

ESR ISOCHRON DATING OF SPELEOTHEMS

ESR ISOCHRON DATING OF SPELEOTHEMS

By

IAKOVOS KARAKOSTANOGLU, B.Sc.

A Thesis

Submitted to the School of Graduate Studies

in Partial Fulfilment of the Requirements

for the Degree

Master of Sciences

McMaster University

November 1982

MASTER OF SCIENCE (1982)  
(Geology)

McMASTER UNIVERSITY  
Hamilton, Ontario

TITLE: ESR Isochron Dating of Speleothems

AUTHOR: Iakovos Karakostanoglou, B.Sc. (National  
University of  
Athens, Greece)

SUPERVISOR: Professor Henry P. Schwarcz

NUMBER OF PAGES: xviii, 209

## Abstract

Calcium carbonate precipitated in caves (speleothem) may contain more than 1 ppm of U but is devoid of Th or K. The major part of its natural radiation dosage (NRD) may have arisen internally from U and its short-lived daughters. By analysing adjacent, approximately coeval samples with varying U content, it is possible to construct an isochron of NRD versus U content which, when extrapolated to zero, gives the external NRD component. The slope of the isochron is a function of the age of the samples, taking into account appropriate corrections for disequilibrium between U-series daughter isotopes, and alpha-particle ESR efficiency ("a"-factor). Using speleothems which have been dated by the  $^{230}\text{Th}/^{234}\text{U}$  method, the above procedure has been reversed to determine the average "a"-factor of the samples, and to establish that its values lie around 0.1.

Several discrete and reproducible ESR peaks of approximately constant g-value have been observed in speleothem calcites. The main peak ( $S_{1A}$ ) with  $g=2.0008(\pm 2)$ , fades at approximately  $220^\circ\text{C}$  and corresponds to the principal TL peak, used for dating so far. Other weaker peaks of various g-values and fading temperatures are also radiation-sensitive. Several other peaks are present which are associated with

$Mn^{2+}$ . Low-temperature annealing has a mild effect on the main peak, probably due to retrapping. This peak varies greatly with grain size, decreasing by more than half for particles less than 100  $\mu m$ .

## Acknowledgements

It was the restless spirits of my friends-brothers in struggle, our faith that "the past is the key to the present", and the all-night discussions with Michalis, walking along the narrow streets of Kokkinia seven years ago, that motivated me to do research on archaeometry. I am grateful to Dr. Aris Poulianos who first showed me that "cave science" does exist, and recommended McMaster University for graduate studies.

I especially thank my supervisor Prof. Henry P. Schwarcz who allowed me to come over from Greece to begin this work. Without his help, guidance, encouragement and financial support this thesis would not have been possible. The original idea of this project was his. I thank also Prof. Derek C. Ford for his interest, the enthusiasm he imparted on me in the classroom and in caves, and the opportunity he gave me to study the karst of Greece, thus keeping my morale up.

Other people have also contributed to the completion of this work. I would like to thank:

- Dr. Melvyn Gascoyne for permission to use his speleothems and data
- Dr. D.J. Huntley of the Physics Department, Simon Fraser University, for his willingness to do alpha irradiations

and thermoluminescence studies of my samples. A large part of this thesis would not have been written without his contribution

- Dr. E.G. Janzen of the Chemistry Department, University of Guelph, for permission to use the Varian ESR spectrometer. His graduate students: Owe, Henry, and Coit are also acknowledged for their technical advice
- Dr. Alfred G. Latham for listening to my research problems, assistance of all kinds and friendship
- M. Leeksma, the laboratory technician of the Biochemistry Department, McMaster University, for her kindness to give me her data on the calibration of the  $^{137}\text{Cs}$  source.
- Martin Knyf, the laboratory technician, for his useful technical advice
- Tammy Middleton, for her excellent performance of some ESR work, the results of which are included in this thesis
- Ali Kameli, for his valuable help in English language problems, some drafting work and friendship, and
- Libby Ginn for her excellent abilities and performance in drafting most of the diagrams and typing the manuscript.

Last, but not least, my sincere thanks go to all those who helped me to adapt in a life style quite new to me.

Particularly to:

- Chas Yong and Pam Burns for their invaluable constant friendship in cave, climbing and skiing trips, pub and parties.
- my compatriots Yannis Missirlis and Vangelis Diamanto-

poulos for personal support of all kinds and for easing my mind in times of trouble.



Science is true;  
do not be misled by 'facts'.

ΚΟΣΜΟΝ (ΤΟΝΔΕ) τόν αὐτόν ἀπάντων ΟΥΤΕ ΤΙΣ ΘΕΩΝ  
ΟΥΤΕ ΑΝΘΡΩΠΩΝ ΕΠΟΙΗΣΕΝ, ΑΛΛ ΗΝ ΔΕΙ ΚΑΙ ΕΣΤΙΝ  
ΚΑΙ ΕΣΤΑΙ· ΠΥΡ ΔΕΙΖΩΝ, ΑΠΤΟΜΕΝΟΝ ΜΕΤΡΑ ΚΑΙ  
ΑΠΟΣΒΕΝΝΥΜΕΝΟΝ ΜΕΤΡΑ.

ΗΡΑΚΛΕΙΤΟΣ

THIS (WORLD-) ORDER the same for all DID NONE OF  
GODS OR MEN MAKE, BUT IT ALWAYS WAS AND IS AND  
SHALL BE; AN EVERLIVING FIRE, KINDLING IN MEASURES  
AND GOING OUT IN MEASURES

HERACLITUS

The thesis is dedicated to

the memory of my father  
who passed away during the completion of this work

## Table of Contents

	Page
CHAPTER 1: RADIATION AND MATTER	
1.1 Introduction (Primary radiational effects)	1
1.2 Charge trapping centers and trapping process	1
1.3 Efficiency of ionization sources	2
1.4 Thermal stability of trapped charges	4
1.4.1 Untrapping	5
1.4.2 Retrapping - Second order kinetics	6
1.5 Detection of trapped charges	7
1.5.1 Thermoluminescence (TL)	7
1.5.2 Electron Spin Resonance (ESR or EPR)	8
1.5.3 Comparison of TL and ESR methods	11
1.6 Natural radiation dose	12
1.6.1 NRD or AD determination	13
1.6.2 a-value determination	13
CHAPTER 2: SPELEOTHEMS	17
2.1 Introduction (Deposition and morphology)	17
2.2 Trace element (TE) geochemistry	19
2.2.1 Radioactive TE	19
2.2.2 Stable TE, radicals and other impurities	20
2.3 Charge trapping centers	21
2.3.1 Nature of traps	21
2.3.2 Abundance of traps	22
2.4 Trap indicators: $g$ and $T^*$	24
2.5 Thermal stability of trapped charges	28
2.6 Traps and artificial irradiation	30

	Page
2.7 Anomalous fading	33
2.8 ED determinations	34
2.9 a-value determinations	36
CHAPTER 3: ESR/TL DATING OF SPELEOTHEMS	38
3.1 Introduction (Conventional dating)	38
3.2 Natural radiation sources	39
3.3 Internal annual dose rate ( $R_{int}$ )	40
3.3.1 Disequilibrium approach	41
3.3.2 Equilibrium approach	42
3.4 External annual dose rate ( $R_{ext}$ )	43
3.4.1 Problems involved in $R_{ext}$ evaluation	44
3.5 Isochron dating: Thesis objective	49
3.6 Isochron applications	52
3.6.1 Method to estimate a gross $t$	53
3.6.2 Age determination	54
3.7 Conditional ESR isochron dating	55
3.7.1 ESR intensity isochron dating	56
3.7.2 Multilayer isochron dating	57
3.8 Isochron diagrams and possible complexities	58
CHAPTER 4: ANALYTICAL TECHNIQUES	61
4.1 Introduction	61
4.2 Sample preparation	62
4.3 Irradiations	63
4.4 Annealing	67
4.5 ESR measurements	71
4.6 Determination of the trace element content	76

	Page
CHAPTER 5: ESR ISOCHRON: TEST ON A STALAGMITE	80
5.1 Introduction	80
5.2 Speleothem 76121 : Given data	81
5.3 Details on analytical procedure	84
5.4 Experimental results	86
5.5 Determination of the IS and $D_{\text{ext}}$	88
5.6 Determination of the $R_{\text{ext}}$ and a-value	93
5.7 Determination of the age $t$	95
5.8 Discussion	97
CHAPTER 6: CONVENTIONAL ESR ISOCHRON DATING: TEST ON A FLOWSTONE	99
6.1 Introduction	99
6.2 Speleothem 77200 : Given data	99
6.3 Details on analytical procedure	101
6.4 Experimental results	106
6.4.1 ESR intensity isochron: complications. The " $[\text{Mn}^{2+}]$ -effect"	116
6.4.2 Experimental determination of a-value	122
6.5 Determination of the IS and $D_{\text{ext}}$	126
6.6 Determination of the $R_{\text{ext}}$ and a-value	131
6.7 Determination of the age $t$	135
6.8 TL study	138
6.8.1 TL experimental results	138
6.8.2 Comparison of TL and ESR results. Inter- pretation: the "grain size effect".	144
6.9 Supplementary ESR data	152
6.10 Discussion	156

	Page
CHAPTER 7: ANNEALING AND GRAIN SIZE EFFECTS OF VARIOUS SPELEOTHEMS	160
7.1 Introduction	160
7.2 Speleothem 76165 . Given data and details on analytical procedure.	161
7.2.1 Experimental results	162
7.2.2 Estimation of the a-value	167
7.3 Thermal study at 'low' T of 76165 powders of various grain sizes	169
7.4 Thermal study at 'high' T	171
7.5 Speleothems 77032 and 77159 . Given data and details on analytical procedure.	176
7.5.1 Experimental results	177
7.5.2 The "grain size effect"	180
7.6 Grain size effect and grain 'surface'	185
7.7 Discussion	189
CHAPTER 8: CONCLUDING REMARKS	190
8.1 Introduction	190
8.2 Distribution of some trace elements in single speleothem layers	190
8.3 Detrital uranium and its effect on the isochron slope	192
8.4 The effect of Mn on the radiation induced ESR signals	193
8.5 Comparison of ESR signals obtained in this work with those in literature	194
8.6 Suggestions for further research	198
References	200
Appendix I: Fricke-Calcite conversion factor cal- culations	205

Appendix II: Sample: 77200-E<sub>3</sub>. Calculation of  $Z_0$   
of the TL active defects chosen for dating.

## List of Figures

	Page	
1.2.1	Illustration of the trapping process.	3
1.5.1.1	Model for thermoluminescence in calcite.	9
1.5.2.1	Electron energy levels. Splitting of energy levels by a magnetic field $H_0$ .	9
1.6.1.1	Signal intensity against dose in an experiment to determine the trapped charge in a mineral.	14
2.1.1	Process and physicochemical mechanisms of speleothem deposition.	18
2.3.2.1	A schematic model of the non-sensitive volume around a defect and an impurity in a crystalline material.	25
2.4.1	Step annealing of the sample "Tautavel 2" (natural).	29
3.4.1	Range of $R_{ext}$ values found in literature.	46
4.3.1	$^{137}\text{Cs}$ source calibration curve.	64
4.3.2	$^{137}\text{Cs}$ $\gamma$ -ray source apparatus.	66
4.3.3	Dose rate dependence on the horizontal distance from the center C, at 9.9 cm from the source.	66
4.4.1	Annealing apparatus; circuitry.	70
4.5.1	Block diagram of ESR spectrometer.	73
4.5.2	$\text{TE}_{011}$ resonance cavity.	74
4.5.3	ESR spectrum of $\text{Mn}^{++}$ in $\text{MgO}$ at room temperature, with $\nu=9.3$ GHz.	74
4.6.1	[U] of various speleothem samples as found by IDA and NAA.	78
5.1.1	Climatic oscillations for the last 120 Ka in Britain, from beetle assemblages.	82

	Page
5.4.1	ESR spectra of spel. 76121-Top (spectrometer: Varian E104A). 87
5.4.2	Stal. 76121, Top and Base samples. Determination of ED's. 89
5.5.1	Stal. 76121, natural $S_{1A}$ : ESR intensity isochron. 91
5.5.2	Stal. 76121, $S_{1A}$ : 'real' isochron. 92
5.6.1	Stal. 76121, Top and Base. Plot of $cf(a,p,q,t)$ versus a-factor. The IS and $IS_{max}$ are shown too. 94
5.7.1	Stal. 76121, Top and Base. Plot of $cf(a,p_o,t)$ versus $\underline{t}$ for $a=0.15$ and $p_o=1$ and 2 (preliminary test plot). 96
5.7.2	Stal. 76121, Top and Base. Plot of $cf(a,p,q,t)$ versus $\underline{t}$ . 96
6.1.1	Stalactite 75037. Natural intensity of the main ESR signal versus U content (NAA). 100
6.3.1	Flowstone 77200: cross section. 105
6.3.2	Flowstone 77200, layer E, grain size 150-300 $\mu m$ . Natural $S_{1A}$ : ESR intensity dependence on sample weight. 107
6.4.1	ESR spectra of f/st 77200- $E_3$ (spectrometer: Varian E104A). 108
6.4.2	Flowstone 77200- $E_3$ , natural; powder of grain size 150-300 $\mu m$ . $^3$ Step annealing: $T=25^\circ C$ , $t^*=6$ min. 110
6.4.3	F/st 77200- $E_3$ , natural: ESR spectra of the thermal study (spectrometer: JEOL JES-3BS-X) 112
6.4.4	F/st 77200- $E_3$ samples. ESR intensity response to additive $\gamma$ -doses. 114
6.4.1.1	F/st 77200. ESR intensity of natural $S_{1A}$ versus [U] for all the available samples. 118
6.4.1.2	F/st 77200. ESR intensity of $Mn^{2+}(-\frac{1}{2})$ peaks versus [Mn]. Calibration curve. 118



	Page
6.4.1.3 F/st 77200. ESR intensity of natural $S_{1A}$ versus $[Mn]$ for all the available samples.	120
6.4.1.4 F/st 77200. ESR intensity of natural $S_{1A}$ versus $[U] / [Mn]$ for all the available samples.	121
6.4.2.1 F/st 77200- $E_3$ . ESR intensity response to additive $\alpha$ -doses. (signal $S_{1A}$ )	125
6.5.1 F/st 77200, natural $S_{1A}$ : ESR intensity multilayer-isochron.	128
6.5.2 $S_{1A}$ sensitivity to $\gamma$ -rays versus $[U] / [Mn]$ for various samples.	130
6.5.3 F/st 77200. 'Real' isochron line and data point for the E layer ( $\overline{ED}$ , $[\overline{U}]$ ).	132
6.6.1 $\alpha$ -factor as a function $\Delta_1$ .	134
6.7.1 F/st 77200. Preliminary test to estimate a gross $t$ .	136
6.7.2 F/st 77200. ESR isochron and U/Th dates for various cases discussed in section (6.7).	139
6.8.1.1 F/st 77200- $E_3$ . TL first glow curves of natural and $\gamma$ irradiated material.	141
6.8.1.2 F/st 77200- $E_2$ . TL intensity response to additive $\gamma$ -doses for the dating TL peak.	142
6.8.1.3 F/st 77200- $E_3$ . First glow growth with gammas of the dating TL peak.	143
6.8.1.4 F/st 77200- $E_3$ . TL first glow curves of natural and $\alpha$ irradiated material.	145
6.8.1.5 F/st 77200- $E_3$ . First glow growth with alphas of the dating TL peak.	146
6.8.2.1 F/st 77200-E. The "grain size effect".	148
6.8.2.2 F/st 77200-E. Equivalent dose versus grain size of powders not treated with acid.	151
6.9.1 F/st 77200 - K and EF layers. ESR signal $S_{1A}$ -growth with additive gamma doses.	154

	Page
6.9.2 F/st 77200. Isochron plot including data from Figure (6.5.3) and from the table in section (6.9).	157
7.2.1.1 F/st 76165. Step annealing of natural and irradiated powders ( $>100 \mu\text{m}$ ), approximately 6 days after irradiation.	163
7.2.1.2.A F/st 76165. Step annealing of the natural powder ( $>100 \mu\text{m}$ ). ESR spectra at characteristic temperatures. ESR spectrometer: JEOL, Gain=250.	164
7.2.1.2.B as Figure 7.2.1.1.A but: Gain=630.	165
7.2.1.3 F/st 76165. ESR intensity response to additive $\gamma$ -doses and fading process.	166
7.2.1.4 F/st 76165. ESR signal growth with gammas (data taken from Figure 7.2.1.1).	168
7.3.1 F/st 76165. Step annealing ( $T=25^\circ\text{C}$ , $t^*=12 \text{ min.}$ ) at low T of coarse ( $>100\mu\text{m}$ ) or fine ( $<100 \mu\text{m}$ ) powders, natural or irradiated with 2.46 Krads of gamma. ESR spectra have been taken soon after irradiation.	170
7.4.1 Step annealing at high T, for various speleothems. $I$ =ESR intensity of $S_X$ .	173
7.4.2.A,B F/st 76165. g-value dependence on temperature for low H (A) and high H (B) $\text{Mn}^{2+}$ Forbidden Transitions.	174
7.5.1.1 Stal. 77032. Step annealing of powder (300-700 $\mu\text{m}$ ) irradiated with 2.4 Krads gamma and annealed (soon after irradiation).	179
7.5.1.2 Stal. 77032. ESR signal $S_{2B}$ : decay at room temperature.	179
7.5.2.1 Stal. 77032 and F/st 77159. The "grain size effect" for various ESR signals. The powders and	182
7.5.2.2 are natural, irradiated (2.4 Krads of gamma), or irradiated and annealed soon after irradiation at $\sim 100^\circ\text{C}$ for about 10 minutes.	183
7.6.1 Stal. 77032. The effect of etching with acetic acid 0.5% on the dating ESR signal ( $S_{1A}$ ) for powders of various ranges of grain size.	187
7.6.2 Acid attack does not affect the ESR intensity of very fine grains ( $<100 \mu\text{m}$ ).	188

		Page
I <sub>1</sub>	Attenuation coefficient of $\gamma$ -rays in water versus gamma energies.	207
II <sub>1</sub>	Annealing rate ( $\beta$ ) dependence on activation temperature ( $T^*$ ).	209

### List of Tables

		Page
2.3.1.1	Radiation-induced defects in calcite.	23
2.5.1	Calculated mean lives for a peak at 275°C for a heating rate of 5°C s <sup>-1</sup> and having a trap depth of 1.75 eV.	29
4.5.1	ESR spectrometer setting	73
5.1.1	Proposed correlation of British Quaternary events to the stable isotope record of speleothem 77151 and the deep sea core ice volume curve.	83
8.5.1	ESR signal Classification	195
8.5.2	Comparison of ESR data of this work with that of Apers <u>et al.</u> , (1981).	196

### List of Plates

		Page
5.3.1	Stalagmite 76121: Longitudinal cross section	85
6.2.1.A	Flowstone 77200. Cross section parallel to the growth direction (actual size). Most of the samples used in this study were taken from this piece.	102
6.2.1.B	Flowstone 77200. Cross section parallel to the growth direction (actual size). Piece used by Gascoyne for U/Th dating.	103

## Glossary

This list includes those symbols and abbreviations which are most frequently used in the thesis. Definitions and other information are given on the indicated page.

<u>Latin</u>	<u>Page</u>
a-factor/value : the degree of effectiveness (%) in inducing trapped charges that the alpha particles have, compared with the beta particles or gamma photons of the same dose.	4
c : constant	42
D : dose or dosage in general	1, 13
$D_n$ : total natural radiation dose $\equiv$ NRD	49
$D_{int}$ : internal component of $D_n$	40
$D_{ext}$ : external component of $D_n$	41, 49
E : charge activation energy, or trap energy depth	5
ED : equivalent dose	13
ESR : electron spin resonance	8-11
g-factor/value : spectroscopic splitting factor	8
H : magnetic field in general	
$H_o$ : external H where ESR occurs	10, 11
$H_m$ : the amplitude of the microwave H in the resonance cavity	72
I : TL or ESR signal intensity in general	8, 11
$I_n$ : I of natural samples, i.e. total natural I of the radiation sensitive ESR signals	56

<u>Latin</u>		<u>Page</u>
$I_{\text{ext}}$	: external component of $I_n$	56
IDA	: isotope dilution analysis	77
IS	: isochron slope	50
MW	: ESR spectrometer modulation width	26
NAA	: neutron activation analysis	76
NRD	: natural radiation dose $\equiv D_n$	12
p	: the present day activity ratio $^{234}\text{U}/^{238}\text{U}$	41
$p_0$	: the initial p at $t=0$	53
q	: the present day activity ratio $^{230}\text{Th}/^{234}\text{U}$	41
$R_n$	: natural annual dose rate	38
$R_{\text{int}}$	: internal component of $R_n$	39-40
$R_{\text{ext}}$	: external component of $R_n$	39,43
$R'_{\alpha, \beta, \gamma}$	: dose rates per ppm of total U, due to $\alpha$ , $\beta$ and $\gamma$ rays respectively, given by Bell	40
s	: the ESR intensity-dose sensitivity $\equiv$ $dI/dD$	15
$s(\alpha)$	: the $\underline{s}$ for alpha particles	15
$s(\gamma)$	: the $\underline{s}$ for gamma photons	15,56
S	: alpha particles source strength	15
$S_{ij}^{i=1,2}$ $j=A,B$	: ESR signal symbols adopted for classification purpose	145
t	: age or date	
$t^*$	: heating time in the process of step annealing	68

<u>Latin</u>		<u>Page</u>
$t_o$	: cooling interval in the process of step annealing	68
T	: temperature in general	
T*	: activation temperature	5,27
$T_o$	: environmental temperature	5
TE	: trace element	19
TL	: thermoluminescence	7
TLD	: TL dosimeter or dosimetry	44
U/Th dating	: dating method based on the isotope ratios p and q	
 <u>Greek</u>		
$\beta$	: annealing rate	5
$\Delta_i, i=1,2,3$	: effective doses; parameters of the Wintle's function	41
$\Delta T$	: temperature interval (step) used in the annealing process	68
$\epsilon(TE)$	: $\epsilon$ -factor indicating that the [TE] range is $\epsilon\%$ of the average of the extreme [TE] -values	190
$\lambda$	: decay constant in general	
$\tau_o$	: lifetime of the trapped charge	5-6

## CHAPTER 1: Radiation and matter

### 1.1 Introduction (Primary radiational effects)

Any radiation passing through matter loses part or the whole of its energy. The portion of this energy dissipated within the object is called the absorbed dose or simply dose (rad). There are two primary radiational effects: a) displacement of atoms through direct energy transfer by charged particles ( $\alpha$ ,  $\beta$ , cosmic rays, etc.). b) ionization by particles or photons ( $X$ ,  $\gamma$ ). Consequently point defects (Schottky, Frenkel, etc.) and ionization electrons/holes are created.

Ionization charges can be produced by agencies other than nuclear radiation, e.g. by pressure, friction, and light (piezo-, tribo-, and photo-electric effects). In the context of dating we are interested only in radiation-induced ionization which is regarded as "true"; all the other types will be regarded as "spurious".

### 1.2. Charge trapping centers and trapping process.

Several charge-defect structures are present in the crystalline lattices, known as charge-traps or color-centers.

They may have thermal, radiational, or other origin. Many of these centers form in connection with impurities. As a matter of fact not all lattice defects are necessarily charge-traps, and some of the charge-traps are not lattice defects. The most important and extensive group of traps in any minerals appear to be different radicals (impurities or not), the foreign cations and a combination of these two types of centers (Marfunin, 1979, section 7.2). Thus the main role of radiation is to supply ionization charges which randomly move about in a solid.

In most non-metallic crystals the holes are quickly captured by hole traps. Electrons usually have a longer life time and one fraction of these are 'permanently' trapped by 'thermally stable' electron traps. The remaining fraction undergoes recombination at recombination centers, which are hole traps located at parent atoms and having the following property: once they have captured a hole, there is a high probability that free or mobile electrons will be recombined with these holes. The concentration of these centers remains substantially constant in any crystal. Figure (1.2.1) illustrates the process described above.

### 1.3 Efficiency of ionization sources

All radiation does not have the same efficiency



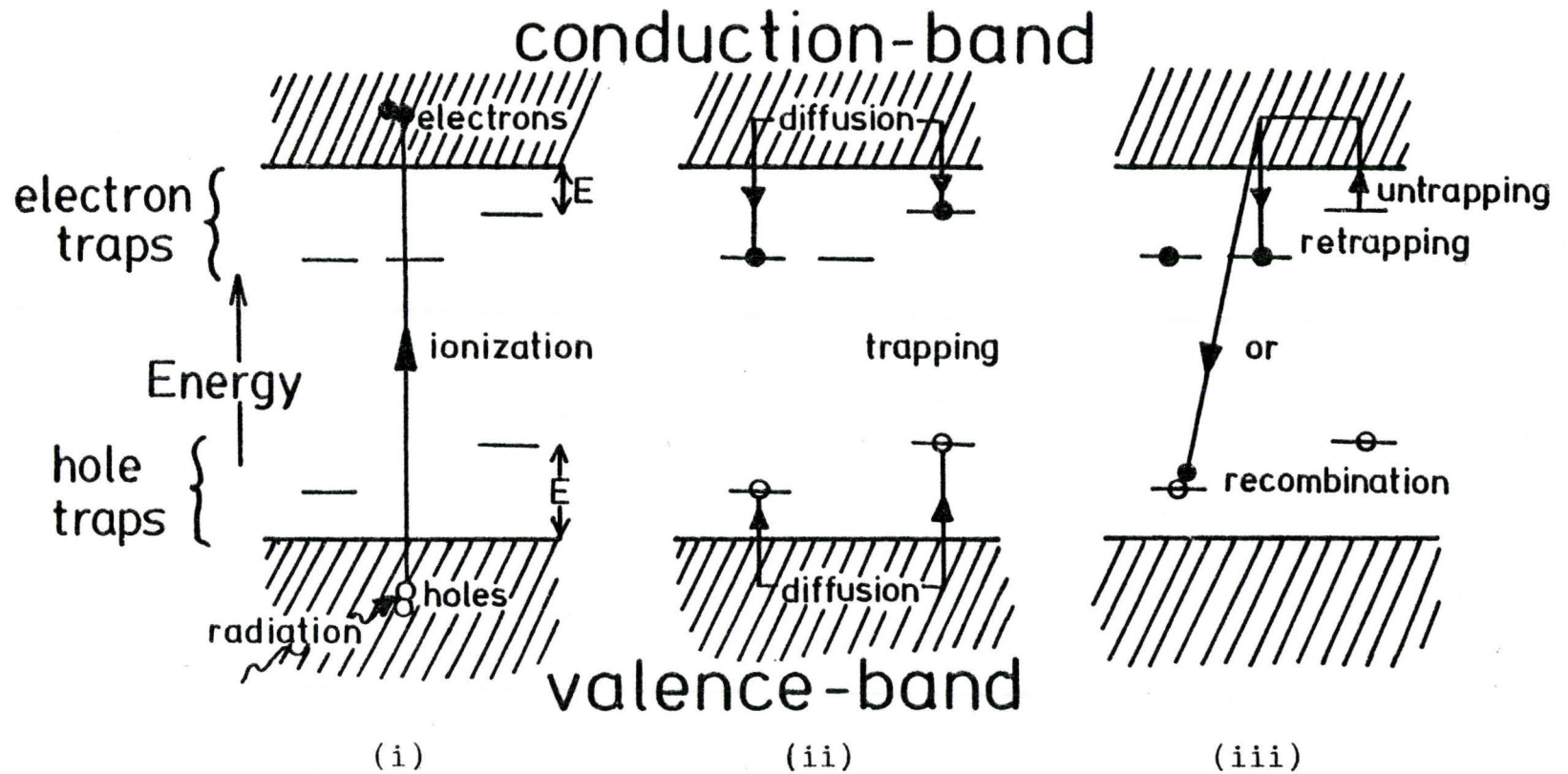


Figure 1.2.1 Illustration of the trapping process: (i) creation of charges, (ii) storage of energy, (iii) release of charges at constant temperature (1st order kinetics).

in creating trapped charges. So, a given dosage from alpha particles is less effective in inducing trapped charges than the same dosage of beta particles or gamma photons. The degree of effectiveness varies from sample to sample and is expressed as the k- or a-value. If  $X_\alpha$  and  $X_{\beta\gamma}$  represent concentrations of trapped charges in a particular trap per unit of absorbed dose induced by  $\alpha$  and,  $\beta$  or  $\gamma$  radiations respectively, then the a-value is given by

$$a = X_\alpha / X_{\beta\gamma} \quad (1.3.1)$$

In other words, the effective alpha dosage is equal to a-times the actual dosage, ie.

$$D_{\text{eff}} = a D_{\text{act}} \quad (1.3.2)$$

The reason for the lower effectiveness of alpha particles seems to be the high ionization density in their tracks which is more than enough to saturate all the traps; the excess is wasted to recombination centers (Zimmerman, 1972).

#### 1.4. Thermal stability of trapped charges

The amount of trapped charge retained in a crystal over an extended period of time depends on several factors, the most important of which are thermal untrapping and retrapping of the thermally released charges (see Figure 1.2.1).

The simplest and most convenient case for mathematical treatment is the one where first order kinetics are employed.

#### 1.4.1 Untrapping

Untrapping is characterized by the life-time  $\tau_0$  of the trapped charge, given by the Arrhenius law:

$$\tau_0 = \frac{1}{s^*} \exp E/kT_0 \quad (1.4.1.1)$$

where  $s^*$  is the frequency factor which expresses the attempts of the trapped charge to escape

$E$  is the activation energy (eV) or the energy depth (Figure 1.2.1)

$T_0$  is the environmental temperature ( $^{\circ}\text{K}$ ) and

$k$  is the Boltzmann's constant ( $k = 0.862 \cdot 10^{-4} \text{ eV}/^{\circ}\text{K}$ )

To estimate  $E$ , Hoogenstraaten derived the following expression (Wintle, 1977)

$$\frac{\beta E}{kT^{*2}} = s^* \exp (-E/kT^*) \quad (1.4.1.2)$$

where  $T^*$  is the temperature ( $^{\circ}\text{K}$ ) at which the trapped charges are fluently released

and  $\beta$  is the annealing rate ( $^{\circ}\text{K}/\text{sec}$ ) of an experiment where temperature increases linearly from  $T_0$  (usually room temperature) to  $T^*$ .

Equations (1.4.1.1) and (1.4.1.2) enable us to evaluate  $\tau_0$  a magnitude characteristic of the material, by means of

$\beta$  and  $T^*$ , magnitudes characteristic of the way of heating. This is a bit odd, because different  $\beta$  and  $T^*$  could yield different  $\tau_0$ . However,  $T^*$  is dependent on  $\beta$ , and the ratio  $\beta/T^{*2}$  remains fairly constant, as we will see later.

There is no critical interference in the experimental evaluation of  $\tau_0$ . Now from equation (1.4.1.1) and (1.4.1.2) we obtain:

$$\tau_0 = \frac{kT^{*2}}{\beta E} \exp \left[ -\frac{E}{k} \left( \frac{1}{T^*} - \frac{1}{T_0} \right) \right] \quad (1.4.1.3)$$

Therefore, to get  $\tau_0$  sufficiently large we must have both  $T^*$  high and  $E$  low. These two requirements are mutually independent, that is  $T^*$  and  $E$  must be measured by independent ways.

#### 1.4.2 Retrapping - Second order kinetics

If the crystal contains a large number of traps, only a fraction of them being filled, there is a high probability that thermally released charge will find its way to an empty trap. However, there is a finite probability that the untrapped charge will undergo recombination and be lost (see Figure 1.2.1). If the concentration of recombination centers  $R$  ( $\#/cm^3$ ) is very large, every thermally released charge is lost by recombination, i.e., retrapping practically does not occur. The effect of recombination has been formulated by Levy (1968). He gives a particular example ( $T_0=27^\circ C$  and  $E=1.4$  eV) where retrapping is significant only for  $R < 1$ . Most of

the minerals which possess trapping centers seem to have  $R \gg 1$ , so the retrapping process is probably negligible for traps of  $E \geq 1.4$  eV at  $T_0 \leq 27^\circ\text{C}$ .

The question "What happens when kinetics are of second or higher order?" is very difficult to answer. However, though the high  $T^*$  trapped charges are more likely to obey second order kinetics the low or intermediate  $T^*$  ( $< 300^\circ\text{C}$ ) ones can be described sufficiently by first order kinetics (Bonfiglioli, 1968).

### 1.5 Detection of trapped charges

There are several methods of measuring the concentration of trapped charges but most of them are indirect or present other difficulties. One of the methods, probably the most popular, is called Thermoluminescence. This method has been widely applied in a large variety of minerals for various purposes. On the other hand, there are distinct advantages in measuring trapped charges by direct methods, such as the so-called Electron Spin Resonance method which has attracted much attention lately.

#### 1.5.1 Thermoluminescence (TL)

TL-method employs a crystal property called Thermoluminescence which is based on the presence of a particular type of defect (usually due to impurities) called a

luminescent center. Crystals including such centers are named phosphors (e.g.  $\text{CaCO}_3$  etc.). If the temperature of the sample is raised, charges escape and some of them reach luminescent centers. In the process of combining into the atom or ion forming the center, photons of visible light are emitted and recorded by TL-devices. Figure (1.5.1.1) illustrates in more detail the TL process in a particular example ( $\text{CaCO}_3$ ). Usually TL-intensity  $I$  is proportional to the charge release rate  $-dn/dt$ , that is

$$I = e (-dn/dt) \quad (1.5.1.1)$$

where  $e$  is the luminescence efficiency and is assumed to be constant. During the process of annealing with constant rate  $\beta$ , several glow peaks are revealed at different activation temperatures  $T^*$ , corresponding to traps with different energy depths  $E$ .

### 1.5.2 Electron Spin Resonance (ESR or EPR)

A single electron, such as a trapped one, possesses intrinsic angular momentum or spin  $S = \frac{1}{2}$  and magnetic moment  $\mu$  associated with the spin by

$$\mu = -g \beta M_S \quad (1.5.2.1)$$

where  $g$  is the spectroscopic splitting factor, which has a value depending on the electron's environment ( $g \cong 2$  for a free electron)

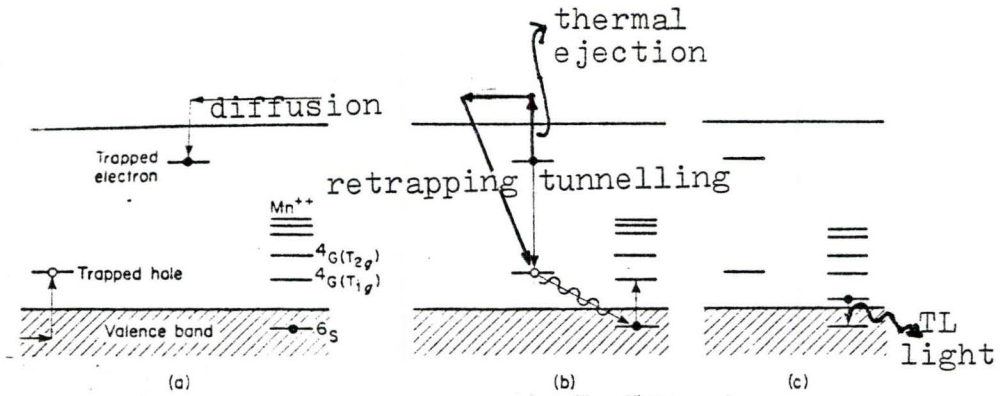


Figure 1.5.1.1 Model for thermoluminescence in calcite showing (a) color center formation, (b) thermal bleaching of color centers and excitation of a  $Mn^{2+}$  center, and (c)  $Mn^{2+}$  emission. (after: Medlin, 1968b. Fig. 4.20)

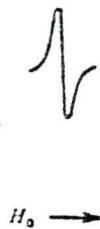
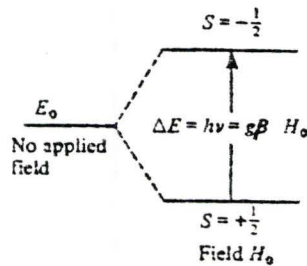


Figure 1.5.2.1 Electron energy levels. Splitting of energy levels by a magnetic field  $H_0$ .

$\beta$  is the Bohr magneton, i.e. a factor converting spin to magnetic moment, and

$M_s$  is the spin quantum number, which can have values of  $+\frac{1}{2}$  or  $-\frac{1}{2}$ .

In the absence of an external magnetic field, the electron may exist in one of two states  $+\frac{1}{2}$  or  $-\frac{1}{2}$  of equal energy (degenerate). When an electron is placed in an external magnetic field,  $H_0$ , the degeneracy is removed and two energy levels are established (Figure 1.5.2.1). The difference between these two levels is given by

$$\Delta E = g \beta H_0 \quad (1.5.2.2)$$

The excess electron population of the lower energy level over that in the upper state is very small. It is governed by the Boltzmann distribution:

$$\frac{N_{\text{upper}}}{N_{\text{lower}}} = \exp(-\Delta E/kT) \quad (1.5.2.3)$$

For example, at  $300^\circ\text{K}$  and  $H_0=3000\text{G}$  for a species of  $g=2$ ,  $N_{\text{upper}} \cong 0.9984 N_{\text{lower}}$ . If an electromagnetic (EM) wave of frequency  $\nu$  and energy  $h\nu$  ( $h$ =Planck's constant) equal to

$\Delta E$  is applied to the electrons, transitions from the lower to the upper energy state occur. The absorption of EM-radiation quanta by electrons in the lower level will exceed spontaneous emission from the upper level because of the Boltzmann distribution, resulting in a net absorption



of energy. This phenomenon is called Electron Spin Resonance. The normal frequency is  $\nu \cong 9$  GHz (X-band) at a magnetic field  $H_0 \cong 3,500$  G. In practice  $\nu$  is kept constant while  $H_0$  varies and when  $H_0 = h\nu/g\beta$ , part of the microwave energy is absorbed and an absorption signal is recorded. Signal intensity  $I$  is proportional to the absorbed energy and thus to the number of transitions, the latter being related to the absolute number of the trapped single electrons of a particular  $g$ -value.

### 1.5.3 Comparison of TL and ESR methods

In correlating TL and ESR data, it is important to realize that TL registers the same electron-hole centers which are identified by the ESR spectra (Marfunin, 1979; section 6.1.2). Peaks on the thermal de-excitation (annealing) curves actually represent an energy spectrum of the centers. However, TL-parameters are only a part of the characteristics featuring these centers, being insufficient to determine its nature. A center's nature is determined from the ESR spectra of a single crystal and by correlating the thermal stability of the centers, established from these spectra, with temperatures of the TL-peaks.

A comparison of TL- and ESR-methods, favouring the latter, is given by Zeller (1968). Some practical advantages of ESR over TL are:

- (i) the radiation induced charge-centers are not des-

- troyed during the measurement;
- (ii) ESR is less sensitive to surface effects than TL (see: Chapter 4);
  - (iii) Sample preparation at room temperature is quite simple.

An advantage of TL is its substantially higher sensitivity and its simplicity of measurements, though the new digital signal averaging technique (Ikeya and Miki, 1980a) and measurements at low temperatures (e.g. 150°K) can improve the poor ESR sensitivity. The different order of TL and ESR sensitivity may cause incomplete TL-ESR correspondence for by using ESR one may not find centers for all the TL-peaks (Marfunin, 1979; section 6.2) and vice versa. Thus, in general, a one-to-one correspondence between TL and ESR cannot be taken for granted (Nambi, 1979). In geological practice, however, the combination of these two methods has been proven most fruitful.

### 1.6 Natural radiation dose

The total "true" dose (TD) acquired by a mineral-phosphor during its geological or archaeological life is also called natural radiation dose (NRD) or archaeological dose (AD), and it is due to any source of radiation (radioactive impurities, cosmic rays) present in the environment of the individual sample. If it is assumed that a suitable means is available for measuring charge-center concentrations,

such as ESR or TL, determination of NRD is possible by using several methods, of which the so called additive method (Levy, 1968; Aitken, 1974, section 3.7) is in common use the last few years.

#### 1.6.1 NRD or AD determination

A hypothetical experiment is illustrated in Figure (1.6.1.1) where a sample containing two centers is irradiated by successively increased doses D of gamma artificial irradiation. As far as the intensity increases linearly, straight lines over the range of the linear response can be drawn, the extrapolation of which to zero intensity ordinate yields the so called prior dose (PD) or equivalent dose (ED). In a first approximation:  $ED = NRD$ , with the assumptions that :

- (i) the ESR signals or TL peaks are due to charges trapped on centers which were completely empty when the sample was formed.
- (ii) the trap is thermally stable.
- (iii) the trapped charge increases linearly with dose.
- (iv) the linear intensity-dose relation is independent of dose rate or irradiation time.

#### 1.6.2 a-value determination

The additive method can be used for the a-value experimental determination, as well. If sample powders,

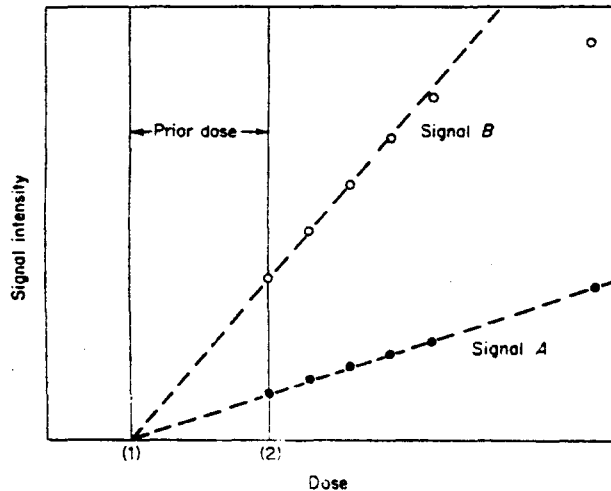


Figure 1.6.1.1 Signal intensity against dose in an experiment to determine the trapped charge in a mineral. This material would have to have two relatively empty traps when measurements were started. For this determination to be meaningful it would be essential to determine, for example by annealing experiments, that the trapped charges were almost completely stable at the highest temperature reached by the sample in the time it acquired the "prior dose". (from: Levy, 1968, Fig. 2.6)

adequately fine to be penetrated by alpha particles, are exposed to alpha irradiation, then the alpha-ED is obtained and formula(1.3.2)gives:

$$a = \frac{D_{\text{effective}}}{D_{\text{actual}}} = \frac{\text{gamma ED}}{\text{alpha ED}} \quad (1.6.2.1)$$

In evaluating a-values by this method, sample preparation may raise some complications (surface effect), which will be discussed later. Alternatively, the intensity-dose sensitivity (dI/dD) of alphas  $s(\alpha)$  and gammas  $s(\gamma)$  (slopes of the corresponding straight lines) can be used and combined with formula (1.3.1) which gives:

$$a = \frac{X_{\alpha}}{X_{\gamma}} = \frac{s(\alpha)}{s(\gamma)} \quad (1.6.2.2)$$

This formula requires both slopes or sensitivities to be given in same units (TL or ESR intensity per rad). This is not always possible because of problems raised in alpha sources calibration. It is suggested by Aitken and Bowman (1975) that specification of alpha source strength in terms of track length delivered to the sample is more convenient than the usual practice of specification in terms of rads. These authors define the a-factor as:

$$a = \frac{x}{1300 S} \quad (1.6.2.3)$$

where S is the source strength in  $\mu\text{m}^{-2} \text{min}^{-1}$

x is the dose (rads) of beta or gamma that gives the same TL (or ESR) intensity as 1 min dose of alpha, and

1300 is a numerical factor chosen so that the a-value given by (1.6.2.3) will be equal to the a-value given by (1.6.2.2) for irradiation with alphas of 3.7 MeV.

In practice, x can be evaluated by the ratio:

$$x = s(\alpha)_t / s(\gamma) \quad (1.6.2.4)$$

where  $s(\alpha)_t$  and  $s(\gamma)$  are alpha and gamma sensitivities expressed in TL or ESR intensity per min of alphas and per rad of gammas respectively.

## CHAPTER 2: Speleothems

### 2.1 Introduction (Deposition and morphology)

Speleothems are mostly calcite deposits formed in caves by a transport process in which material is carried into the cave by moving groundwater and left behind as a stalactite, stalagmite, flowstone or other formation. The physico-chemical mechanisms for such a calcite deposition are outlined in Figure (2.1.1). Speleothems are basically ionic  $\text{CaCO}_3$  crystals, usually oriented perpendicular to the growth surface. They form under relatively constant cave-atmosphere conditions of pressure and temperature, the latter being approximately equal to the average annual temperature of its surroundings and having annual variation of less than  $1^\circ\text{C}$  (Moore and Sullivan, 1978; p.27-29).

Most speleothems are characterized by growth rings or laminations which can represent up to several thousand years of growth for one "band". These layers can be distinguished from one another by changes in colour, texture and impurity content. Hiatuses are often seen, which represent temporary cessation of speleothem growth. They often appear as a thin layer of detritus or as sudden change in colour or texture of the growth layers.

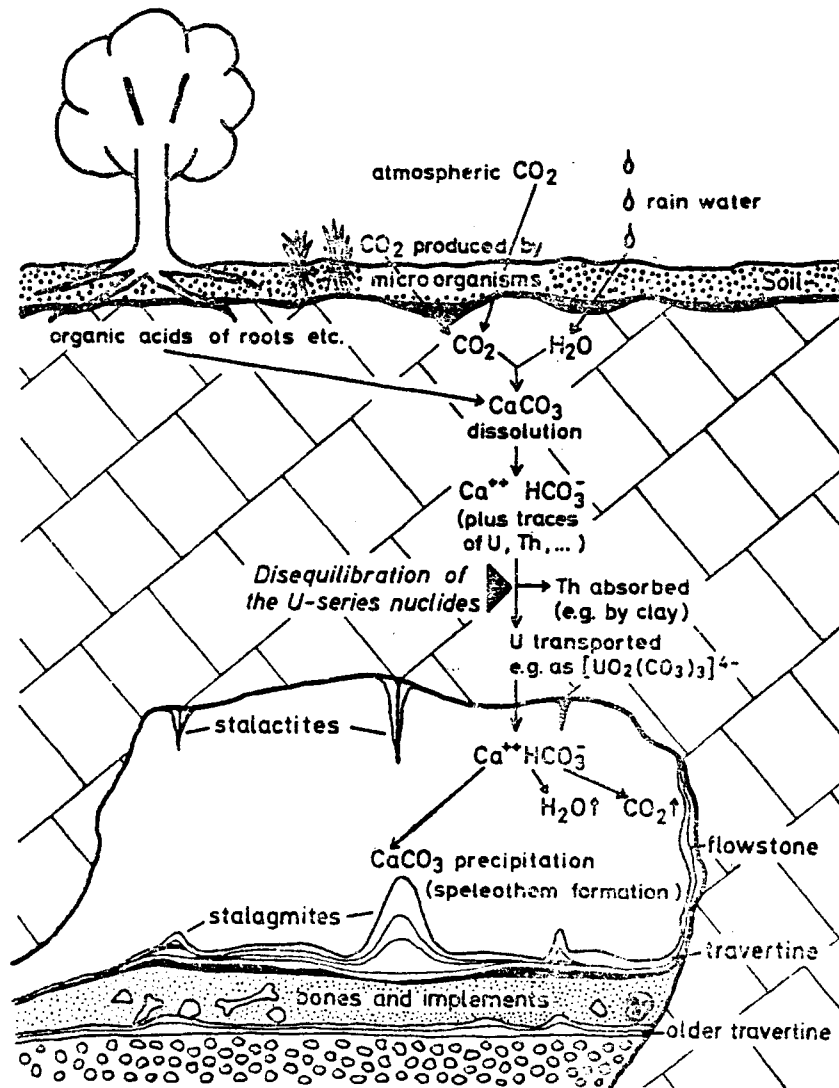


Figure 2.1.1 Process and physicochemical mechanisms of speleothem deposition. (from: Hennig *et al.*, 1980, Fig. 2)



## 2.2 Trace element (TE) geochemistry

Speleothem-depositing cave waters contain mainly the cations  $\text{Ca}^{2+}$  and  $\text{Mg}^{2+}$  as major elements. Other cationic species are minor or trace elements, being incorporated into the calcite lattice in several ways, and their content may vary for several reasons too (see for example: Gascoyne, 1979; Chapter 9). In this study we are concerned mostly in the content of radioactive elements.

### 2.2.1 Radioactive TE

Most geological materials, including speleothems, contain such radionuclides as  $^{238}\text{U}$ ,  $^{232}\text{Th}$ , their daughter products,  $^{40}\text{K}$  etc. However, in 'pure' speleothems, i.e. those with little or no detrital inclusions (clay particles etc.), only  $^{238}\text{U}$  and its products are present, the others being negligible. This can be understood from the distinct geochemical behaviour of these elements. Uranium concentration in speleothems is not uniform. It may vary considerably both parallel and normal to the speleothem growth direction. [U] -variations range from less than 0.01 ppm to about 90 ppm (Gascoyne, 1979; section 2.2). But most values fall in the range 0.1 to 2.0 ppm (Gascoyne, 1978).

The distribution of U and other foreign ions within a single layer of speleothem has rarely been studied. It is more likely that a rather inhomogeneous trace element distribution should be expected, particularly

for non-substitutional ions, such as U-complexes. Fission track analysis of stalagmites (Wintle, 1978) showed variations in the uranium content in adjacent slices 2 mm by 2 mm of a single layer. The mean U-content for each slice varied from  $\sim 0.11$  to  $\sim 0.44$  ppm. The U-content of adjacent growth layers in a stalactite was found to vary by factors of 2-50 or more. Another similar analysis showed great variation of microdistribution of U within an area of  $0.58 \text{ cm}^2$  of a speleothem sample (Liritzis, 1980).

### 2.2.2 Stable TE, radicals and other impurities

Various TE have been found in speleothems in concentrations from a few ppm to several hundreds of ppm (Gascoyne, 1977; Apers *et al.*, 1980; Hennig *et al.*, 1981a). Their valence state can be determined from ESR spectra of single crystals. The presence of cations substituting  $\text{Ca}^{2+}$  were established by ESR in case of 'pure' calcites (Marfunin, 1979, section 7.3.9). So,  $\text{Mn}^{2+}$ ,  $\text{Fe}^{2+}$ ,  $\text{Fe}^{3+}$ ,  $\text{Y}^{3+}$  and other metals or rare earths were found, some of them being related with electron or hole centers. Besides, anions substituting  $\text{CO}_3^{2-}$  were also identified, such as  $\text{PO}_3^{2-}$ ,  $\text{PO}_3^0$ ,  $\text{PO}_2^{2-}$ ,  $\text{PO}_2^0$ , to mention only phosphorus radicals.

The presence of TE was often cited as being the cause of colour banding and opacity differences which some speleothem growth-horizons exhibit. Gascoyne (1977), however, found no direct correlation between colour and TE content,

proposing that organics may often control speleothem colour. Thus, a 'pure', white speleothem may indicate a calcite quite free of humic complexes, clay particulates or other detrital impurities, without excluding the presence of TE.

### 2.3 Charge trapping centers

As in most minerals, so in calcites, the most numerous traps seem to be the different radicals, the foreign cations and a combination of these two. More specifically, the centers related to the  $\text{CO}_3^{3-}$ ,  $\text{CO}_3^-$  and  $\text{CO}_2^-$  radicals appear to have particular importance in dating purposes.

#### 2.3.1 Nature of traps

Centers unstable at room temperature exist largely due to thermal defects (Marfunin, 1979; section 6.1.2). Accumulation of such charge centers is impossible under natural conditions. Irradiation at room temperature (presumably natural conditions) induces electrons and holes trapped primarily at calcite's planar carbonate ions and produces free radicals  $\text{CO}_3^{3-}$  and  $\text{CO}_3^-$  at the lattice sites of  $\text{CO}_3^{2-}$  (Marshall et al., 1968). Some pairs of  $\text{CO}_3^{3-}$  and  $\text{CO}_3^-$  are restored to  $\text{CO}_3^{2-}$  even at low temperatures by electron transfer through tunnelling process and give a long-lasting phosphorescence (Ikeya, 1978a). Besides, irradiation

'uncovers' impurity defects which did not become fully converted into the ionized state under natural conditions.

If a sample's temperature is increased,  $\text{CO}_3^-$  changes electronic symmetry, becomes mobile, and some of them are stabilized in some place. The ESR of this stable hole trap has not been detected in natural calcites so far (Ikeya, 1978a).

The  $\text{CO}_3^{3-}$  free radical seems to play the major role in forming radiation induced defects in calcite, stable at high temperatures. Ikeya (1978a) describes the models of four defects, associated with the  $\text{CO}_3^{3-}$  radical, and being stable up to  $50^\circ\text{C}$ ,  $230^\circ\text{C}$ ,  $330^\circ\text{C}$  and  $430^\circ\text{C}$  respectively. Table(2.3.1.1) summarizes his discussion. Of these, the one stable up to  $\sim 230^\circ\text{C}$  seems to be the main ESR or TL signal mostly used for dating. In addition to  $\text{CO}_3^{3-}$  and  $\text{CO}_3^-$  centers, the  $\text{CO}_2^-$  center is also formed but less efficiently than the former two. Its formation has been found to be closely associated with a  $\text{F}^-$  impurity ion. Since  $\text{F}^-$  anions are of minor importance in speleothems, this center has rarely been observed in such materials (see for instance: de Canniere *et al.*, 1982).

### 2.3.2 Abundance of traps

To date, calcites by measuring concentrations of trapped charges, an essential requirement is the presence of abundant traps. Both  $\text{Ca}^{2+}$  and  $\text{CO}_3^{2-}$  lattice sites may become traps if a trivalent cation substitutes for  $\text{Ca}^{2+}$ .

Table 2.3.1.1 Radiation-induced defects in calcite.  
(from: Ikeya, 1978a, Table 1)

<i>Defect</i>	<i>Model</i>	<i>Symmetry from ESR spectrum</i>	<i>TL peak (°C)</i>	<i>Decay time at 27°C</i>	<i>Comment</i>
I	CO <sub>3</sub> <sup>2-</sup>	Tetragonal	50	1 day	Unstable at room temperature
II	Y <sup>3+</sup> -CO <sub>3</sub> <sup>2-</sup> or CO <sub>3</sub> <sup>2-</sup> associated with a trivalent cation	Rhombic	230	2 × 10 <sup>4</sup> years	Dating is possible
III	Aggregate or pairs of defect II or defects densely populated in presumably α tracks	Rhombic (in distortion or exchange interaction)	330	3-5 × 10 <sup>6</sup> years	Most abundant in cave deposits
IV	Defects in an amorphous phase presumably in fission tracks or α tracks	Isotropic	430	10 <sup>9</sup> years	Amount is small. Dating of geological materials may be possible with these defects

Hole type defects such as CO<sub>3</sub> molecular ions are unstable at room temperature. The structure of hole type defects which are at room temperature is not clear at present.

The concentration of  $\text{Ca}^{2+}$  or  $\text{CO}_3^{2-}$  in a calcite lattice is:  $N_0 \cong 10^{22}/\text{cm}^3$ . Interaction and recombination of centers, however, reduces this abundance. Surrounding a defect or impurity atom, a certain volume  $V_i$  with  $n_i \cong 10^3-10^4$  atoms becomes inefficient for more than one center production (Ikeya, 1981). Figure (2.3.2.1) illustrates the phenomenon. This is in fact the interaction volume known in solid state physics. Thus, the maximum concentration of  $\text{CO}_3^{3-}$  centers or the saturation value is:  $N_0/n_i \cong 10^{18}-10^{19}/\text{cm}^3$ .

The abundance of  $\text{Y}^{3+}-\text{CO}_3^{3-}$  centers (main ESR signal) depends on the concentration  $N_I$  of substitutional  $\text{Y}^{3+}$  cations, which is given by:

$$N_I = C N_0 10^{-6} \text{ cm}^{-3} \quad (2.3.2.1)$$

where  $C$  is the concentration in ppm. For instance, if  $C=0.001$  ppm,  $N_I$  becomes  $\cong 10^{13}/\text{cm}^3$ , a value much lower than the saturation one, but high enough to be detected by any ESR instrument (minimum detectable number of spins  $\cong 10^{11}$ ). In case of very high concentrations, e.g.  $C=1000$  ppm,  $N_I$  becomes  $\cong 10^{19}/\text{cm}^3$  and the center cannot be produced in a stable form.

#### 2.4 Trap indicators: $g$ and $T^*$

The characterization of ESR signals only by their  $g$ -values leads to some complications due to:

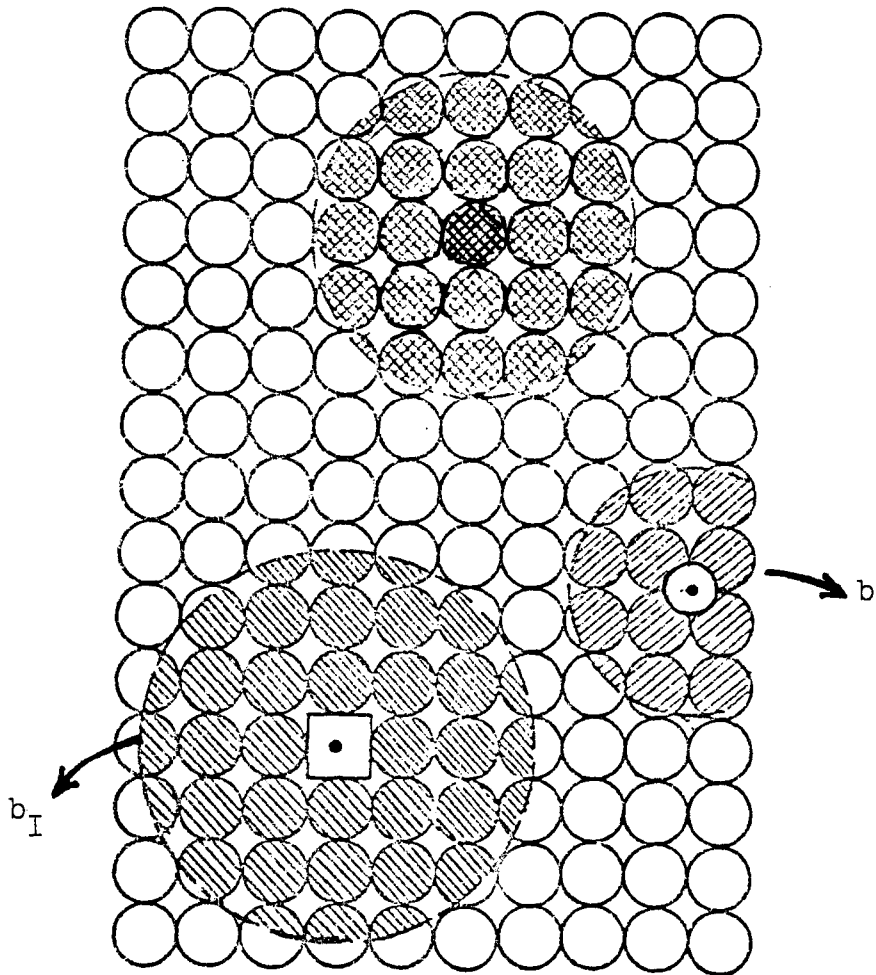


Figure 2.3.2.1 A schematic model of the non-sensitive volume around a defect and an impurity in a crystalline material. A volume of about  $\underline{b}$  atoms around the defect and  $\underline{b_I}$  atoms around an impurity are not sensitive to radiation. (from: Ikeya, 1981, Fig. 5)

- (i) the dependence of  $g$  on: a) the sample form (single crystal/powder), and b) the ESR-instrument modulation width (MW), the latter representing the instrument's 'reading' ability. So, ESR signals which are 'very close' to each other require a 'short' MW in order to be distinguished, otherwise they are unresolved.
- (ii) the possibility that more than one trap may have very similar  $g$ -values, so that their signals cannot be distinguished even though a 'short' MW is used.

So, the  $Y^{3+}-CO_3^{3-}$  electron trap, stable up to  $500^\circ K$ , of a single crystal of calcite gave:  $g_x=2.0012$ ,  $g_y=2.0024$ ,  $g_z=2.0038$  (Marshall et al., 1968) and the  $CO_2^-$  hole trap gave:  $g_x=2.0032$ ,  $g_y=1.9973$ ,  $g_z=2.0016$  (Marshall et al., 1964), where  $x, y, z$  are crystal orientations with respect to the external magnetic field. On the other hand, powders of speleothems were found to have  $g=2.003 \pm 0.001$  for the signals stable up to  $500^\circ K$  (Ikeya, 1975) or  $600^\circ K$  (Ikeya, 1978a). Besides, a recent study (de Canniere et al., 1982) showed that a powdered speleothem had five peaks at  $g=2.0057$ ,  $2.0036$ ,  $2.000-2.002$ ,  $1.9997$ , and  $1.9970$  if a MW=0.5 gauss was used, while the same sample showed only one large peak of  $g=2.0038$  with MW=10 gauss.

Since attribution of certain ESR signals (and  $g$ -values) to centers can be done only by studying single



crystals, the best, though indirect, way to find a center-ESR signal correlation for powdered samples seems to be the thermal study. By determining activation temperatures,  $T^*$ , it becomes also possible to assign certain TL peaks to ESR signals. This practice is quite common in ESR-dating (e.g. Ikeya, 1978a; Miki and Ikeya, 1978; Hennig et al., 1981a).

During an annealing experiment retrapping of released charges may raise severe complications. Yokoyama et al. (1981b) studied powdered speleothems using  $MW=0.4$  gauss, and found three signals  $h_1$ ,  $h_2$ ,  $h_3$  of various intensities corresponding to  $g$ -values=2.0067, 2.0037 and 2.0008 respectively. Above 120-140°C  $h_2$  and  $h_3$  signals disappeared and the  $h_1$  signal was greatly enhanced but the total peak area of the three lines ( $h_1+h_2+h_3$ ) was not changed during the annealing. They proposed that either:

(i) transfer of the trapped electrons from  $h_2$  and  $h_3$  to  $h_1$  occurred or

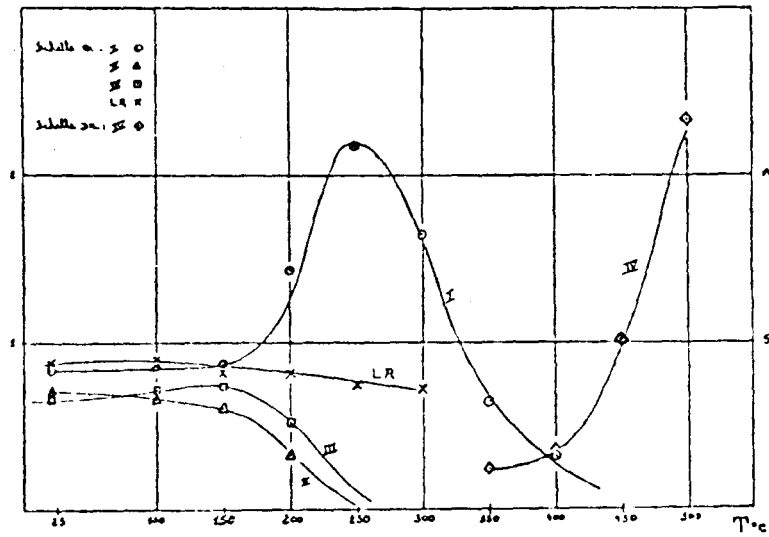
(ii) simply, the  $g$ -values were modified due to the change of the nature of traps by the annealing, and they used the total area of three signals for ED and  $a$ -value determinations. It is possible that they would not observe this complication if they had used larger  $MW$ ; this choice possibly would not affect their ED and  $a$ -value results. Other annealing experiments have been proven less confusing. Apers et al. (1981) studied several

speleothems and found three radiation-induced signals I, II, III at  $g=2.0057$ ,  $2.0035$ , and  $2.0002$  respectively (MW=0.5 gauss). Their thermal study (steps of  $50^{\circ}\text{C}$ , heating for 1 h, measurement  $\frac{1}{2}$ h later) is shown in Figure (2.4.1). Signals II and III fade at  $\sim 210^{\circ}\text{C}$  while signal

I fades at  $\sim 330^{\circ}\text{C}$ , the latter displaying strong retrapping effect before it starts fading. Another signal (IV) of  $g=2.0029$ , not related to radiation, is revealed above  $300^{\circ}\text{C}$  and its intensity increases by increasing temperature. Such a signal was not observed in pure calcite of chemical origin. They propose that signal IV is due to the pyrolysis of organic impurities possibly present in the speleothem, since heating was done in open air. It seems therefore that a thermal study of the ESR signals, combined with an appropriate MW, is adequate for traps distinction, based on activation temperatures  $T^*$ .  $g$ -values, though not critical for ESR-dating of powdered speleothems, might be informative when traps between different samples are compared.

### 2.5 Thermal stability of trapped charges

The lifetime  $\tau_0$  is a measure of trapped charges' stability. Table(2.3.1.1) shows  $\tau_0$ -values at  $27^{\circ}\text{C}$ , a rather high average annual temperature for the cave environment. Wintle (1977) determined the energy depth  $E$  of the  $275^{\circ}\text{C}$  ( $5^{\circ}\text{C}/\text{sec}$ ) TL peak of calcite by using more than one method.



RECUIIT ISOCROME DE L'ECHANTILLON "TAUTAVEL 2".

Figure 2.4.1 Step annealing of the sample "Tautavel 2" (natural). (from: Apers et al., 1981, Fig. 3)

Table 2.5.1 (from: Wintle, 1977, Table 3)

Calculated mean lives for a peak at 275°C for a heating rate of 5°C s<sup>-1</sup> and having a trap depth of 1.75 eV

Temperature (°C)	Mean life (x 10 <sup>6</sup> years)
0	1500
5	390
10	110
15	31
20	9
25	3

She found a range of depths: 1.60-1.80 eV, yielding an average value:  $\bar{E}=1.74$  eV. Based on these data she calculated "mean lives"  $\tau_0$ , as shown in Table (2.5.1). Miki and Ikeya (1978) calculated the "decay time"  $\tau_0$  of the 500°K (0.5°C/sec?) TL-peak, for  $T_0=18^\circ\text{C}$ . They found  $\tau_0 \cong 10^6$  yrs. Hennig et al. (1981a) performed isothermal annealing experiments on ESR active defects fading at 200-250°C. They calculated a trap depth  $E=1.65 \pm 0.1$  eV and mean defect "annealing times"  $\tau_0 = 90$  Ma and 300 Ma for storage temperatures of 15°C and 10°C respectively. These ESR data are in good agreement with the mean lives given by Wintle (Table 2.5.1) for TL-dating.

To secure traps sufficiently deep for there to have been no thermal leakage of charges during archaeological or geological time, Wintle and Aitken (1977a) point out that the trap lifetime should be at least 20 times greater than the sample's age. Therefore, speleothems of middle or upper Pleistocene age should be datable by TL or ESR techniques, on the 225-275°C (TL) or 200-250°C (ESR) trapping center, without significant correction for annealing.

## 2.6 Traps and artificial irradiation

The simulation of the natural processes in speleothem is currently done by exposing the object to various sources of  $\alpha$ ,  $\beta$  or  $\gamma$  rays. Regarding this, the following

problems have to be considered. Incident radiations vary with projectile type (PT) and energy (PE), and created charges are trapped on centers of variable type (CT) and sensitivity (CS). Thus, four correlations have to be examined: (i) PT-CT, (ii) PE-CT, (iii) PT-CS, and (iv) PE-CS. Besides, the sample form might make difficult the achievement of a good simulation. Research on these issues is limited at the moment. Fruitful results from TL and ESR dating have probably led investigators to temporarily neglect some ambiguities that, according to present understanding, will not be critical. Despite this scarcity, the available information suggests some trends and indicates possible problems:

- (i) The existing model of the trapping centers in calcite does not allow any correlation between PT's and CT's. This model considers that all projectiles create equivalent electrons or holes which are 'blind' regarding the centers. The model is based mostly on TL studies of calcites and other minerals, which show that the same TL-peaks are induced regardless of the type of radiation ( $\alpha$ ,  $\beta$ ,  $\gamma$ ). The recent ESR work of de Canniere et al. (1982), however, indicated that internal  $\alpha$ -bombardment effects on chemically synthesized  $\text{CaCO}_3$  doped with  $^{210}\text{Po}$   $\alpha$ -emitter, could be distinguished from those of external

$\gamma$ -irradiation, regarding the centers which  $\alpha$ - or  $\gamma$ -rays are affiliated with.

- (ii) We do not know of any study which correlates PE's with CT's.
- (iii) The correlation of PT's with CS's was considered from the beginning of TL/ESR dating. It deals with the already mentioned variable efficiency of the ionization sources (section 1.3) and is expressed by the  $a$ -factor. This correlation, however, rests upon the assumption that a PT-CT correlation does not exist. This is now in question, as was shown in (i) above.
- (iv) The major problem in PE-CS correlation is the strong  $\alpha$ -particle attenuation. Materials which have beta absorption response similar to calcite ( $\text{CaF}_2:\text{Mn}$ ) have shown (Zimmerman, 1972) a decrease in  $\alpha$ -efficiency ( $\alpha\text{-TL/rad} \div \beta\text{-TL/rad}$ ) with decreasing incident  $\alpha$ -particle energy. It is proposed that as  $\alpha$ -particle energy decreases the ionization density increases and more excess charge (section 1.3) is wasted to recombination centers, so that there is a fall off of the  $a$ -value. However, over the range 1 to 3.7 MeV (Zimmerman, 1972) and even up to 7.3 MeV (Aitken and Bowman, 1975) the TL per unit length of alpha track is approximately independent of energy. The same.

range of independence presumably holds for calcite too.

As far as a sample's form is concerned, the above discussion (iv) indicates that very fine powders or very thin slices should be used for  $\alpha$ -irradiations, so that  $\alpha$ -particles not only penetrate (average  $\alpha$ -range in calcite  $\sim 20 \mu\text{m}$ ) but do not lose significant portions of their energy as they pass through the object. A further consideration is that in the case of alpha particles in the natural radiation environment, total absorption occurs. So, the already mentioned decrease in  $\alpha$ -efficiency should also occur at the end of the alpha track, as  $\alpha$ -particle energy becomes  $< 1\text{MeV}$ . The sample's actual  $\alpha$ -efficiency, therefore, should be smaller than the one indicated by the  $a$ -value, as it is evaluated by using very fine grains. Several TL studies have developed ways to overcome this problem (e.g. Aitken and Bowman, 1975; Aitken and Wintle, 1977, etc.). But it seems that still much has to be done in order to get a true simulation of the natural process.

## 2.7 Anomalous fading

TL studies have demonstrated a 'short term' non-thermal instability of the high temperature TL-peaks to occur in some irradiated minerals. This loss of TL was termed anomalous fading. Three mechanisms have been proposed

(Wintle, 1977), as likely explanations of this fading, the most likely of which are:

(i) direct transfer of an electron from a trap to a recombination center by a tunnelling process.

(ii) decay of available activated luminescence centers.

Various minerals have been examined regarding this phenomenon (Wintle, 1973) but, within  $\pm 5\%$  reproducibility, speleothems have shown no fading of the  $275^{\circ}\text{C}$  ( $5^{\circ}\text{C}/\text{sec}$ ) TL-peak, for storage over several months (Wintle, 1978). However, failure to observe fading in a 'short term' experiment does not exclude longer term fading. If the proposed mechanism (ii) does occur, then ESR measurements should not show such fading, because traps are not involved in (ii). No fading of the main ESR signal of natural and  $\gamma$ -irradiated stalagmites was found when they were re-measured by ESR after more than one year interval (Yokoyama *et al.*, 1981a).

## 2.8 ED determinations

Speleothems seem to satisfy most of the four assumptions (see section 1.6.1) required to determine ED's by the additive method:

(i) speleothem deposition guarantees empty traps at the beginning of its formation.

(ii) thermally stable traps are considered those of  $T^* > 200^{\circ}\text{C}$ .



(iii) the linear relationship between the main ESR signal or TL peak and the artificial dose has been established so far, within some limits, by all the ESR or TL dating attempts, and this regardless of the type of radiation or source used (eg.  $^{242}\text{Cm}$ ,  $^{241}\text{Am}$ ,  $^{238}\text{Pu}$ :  $\alpha$ -particles -  $^{90}\text{Sr}/^{90}\text{Y}$ :  $\beta$ -particles -  $^{60}\text{Co}$ :  $\gamma$ -photons). A tendency to saturation, due to trapping-centers' interaction (Ikeya, 1981), occurs at about  $10^5$ - $10^6$  rads of  $\beta$ -particles (Wintle, 1978) or  $\gamma$ -photons (Ikeya, 1975 and 1978a). However, the pre-dose portion due to the natural radiation is still assumed to be linear, though there are some indications (Wintle, 1975) that the dose previously received does not influence substantially the sensitivity of the  $275^\circ\text{C}$  ( $5^\circ\text{C}/\text{sec}$ ) TL-peak (pre-dose effect).

(iv) The rates of the natural doses absorbed by speleothems are much lower than any practically possible artificial dose rate. Thus, the assumption that the linearity described above is independent of the dose-rate is a necessity at the moment.

Despite the uncertainties discussed previously and others related to sample preparation and analytical techniques (see Chapter 4), EDs have been determined for several speleothems by either ESR or TL methods. The obtained

results are usually compared with theoretically predicted values, or the date derived from these results is compared with the sample's age, if the latter is already known. In many cases there is good agreement between these estimates. Reported ED values range from  $\sim 0.8$  to  $\sim 210$  krads. Some studies (Ikeya, 1978a; Miki and Ikeya, 1978) have compared ED's of the same sample, obtained by means of ESR and TL. They indicate good agreement between the two methods.

### 2.9 a-value determinations

It is quite significant in ESR/TL dating to have a reliable estimation of the a-value. Though this was realized from the very beginning of the dating practice, the first a-value determination of speleothems were reported a few years ago by Wintle (1978). Earlier studies assumed various values ranging from 0.10 (Ikeya, 1977) to 0.38 (Miki and Ikeya, 1978). Their acceptance was based on the rationality of either the dates of the corresponding samples or the total annual doses absorbed by the substances. Wintle's TL-determination of a-values lie in the range of 0.24-0.56 (average 0.40). The same value (0.4) was accepted by both Ikeya (1980) and Hennig et al. (1981b) for use in ESR dating of speleothems. However, other attempts to date speleothems by TL have determined a-values as low as 0.20 (Hennig et al., 1980) or generally falling within the range 0.20-0.35

(Aitken, 1981).

ESR a-value determinations first appeared in 1981. Hennig et al. (1981a) presented a value of  $0.30 \pm 0.06$ , which falls well within the ranges given by Wintle or Aitken. On the other hand, Yokoyama et al. (1981b) obtained values 0.083-0.110 (average 0.1) which are remarkably lower than the values generally found by TL. The cause of this difference was thought to be related to the surface effect in TL (Yokoyama et al., 1981b). Besides, Apers et al. (1981) point out that ESR dates of speleothems from the cave "Caune de l'Arago" are more reasonable if the value 0.1 is used.

The above discussion shows that a-values, fluctuating so far from  $\sim 0.08$  to  $\sim 0.56$ , not only may vary from sample to sample but even from method to method. It seems that ESR a-values tend to be generally lower than the TL ones, though, inter-method or inter-laboratory comparisons have not been done so far (June, 1982). Therefore, it becomes obvious that a TL or ESR dating project should include a-value determination for each one of the individual samples, if possible, and that both ED and a-value should be measured by the same method, either ESR or TL.

## CHAPTER 3: ESR/TL dating of speleothems

### 3.1 Introduction (Conventional dating)

ESR/TL dating basically consists of two steps. First is the measurement of the ED by ESR or TL (section 2.8), and second is the evaluation of the annual dose rate  $R_n$  of the natural radiation environment. Then the age  $t$  is deduced by:

$$t = ED/R_n \quad (3.1.1)$$

$R_n$  is calculated and/or measured so far from radiometric or chemical analysis of radioactive element contents of the sample and its surroundings, and it is often assumed constant since the sample deposition.

The more or less complicated techniques in the  $R_n$  evaluation led Ikeya and Miki (1980b) to propose the use of a simplified  $R_n$ -determination. From the comparison of EDs of samples whose ages were known, they calculated that  $R_n$  is 0.1 to 0.2 rad/yr for speleothems or fossilized bones excavated from calcareous caves. The proposal was motivated by the agreement Ikeya (1978b) had observed between ESR-dating (using tentative- $R_n$ ) and other dating methods ( $^{14}\text{C}$ ,  $^{234}\text{U}/^{230}\text{Th}$ ). This method, however, yields relatively high uncertainty ( $\pm 33\%$ ) because for  $R_n = 0.15 \pm 0.05$  rad/yr the

age becomes  $t = 7.5 \text{ ED} \pm 2.5 \text{ ED}$ . Besides, the range 0.1-0.2 rad/yr may not be universal. A new dating method with a digital ESR instrument (Ikeya and Miki, 1980a) was intended to determine the age by measuring the day-by-day accumulating defects in the materials without knowing the  $R_n$ . This method, however, is not practical at present for speleothems as the daily increase of defects is too small to be detected by conventional ESR instruments.

### 3.2 Natural radiation sources

In the attempt to evaluate  $R_n$ , a distinction between variable radiation sources has to be considered. So we have:

- (i) the internal radiation ( $\alpha$ -,  $\beta$ - and  $\gamma$ -rays) of radioactive impurities present in a particular speleothem sample.
- (ii) the external radiation (mostly  $\gamma$ -rays) of any radiation source outside the sample boundary.

A further separation of the external component distinguishes between the radiation coming from radioactive impurities present in the speleothem which the sample belongs to, and the radiation originating in the surrounding environment (carbonate bedrock and deposits, soils, air etc.). Thus,  $R_n$  has two components, the  $R_{int}$  and the  $R_{ext}$ , the latter being split to  $R_{spel}$  and  $R_{env.}$ , so that:

$$R_n = R_{int} + R_{ext} \quad (3.2.1)$$

$$R_{ext} = R_{spel} + R_{env} \quad (3.2.2)$$

### 3.3 Internal annual dose rate ( $R_{int}$ )

The internal radiation dose  $D_{int}$  received by a pure speleothem sample is mostly due to  $^{238}\text{U}$  decay chain (section 2.2.1) with no radon loss (closed system). Early ESR/TL dating attempts assumed that the decay series was in equilibrium. It was then possible to calculate the dose rates for a given concentration of the parent nuclei from the data given by Bell (1975, 1977 or 1979). In Bell's tables the U-series comprises not only the  $^{238}\text{U}$  series but the  $^{235}\text{U}$  series as well, at a natural abundance of 0.72%. Besides, dose rates are given in cases of no radon or 100% radon loss. If the total uranium concentration  $[U]$  and the a-factor are known, then  $R_{int}$  is calculated by the equation:

$$R_{int} = [U] (aR'_a + R'_\beta + R'_\gamma) \quad (3.3.1)$$

where  $R'_a$ ,  $R'_\beta$  and  $R'_\gamma$  are Bell's dose rates per ppm of total U (dR/d [U], given in mrad/yr ppmU) due to  $\alpha$ ,  $\beta$  and  $\gamma$  rays respectively.

The first attempt to introduce disequilibrium in TL dating of speleothems was done by Wintle (1978) and followed by Yokoyama et al. (1980) in their ESR dating of fossil bones and speleothems. Since the annual dose rate increases

according to the growth of U daughter nuclides,  $R_{int}$  is not constant, so that the use of equation (3.1.1) is not practical. Instead, the accumulated  $D_{int}$  can be calculated as a function of time, and the sample's age can be deduced from the comparison of the ED with the  $D_{int}$ , taking into account the  $D_{ext}$  component. This comparison requires the sample to be homogeneous at the 20  $\mu\text{m}$  scale, regarding the concentration  $[U]$  or the sensitivity  $\underline{s}$ . The effect of zoning of  $[U]$  and  $\underline{s}$  on bulk TL measurements is thoroughly discussed by Wintle (1978).

### 3.3.1 Disequilibrium approach

The total  $D_{int}$  received by a sample, containing  $\underline{r}$  atoms per gram of U,  $\underline{t}$  years after its formation, is given by the following equation derived by Wintle (1978).

$$D_{int} = \lambda_{238} r f(a, p, q, t) \quad (3.3.1.1)$$

$$f(a, p, q, t) \equiv \Delta_1 t + \Delta_2 (p-1) (e^{\lambda_{234} t} - 1) / \lambda_{234} - \Delta_3 p q / \lambda_{230} \quad (3.3.1.2)$$

where:  $p$  and  $q$  are the present day activity ratios  $^{234}\text{U}/^{238}\text{U}$  and  $^{230}\text{Th}/^{234}\text{U}$ , respectively;  $\lambda_{238}$ ,  $\lambda_{234}$  and  $\lambda_{230}$  are the decay constants of  $^{238}\text{U}$ ,  $^{234}\text{U}$  and  $^{230}\text{Th}$ ; and  $\Delta_1$ ,  $\Delta_2$  and  $\Delta_3$  are the effective doses due to the decay of one parent atom in 1 g of calcite for the decays:  $^{238}\text{U}$  to  $^{206}\text{Pb}$ ,  $^{234}\text{U}$  to  $^{206}\text{Pb}$  and  $^{230}\text{Th}$  to

$^{206}\text{Pb}$ , respectively.

$\Delta$ -parameters are a-factor dependent and their values have been calculated by Wintle for several a's. It is practical to express [U] in ppm,  $\lambda$  in  $\text{Ma}^{-1}$ ,  $\Delta$  in  $10^{-11}$  Krads, t in Ma and  $D_{\text{int}}$  in Krads. Since 1 ppmU is equivalent to  $2.531 \cdot 10^{15}$  atoms of U per gram of calcite, r is equal to  $2.531 \cdot 10^{15} [\text{U}]$  and  $\lambda_{238}r$  becomes  $3.7965 \cdot 10^{11} [\text{U}] \text{Ma}^{-1}$ . So, equation (3.3.1.1) gets the form:

$$D_{\text{int}} = c [\text{U}] f(a,p,q,t) \quad (3.3.1.3)$$

where  $c = 3.7965 \cdot 10^{11} \text{Ma}^{-1} \text{ppmU}^{-1}$

A typical plot of  $D_{\text{int}}$  as a function of t (Wintle, 1978, Fig. 4) shows that from  $\sim 0.15$  Ma to  $\sim 0.8$  Ma the rate of change of dose is slightly greater than it would be for the equilibrium decay with the same parent concentration.

### 3.3.2 Equilibrium approach

If a sample's age allows one to assume secular radioactive equilibrium, the function  $f(a,p,q,t)$  becomes equal to  $\Delta_1 t$ , the rest of the components of (3.3.1.2) being neglected due to the equilibrium simplification. So, equation (3.3.1.3) becomes:

$$D_{\text{int}} = c [\text{U}] \Delta_1 t \quad (3.3.2.1)$$

and the  $R_{\text{int}} \equiv D_{\text{int}}/t$  is expressed as



$$R_{\text{int}} = [U] \ c \ \Delta_1 \quad (3.3.2.2)$$

A comparison of (3.3.2.2) with (3.3.1) indicates that in equilibrium we should expect:  $c \ \Delta_1 = aR'_\alpha + R'_\beta + R'_\gamma$ , so that  $R_{\text{int}}(\text{Wintle}) = R_{\text{int}}(\text{Bell})$  for  $t > 0.2 \text{ Ma}$ . In fact this equality does not exist. Instead, the ratio  $R_{\text{int}}(\text{Wintle})/R_{\text{ind}}(\text{Bell}) \equiv c \ \Delta_1 / (aR'_\alpha + R'_\beta + R'_\gamma)$  is a-factor dependent and ranges from 0.85 ( $a=0.1$ ) to 0.78 ( $a=0.5$ ). The following reasons might be given to explain this discrepancy:

- (i) Wintle's model does not consider any  $^{235}\text{U}$  series contribution to  $D_{\text{int}}$  evaluation while Bell's model does.
- (ii) Wintle's  $\Delta_1$  parameter can be split into two components: the effective alpha dose  $\Delta_\alpha$  and the beta-gamma dose  $\Delta_{\beta\gamma}$ , so that
 
$$\Delta_1 = \Delta_\alpha + \Delta_{\beta\gamma}$$
 .  $\Delta_{\beta\gamma}$  is calculated from Bell's data, so that the rates:  $c\Delta_{\beta\gamma} = 25.21 \text{ mrad/yr ppmU}$  and  $R'_\beta + R'_\gamma = 26.1 \text{ mrad/yr ppmU}$  agree fairly well. For  $\Delta_\alpha$ , however, Wintle made a different consideration, causing her parameter to yield lower dose rates than Bell's ones. For instance ( $a=0.1$ ),  $c\Delta_\alpha = 20.8 \text{ mrad/yr ppmU}$  while  $aR'_\alpha = 27.83 \text{ mrad/yr ppmU}$ .

### 3.4 External annual dose rate ( $R_{\text{ext}}$ )

The very first radiation survey of a cave was done

by Ikeya (1976). Since then, other surveys followed in various caves all over the world. Their main goal was to estimate  $R_{\text{ext}}$  values for dating purposes. Several techniques have been applied, from TL-Dosimetry to  $\gamma$ -ray spectroscopy, and various monitors have been used, from  $\text{CaSO}_4$ : Dy or Tm TLD phosphors to NaI (TL)  $\gamma$ -scintillometers. The monitors, mostly TLDs, are placed in a variety of locations, e.g. in deep boreholes in speleothems, in clay-rich areas, on the surface of travertine floors etc., and left there for several months. Thus, a wide range of  $R_{\text{ext}}$  values have been reported so far (Figure 3.4.1), from a minimum 14.4 mrad/yr (Ikeya, 1976) to a maximum  $190 \pm 20$  mrad/yr (Hennig *et al.*, 1981a). In cases where  $R_{\text{ext}}$  evaluation was not available, the tentative dose of 100 mrad/yr has been used (Hennig *et al.*, 1981b).

### 3.4.1 Problems involved in $R_{\text{ext}}$ evaluation

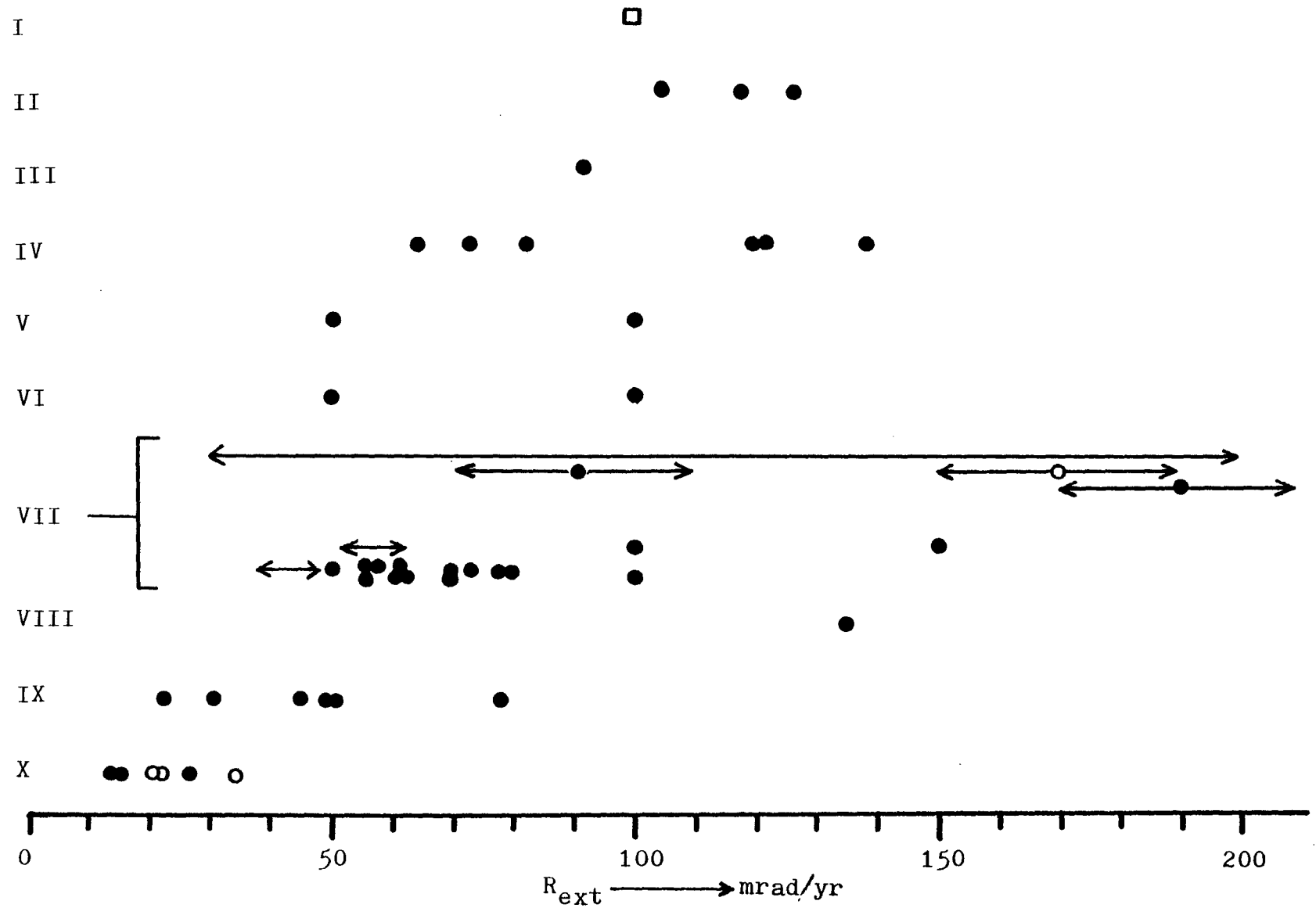
In ESR/TL dating practice it is commonly assumed that the measured  $R_{\text{ext}}$  has remained constant since the time of sample deposition. This assumption for a cave environment might be debatable for two reasons:

- (i) If speleothem is a closed system, the  $R_{\text{spel}}$  component (section 3.2) might be considered as constant, for material old enough so that U-series is in equilibrium. For young speleothems (U-series in disequilibrium) however,  $R_{\text{spel}}$  is not constant.

Figure 3.4.1 Range of  $R_{ext}$  values found in literature

		<u>Reference</u>
I	tentative	Hennig <u>et al.</u> , 1981b
II	Sa Cambana (MAJ)	] Liritzis and Poulianos, 1980
III	Alexandres (MAJ)	
IV	Canet (MAJ)	
V	Flint Ridge (KY)	] Wintle, 1978
VI	Great Onyx (KY)	
VII	Petralona (GR)	[ Ikeya, 1977; Liritzis and Poulianos, 1980; Hennig <u>et al.</u> , 1981a
VIII	L'Aven d'Orgnac (FR)	Wintle, 1978
IX	Caune de l'Arago (FR)	[ Yokoyama <u>et al.</u> , 1981a, 1981b; Wintle, 1978
X	Akiyoshi (JAP)	Ikeya, 1976

Figure 3.4.1 Range of  $R_{ext}$  values found in literature



(ii) It is not very likely that the  $R_{env}$  component (section 3.2) has remained constant. Though limestone bedrock contribution (U-, Th-series in equilibrium) does not change with time, cave soils (mostly limestone-derived clays) can not be considered closed systems. This becomes particularly important when the soil background radiation comprises the major source of  $R_{env}$  (see for instance: Liritzis and Poulianos, 1980). Constant radon emanation from the bedrock or other sources does not guarantee constant radon concentration in the cave atmosphere, due to air-flow effects.

In addition to this major problem, other aspects of the analytical techniques for  $R_{ext}$  raise some uncertainty of the obtained values:

- (i) The monitors in use measure only  $\gamma$ -doses, the  $R_{ext}$  component due to  $\beta$ -particles or cosmic rays being unrecorded.
- (ii) The environmental  $\gamma$ -dose has been found in situ to suffer unexpected attenuation inside the calcite (Hennig et al., 1980), a fact confirmed by laboratory experiments too (Hennig et al., 1981a). Thus, the  $R_{ext}$  measured outside the speleothem body may differ from the  $R_{ext}$  that occurs just around the boundary of a deep sample.

- (iii) TLD monitors are usually packed in glass or plastic capsules, which may partly absorb low energy  $\gamma$ -rays.
- (iv) Both capsules and TLD may contain radionuclides, and the dose of self exposure is added to the external dose.
- (v) Some TLD phosphors may have high sensitivity for low energy ( $<0.1$  MeV)  $\gamma$ -photons, and a supplementary study of the natural  $\gamma$ -ray spectrum may be necessary.
- (vi) Crystal  $\gamma$ -scintillometers and TLD phosphors have differential sensitivities to gamma radiation.
- (vii)  $\gamma$ -scintillometer readings are easily taken on  $2\pi$  geometry and thereafter converted to  $4\pi$  , while readings on  $4\pi$  geometry may be questionable.
- (viii) The  $\gamma$ -dose rates monitored by  $\gamma$ -scintillometers may be smaller than those recorded by TLD-monitors, because of geometry-factors. In general, TLD-monitors have higher spatial resolution in recording the  $\gamma$ -dose rates, which generally show considerable variation (on a cm scale) normal to the speleothem growth horizons (Hennig et al., 1981a).

Each one of these problems is susceptible to its own corrections, and in practice, these corrections are always applied. Nevertheless, the above discussion shows that not

only discrepancies between  $\gamma$ -spectroscopy and TL-dosimetry might be observed (Liritzis and Poulianos, 1980; Hennig et al., 1981a), but also between variable  $\gamma$ -scintillation crystals or TLD-phosphors as well.

The significance of a reliable  $R_{\text{ext}}$  evaluation is realized when samples of very low U-content have to be dated. In such a case Yokoyama et al. (1981b) followed a more complicated method to calculate  $R_{\text{ext}}$ , which was checked independently by the conventional way of TL dosimetry. The agreement they found, however, neither refutes the criticism on the assumption of  $R_{\text{ext}}$  constancy, nor establishes an error-free method for the evaluation of  $R_{\text{ext}}$ .

### 3.5 Isochron dating: Thesis objective

The uncertainties of  $R_{\text{ext}}$  determination, and the more or less inconvenience of doing a radiation survey in situ, urged us to try to devise a dating method independent of  $R_{\text{ext}}$ . The idea came from a careful observation of equation (3.3.1.3): a linear relation between  $D_{\text{int}}$  and  $[U]$  is shown, if  $f(a,p,q,t)$  is kept constant. If  $D_{\text{int}}$  is added to the external radiation dose  $D_{\text{ext}}$ , the total natural radiation dose  $D_{\text{n}}$  or NRD (section 1.6) is obtained, and the linear relation, now between  $D_{\text{n}}$  and  $[U]$ , is expressed by the equation:

$$D_{\text{n}} = D_{\text{ext}} + c [U] f(a,p,q,t) \quad (3.5.1)$$

The known process of stalagmite or flowstone formation and their morphology makes us expect that a single layer:

- (i) was formed during a relatively short time-period.
- (ii) could display uniformity to some physical constants, including a-factor.
- (iii) should display uniformity of the p and q isotope ratios (closed system), and this regardless of the U-concentration.
- (iv) has experienced uniform exposure to external radiation, so that the  $D_{\text{ext}}$  received since the layer's formation might be very similar throughout the layer.

In contrast, geochemical uniformity at the ppm level is not necessarily present (section 2.2.1). Therefore, in case several samples taken from a single layer display a 'good' range of [U], the plot of their ED's versus [U] (assuming  $ED \equiv D_n$ ) should yield a linear correlation. Such a roughly linear relation has been found to occur in fossilized bones excavated from cave sediments (Yokoyama et al., 1981a). Since all the speleothem samples presumably have the same age, the best-fit straight line is called an "isochron". The isochron intercept at [U] = 0 gives the  $D_{\text{ext}}$ , which presumably ((iv) above) is a common component of all  $D_n$ 's. The isochron slope IS is decisive in our dating method. It can be derived from both equations (3.3.1.3) or (3.5.1)



by differentiation with respect to  $[U]$  ( $dD_{int}/d[U] = dD_n/d[U] \equiv IS$ ). So:

$$IS = cf(a,p,q,t) \quad (3.5.2)$$

In the case of the equilibrium simplification, eq. (3.5.2) becomes:

$$IS = c \Delta_1 t \quad (3.5.3)$$

Alternatively, the equation:

$$IS = (aR'_\alpha + R'_\beta + R'_\gamma) t \quad (3.5.4)$$

can be used, according to Bell's model (see section 3.3.2). Previous ESR/TL dating methods have been based on the following equations:

$$ED - R_{ext} t = c [U] f(a,p,q,t) \quad (3.5.5)$$

$$ED - R_{ext} t = [U] (aR'_\alpha + R'_\beta + R'_\gamma) \quad (3.5.6)$$

for disequilibrium (Wintle) and equilibrium (Bell) approaches respectively. A comparison of (3.5.2) and (3.5.4) with (3.5.5) and (3.5.6) respectively, illustrates the isochron-dating advantage:  $R_{ext}$  need not be independently determined. Furthermore, the isochron method potentially can evaluate both  $D_{ext}$  and  $t$ , the ratio of which offers an estimation of the average external dose rate  $\overline{R_{ext}}$ .

The isochron method nevertheless suffers from similar

infirmities as the conventional methods. For instance, the requirement that a sample has to display microhomogeneity regarding either  $[U]$  or  $\underline{g}$  in order for ED and  $D_n$  to coincide (Wintle, 1978) may not be always satisfied (see section 2.2.1 for U-microdistribution). Possible divergence of ED from  $D_n$  of various coeval samples, however, could be averaged in an isochron plot, so that  $dED/d [U] \cong dD_n/d [U]$ . Besides,  $[U]$ -microinhomogeneity may affect IS less than ED because the former incorporates  $[U]$  variability by definition, though this variability (bulk  $[U]$ -inhomogeneity) is not referred to a single sample.

### 3.6 Isochron applications

Equation (3.5.2) indicates that isochron dating requires determination of IS, a, p and q parameters. This seems to be a bit odd because p and q alone can determine the sample's age (U/Th-dating). We have developed a method which partly overcomes this dependency of isochron dating on p and q. Nevertheless, the determination of all four parameters allows us:

- (i) to find dates using both isochron and U/Th-dating methods.
- (ii) to test the reliability of the new isochron method by the well established U/Th method.
- (iii) to check the two methods mutually, since all three

ED, p and q arise as a result of the same physical process, i.e. the  $^{238}\text{U}$ -series disequilibrium decay, and any excess of  $^{234}\text{U}$  affects all of them.

In the case of agreement, the derived date is more solid than a single date given by either of the methods alone. A side-application of the isochron method is the determination of the average a-factor, if the remaining three parameters are available. So, p and q can give a U/Th date t, and equation (3.5.2) yields the  $\bar{a}$ -value.

### 3.6.1 Method to estimate a gross t

The basic equation of U/Th dating is:

$$q = \frac{1 - e^{-\lambda_{230}t}}{p} + \frac{\lambda_{230}}{\lambda_{230} - \lambda_{234}} \left(1 - \frac{1}{p}\right) (1 - e^{-(\lambda_{230} - \lambda_{234})t}) \quad (3.6.1.1)$$

that is, q is p and t dependent. The ratio p is given by:

$$p = 1 + (p_0 - 1)e^{-\lambda_{234}t} \quad (3.6.1.2)$$

where  $p_0$  is the initial p ( $t=0$ ). We see that p is  $p_0$  and t dependent. Thus, function  $f(a, p, q, t)$  can become  $a, p_0, t$  dependent by substituting (3.6.1.1) and (3.6.1.2) into (3.3.1.2). What we get is a function  $f(a, p_0, t)$  equivalent to  $f(a, p, q, t)$ , given by:

$$f(a, p_0, t) = \Delta_1 t + \Delta_2 (p_0 - 1) (1 - e^{-\lambda_{234}t}) / \lambda_{234} - \Delta_3 (1 - e^{-\lambda_{230}t}) / \lambda_{230} - \Delta_3 (p_0 - 1) (e^{-\lambda_{234}t} - e^{-\lambda_{230}t}) / (\lambda_{230} - \lambda_{234}) \quad (3.6.1.3)$$

Now, isochron equation (3.5.2) takes the form:

$$IS = cf(a, p_0, t) \quad (3.6.1.4)$$

This equation cannot be used for precise dating, because  $p_0$  cannot generally be assumed to be known, though it can be independently calculated from  $p, q$  and  $t$ . An independent dating method, however, should use parameters whose evaluation does not require dating by another method. This problem is also present in  $^{234}\text{U}/^{238}\text{U}$  dating. Equation (3.6.1.4) is to be used for only a gross age estimation. It is based on the observation that  $p_0$  values of speleothems lie mostly in the range 1-2, only few of them being as low as 0.7 or as high as 3.7 (Gascoyne, 1979; Appendix 3,4,5). Thus a diagram of  $f(a, p_0, t)$  versus  $t$  for  $p_0=1$  and 2, on which the determined IS is indicated, could give a feeling of what the layer's age should be, and show the most probable range of age. Besides, the curves mentioned above give some idea of the dependence of  $t$  on  $p_0$ .

### 3.6.2 Age determination

The gross  $t$  estimation serves as a preliminary test which shows whether the disequilibrium or equilibrium approach (and the use of the corresponding equation) should be considered. Thus:

- (i) if disequilibrium is indicated,  $p$  and  $q$  are required for dating, or alternatively an  $a$ -value

can be determined (see section 3.6).

- (ii) if equilibrium is indicated, equations (3.5.3) or (3.5.4) can be used to find the isochron age of the speleothem layer.

Isochron application basically utilizes three plots:

- (i) ED versus  $[U]$ , i.e. the isochron plot.
- (ii)  $cf(a, p_0, t)$  versus  $\underline{t}$ , i.e. the preliminary test plot
- (iii)  $cf(a, p, q, t)$  versus  $\underline{t}$  or a-values, for dating or a-factor determination respectively, when  $^{238}\text{U}$ -series are considered to be in disequilibrium. Equilibrium cases do not need this plot.

### 3.7 Conditional ESR isochron dating

ESR dating techniques (Chapter 4) usually demand more sample weight than TL techniques, for ED-determinations. In general, the more the sample weight the better the ESR-ED and  $[U]$  determinations. In looking for a good  $[U]$  -range, it may be necessary to extract many samples from a single layer, more than enough to construct the isochron plot. Therefore, a possible shortage of speleothem material and/or a lack of sufficient  $[U]$  -range, may become problematic. Here, we suggest two means which might help the situation, if some conditions are fulfilled.

### 3.7.1 ESR-intensity isochron dating

The method requires determination of the following:

- (i) ED for only one 'principal' sample.
- (ii) only  $I_n$  (natural ESR intensity) for the rest of the samples.
- (iii)  $[U]$  for all samples.

The new idea is that "isochron" line could be drawn not only on the plot of ED versus  $[U]$  but on the plot of  $I_n$  versus  $[U]$ , as well. The discussion made previously (see section 2.8) on the validity of the assumption:  $ED \equiv D_n$ , allows one to write:

$$I_n = sD_n \quad (3.7.1.1)$$

where  $\underline{s}$  is sample's ESR-sensitivity to  $\gamma$ -rays ( $s \equiv s(\gamma)$ , see section 1.6.2). Substitution for  $D_n$  from equation (3.5.1), gives:

$$I_n = I_{\text{ext}} + sc[U]f(a,p,q,t) \quad (3.7.1.2)$$

where  $I_{\text{ext}}$  is the common component of samples'  $I_n$ , due to the  $D_{\text{ext}}$ . This equation displays linear relation between  $I_n$  and  $[U]$ , if  $f(a,p,q,t)$  and  $s$  are kept constant. Thus, a  $I_n$ - $[U]$  isochron may have meaning if uniformity of  $a,p,q,t$  and  $s$  throughout a single layer is assumed. Given  $I_{\text{ext}}$  and  $\underline{s}$ , their ratio yields:

$$D_{\text{ext}} = I_{\text{ext}}/s \quad (3.7.1.3)$$

and the 'real' isochron of ED versus [U] determines the IS as the slope of the line which connects two points:  $(0, D_{\text{ext}})$  and  $([U]\text{-principal}, \text{ED-principal})$ . Alternatively, IS is determined by:

$$\text{IS} = (\text{intensity isochron slope})/s \quad (3.7.1.4)$$

Now the regular isochron dating process follows, as described in previous sections. Of the required assumptions, the constancy of  $f(a,p,q,t)$  has already been discussed (see section 3.5), the  $\underline{g}$  uniformity, however, might be questionable. It has been mentioned several times (Ikeya, 1975; Miki and Ikeya, 1978 etc.) that some trace elements (e.g.  $\text{Mn}^{2+}$ ,  $\text{Fe}^{2+}$ , etc.) are likely to affect natural calcite's sensitivity to  $\gamma$ -rays, and geochemical uniformity is not expected to occur in a single layer (see section 2.2.1). Ikeya (1975) found that the  $\underline{g}$  variation - due to the microdistribution of impurities - among samples from different locations of a latitudinal stalactite section are within experimental error. Since the degree of distribution of trace elements - ESR sensitizers - in single speleothem layers has not been studied so far (June, 1982), it is felt that this proposal has some chance to be proven applicable.

### 3.7.2 Multilayer isochron dating

The flexibility of the "isochron" concept could

allow the expansion of the "single layer" isochron dating to a "multilayer" one. To use samples from several layers for the isochron plot construction seems to be a bit odd. This practice, however, may be permissible if:

- (i) hiatuses do not interrupt the layers' sequence.
- (ii) the layers are not very well distinguished from one another, so that the layer identification might be a more or less subjective decision.
- (iii) there are indications, other than dates, that the layers being used were deposited in a short time period relative to their expected age.

Under such a situation, 'real' and/or intensity isochron dating might be applicable.

### 3.8 Isochron diagrams and possible complications

The isochron dating method assumes that a graph of ED versus  $[U]$  falls on a straight line. In order for the method to be applicable, several (more than 3) samples must be plotted to assure that a linear array does result. In doing this, the following complications might arise:

- (i) The isochron intercept at  $[U] = 0$  is negative, yielding meaningless values of  $D_{ext}$  (negative) and IS (too high). This might happen, for instance, as a result of lack of sufficient data (small  $[U]$ -range). In such a case, the maximum slope



possible,  $IS_{\max}$ , (that is the slope of a line passing through the origin :  $[U] = 0$ ,  $ED = 0$  i.e.  $R_{\text{ext}} = 0$ ), could give the maximum age possible,  $t_{\max}$ .

- (ii) The points do not fall on a straight line. This might be because all or some of the parameters: a-factor,  $p$ ,  $q$ ,  $D_{\text{ext}}$ , vary from sample to sample. The  $p$  and  $q$  variations could only be because the speleothem layer was not a closed system, and samples were geochemically disturbed. If it is so, isochron dating - a method dependent on  $[U]$  - has no meaning. If samples are very old ( $t \approx \tau_0$ ) a possible trap depth  $E$  and leakage variability may affect the points' linearity, as well.

- (a) If more than one center of variable  $E$  display very similar  $g$ -values, these centers are not distinguishable in the ESR spectra (see section 2.4). A possible leakage of electrons from the traps of low  $E$ , thus, results in getting small ED's. The thermal study of these samples might show the presence of such a trap depth variability.
- (b) The approach to equilibrium between center production by natural radiation and thermal fading (leaking) results in obtaining smaller ED than the real one (Ikeya, 1981).

These factors limit isochron applicability to samples of  $t \ll \tau_0$  (see section 2.5).

## CHAPTER 4: Analytical Techniques

### 4.1 Introduction

The analytical procedure being followed in this study is neither original nor uniform. It is mostly a repeat of what was found in the literature, the detailed steps being adjusted each time to the particular goal. In general, sample preparation was followed by irradiation, annealing, ESR measurement and determination of trace element concentration. Some of these stages attracted more attention due to their critical affect on the isochron slope. For instance, some of the sample preparation techniques, suggested in literature, were tested and partially modified. The whole treatment of our samples was done in rooms illuminated with fluor lamps or daylight passing through glass windows. Though in TL-dating samples are usually treated in red light to reduce any bleaching of electrons that can possibly be induced by short wavelength light (Wintle, 1978), such a light effect on ESR signal amplitude has been found to be negligible, at least for laboratory conditions (Yokayama et al., 1981a). We did not observe any such light effect either. Some physical magnitudes were measured by two different models of instruments, whenever it was possible, to ensure reliable values.

#### 4.2 Sample preparation

Samples used in ESR dating are generally powders. Such a preference is mostly because of the ease with which powders are obtained, manipulated and divided into aliquots. In fact, to get a sizeable single crystal of speleothem one would be very lucky. Powders were prepared for irradiation by the following steps:

- (i) Sampling by using a small compressed-air chipper. The extracted material was about 1 gram.
- (ii) Grinding in a porcelain mortar for about 1 min.
- (iii) Sieving to get an appropriate grain size. The coarse and fine powder fractions were used to obtain ED and [U] , respectively. The grain size limits were determined after the study of the "grain size effect" (see chapter 7).
- (iv) Etching with acetic acid 0.5%, for 1 or 2 min, to eliminate possible surface effects. Only the coarse powders were etched, in general.
- (v) Washing with acetone to remove any dust from the coarse fraction. The powder was then left to dry for several hours, at room temperature.
- (vi) Homogenization and formation of 5 aliquots by distributing the powder uniformly on 5 small sheets of powder-paper.
- (vii) Weighing by using analytical balances (E. METTLER,

No. 1-911 or HL52).

The above procedure was decided upon after a consideration of the existing (published) experience as well as of our results. In brief, though it has been mentioned several times that grain size of speleothem powder does not affect the ESR intensity (Ikeya, 1975, 1978; Yokoyama *et al.*, 1981a) we found that it does. A more comprehensive discussion of the grinding-sizing-etching effects on the ESR signal will be found in connection with the experimental results (Chapter 7).

### 4.3 Irradiations

Irradiations were performed with a  $^{137}\text{Cs}/^{137}\text{Ba}$   $\gamma$ -ray source (1.4 KCi; summer 1981) and were carried out with the samples placed either in 1 mm thick glass vials or in glassine paper cases. The  $^{137}\text{Cs}$  source was calibrated with Fricke-solution ( $\text{FeSO}_4$ ) dosimetry, as it is described by Arena (1971, p.312). Calibration was done by M. Leeksma of the Biochemistry Dept. at McMaster University (1-10 May, 1979). The dose rates obtained from the calibration curve (Figure 4.3.1) were susceptible to several corrections.

#### (i) Precision correction

The dose rate at 9.9 cm (Figure 4.3.2) was found to be  $558 \pm 10^{\circ}$  rad/min (May, 1979) or  $485 \pm 4$  rad/min (November, 1979). Six months decay, however does

---

$^{\circ}$  all the  $\pm$  errors in this thesis are  $1\sigma$  standard errors.

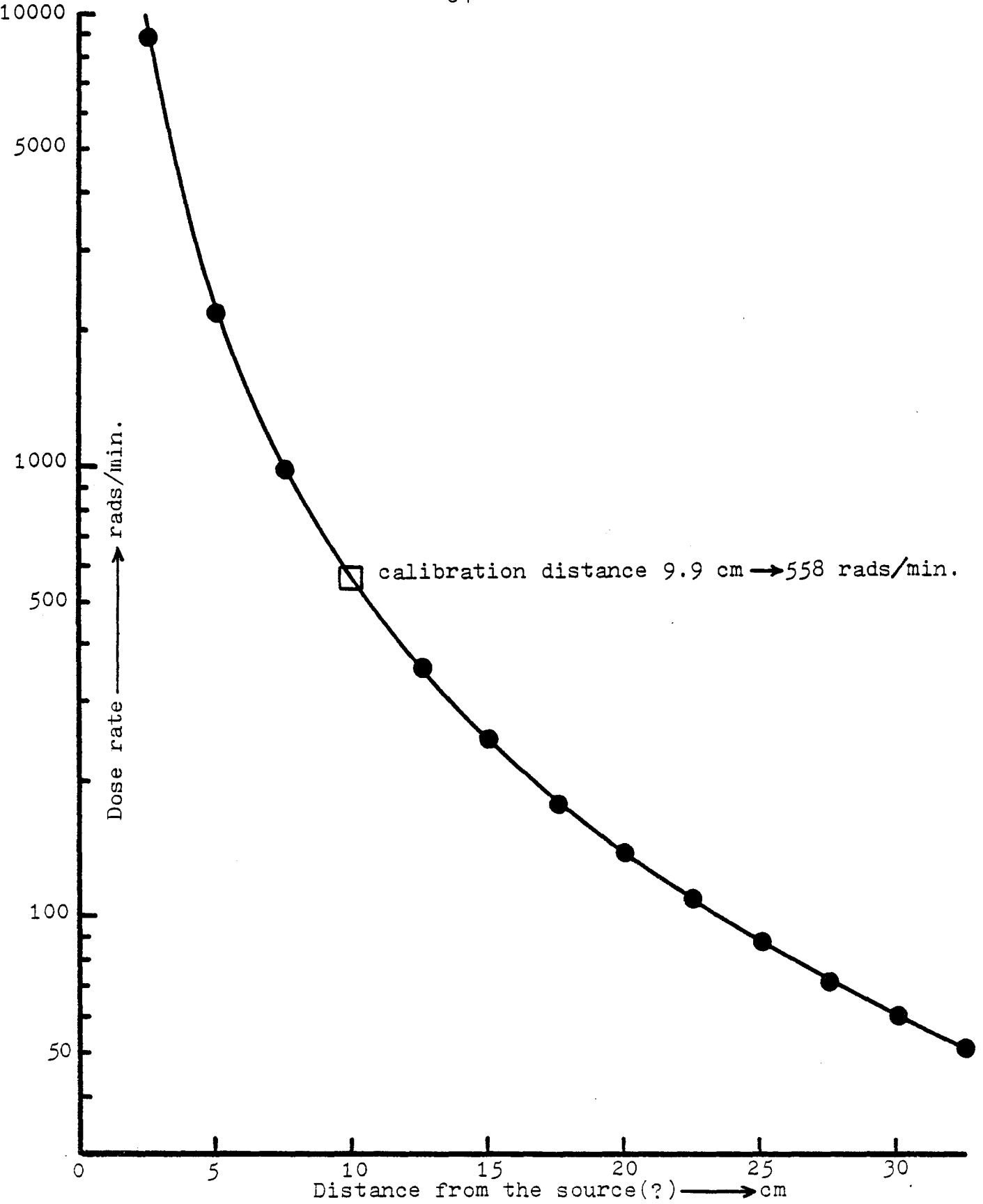


Figure 4.3.1  $^{137}\text{Cs}$  source calibration curve

not justify such a drop. We considered that the 'true' dose rate at 9.9 cm was  $522 \pm 11$  rad/min, i.e. 6.5% off, or  $\sim 94\%$  of the value displayed on the calibration curve.

(ii) Off center correction

The calibration curve values correspond to dose rates at the center of the stage-sample holder (Figure 4.3.2). Figure (4.3.3) shows how dose rate depends on the distance from the center. The samples were placed either at the center or on circles of various radii, depending on the number of samples.

(iii) Decay correction

Dose rates were corrected for the source natural decay, according to the decay law:

$$A = A_0 e^{-\lambda t} \quad (4.3.1)$$

Where:  $A_0$  is the dose rate as indicated in the calibration curve

A is the corrected dose rate

$\lambda$  is the  $^{137}\text{Cs}$  decay constant;  $\lambda = 0.693/T_{\frac{1}{2}}$ ,

$T_{\frac{1}{2}}(^{137}\text{Cs}) \cong 30$  years

t is the time elapsed since calibration was done (May, 1979), given in years by:

$t = m/12$  (m=number of months).

In practise, the following equation was used:

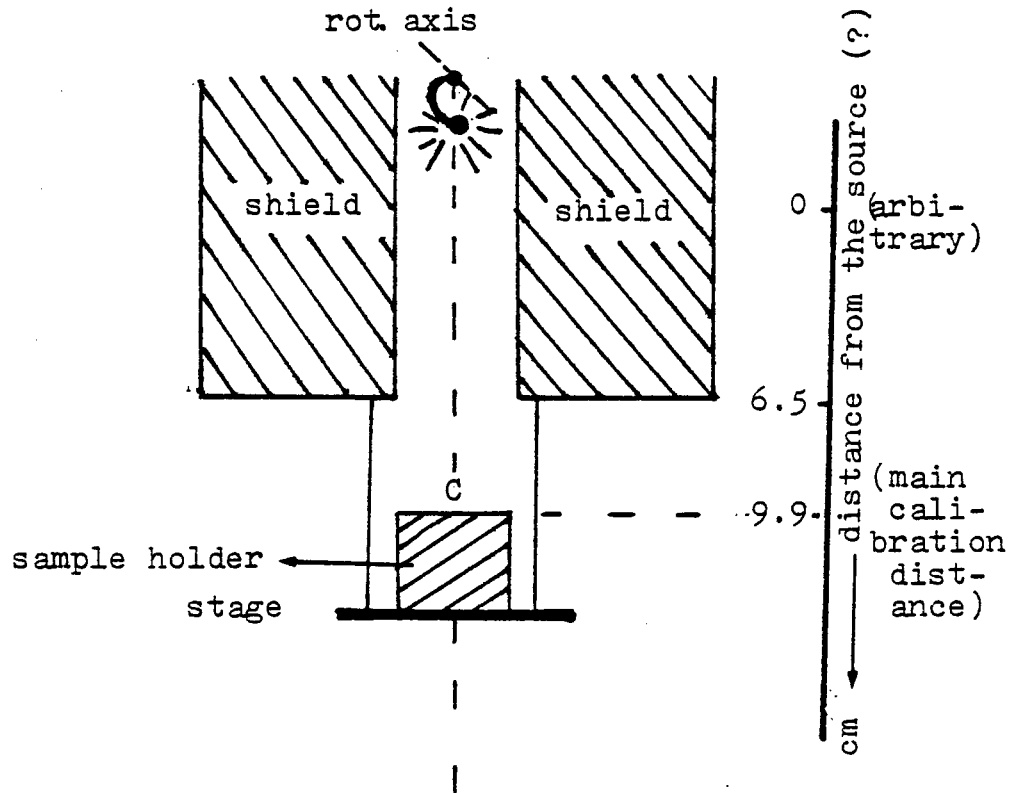


Figure 4.3.2  $^{137}\text{Cs}$   $\gamma$ -ray source apparatus

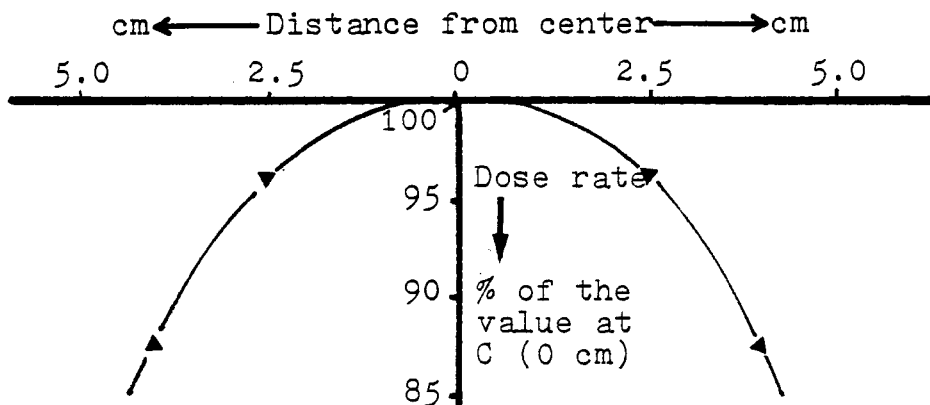


Figure 4.3.3 Dose rate dependence on the horizontal distance from the center C, at 9.9 cm from the source.



$$A = A_0 \exp(-19.25 \cdot 10^{-4} m) \quad (4.3.2)$$

(iv) Fricke-Calcite correction

The conversion of the Fricke absorbed dose to the speleothem one was grossly calculated to 94% (Appendix I). Yokoyama et al., (1981a) used a correction factor of 1.0, while Apers et al. (1981) applied the relation:  $D(\text{CaCO}_3) = 0.905 D(\text{Fricke})$ . Our factor (0.94), therefore, seems to be reasonable.

On the whole, the corrections applied on the calibration curve dose rates range from 76% to 86%.

#### 4.4 Annealing

The idea of annealing speleothems to study their ESR signal thermal stability came from the TL practice. The gradual annealing of TL, however, is not applicable in ESR techniques. What can be done in ESR is isothermal or step annealing.

- (i) In isothermal annealing the sample is kept at constant temperature  $T$  either for some time to let undesirable low  $T^*$  centers (see section 1.4.1) fade or for time  $\Delta t$  to let a center fade partially, then reheat at  $T$  for  $\Delta t$  and so on, each time measuring the ESR intensity.

The first practice has been used quite often (e.g. Ikeya, 1978; Hennig et al., 1981a) because it allows the low  $T^*$  signals, arising after irradiation and interfering with the dating signal, to decay quickly ( $T \cong 100^\circ\text{C}$ ). These signals decay completely at room temperature too, a few days after irradiation. In this study we chose the 'natural' decay because we observed severe variation of the dating signal ESR intensity above room temperature (see Chapter 7).

The second practice has been used as a method to evaluate center's lifetime (Hennig et al., 1981a). We employed this method only incidentally.

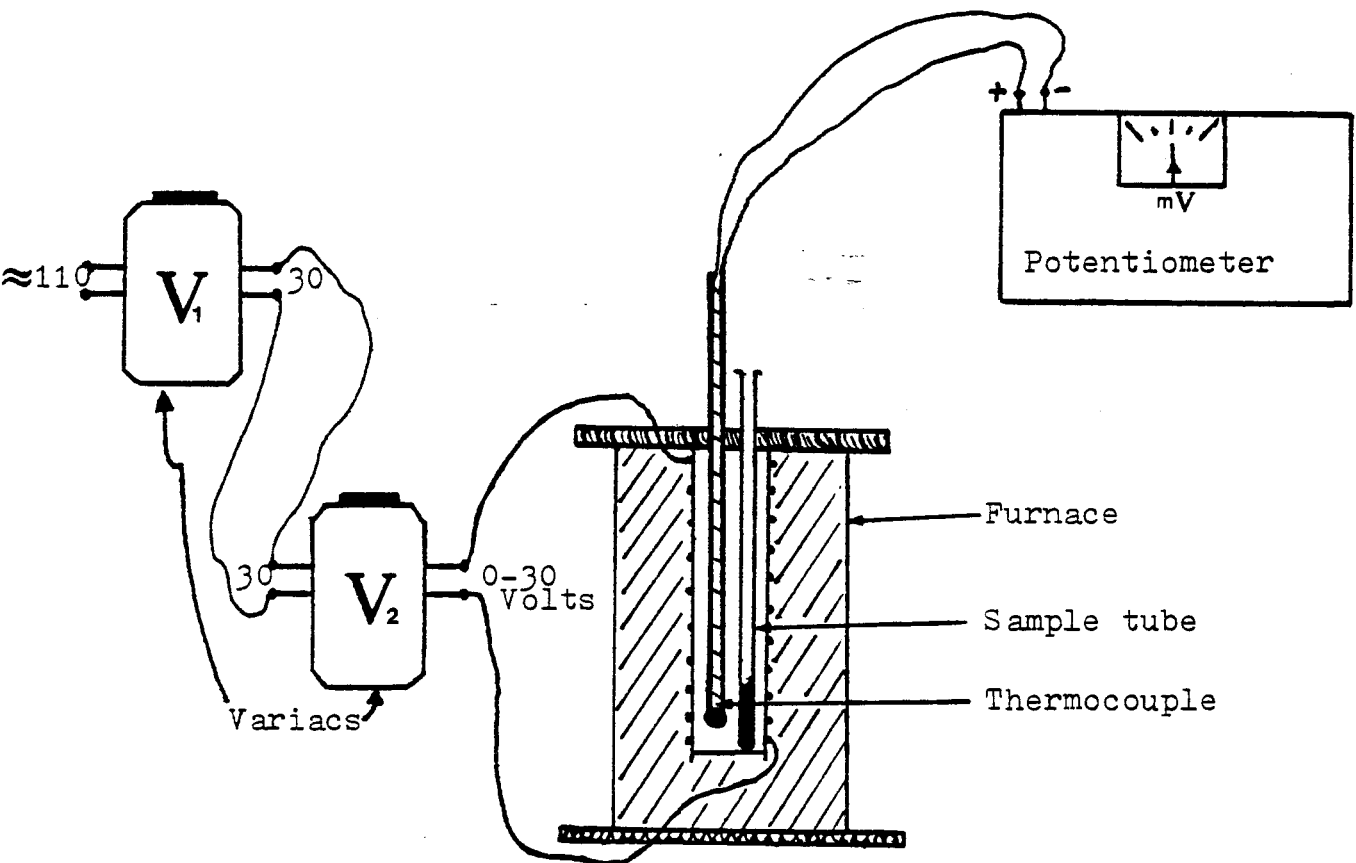
- (ii) Step annealing means that the sample is heated at a certain temperature  $T_1$  for certain time  $t^*$ , then it is cooled to room temperature, and after a time interval  $t_0$  ESR measurement follows. Next, the sample is heated at higher temperature  $T_2 = T_1 + \Delta T$  and so on. The final plot of ESR intensity versus  $T$  has a certain profile but its horizontal position depends on the 'step'  $\Delta T$ , the heating time  $t^*$ , and possibly the interval  $t_0$ .

Step annealing studies of radiation-induced ESR signals were first performed by Zeller (1968), but Apers et al. (1981) were the

first who applied this method to speleothems (see Figure 2.4.1 ). They used:  $\Delta T=50^{\circ}\text{C}$ ,  $t^*=60$  min, and  $t_0=30$  min. We independently applied step annealing with  $\Delta T=25^{\circ}\text{C}$ ,  $t^*=6-12$  min, and  $t_0=5-15$  min.

The furnace design and construction was quite simple. A quartz tube  $\sim 1$  cm by 8 cm was wrapped up with  $\sim 3.56$  feet element of 2.17 Ohm/foot (total Resistance  $\sim 7.73$  Ohm) so that the 38 loops were uniformly distributed along the tube. The 'reel' was placed in a copper tube  $\sim 3$  cm by 10 cm and the space between them was filled up with wet clay so that the axes of the quartz and copper cylinders coincided. After the clay had dried, both top and bottom of the furnace were insulated with asbestos sheets, leaving a small hole at the top for the sample insertion. The power supply consisted of two variacs: the stable  $V_1$  (110/30 Volts) and the variable  $V_2$  (30/0-30 Volts). Temperatures were measured with a Chromel-Alumel Thermocouple Potentiometer (type P4-CROUDON PREC. INSTR. CO.). Calibration tables were taken from the "Handbook of Chemistry and Physics", 57th ed., 1976-1977, CRC Press (p. E107-E108). The whole circuitry is shown in Figure (4.4.1). The temperature variations along the quartz tube were first examined. Since the appropriate depth was fixed, the variac  $V_2$  was then calibrated in order to know approximately the voltage required to reach a certain temperature at that depth, taking into

Figure 4.4.1 Annealing apparatus; circuitry.



account the time needed for the temperature to reach the predecided level. Finally, a precision of  $\pm 1^{\circ}\text{C}$  was achieved at  $T < 400^{\circ}\text{C}$ .

#### 4.5 ESR measurements

Two ESR spectrometer models were used in this study:

- (i) JEOL: JES-3BS-X of the Chemistry Department at McMaster University, installed in 1967.
- (ii) Varian: E104A of the Chemistry Department at the University of Guelph, installed in 1975.

Basic ESR instrumentation, operating procedures, and criteria to choose experimental conditions can be found in instrument instruction manuals or in various books on ESR spectroscopy (e.g. Wertz and Bolton, 1972; Poole, 1967; etc.). In brief, the principal components of an ESR spectrometer are:

- (i) A large electromagnet and its associated power supply.
- (ii) A microwave bridge which houses a klystron that generates microwaves. Attached to this bridge is a waveguide arm at the end of which is found a waveguide (resonance) cavity suspended between the magnet polepieces.
- (iii) Electronic circuitry which detects and amplifies the microwave signal, removes noise, and displays the results on a chart recorder.

A simplified block diagram of a typical ESR spectrometer is shown in Figure (4.5.1). The instrument operating conditions (setting), chosen to yield satisfactory spectral resolution, are displayed in Table (4.5.1). To get ESR spectra, samples mostly of equal weight were poured into quartz tubes ( $\sim 3$  mm inner diameter), and the tubes were placed into the resonance cavity, so that the cavity and sample centers coincided. The sample position in the cavity plays a significant role in quantitative ESR spectroscopy. Factors which determine the absolute intensity  $I$  of the ESR signal are discussed by Wertz and Bolton (1972, p. 462). Of them, we notice the following:

- (i) The amplitude  $H_m$  of the microwave magnetic field. More specifically:  $I \approx \bar{H}_m^2$  (Poole, 1967, p. 291).
- (ii) The filling factor  $\underline{n}$ , which is a measure of the efficiency with which  $H_m$  is concentrated in the sample (Poole, 1967, p. 524). For small samples ( $V_s \ll V_c$ ) in some cavity types we have:  $n \approx V_s/V_c$ , where  $V_s$  and  $V_c$  are the sample and cavity volumes, respectively.

The microwave electromagnetic field existing in the cavity is not homogeneous. Figure (4.5.2) shows this inhomogeneity for the  $TE_{011}$  cylindrical cavity of the JEOL spectrometer.  $H_m$  is symmetrical with respect to the central axis  $x-x'$  and it is maximum at 0 and on a sine-functional decrease on this said axis (JEOL instr. manual, section

## ESR Spectrometer Operation

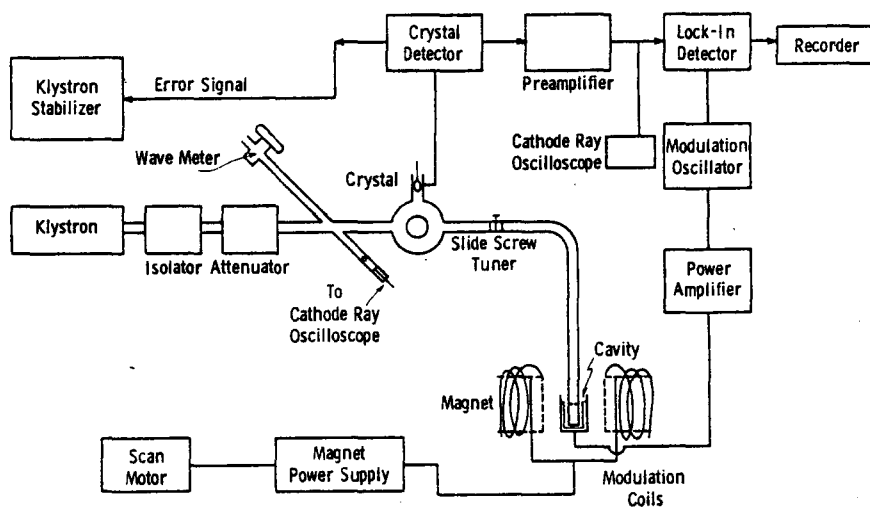
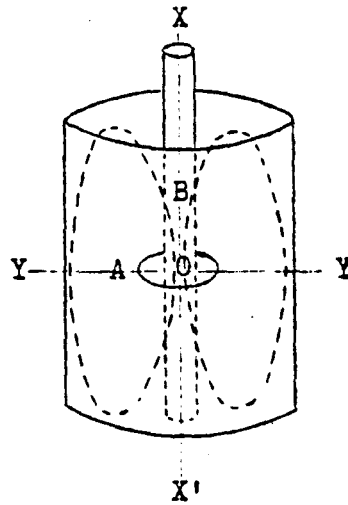


Figure 4.5.1 Block diagram of ESR spectrometer.  
(from: Poole, 1972, Fig. 8.5)

Table 4.5.1 : ESR spectrometer setting

Spectrometer	JEOL	Varian
Quantity		
Resonance frequency (see section 1.5.2)	X-band ( 9.4 GHz)	
Microwave power attenuation	10 db (20 mW)	
Microwave modulation frequency	100 KHz	
Microwave modulation amplitude or width (see section 2.4)	3 or 4 gauss	0.05 gauss
Response or time constant	0.03 or 0.1 sec	1 sec
Resonance magnetic field	3220 gauss	3350 gauss

— Electric field  
 --- Magnetic field



$TE_{011}$  resonance cavity

Figure 4.5.2 (from: JES-3BS-X ESR Instr. Instruction manual, Fig. 2-1)

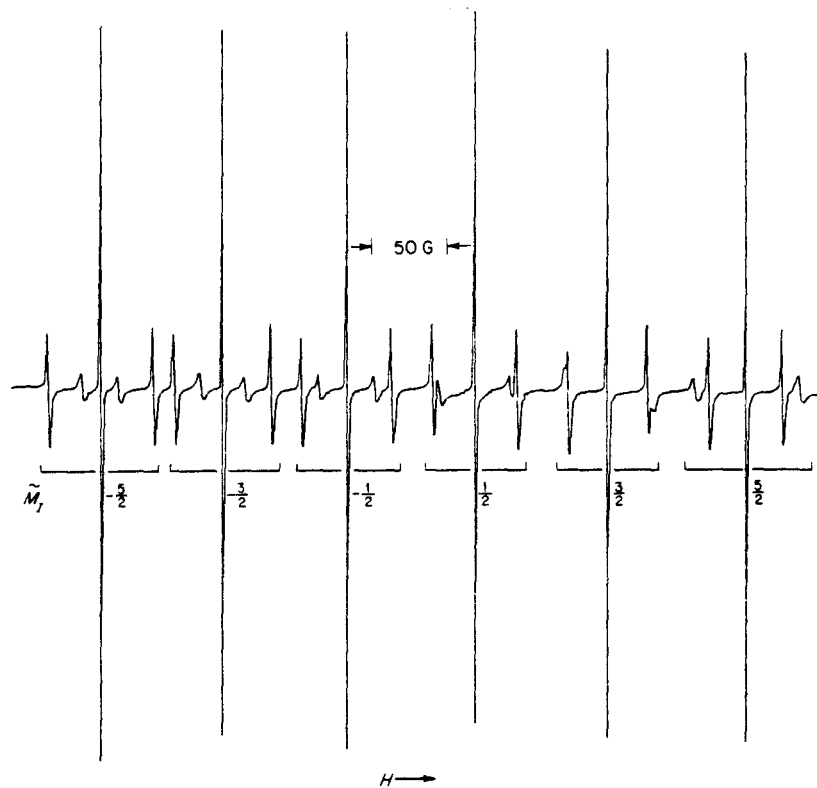


Figure 4.5.3 ESR spectrum of  $Mn^{++}$  in  $MgO$  at room temperature, with  $\nu=9.3$  GHz. (from: Wertz and Bolton, 1972, Fig. 11-22)



2.1). Therefore, samples of small  $V_s$  around the center should yield higher  $I$  per mg than those of large  $V_s$  or those being off center.

Though the sample weight was easily controlled ( $\pm 1$  mg), the sample centricity was not guaranteed, resulting in an experimental error higher than expected. Calibration of the obtained signals varied, according to the type of instrument.

(i) The JEOL spectrometer had a Marker ( $Mn^{2+}$  in  $MgO$ ) available within the resonance cavity. A typical spectrum of  $Mn^{2+}$  in  $MgO$  is shown in Figure (4.5.3). The central part of such a spectrum was always recorded on the chart. Thus, calibration was done by any of these: weight, Marker (average of the  $Mn^{2+}(+\frac{1}{2})$  and  $Mn^{2+}(-\frac{1}{2})$  peak to peak heights), or both weight and Marker. Signal normalized intensity was expressed in terms of ESR/mg, ESR/Marker, or ESR/mgMarker, respectively (ESR=number of ESR chart units).

Marker  $Mn^{2+}$  peaks were also used as a reference for g-value determinations. The following formula was applied:

$$g_i = \frac{6726.9}{3395.7 - 87.5 l_i/l} \quad (4.5.1)$$

where  $l_i$  and  $l$  are distances of signal "i" and  $Mn^{2+}(-\frac{1}{2})$  peaks from  $Mn^{2+}(+\frac{1}{2})$  peak, respectively. Formula (4.5.1)

is taken from the spectrometer's instruction manual, and it is slightly modified to accommodate our resonance frequency ( $\sim 9.415$  GHz).

(ii) Varian spectrometer signals were calibrated by weight only. Several workers have used the signal of  $\text{Mn}^{2+}$  inherent in the sample for calibration purposes. Whenever tested, both  $\text{Mn}^{2+}$  and weight calibrations showed good agreement in the ED determinations (e.g. Hennig *et al.*, 1981a). In calibrating by a sample's  $\text{Mn}^{2+}$ , it is assumed that the  $\text{Mn}^{2+}$  signal intensity is not altered by irradiation. Hennig *et al.* (1981b), however, observed that the  $\text{Mn}^{2+}$  signals are slowly decreasing with additional  $\gamma$ -doses (10-15% for 100 Krads). This, and isochron peculiarities (possible  $[\text{Mn}^{2+}]$  variability within a single layer) as well as the absence of  $\text{Mn}^{2+}$  signals in some cases, led us to normalize the samples in regard to their mass only (units:  $\text{ESR mg}^{-1}$ ).

All ESR measurements were carried out at room temperature ( $\sim 24^\circ\text{C}$ ).

The peak-to peak height of the 1st derivative of the ESR absorption curve was considered to be a good approximation of the ESR intensity.

#### 4.6 Determination of the trace element content

Uranium and other trace element concentrations were determined by Neutron Activation Analysis (NAA), performed

by the Nuclear Activation Services Limited at McMaster University. Each sample sent to the Reactor, usually the fine fraction of the sieving process (see section 4.2 (iii)) without any additional treatment, was pre-weighed at 0.5 g. The NAA detection limits for various elements were:

Element	U	Th	Rb	K	Mn
det. limit	0.03-0.2	0.5	10	0.1	1
units	ppm	ppm	ppm	%	ppm

Since our samples were taken from speleothem layers which had already been dated by U/Th dating, a [U]-value was available, determined by means of Isotope Dilution Analysis (IDA). This value might be considered as an average [U] of the whole layer or as an indicator of the layer's [U] level. Regarding this consideration, two problems are involved:

- (i) The IDA [U]-values of many speleothem samples have been found to be lower than the NAA [U]-values, as it is shown in Figure (4.6.1). This is possible because U in detritus, present more or less in all speleothems, is excluded as it is filtered off in IDA.
- (ii) The samples used in this study and in U/Th dating were taken from distinct parts of the same growth layer and [U] homogeneity is rather

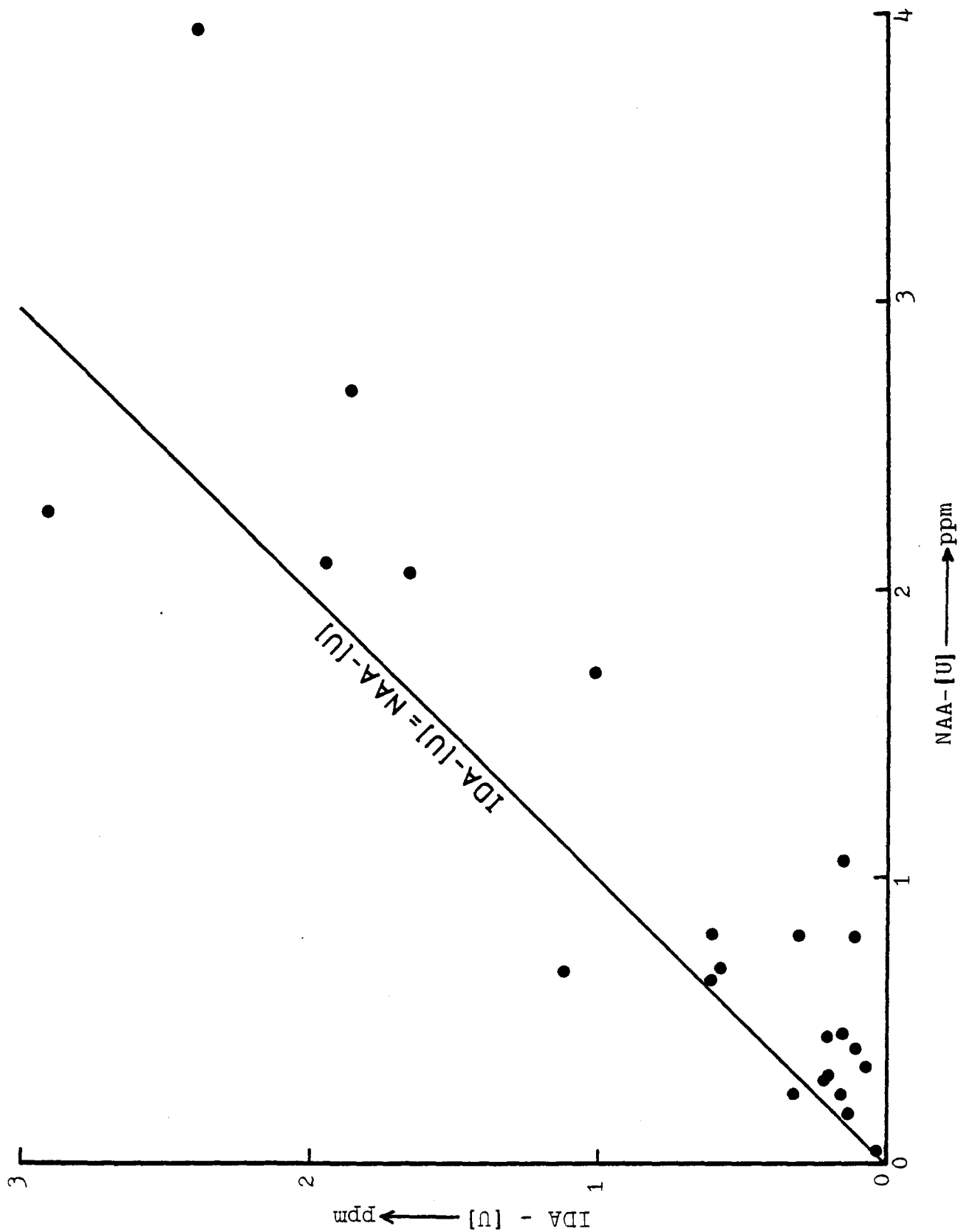


Figure 4.6.1 [U] of various speleothem samples as found by IDA and NAA (courtesy of A.G.Latham).

unlikely (see section 2.2.1).

Any divergence of our NAA [U] -values from the IDA ones, therefore, should not be surprising.

The experimental error of NAA was checked by using powder of the standard speleothem 76001. The reported interlaboratory IDA-[U] values of this standard (Harwell AERE-R 10044, Table 3.1 and 3.3) are:  $0.78 \pm 0.054$  ppm (Lab. spike),  $0.80 \pm 0.028$  ppm (USIP spike),  $0.81 \pm 0.03$  ppm (USIP spike, 19 laboratories). The NAA results are:  $0.805 \pm 0.027$  ppm (1979), and 0.78 ppm, 0.93 ppm, 1.00 ppm (1982, NAA Report 933, preweighed samples 501-502 mg); their mean is  $0.88 \pm 0.05$  ppm. We notice that:

(i) The IDA and NAA results ( $1\sigma$  level) overlap at 0.83-0.84 ppm.

(ii) The NAA results yield a standard error:  $\pm 5.7\%$ .

This value is assumed to remain constant. for all the NAA-[U] measurements of this thesis.

## CHAPTER 5: ESR isochron: test on a stalagmite

### 5.1 Introduction

The choice of material to test the "isochron" idea was done according to the following criteria:

- (i) The speleothem should have been dated by a reliable method, such as U/Th dating method.
- (ii) The speleothem layer for which the date was given, should be a dense, white, 'pure' calcite (see section 2.2.2) in order to assure uniformity of p, q and a-value (section 3.5 and 3.8). Besides, the growth layer should have sufficient size to get enough samples for the isochron plot (see section 3.7).
- (iii) The temperatures which the speleothem has experienced should be quite low (see section 2.5) in order to guarantee that thermal fading of the dating ESR signal did not occur since the speleothem was formed.

M. Gascoyne's work in McMaster University offered both abundant specimens and precise U/Th dates; so the choice of speleothems was not at all problematic.

The speleothems used in this study come from caves

of N.W. England. The climatic oscillations in Britain during the middle and upper Pleistocene are shown in Figure (5.1.1) and Table (5.1.1). The average annual temperature does not seem to exceed  $\sim 20^{\circ}\text{C}$ . The warm periods ( $15\text{-}20^{\circ}\text{C}$ ) constitute only a small fraction ( $\sim 10\%$ ) of a period of  $\sim 300$  Ka, while the cool-cold periods ( $0\text{-}10^{\circ}\text{C}$ ) are dominant. Therefore, the mean average annual cave temperature (see section 2.1) in Britain over the last 300-400Ka could reasonably be considered to be:  $T_0 \cong 10^{\circ}\text{C}$ . This value will be used later in the evaluation of  $\tau_0$  (see section 1.4.1).

### 5.2 Speleothem 76121 : Given data

76121 is a dense, white, laminated stalagmite from the Lancaster Hole cave system, showing surface erosion features and continuous growth. It was formed during a very short time period, as inferred from U/Th dating. The following data are available (Gascoyne, 1979 p.451).

Sample	[U] ppm	p	$P_0$	q	$^{230}\text{Th}/^{232}\text{Th}$	t Ka
Top 1 cm	2.42	1.073	1.100	0.656	110	$113.6^{+7.6}_{-7.1}$
Base 2 cm	1.49	1.130	1.179	0.661	129	$114.0^{+7.5}_{-7.1}$

Both materials seem to be free of detrital impurities, because their  $^{230}\text{Th}/^{232}\text{Th}$  isotope ratios lie well above the limit of 20, taken by Gascoyne (1979, p. 68) to distinguish

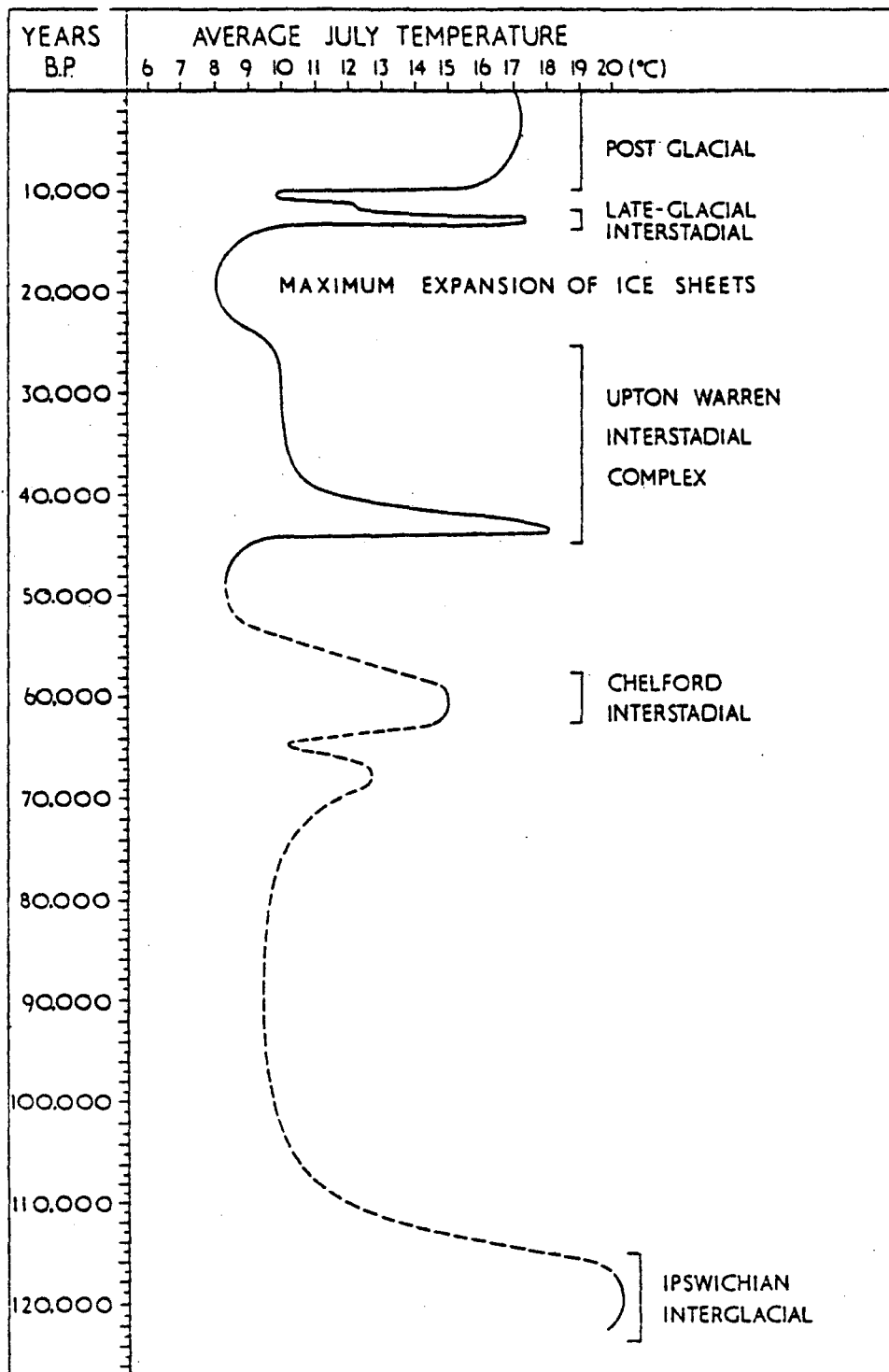


Figure 5.1.1 Climatic oscillations for the last 120 Ka in Britain, from beetle assemblages (from Coope 1975).



$^{230}\text{Th}/^{234}\text{U}$ age (Ka)	Isotopic stage and substage		British Quaternary stage and substage		Climate *
140					
170	6	-	WOLSTONIAN		glacial
190-195		a			mild-warm
195-200	7	b	HOXNIAN		cool
- 210		c			warm
210-220			A		
	8	-	N	Lowestoft Stadial	arctic-glacial
230-240			G		
- 240	9	a	L	Corton Interstadial	cold
			I		
			A		
	9	b	N	Gromer Stadial	cold-arctic
--- 250					
	9	c		C R ?	mild
--- 270				O ?	
	9	d		M E ?	cool
--- 275				R ?	
	9	e		I A ?	warm
--- 280				N	
	10 ?	-		?	arctic-glacial ?
---> 285					
	11 ?	?		?	mild ?

\* the terms used to define climate are based on stable isotope signal of both deep sea cores and speleothem and on presence or absence of speleothem growth as described below:

- arctic - generally non-glacial but with presence of perma-frost and tundra
- cold - mean annual temperatures about zero because speleothem growth did not occur
- cool - mean annual temperatures were > 0 because speleothem growth did not cease
- mild - climate somewhat cooler than present
- warm - climate comparable to today

Table 5.1.1 Proposed correlation of British Quaternary events to the stable isotope record of speleothem 77151 and the deep sea core ice volume curve. Radiometric ages are determined from speleothem only. (from Gascoyne, 1979, Table 5.6)

between 'pure' and 'dirty' calcites. Both materials have 'identical' dates ( $t \cong 114 \pm 7.3$  Ka) and very similar p and q isotope ratios ( $p \cong 1.10 \pm 0.03$ ,  $q \cong 0.658$ ).

### 5.3 Details on analytical procedure

The samples were taken as closely as possible to the sites indicated by M. Gascoyne (Plate 5.3.1), in order to allow the data given in section(5.2) to be used in the present study too. The sample preparation was done as described in section(4.2). The grain size range was 0.18-0.71 mm. Five 'aliquots' of each sample were formed before the powders were homogenized, and their natural ESR intensity was measured in order to see the necessity of the homogenization. Differences up to  $\sim 15\%$  were found. The 'aliquots' were remixed and new ones were formed as described in section(4.2). These 'true' aliquots were given 2.6, 5.2, 7.8 and 10.4 Krads of  $\gamma$ -rays and one of them was left unirradiated to get the natural signal. The Varian and JEOL ESR spectrometers were used to get ESR spectra for the determination of ED's and g-values respectively. All samples had identical weight  $\sim 100$  mg. The Top-aliquots were measured 3 times and the Base-aliquots 2 times, in order to test the reproducibility of the slopes and ED's.



Plate 5.3.1 Stalagmite 76121: Longitudinal cross section ( ~85%  
of the actual size).

#### 5.4 Experimental results

The ESR spectra of both Top and Base samples display strong resonance peaks (Figure 5.4.1) with  $g$ -factors of about 2.00075; this value does not seem to be dependent on additional  $\gamma$ -irradiation. Thermal study of this signal has not been carried out. We assume that the fading temperature of  $\sim 230^{\circ}\text{C}$ , occurring in cases of other speleothems, e.g. 77200-E<sub>3</sub> (Chapter 6), which display the same  $g$ -values, could be expected here too. If this is correct,  $T^* \cong 230^{\circ}\text{C}$  ensures a stable trap for storage temperature  $\sim 10^{\circ}\text{C}$  (see section 2.5).

Other signals have been revealed in the ESR spectra as well. Their  $g$ -values are: 2.0070 and 2.0117. These values do not seem to be affected by the additional irradiation, as well. The ESR spectra did not show any  $\text{Mn}^{2+}$  peaks. A notation has been adopted for the above ESR signals, as shown in the following table:

Signal's symbol	$g$ -factor	notes
S <sub>1A</sub>	2.00075( $\pm 5$ )	strong signal, used for dating
S <sub>1B'</sub>	2.00700( $\pm 20$ )	very weak signal
S <sub>2B</sub>	2.01170( $\pm 10$ )	not present at sample's natural (unirradiated) state

All, S<sub>1A</sub>, S<sub>1B'</sub>, S<sub>2B</sub> signals are sensitive to  $\gamma$ -irradiation.

The results of the additive-dose method used to deter-

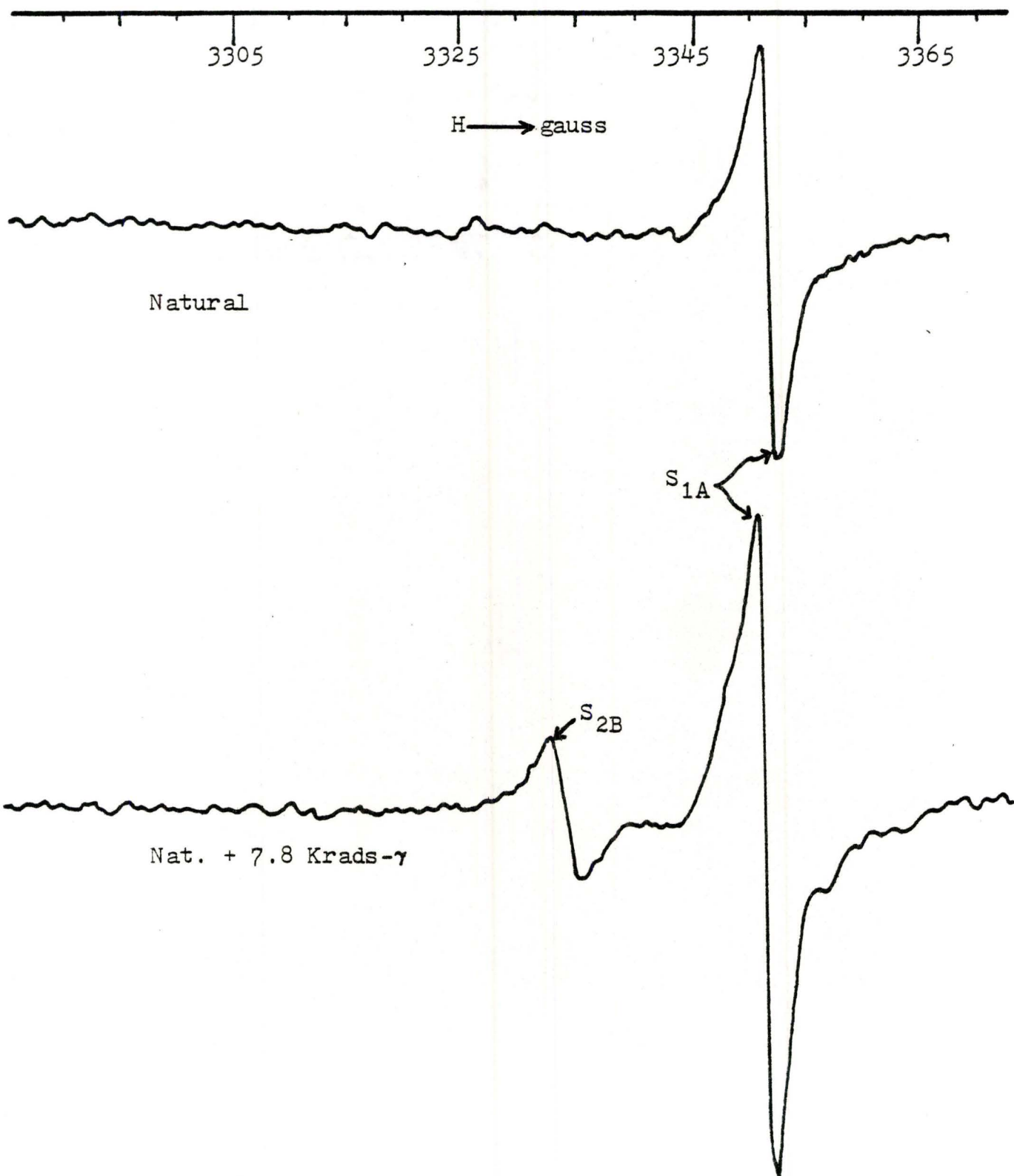


Figure 5.4.1 ESR spectra of Spel. 76121-Top (spectrometer: Varian E104A)

mine EDs (see section 1.6.1) are shown in Figure (5.4.2). Both Top and Base seem to respond linearly to additional doses. Their EDs are:  $ED_{\text{Top}} = 10.9 \pm 0.4$  Krads and  $ED_{\text{Base}} = 8.35 \pm 0.15$  Krads. It is obvious that Top and Base sensitivities to  $\gamma$ -rays are different. In general,  $s(\text{Top}) > s(\text{Base})$  for both  $S_{1A}$  and  $S_{2B}$  signals.  $S_{1A}$  sensitivities are:  $s(\text{Top}) \cong 0.032(+3)$  ESR  $\text{mg}^{-1}/\text{Krad}$  and  $s(\text{Base}) \cong 0.025(+2)$  ESR  $\text{mg}^{-1}/\text{Krad}$ .

The NAA results:  $[U]_{\text{Top}} = 2.6 \pm 0.15$  ppm and  $[U]_{\text{Base}} = 1.9 \pm 0.1$  ppm are higher than the IDA-  $[U]$  values given by Gascoyne (see section 5.2). Such a 'discrepancy', however, was more or less expected (section 4.6). The Mn content of the Top sample was found  $< 1$  ppm. The Rb content of the Base sample was 20 ppm<sup>®</sup>.

### 5.5 Determination of the IS and $D_{\text{ext}}$

The very first test of a new idea should be allowed to contain simplifications and use materials which will facilitate the features of the behaviour to be uncovered. So, in the present test of the "isochron" idea only two samples are used. Besides, the samples do not belong to the same growth layer, but they can be considered as being 'coeval'.

---

<sup>®</sup> The low  $[Rb]$  will contribute to the total  $D_{\text{int}}$  of the Base about 0.1 Krads (Bell, 1979). This is 1.2% of the ED (Base), even lower than the experimental error ( $0.15 > 0.1$ ). In general, such low Rb contents are neglected (e.g. see: Hennig et al., 1981a).

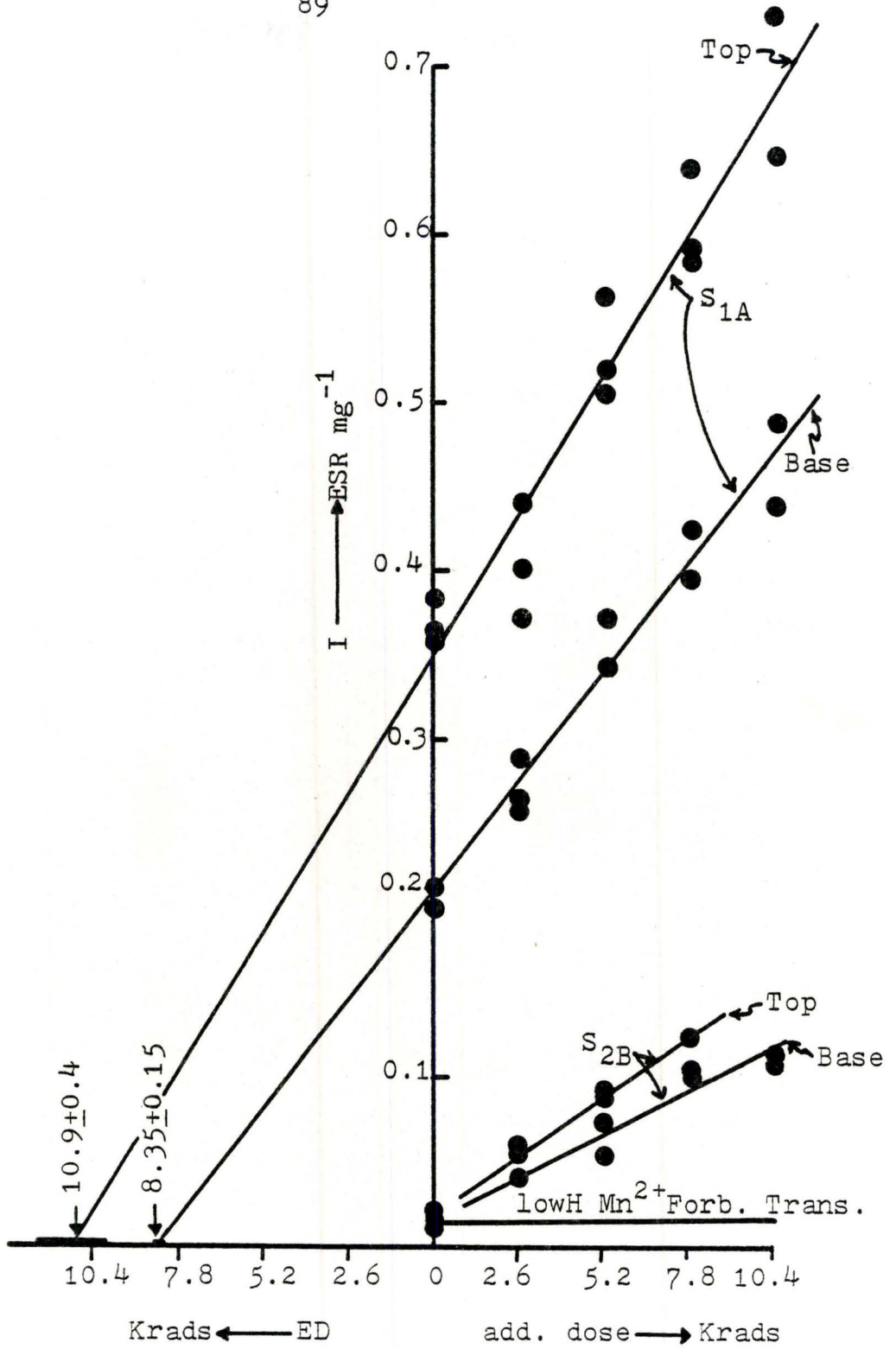


Figure 5.4.2 Stal. 76121, Top and Base samples. Determination of EDs.

By plotting the Top and Base  $I_n$  (natural ESR norm. intensity) versus  $[U]$  (ESR-intensity isochron), a very steep 'isochron' line is obtained and the intercept at  $[U] = 0$  is meaningless (Figure 5.5.1). This is due to the already mentioned sensitivity differences and a possible a-factor difference. On the contrary, the plot of ED versus  $[U]$  (Figure 5.5.2) shows a reasonable correlation. The isochron intercept at  $[U] = 0$  is  $ED_0 = 1.27 \pm 1.63$  Krads and its slope is  $IS = 3.8 \pm 0.7$  Krads/ppmU. The maximum slope (see section 3.8.(i)) is:  $IS_{\max} \cong 4.35$  Krads/ppmU.

The a-values of Top and Base have not been determined. If both samples have the same a-factor ( $a(\text{Top}) = a(\text{Base})$ ) then  $ED_0 = D_{\text{ext}}$ . Possible a-factor differences, however, will affect both  $ED_0$  and IS values. If  $a(\text{Top}) < a(\text{Base})$  then to get an isochron with  $a(\text{Top}) = a(\text{Base})$  either the Base ED must be lowered or the Top ED must be raised. Both result in getting a steeper isochron with  $ED_0 < 1.27$  Krads and possibly zero or even negative intercept, which is rather unlikely to occur. On the other hand, if  $a(\text{Top}) > a(\text{Base})$  then the above reasoning is reversed and the  $ED_0$  becomes  $> 1.27$  Krads. Therefore, if  $a(\text{Top}) \neq a(\text{Base})$ , a high  $a(\text{Top})$  is more likely to occur and the 'true' magnitudes of  $D_{\text{ext}}$  and IS seem to be:  $D_{\text{ext}} \geq 1.27 \pm 1.63$  Krads,  $IS \leq 3.8 \pm 0.7$  Krads/ppmU.



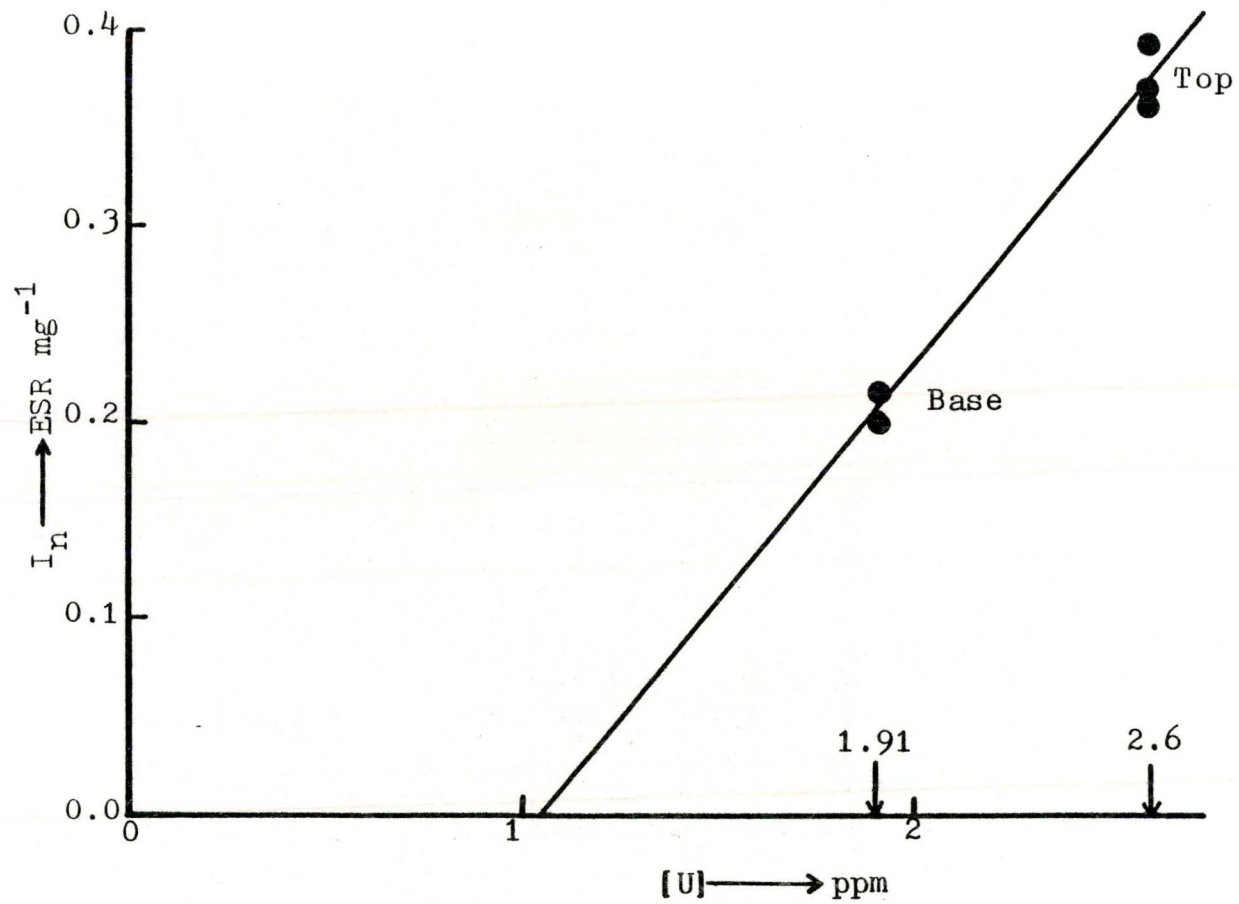


Figure 5.5.1 Stal. 76121, natural  $S_{1A}$ : ESR intensity isochron

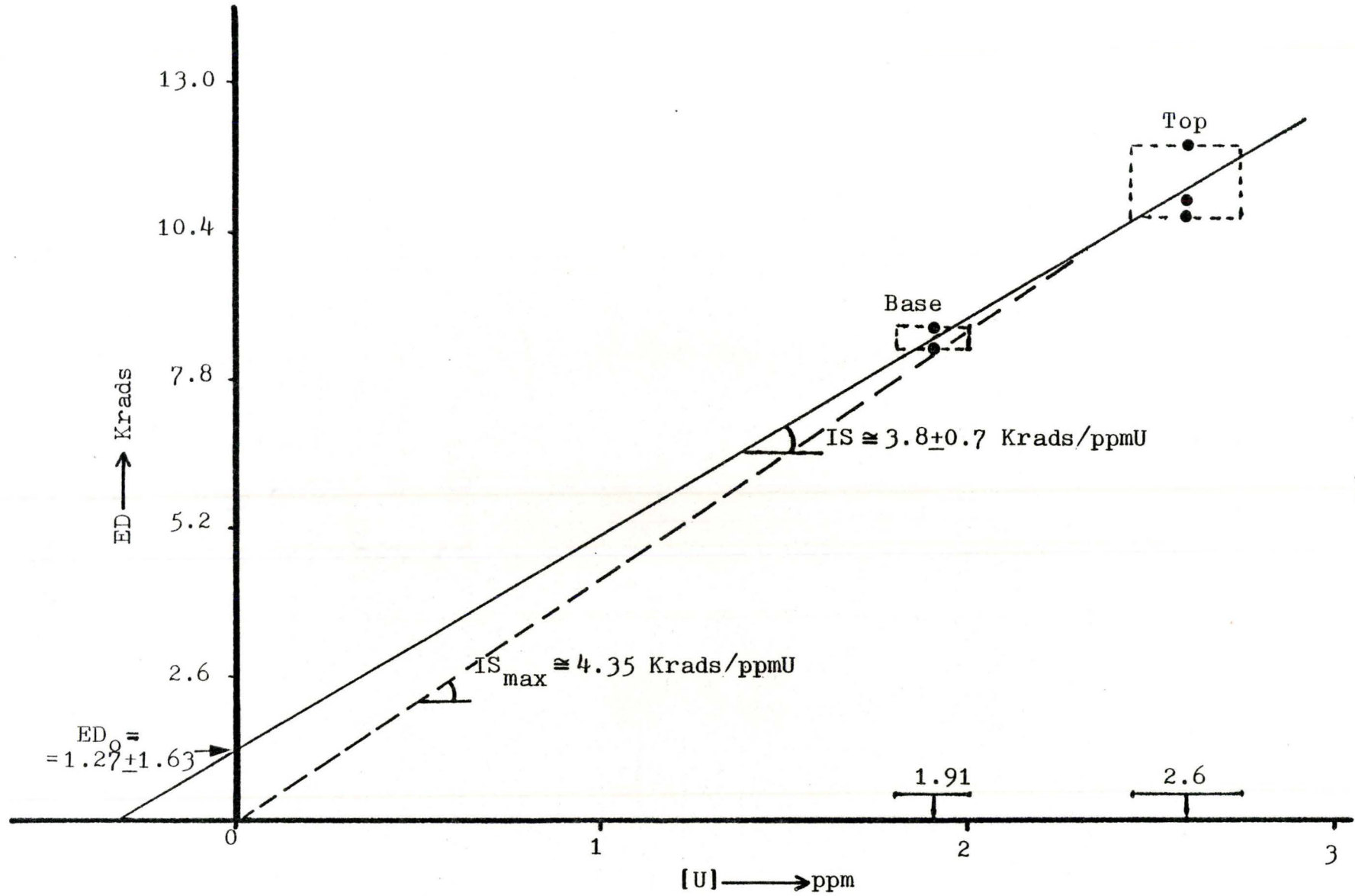


Figure 5.5.2 Stal. 76121, S<sub>1A</sub>: 'real' isochron.

### 5.6 Determination of the $R_{ext}$ and a-value

Given the age  $t$ ,  $\overline{R}_{ext} = D_{ext}/t$  comes to be  $\overline{R}_{ext} \geq \frac{1.27 \pm 1.63}{114 \pm 7.3}$  Krads/Ka or  $\overline{R}_{ext} \geq 11 \pm 14$  mrad/yr, a dose rate rather low compared with present day in situ  $R_{ext}$  evaluations in various caves (see section 3.4). This fact reinforces the thought that  $a(\text{Top})$  could be  $\geq a(\text{Base})$ . Hence, the following attempt to evaluate an  $\bar{a}$ -value is in effect, the evaluation of an upper limit for the a-values.

Since  $p, q$  and  $t$  are given for both samples, equation (3.5.2) allows one to draw a diagram of  $cf(a, p, q, t)$  versus a-factor (Figure 5.6.1). Having known the IS, the a-values' upper limit comes to be  $\sim 0.17 \pm 0.04$ . If we take into account that the lowest reported a-value of speleothems, determined by means of ESR techniques, is about 0.08 (Yokoyama et al., 1981b), it could be expected the a-values of Top and Base to lie within the interval 0.08-0.26, being probably very close to 0.15. The highest ESR a-value, reported by Hennig et al. (1981a) is  $0.30 \pm 0.06$  but the corresponding sample (Pet-a), an opaque, reddish-brown calcite, had a high fraction, probably a few%, of clay minerals and a Mn content of 42.3 ppm. Our samples are quite free of detrital impurities; the Top sample has very low [Mn] ( $< 1$ ppm) and probably so does the Base sample, as it is inferred from their ESR spectra. If a-value is affected by the presence of "active" impurities such as  $Mn^{2+}$  (Ikeya, 1975), a low

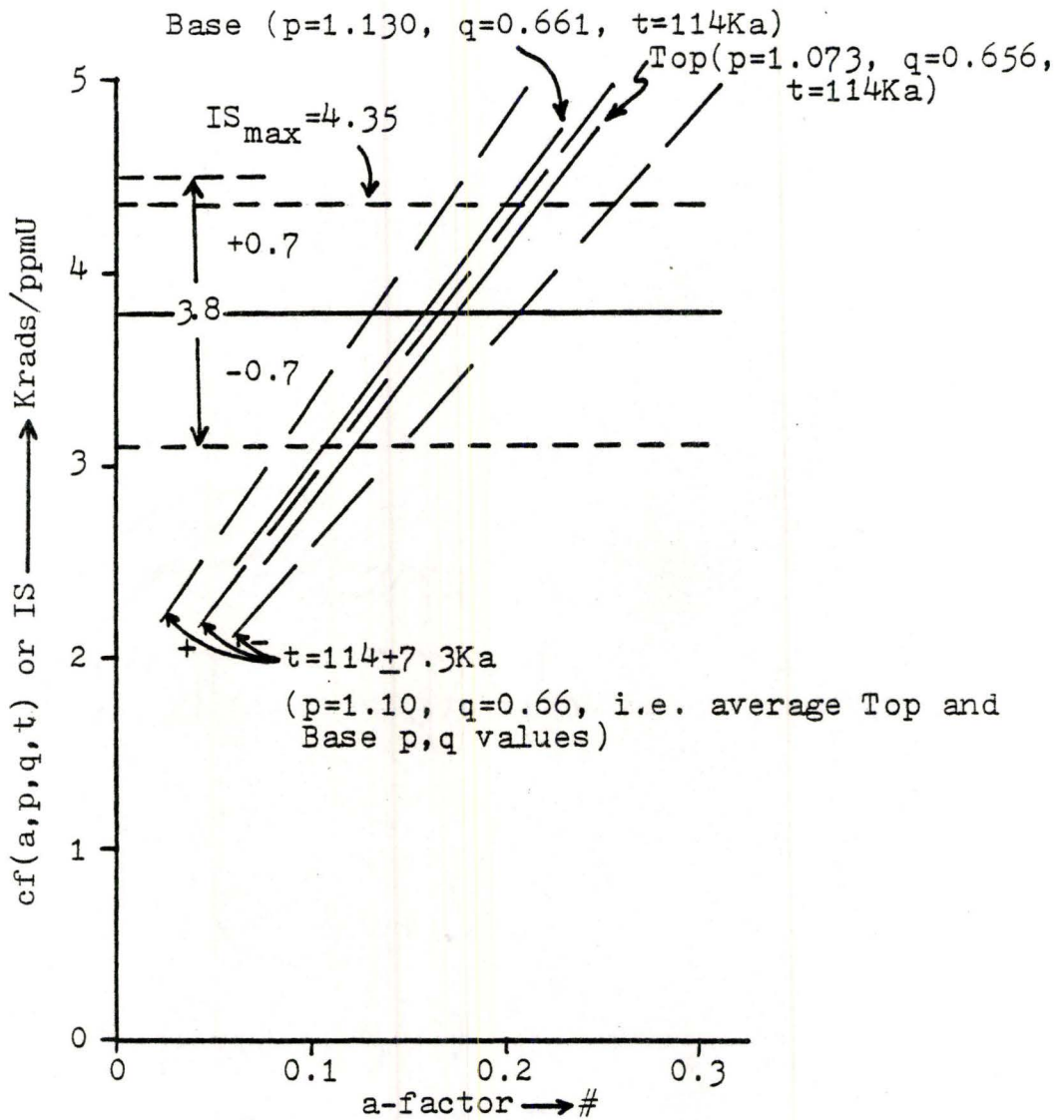


Figure 5.6.1 Stal. 76121, Top and Base. Plot of  $cf(a,p,q,t)$  versus a-factor. The IS and  $IS_{\max}$  are shown too.

a-value seems to be more appropriate for our samples. In the following text we assume an a-value of 0.15.

### 5.7 Determination of the age $t$

Given the a-value, the preliminary test plot (see section 3.6.1) can be drawn for  $p_0=1$  and 2 (Figure 5.7.1). The IS value indicates an age well below 200 Ka, which means that U series should be considered in disequilibrium. Since the Top and Base  $p_0$  values are available from U/Th dating, the  $cf(a, p_0, t)$  curves corresponding to these values are also shown, as well as the U/Th date. The plot indicates that  $t$  would be  $114 \pm 7.3$  Ka if IS lies in the range 3.1-3.9 Krads/ppmU, i.e. if  $IS = 3.5 \pm 0.4$  Krads/ppmU. Since  $p$  and  $q$  are given, the plot of  $cf(a, p, q, t)$  versus  $t$  allows the age to be determined. Figure (5.7.2) illustrates the  $cf(a, p, q, t)$  changes for a-value=0.1, 0.15, and 0.2. The drawn lines correspond to the present day  $p, q$ , activity ratios (Top and Base average values). These lines have no meaning far away from  $t=114 \pm 7.3$  Ka, because  $p$  and  $q$  are time dependent. The  $a=0.15$  line and the IS limits indicate an age  $t=116 \pm 11$  Ka. And something else: for  $t \cong 114$  Ka, the  $a=0.1$  and  $a=0.2$  lines yield  $IS \cong 2.9$  Krads/ppmU and  $IS \cong 4.2$  Krads/ppmU respectively. These values bracket the previously defined range of  $IS=3.1-3.9$  Krads/ppmU and tend to reinforce the assignment of the  $a=0.15$ .

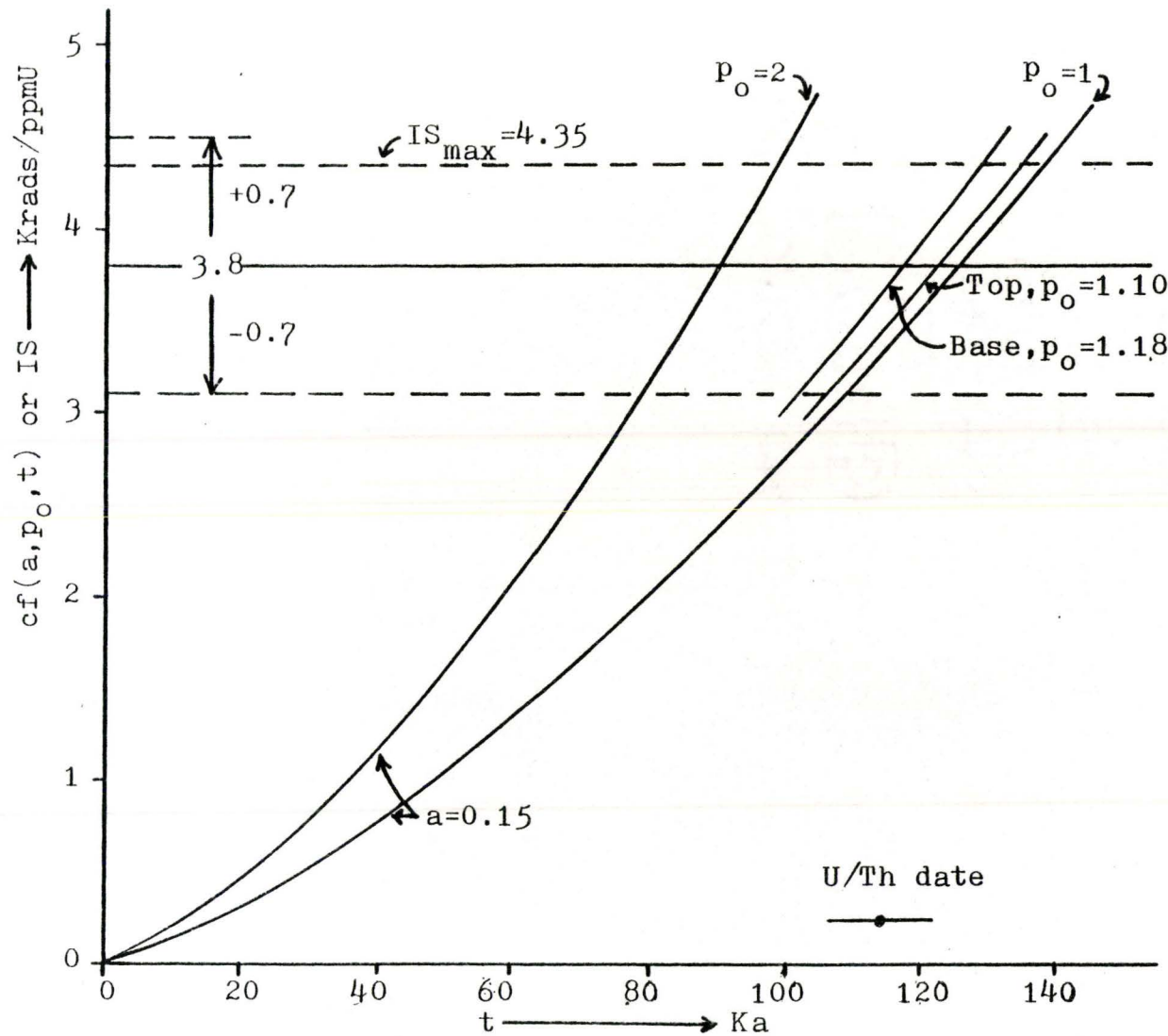


Figure 5.7.1 Stal. 76121, Top and Base. Plot of  $cf(a, p_o, t)$  versus  $t$  for  $a=0.15$  and  $p_o=1$  and  $2$  (preliminary test plot).

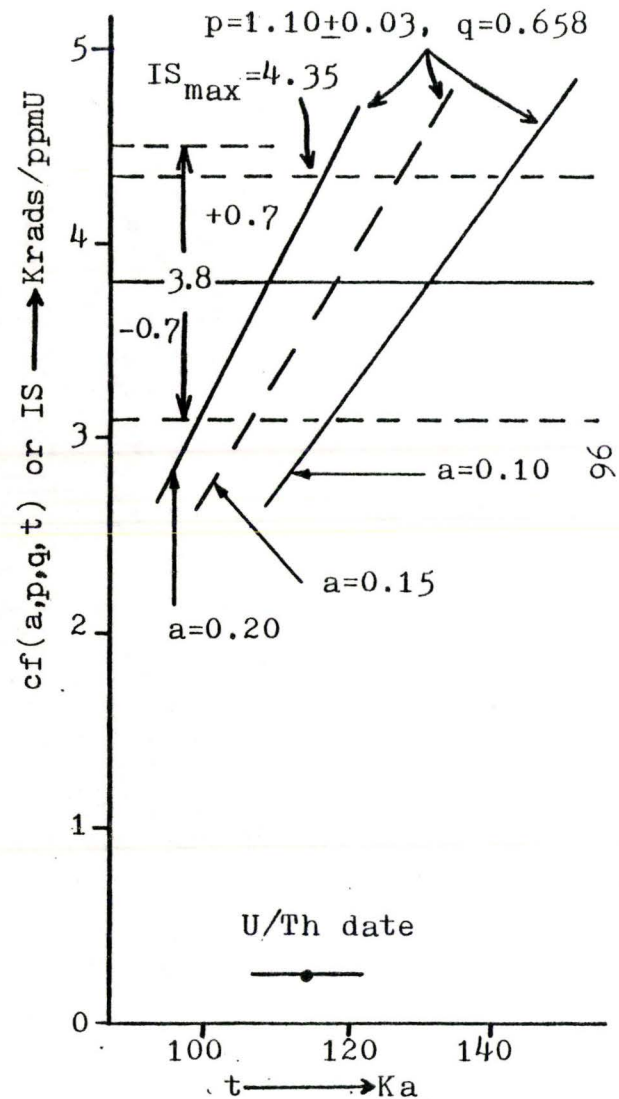


Figure 5.7.2 Stal. 76121, Top and Base. Plot of  $cf(a, p, q, t)$  versus  $t$ .

## 5.8 Discussion

The problems that arose during the a-value and t determination are due to two factors:

- (i) the small number of samples used to determine the IS.
- (ii) the lack of experimental determination of the a-values.

The "isochron" results of the stalagmite 76121 fit together with the U/Th date ( $t \cong 114$  Ka), for  $IS \cong 3.5$  Krads/ppmU and a-value  $\cong 0.15$ . These values require a confirmation; this is hoped to be obtained by a new experiment being performed in our laboratory.

It has already been mentioned (see section 3.3) that early ESR dating attempts assumed the U-series to be in equilibrium. To illustrate the extent to which equilibrium-disequilibrium approaches yield distinct results in cases of young ( $t < 200$  Ka) speleothems, an 'equilibrium' date is derived for the stalagmite 76121. For:  $IS = 3.5$  Krads/ppmU,  $a = 0.15$ ,  $\Delta_1 = 14.865 \cdot 10^{-11}$  Krads,  $c = 3.7965 \cdot 10^{11}$  Ma<sup>-1</sup>ppmU<sup>-1</sup>,  $R_d' = 278.3$  mrad/yr ppmU,  $R_\beta' + R_\gamma' = 26.1$  mrad/yr ppmU (no radon loss), equations (3.5.3) and (3.5.4) give:  $t(\text{Bell}) \cong 52$  Ka and  $t(\text{Wintle}) \cong 62$  Ka. We notice that:

- (i) the two equilibrium dates do not coincide because of reasons discussed in section(3.3.2).
- (ii) both 'equilibrium' dates are significantly lower

(~50%) than the 'disequilibrium' date (114 Ka).  
This example shows clearly the importance of considering  
disequilibrium for young speleothems in ESR/TL dating.



CHAPTER 6: Conventional ESR isochron dating:  
test on a flowstone

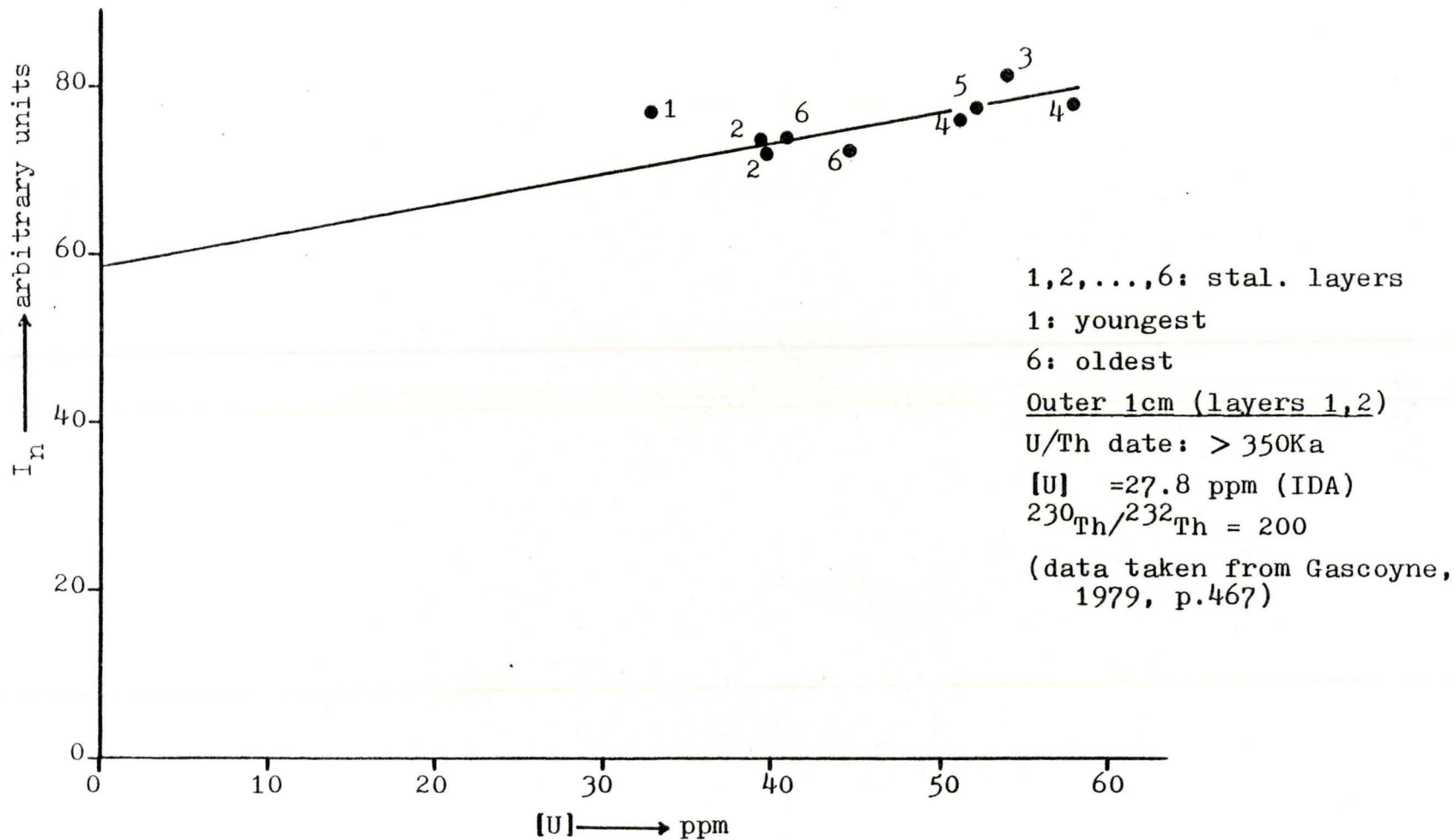
6.1 Introduction

The promising results of the speleothem 76121 induced us to retest the "isochron" idea, this time on a flowstone. The initial aim was to apply 'real' isochron dating, but unexpected complications during the course of the experiment made this aim practically impossible. The motivation to apply intensity isochron dating came from another speleothem (75037) which had been studied in our laboratory during the summer of 1979. Figure (6.1.1) shows the plot of  $I_n$  versus [U] for several samples taken from 6 consecutive layers of the 75037. This plot indicates that multilayer ESR intensity isochron could be feasible. This said speleothem, however, was not chosen for detailed study because of the lack of clear U/Th dates. The flowstone 77200 was studied instead, which satisfied the choice-criteria laid down in section (5.1).

6.2 Speleothem 77200 : Given data

77200 is an approximately 17 cm thick piece of indurated flowstone, mostly white laminated calcite, showing

Figure 6.1.1 Stalactite 75037 (Grotte Valerie, Nahanni, N.W.T.). Natural intensity of the main ESR signal versus U content (NAA).



surface resolution. It was taken from a fallen block in the North Craven Passage of the Gaping Gill cave system. The following data are available (Gascoyne, 1979, p.458)

Sample	[U] ppm	p	p <sub>0</sub>	q	<sup>230</sup> Th/ <sup>232</sup> Th	t	Ka
Top(?)2cm	0.95	1.296	1.665	0.994	181	288.7	<sup>+23.9</sup> <sub>-20.0</sub>
Base(?)2.5cm	1.94	1.239	--	1.032	69	>350	

No hiatus is seen in between 2 cm from Top and 2.5 cm from the Base (Plates 6.2.1A,B). Both materials seem to be free of detrital impurities, because their <sup>230</sup>Th/<sup>232</sup>Th ratios are well above 20 (Gascoyne, 1979, p.68).

### 6.3 Details on analytical procedure

Figure (6.3.1) shows a cross section of the flowstone (the piece used in this study) with the various growth layers named: A,B,C, etc.. The E layer corresponds to a distance approximately 2 cm from the Top. This layer was chosen for sampling because:

- (i) it is very close to the site indicated by Gascoyne
- (ii) it is white, and the closest coloured layer (C) is approximately 0.5 cm away, so contamination during sampling can be avoided.
- (iii) several samples from F layer were available, which could be used if there was such a need.

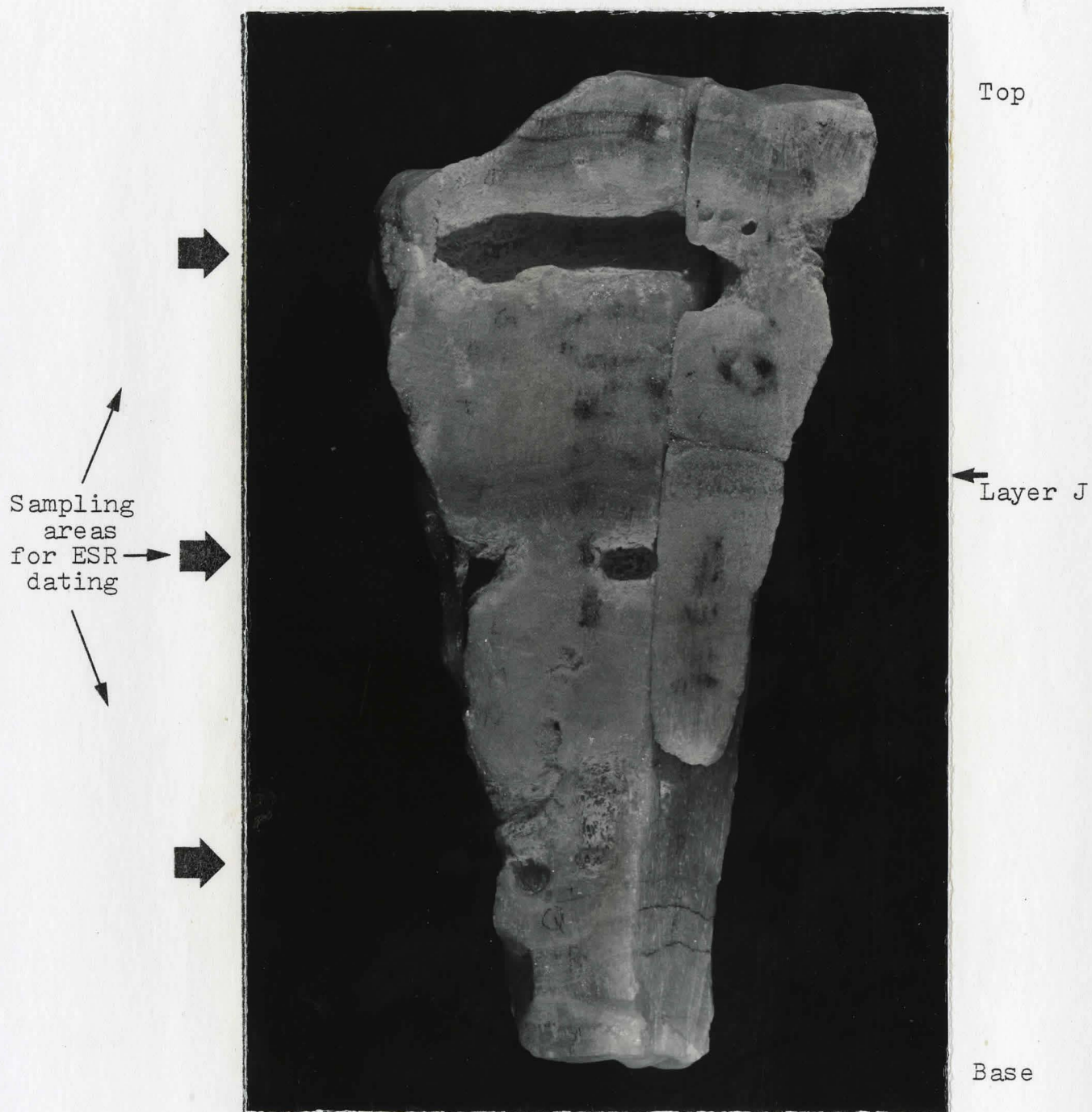


Plate 6.2.1 A Flowstone 77200. Cross section parallel to the growth direction (actual size). Most of the samples used in this study were taken from this piece.

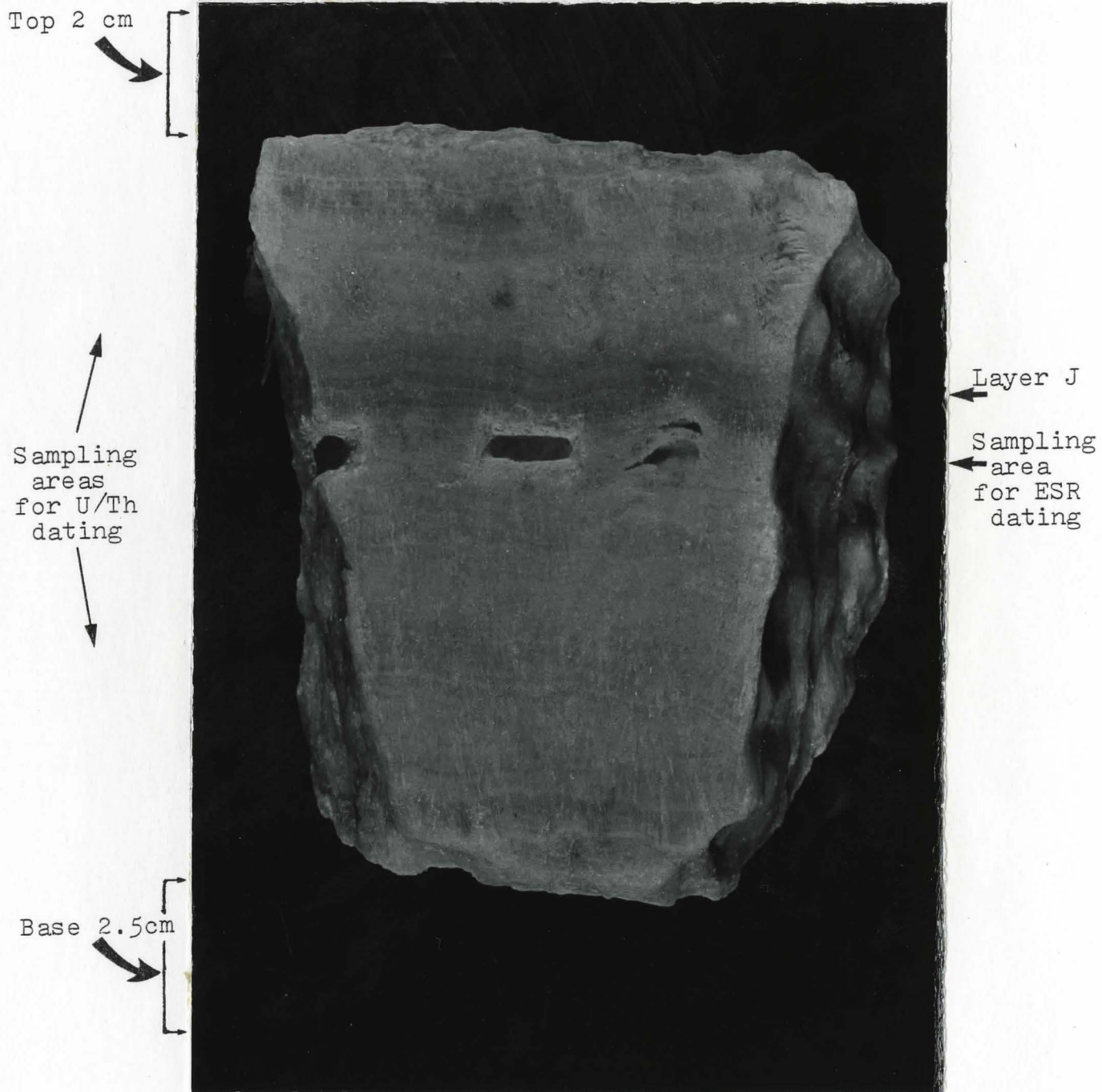






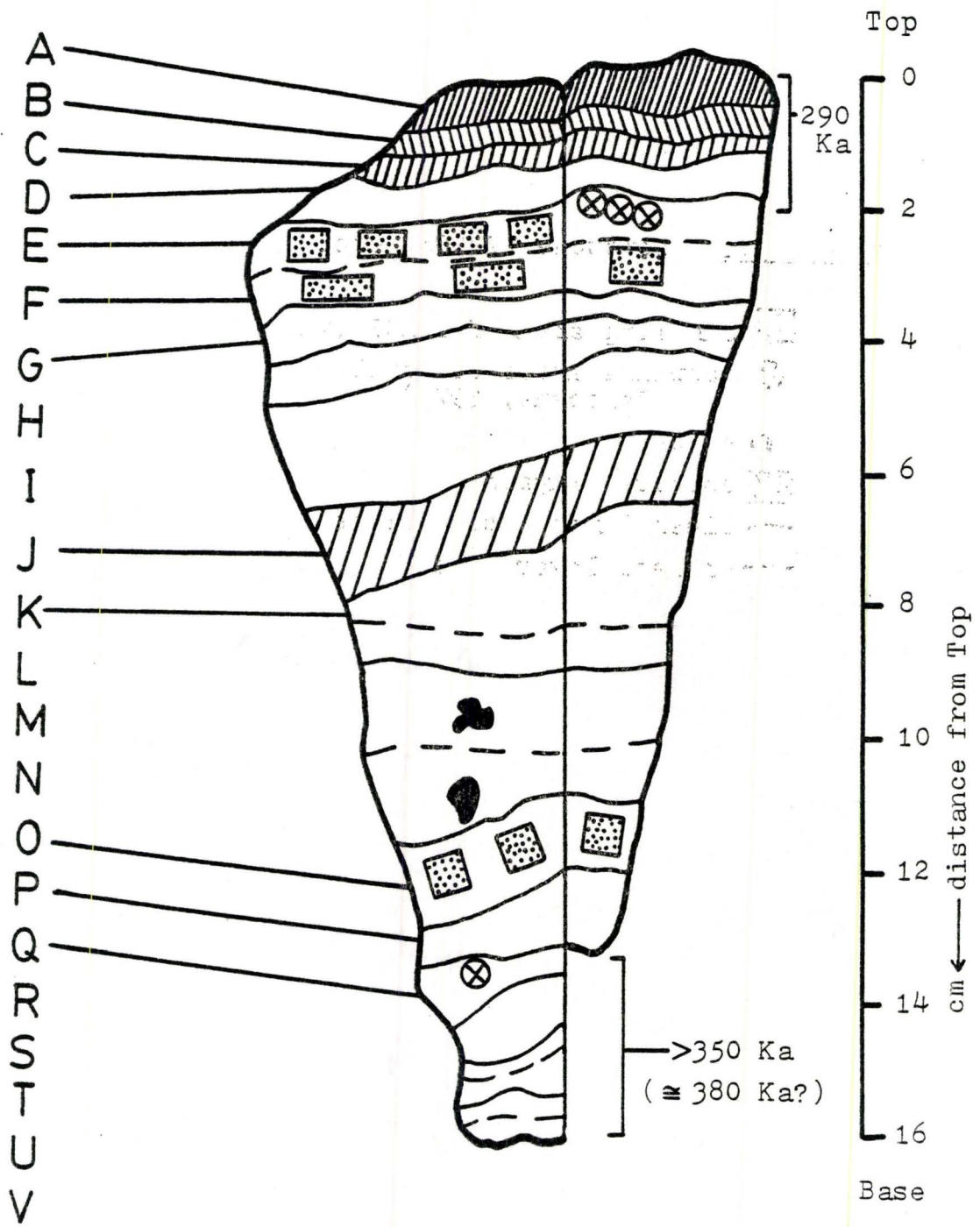


Plate 6.2.1. B Flowstone 77200. Cross section parallel to the growth direction (actual size). Piece used by Gascoyne for U/Th dating.

Figure 6.3.1 Flowstone 77200: cross section.

-  sampling areas for ESR (this study)
-  sampling areas for stable isotope analysis  
(Gascoyne, 1979)
-  voids
-  coloured layers
-  clear layer boundaries
-  unclear layer boundaries



Thus, four samples were taken from the layer E, named  $E_1$ ,  $E_2$ ,  $E_3$ , and  $E_4$ .

The whole procedure, from sample preparation to ESR spectroscopy was done as described in Chapter 4 (same as for 76121). The details are listed below:

powders of grain size: 0.15-0.30 mm were used for  
 $\gamma$ -irradiation.

powders of grain size: 0.075-0.15 mm were used for  
[U]-determination

powders of grain size:  $<0.075$  mm were used for  
 $\alpha$ -irradiation

additive  $\gamma$ -doses (Krad): 2.35, 4.70, 7.05, 9.40

sample weight in quartz tubes:  $75 \pm 1$ mg

The sample weight was kept approximately constant because, regardless of calibration by weight, ESR intensity per mg does not remain constant when weight varies (Figure 6.3.2). This issue is discussed more thoroughly in section (4.5).

#### 6.4 Experimental results

The ESR spectra of all  $E_i$  samples display strong resonance peaks. One of these spectra (Sample  $E_3$ ) is shown in Figure (6.4.1). The peaks of all four spectra have g-values similar to those of the stalagmite 76121; these g-values are not affected by additional  $\gamma$ -irradiation. All spectra display prominent  $Mn^{2+}$  peaks of various intensities,



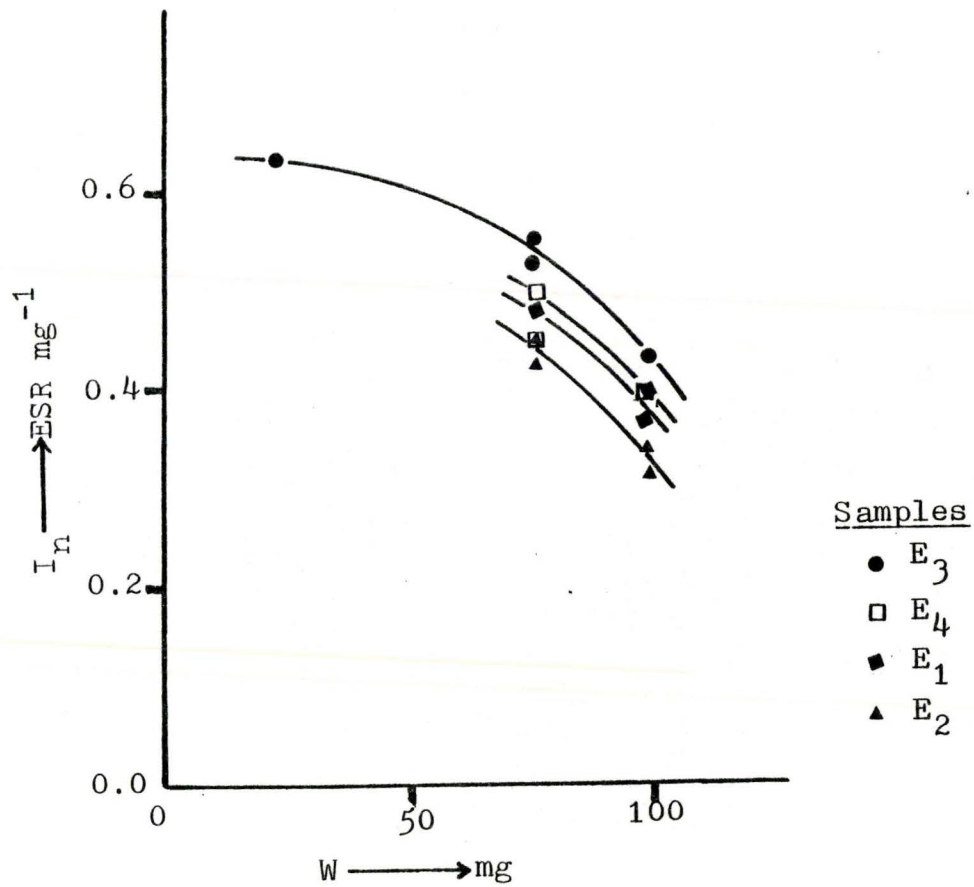


Figure 6.3.2 Flowstone 77200, layer E, grain size 150-300  $\mu\text{m}$ .  
 Natural  $S_{1A}$ : ESR intensity dependence on sample's weight.

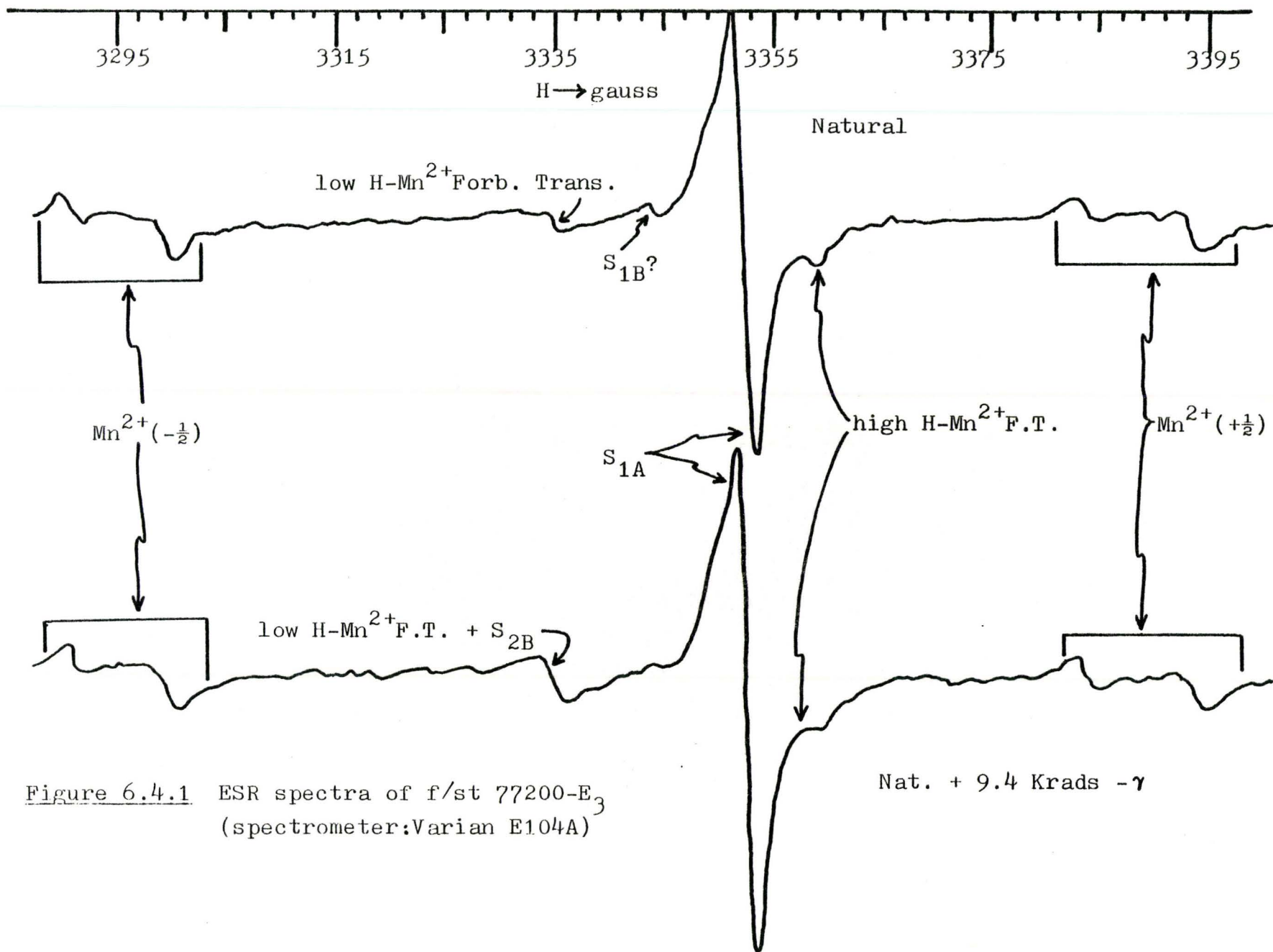


Figure 6.4.1 ESR spectra of f/st 77200-E<sub>3</sub>  
 (spectrometer: Varian E104A)

corresponding probably to variable Mn-content. Thermal study of the  $E_3$ -natural (unirradiated) sample indicates a fading temperature  $T^* \cong 230^\circ\text{C}$  for  $S_{1A}$  and  $T^* \cong 390^\circ\text{C}$  for  $S_{1B}$  (Figure 6.4.2). Retrapping at  $\sim 150^\circ\text{C}$  is evident though signal evolution from  $24^\circ\text{C}$  to  $150^\circ\text{C}$  does not show clearly the features found to occur in other speleothems (Chapter 7). Figure (6.4.3) shows some characteristic spectra of this thermal study.

The following table summarizes the results.

signal's symbol	g-factor	$T^*^\circ\text{C}$	notes
$S_{1A}$	$2.00070(^{\pm}10)$	$\sim 230$	strong signal used for dating
$S_{1B}$	$2.00595(^{\pm}10)$	$\sim 390$	signal revealed only by annealing
$S_{2B}$	$2.01200(^{\pm}10)$	--	signal present only in irradiated materials

The natural signals of all  $E_i$  samples were measured first, and showed a good range of  $I_n$ -values ( $\sim 0.45$ - $0.55$   $\text{ESRmg}^{-1}$ ). It was thought that this range could be due to [U] variations; then the  $\gamma$ -irradiations followed.

Figure (6.4.4) shows the results. All four  $S_{1A}$  signals seem to have a rough linear response to additive doses. Signals related to  $\text{Mn}^{2+}$  are not affected by  $\gamma$ -rays up to  $\sim 10$  Krads. To get ED's, the best fit lines have to be extrapolated back to  $I=0$ . Two features make this task problematic:

Figure 6.4.2 Flowstone 77200-E<sub>3</sub>, natural; powder of grain size 150-300  $\mu\text{m}$ .  
Step annealing:  $\Delta T=25^\circ\text{C}$ ,  $t^*=6$  min.

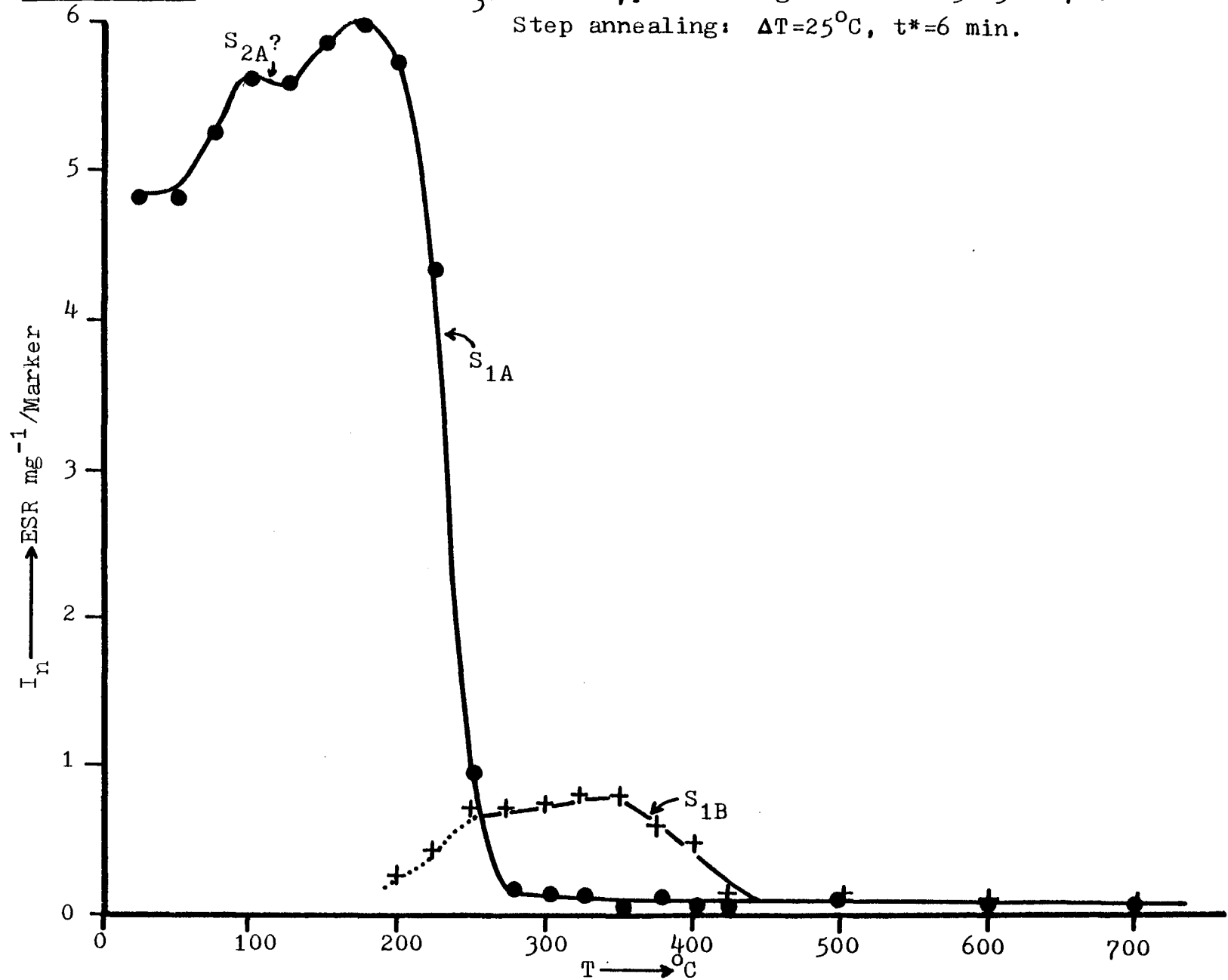


Figure 6.4.3 F/st 77200-E<sub>3</sub>, natural: ESR spectra of the thermal study (spectrometer: JEOL JES-3BS-X).

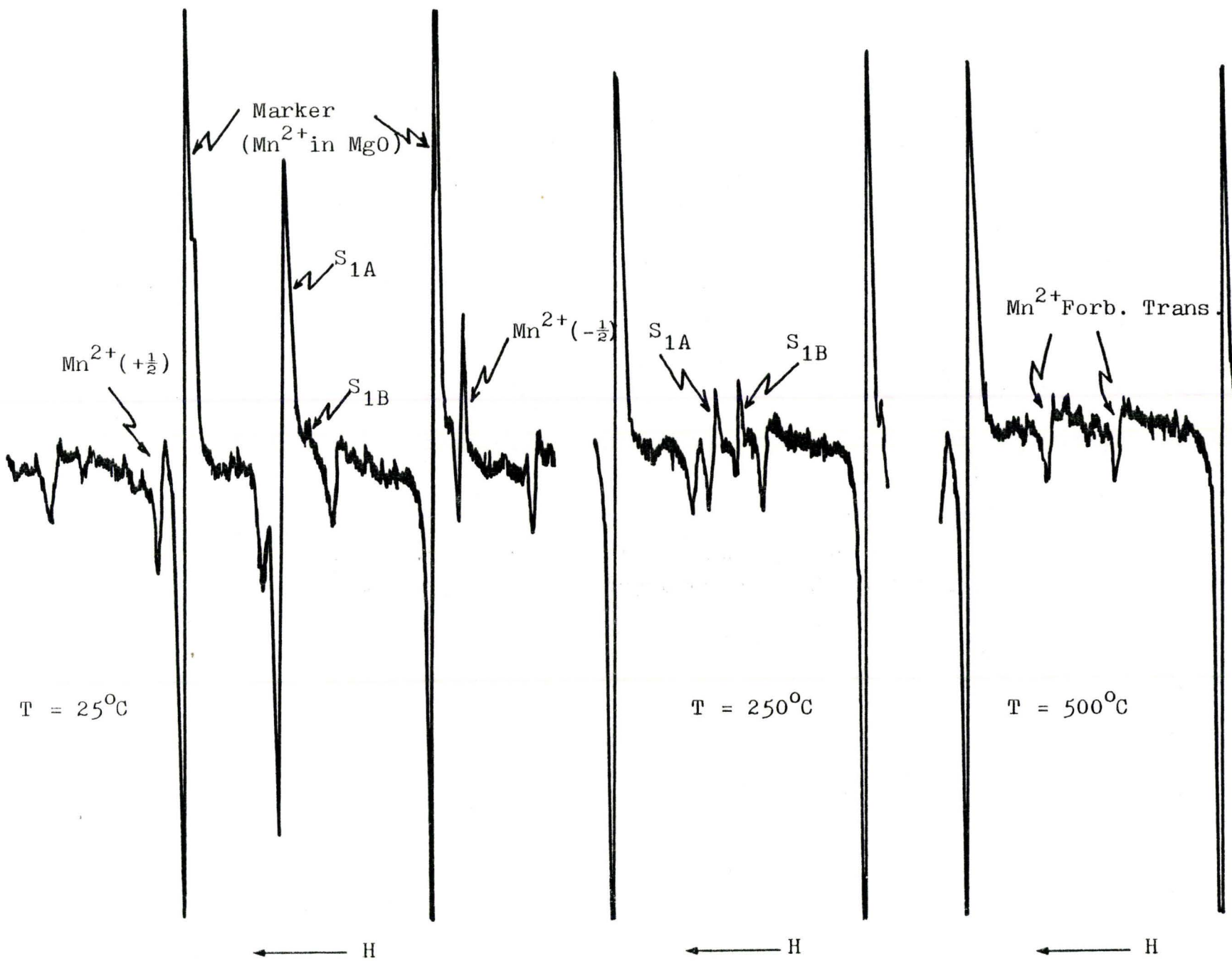





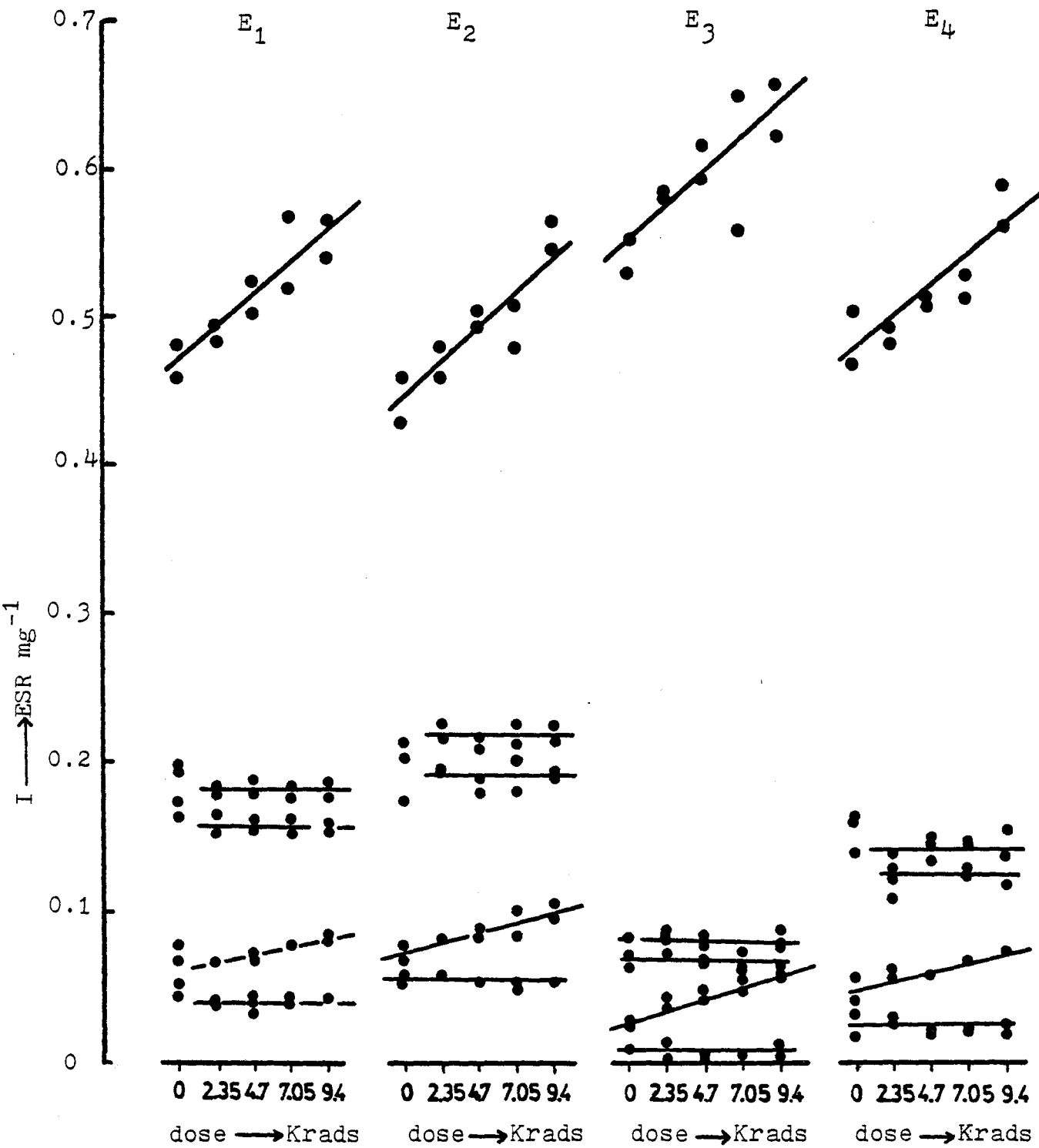


Figure 6.4.4 F/st 77200-E<sub>i</sub> samples. ESR intensity response to additive  $\gamma$ -doses

Legend

-  S<sub>1A</sub>
-  Mn<sup>+2</sup>(- $\frac{1}{2}$ )
-  Mn<sup>+2</sup>(+ $\frac{1}{2}$ )
-  Mn<sup>+2</sup>Forb. Trans. + S<sub>2B</sub>
-  Mn<sup>+2</sup>Forb. Trans.





- (i) the points of each line show an undesirable dispersion.
- (ii) extrapolations have to go back too far, and an unwarranted assumption about linearity far beyond what is acceptable has to be made.

However, all four lines have very similar slopes, a fact which makes the above uncertainties more mild. The extrapolations yield:  $ED_1 = 51 \pm 8$  Krads,  $ED_2 = 43 \pm 7$  Krads,  $ED_3 = 54 \pm 15$  Krads,  $ED_4 = 53 \pm 9$  Krads, with an average:  $\overline{ED}_i = 51.5 \pm 8.0$  Krads\* and an average sensitivity  $\overline{s}_i = 0.0094 \pm 0.0018$  ( $\pm 20\%$ ) ESR  $\text{mg}^{-1}/\text{Krad}$ .

NAA gave the following results for U-contents:  $[U]_1 = 2.75\text{ppm}$ ,  $[U]_2 = 2.74\text{ppm}$ ,  $[U]_3 = 2.88\text{ppm}$ , and  $[U]_4 = 2.63$ . Their average value is  $[\overline{U}]_i = 2.75 \pm 0.15$  (5.7% NAA exp. error, section 4.6). Radioactive element contents other than U (i.e. Th, K, Rb) were found to be below the NAA detection limit. Regarding the above results, we remark on the following:

- (i) It is obvious that the range of the additional  $\gamma$ -doses is too small. This causes the high error of the ED's (up to  $\pm 25\%$ ) and the relatively high dispersion of their values. On the other hand, all the ED values overlap at  $\pm 1\sigma$  level. Their average value (51.5 Krads) could

---

\* the  $\pm$  error is:  $\pm \sigma / n$  where  $\sigma^2 = \frac{\sum_{i=1}^4 \sigma_i^2}{n^2}$  and  $n = 4$ .

be considered to represent the natural dose  $D_n$  absorbed by regions of the E layer which contain approximately 2.75 ppm of uranium.

- (ii) The low  $\bar{s}$  of the E layer is remarkable, in contrast to the stalagmite 76121 (average Top and Base  $\bar{s}=0.029$  ESR  $\text{mg}^{-1}/\text{Krad}$ ). The meaning of this difference will be examined later (see section 6.5).
- (iii) Though the  $I_n$  values display a sufficient range (0.45-0.55 ESR  $\text{mg}^{-1}$ ), the  $[U]$  range is very small, all four  $[U]_i$  being within the  $\pm 5.7\%$  NAA experimental error. This is explained by considering the  $E_i$  samples to have different sensitivities, so that for the same  $D_n$ , different  $I_n$  is obtained ( $I_n = sD_n$ ). The  $\pm 20\%$  uncertainty of the average  $\bar{s}$  and the 51.5 Krads of the average ED (presumably  $D_n$ ) yield :  $I_n = 0.485 \pm 0.095$  ESR  $\text{mg}^{-1}$ . The approximately  $\pm 0.1$  ESR  $\text{mg}^{-1}$  error yields an expected  $I_n$  range: 0.43-0.55 ESR  $\text{mg}^{-1}$ , which can explain the spread of the measured  $I_n$  values. In the following we consider that  $D_n \cong \bar{ED}_i = 51.5 \pm 8.0$  Krads for  $[U] \cong [\bar{U}]_i = 2.75 \pm 0.15$  ppm.

#### 6.4.1 ESR intensity isochron: complications. The "[Mn<sup>2+</sup>]-effect"

The small  $[U]$ -range  $E_i$  samples displayed made the

isochron construction impossible. To overcome this, samples from the F and O layers were used (see section 6.3-(iii)). The eight samples, namely,  $F_1, F_2, F_3, F_4, O_1, O_2, O_3, O_4$  were powders of grain size: 0.075-0.100 mm. Their  $I_n$  and [U] were measured as in the case of  $E_i$  samples. The results were encouraging because besides the good range of  $I_n$ , we observed a reasonable range of [U], i.e. 2.3-3.2 ppm U for  $F_i$  samples and 1.6-2.1 ppm U for  $O_i$  samples. Figure (6.4.1.1) shows the plot of  $I_n$  versus [U] for all the available samples, i.e.  $E_i, F_i$  and  $O_i$  (twelve).

On first inspection, Figure (6.4.1.1) shows a relatively good linear correlation between  $I_n$  and [U]. However, we note that for each of the three layers (E,F,O) there is one sample ( $E_3, F_3, O_1$ ) which is distinctly aberrant. We note that in each case this is a sample which also displays an exceptionally low  $Mn^{2+}$  ESR signal. Ikeya (1975) has noted that Mn appears to suppress the intensity of the trapped free-electron signal in calcite, presumably due to the high recombination rate resulting from the presence of such an ion. To test this, the samples have been analysed for Mn content by INAA. Unfortunately, INA analyses are not very precise in determining [Mn], so we have chosen to use the  $Mn^{2+}$  ESR signal as a monitor of [Mn], calibrating a working curve from the INAA data (Figure 6.4.1.2). It was assumed that all the samples have almost identical  $[Mn^{2+}]/[Mn]$  ratios. From that curve we calculated the

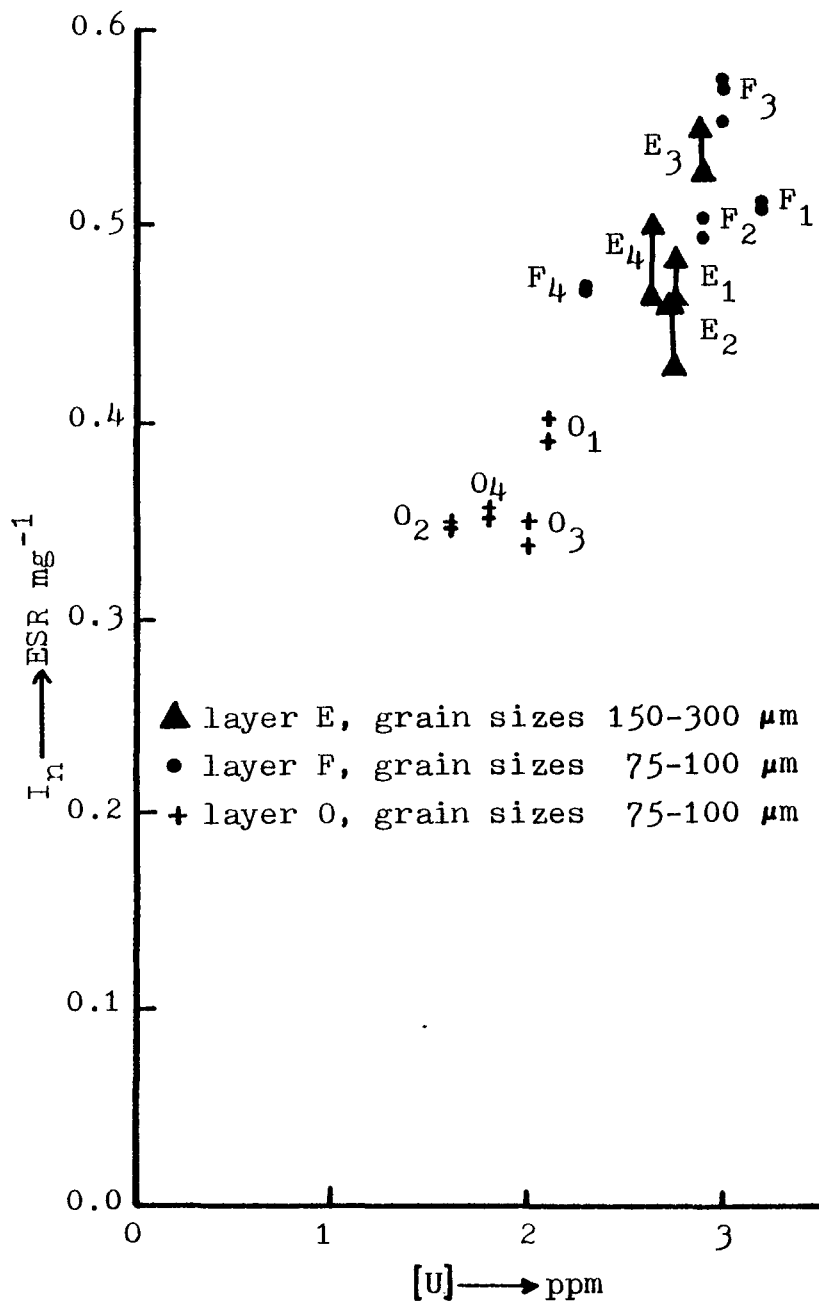


Figure 6.4.1.1 F/st 77200. ESR intensity of natural  $S_{1A}$  versus [U] for all the available samples.

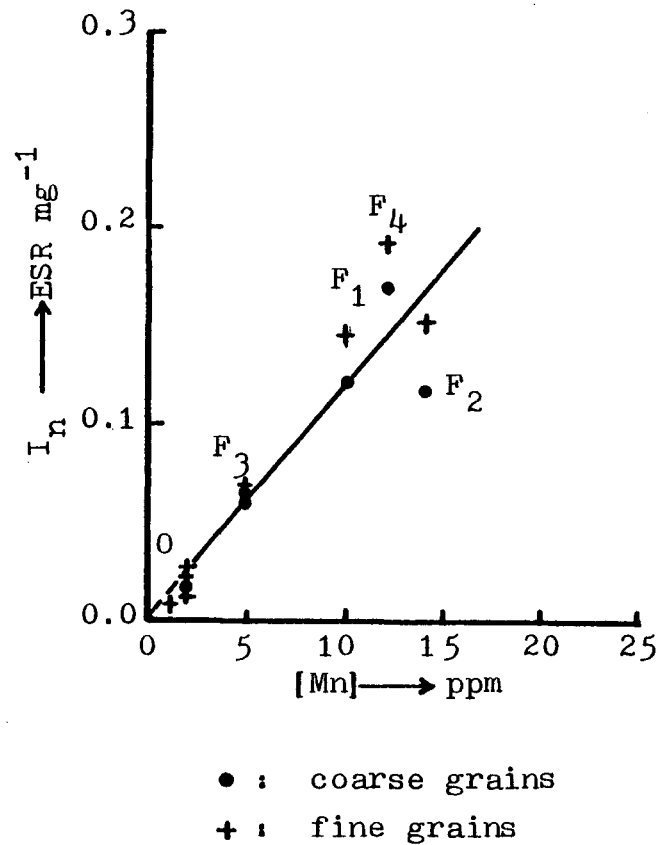


Figure 6.4.1.2 F/st 77200. ESR intensity of  $\text{Mn}^{2+}(-\frac{1}{2})$  peaks versus [Mn]. Calibration curve.

Mn contents of all  $E_i$ ,  $F_i$  and  $O_i$  samples and plotted their  $I_n$  versus  $[Mn]$  (Figure 6.4.1.3). We note a clear suppression of  $I_n$  as  $[Mn]$  increases for a single layer, although different layers (with presumably different  $D_n$ ) define different lines. If  $[Mn]$  differences are indeed the reason that the  $(I_n, [U])$  points in Figure (6.4.1.1) are scattered, and if the negative slopes of  $I_n$ - $[Mn]$  lines in Figure (6.4.1.3) are due to an inverse relationship between  $\underline{s}$  and  $[Mn]$ , then we could expect a plot of  $I_n$  versus the ratio  $[U]/[Mn]$  to align the points. Figure (6.4.1.4) shows such a plot. All  $F_i$  and  $E_i$  points lie around a line. We note that:

(i)  $E_3$  and  $F_3$  lie above  $F_1$ , the point with the highest  $[U]$ .

(ii)  $E_2$  occupy the lower end of the line, as having the lowest  $I_n$ .

The  $O_i$  points are distinct from the  $F_i$  and  $E_i$  points, because the corresponding samples belong to a distinct geochemical environment, as shown by their lower  $[U]$  and  $[Mn]$ . On the other hand, both E and F layers seem to have been formed under similar geochemical conditions and could be considered as a single layer, the "EF" layer.

Speaking on Mn, it is worthy to recall Gascoyne's opinion (1979, p. 367) that Mn probably is incorporated in most speleothems as adsorbed or detrital oxides, hydroxides, carbonates and organic compounds. In these cases, Mn could no possibly affect  $I_n$ . Only if Mn is incorporated in the

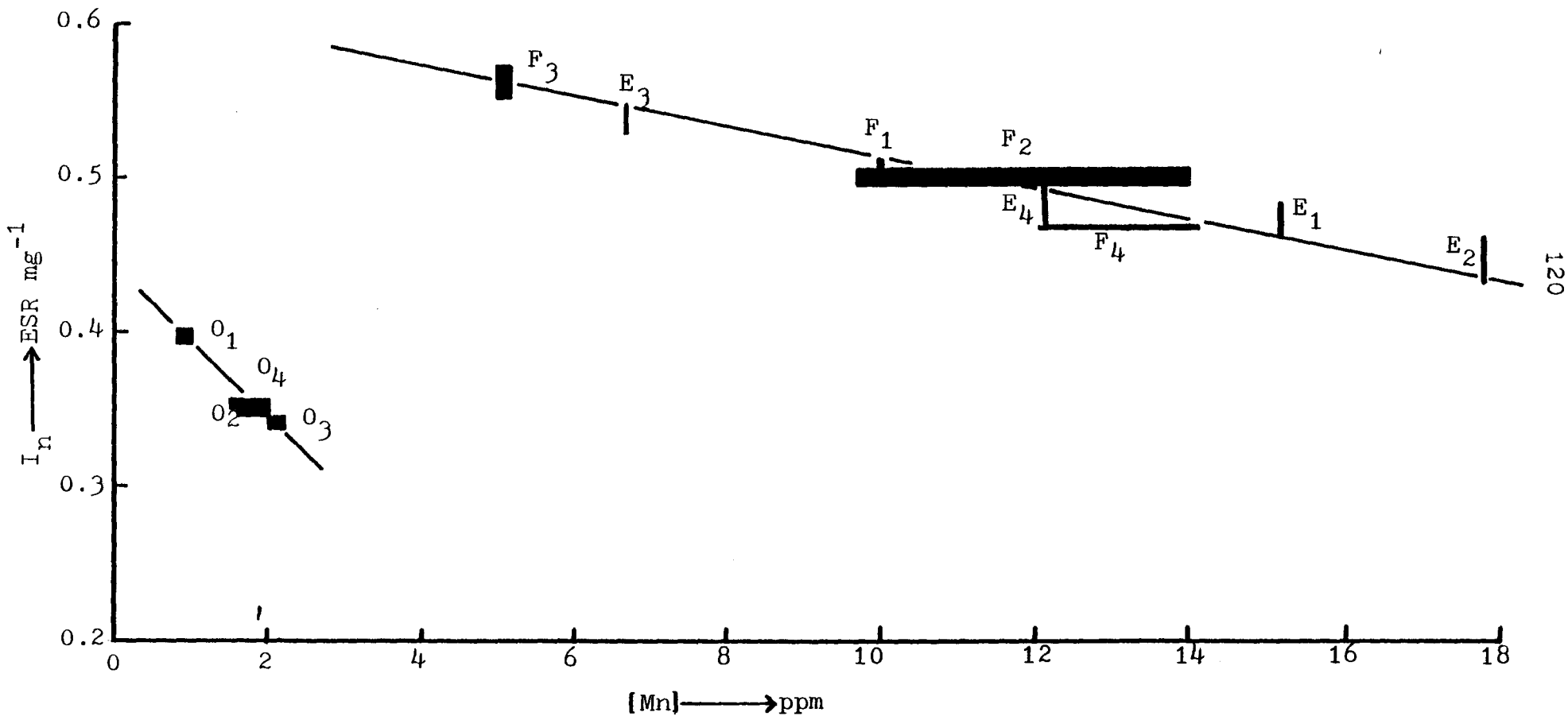
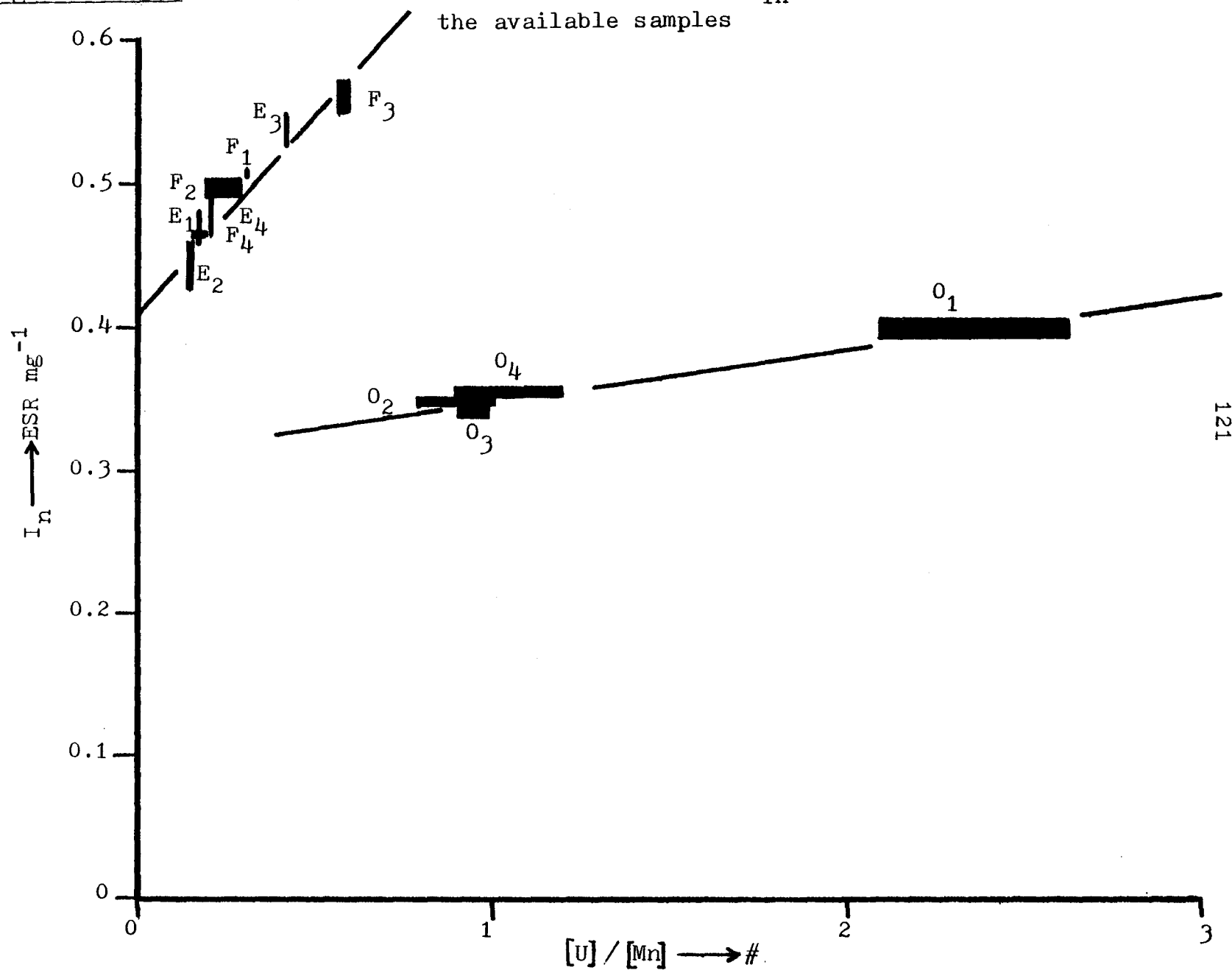


Figure 6.4.1.3 F/st 77200. ESR intensity of natural  $S_{1A}$  versus  $[\text{Mn}]$  for all the available samples.

Figure 6.4.1.4 F/st 77200. ESR intensity of natural S<sub>1A</sub> versus [U]/[Mn] for all the available samples



calcite itself can it suppress the  $I_n$  of trapped electrons, as it does in our case. This is quite an indication that the Mn of the 77200-E,F,0 calcites has occupied a structural site in the lattice, most likely as  $Mn^{2+}$  substitutional for  $Ca^{2+}$ .

In conclusion, we feel that:

- (i) variations of  $I_n$  within a single speleothem layer are determined not only by the U-content but also by the concentration of element -ESR sensitizers, such as structural  $Mn^{2+}$ .
- (ii) variations of  $I_n$  between different layers are determined by the radioactive element content and the age.

#### 6.4.2 Experimental determination of a-value

To estimate an ESR isochron age, an a-factor has to be known. The a-value of  $E_3$  was measured by alpha irradiations followed by ESR analysis. This value was considered to be representative of the EF layer and possibly of the O layer too (see next section). The a-value of  $E_3$  was also measured by TL analysis (see section 6.8.2) to check the ESR result.

Sample preparation and alpha irradiations were done by D.J. Huntley of the Department of Physics, Simon Fraser University, Burnaby, B.C. He separated by settling grains  $<10 \mu m$  (section 2.6 - sample form) and did irradiations



using six  $^{241}\text{Am}$  alpha sources of average strength  $S=0.385 \mu\text{m}^{-2}\text{min}^{-1}$  (Oxford calibration figure). Two aliquots, a few mg each, were given 3h and 6h of alphas respectively, and were sent back for ESR analysis. The process of the samples' removal from the vials\* resulted in a suspension of calcite grains and paper fibers in acetone. The two suspensions were poured onto separate glass plates and left to dry at approximately  $40^{\circ}\text{C}$ . Finally, a mixture of calcite grains and paper fibers was obtained. To get the natural ESR intensity, grains less than  $10 \mu\text{m}$  had to be used because of the "grain size effect" (see section 4.2) which is discussed thoroughly in connection with the TL results (see section 6.8.3). That fraction ( $\sim 10-1 \mu\text{m}$ ) was obtained by settling (15 min-16h) in methanol (see: Muller, 1967, p.76-78). Microscopic examination showed that all  $\text{E}_3$  powders (natural and irradiated) had very similar ranges of grain sizes. Besides, the volume fraction occupied by calcite in the grain-fiber mixtures seemed to be much the same in both of them. This means that both mixtures have probably the same weight fraction  $f$  (%) of calcite grains. The samples were placed in quartz tubes and their ESR signals were obtained several weeks after irradiation (Varian ESR

---

\* The vials were filled with acetone and left a couple of days to let the powders come unstuck, but only the use of ultrasonic rod solved the problem. The bottom of the vial cups is usually covered with sheets of paper and plastic, to make the closed vials impermeable.

spectrometer). Calibration was done by weight, which was not identical for all the samples but quite small (5-20 mg) for the problems arising from the  $H_m$  inhomogeneity (see section 4.5) to be ineffective.

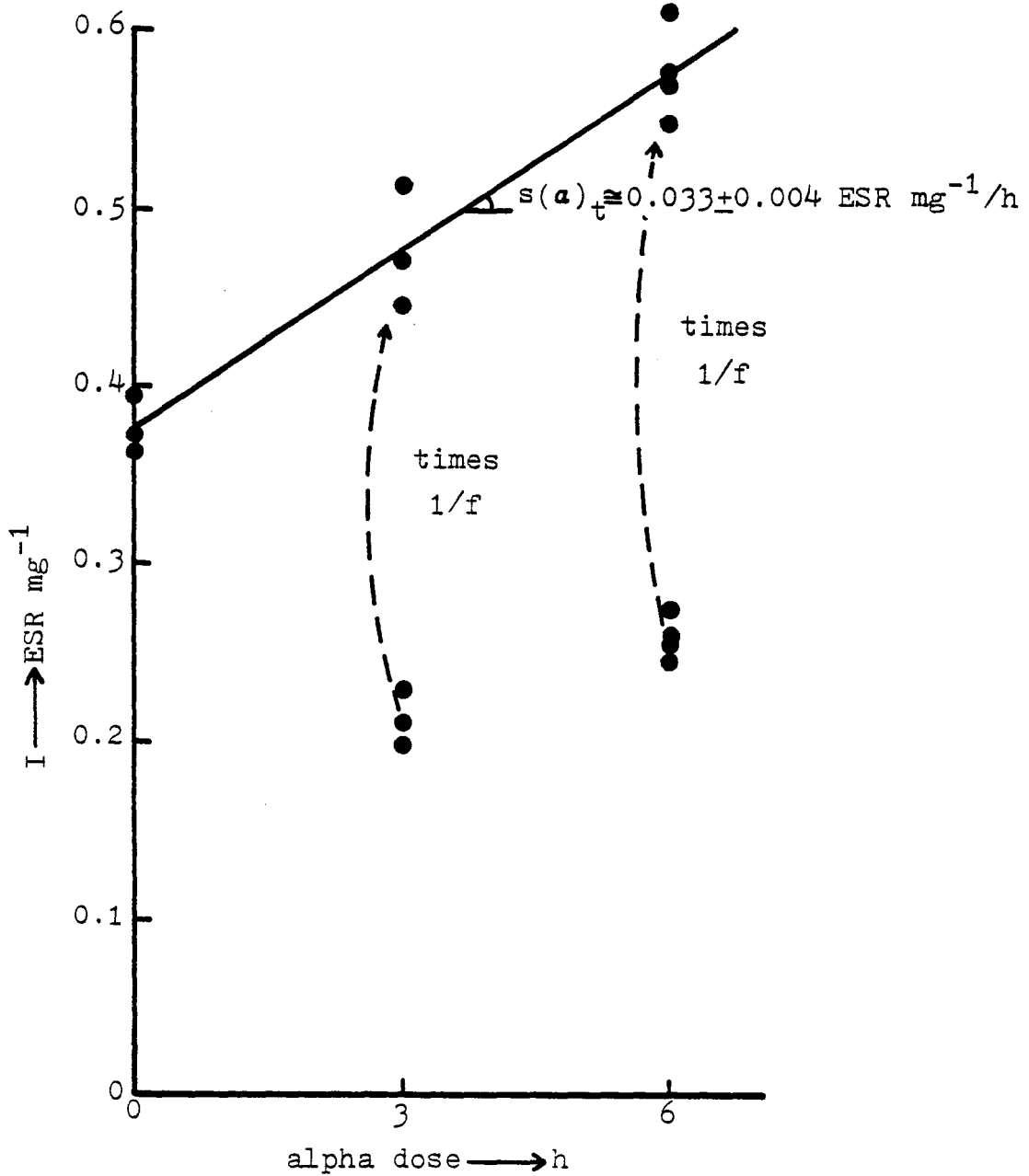
Figure (6.4.2.1) shows the results. The  $I$  of both mixtures was multiplied by a factor of  $1/f$  ( $f \cong 0.45^*$ ), so that the corrected  $I$  ( $\text{ESR mg}^{-1}$ ) will be calibrated by the calcite weight only. The best fit line yields an  $\text{ED} = 11.4 \pm 0.5$  h and a slope  $s(\mathbf{a})_t = 0.033 \pm 0.004 \text{ ESR mg}^{-1}/\text{h}$ , but the error may be higher due to uncertainties arising from the  $1/f$  correction. The  $a$ -value is calculated from the formula (1.6.2.3), some parameters of which have been defined ( $x$ ) or determined (1300) for irradiation with alphas of 3.7 MeV. These parameters, however, seem to be independent of  $\mathbf{a}$ -particle energy over the range of 1-7.3 MeV (see section 2.6 (iv)) in the case of TL. This independence may be acceptable in ESR, too. Now, for  $s(\mathbf{a})_t = 0.033 \pm 0.004 \text{ ESR}$

\* To estimate  $f$ , it is accepted that ESR intensity should have a linear response to additive alpha dose, as in the case of TL intensity (see section 6.8.1). If  $I_0$ ,  $I_3$  and  $I_6$  are ESR intensities of natural (0h) and irradiated (3h, 6h) samples, the latter ones should have  $I_3/f$  and  $I_6/f$  intensities instead of  $I_3$  and  $I_6$  respectively. Linearity between  $I_0$ ,  $I_3/f$  and  $I_6/f$  means that the slope:  $(I_3/f - I_0)/3h$  should be equal to the slope:  $(I_6/f - I_3/f)/3h$ , i.e.

$$\frac{I_3}{f} - I_0 = \frac{I_6}{f} - \frac{I_3}{f} \longrightarrow \frac{1}{f} = \frac{I_0}{2I_3 - I_6}$$

If we use the average values ( $\text{ESR mg}^{-1}$ ) of  $I_0$ ,  $I_3$  and  $I_6$  (0.3755, 0.2120, 0.2562), we get:  $f = 0.4467 \cong 0.45$

Figure 6.4.2.1 F/st 77200-E<sub>3</sub>. ESR intensity response to additive  $\alpha$ -doses (signal S<sub>1A</sub>).



$\text{mg}^{-1}/\text{h}$ ,  $s(\gamma) = 0.0094 \pm 0.0018$  ESR  $\text{mg}^{-1}/\text{Krad}$ , and  $S = 0.385$   
 $\mu\text{m}^{-2}\text{min}^{-1}$ , formulas (1.6.2.4) and (1.6.2.3) give: a-value =  
 $0.12 \pm 0.02$ , the  $\pm$  error being in fact higher due to uncer-  
 tainties in  $s(a)_t$  determination. The a-value given by  
 TL for the same material is  $0.140 \pm 0.014$  (see section 6.8.2).  
 There is good agreement between the ESR and TL a-values.  
 In the following calculations we use the a-value  $0.13 \pm 0.02$ .

### 6.5 Determination of the IS and $D_{\text{ext}}$

The limited duration of this project did not allow  
 ED's of  $F_i$  and  $O_i$  samples to be obtained. The only product,  
 therefore, was the ESR intensity isochron (section 3.7.1).  
 This requires all samples to have very similar values of  $p$ ,  
 $q$ ,  $t$ ,  $a$ , and  $\underline{s}$ . In the case of the EF layer, similarity of  
 $p$ ,  $q$ ,  $t$  is very likely, but a-factor and  $\underline{s}$  may vary, yielding  
 scattered  $E_i$ ,  $F_i$  points in Figure (6.4.1.1). The best fit  
 line drawn through the  $E_i$ ,  $F_i$  points could average possible  
 a-factor and  $\underline{s}$  differences. Such a line, however, yields  
 an IS and  $I_{\text{ext}}$  (intercept at  $[U] = 0$ ) both with great  
 uncertainty. The alternative is to use all  $E_i$ ,  $F_i$ , and  $O_i$   
 points, and draw an ESR intensity multilayer isochron.  
 Such an isochron would give an average date for the  
 EF-0 speleothem layers.

Multilayer isochron dating requires a continuous and  
 rapid growth of the speleothem between the layers being

used (see section 3.7.2). The continuous growth from the O layer to the FE layer is indicated by the absence of hiatus in between. The relatively rapid growth between the said layers is indicated by the location of the  $O_i$  points on the isochron plot (Figure 6.5.1). The average  $[U]$  and  $I_n$  values of  $E_i$  and  $F_i$  points are approximately 2.80 ppm and 0.500 ESR  $\text{mg}^{-1}$  respectively. If  $D_{\text{ext}}$  was negligible ( $I_{\text{ext}}=0$ ), the isochron line would be determined by the points  $(I_n, [U]) = (0,0)$  and  $(I_n, [U]) = (0.5, 2.8)$ . Such a line yields:  $IS_{\text{max}} = 0.18 \pm 0.03$  ESR  $\text{mg}^{-1}/\text{ppmU}$ . It is clear that  $O_i$  points lie very close to that line, although the O layer is older than layer EF. This feature might mean that the O layer:

- (i) -is not much older than the EF layer
  - has  $\underline{g}$  and a-value similar to those of layer EF
  - absorbed relatively small external dose
- (ii) -is sufficiently older than layer EF
  - has  $\underline{g}$  and a-value sufficiently lower than those of layer EF, so that the  $\underline{g}$  and a-value effect on  $I_n$  competes with that of  $\underline{t}$ .

The following observations, however, seem to support the first case. All the speleothem materials we have studied are white and dense calcites. Some of their data are listed below:

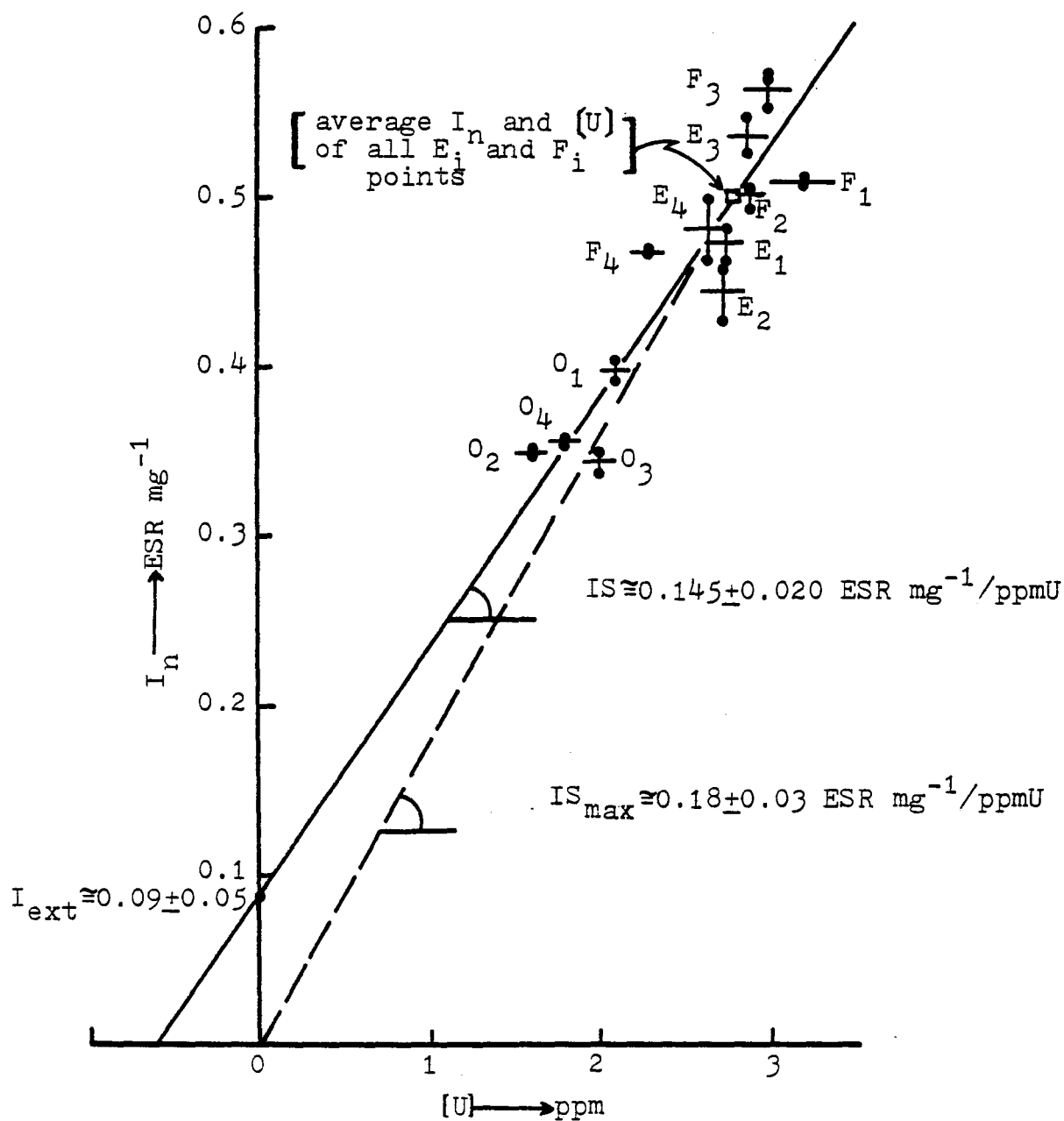


Figure 6.5.1 F/st 77200, natural  $S_{1A}$ : ESR intensity multilayer-isochron.

#	Sample	[U] ppm	[Mn] ppm	[U] / [Mn]	$\underline{s}$ ESR $\text{mg}^{-1}/\text{Krad}$
1	76121-Top	2.6	<1	>2.6	0.0323 $\pm$ 0.0027
2	76121-Base	1.9	<1	>1.9	0.0250 $\pm$ 0.0015
3	77200-E	2.65-2.85	7-18	0.15-0.40	0.0094 $\pm$ 0.0018
4	77200-0	1.6 -2.1	1-2	0.8-2.1	?

We note that:

-samples of low [Mn] yield high  $\underline{s}$  (#1,2) while those of high [Mn] yield low  $\underline{s}$  (#3).

-in samples of similar [Mn] in ppm level (#1,2), the higher the [U] they have, the higher the  $\underline{s}$  they yield (#1).

-in samples of similar [U] (#1,3), the lower the [Mn] they have, the higher the  $\underline{s}$  they yield (#1). Thus in samples of similar [U] (#2,4), the higher the [Mn] they have the lower the  $\underline{s}$  they should yield (#4).

Therefore, for 77200-0, the  $\underline{s}$  value might be expected to be lower than 0.025 ESR  $\text{mg}^{-1}/\text{Krad}$ . Considering the above remarks, it seems that  $\underline{s}$  depends directly on [U] and [Mn]<sup>-1</sup>, so that a plot of  $\underline{s}$  versus [U] / [Mn] may have some meaning. Figure (6.5.2) shows that the 77200-0 sample may have an  $\underline{s}$  value higher than 0.0094 ESR  $\text{mg}^{-1}/\text{Krad}$ . If such is the case, the consideration (ii) is not very likely to occur.

The best fit of the E<sub>i</sub>, F<sub>i</sub> and O<sub>i</sub> points (Figure 6.5.1) yields an intensity-IS=0.145 $\pm$ 0.020 ESR  $\text{mg}^{-1}/\text{ppmU}$  and an I<sub>ext</sub>=0.09 $\pm$ 0.05 ESR  $\text{mg}^{-1}$ . To convert ESR intensity to dose

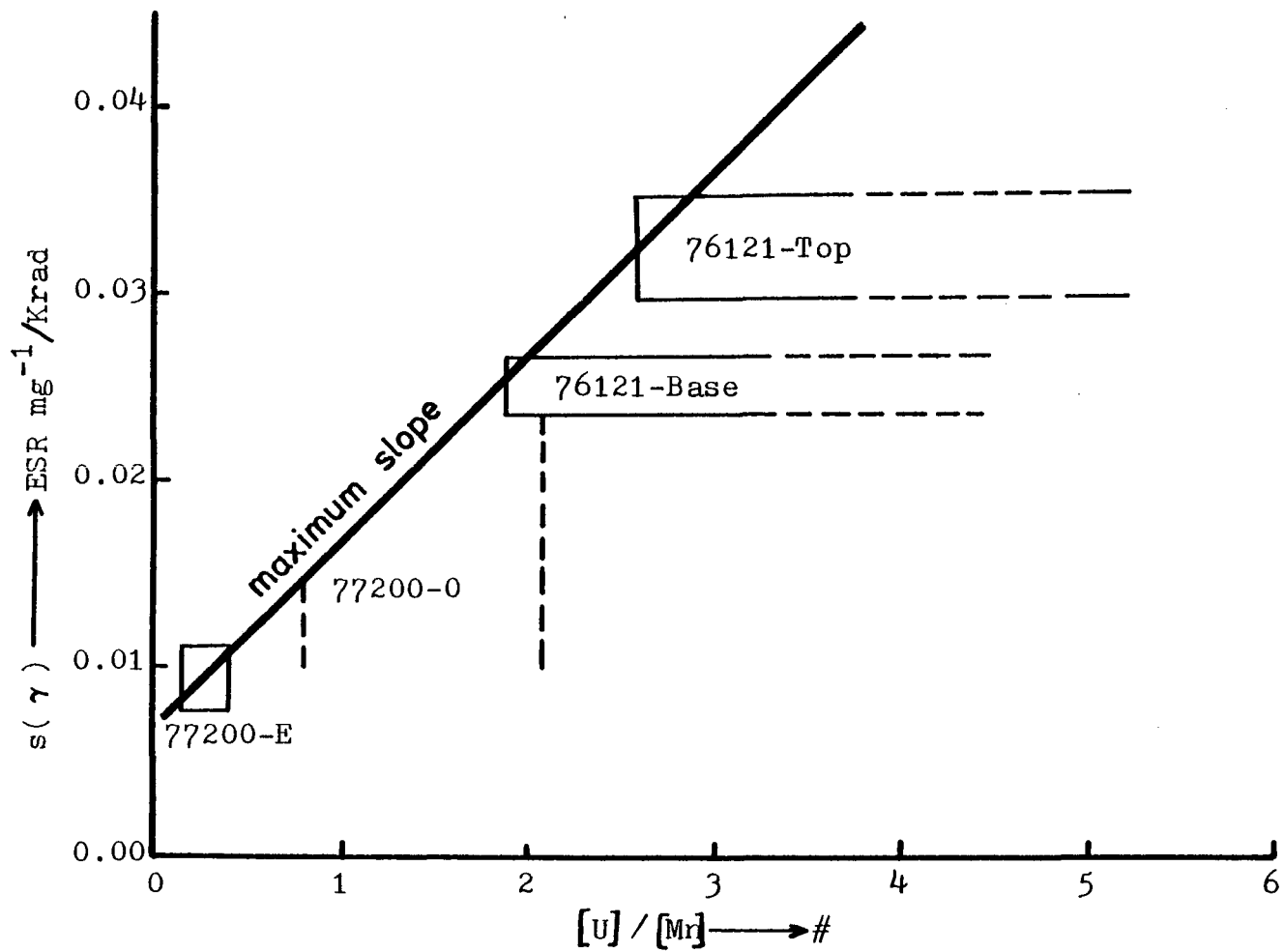


Figure 6.5.2  $S_{1A}$  sensitivity to  $\gamma$ -rays versus  $[U]/[Mn]$  for various samples



the already measured  $s=0.0094\pm 0.0018$  ESR  $\text{mg}^{-1}/\text{Krad}$  is used; so equation  $D_{\text{ext}}=I_{\text{ext}}/s$  gives:  $D_{\text{ext}}=9.6\pm 5.3$  Krads and slopes become:  $IS=\frac{\text{intensity}-IS}{s}=15.4\pm 2.1$  Krads/ppmU and  $IS_{\text{max}}=19.0\pm 3.2$  Krads/ppmU. The above conversion is valid only if the samples involved in the isochron plot have uniform  $s$ ,  $t$ , and  $a$ -value. In our case, the relatively large number of samples (12) may average possible small differences of these parameters, thus justifying the conversion. To see how the above results fit with the ED of the E layer, a diagram of  $D_n$  versus  $[U]$  was made (Figure 6.5.3) by plotting the data point for the E layer for which ED has actually been determined and comparing it with the line estimated above. There is good agreement.

### 6.6 Determination of the $\overline{R}_{\text{ext}}$ and $\bar{a}$ -value

To determine the  $\overline{R}_{\text{ext}}$ ,  $t$  is considered as the average U/Th age of EF and O layers. The Top 2 cm and Base 2.5 cm samples yielded U/Th dates:  $289\pm 22$  Ka and  $>350$  Ka respectively. The Base sample has  $p=1.239$  and  $q=1.032$  which yield an U/Th date  $\sim 380$  Ka. Gascoyne (1979, p. 94) felt that any attempt to push the limit of U/Th dating method back beyond 400 Ka, does not yield reliable dates, and he accepted a safe maximum age of 350 Ka. If the date, 380 Ka, has some meaning, then the O layer may have an age of approximately 350 Ka, being younger than Q and older than EF layers.

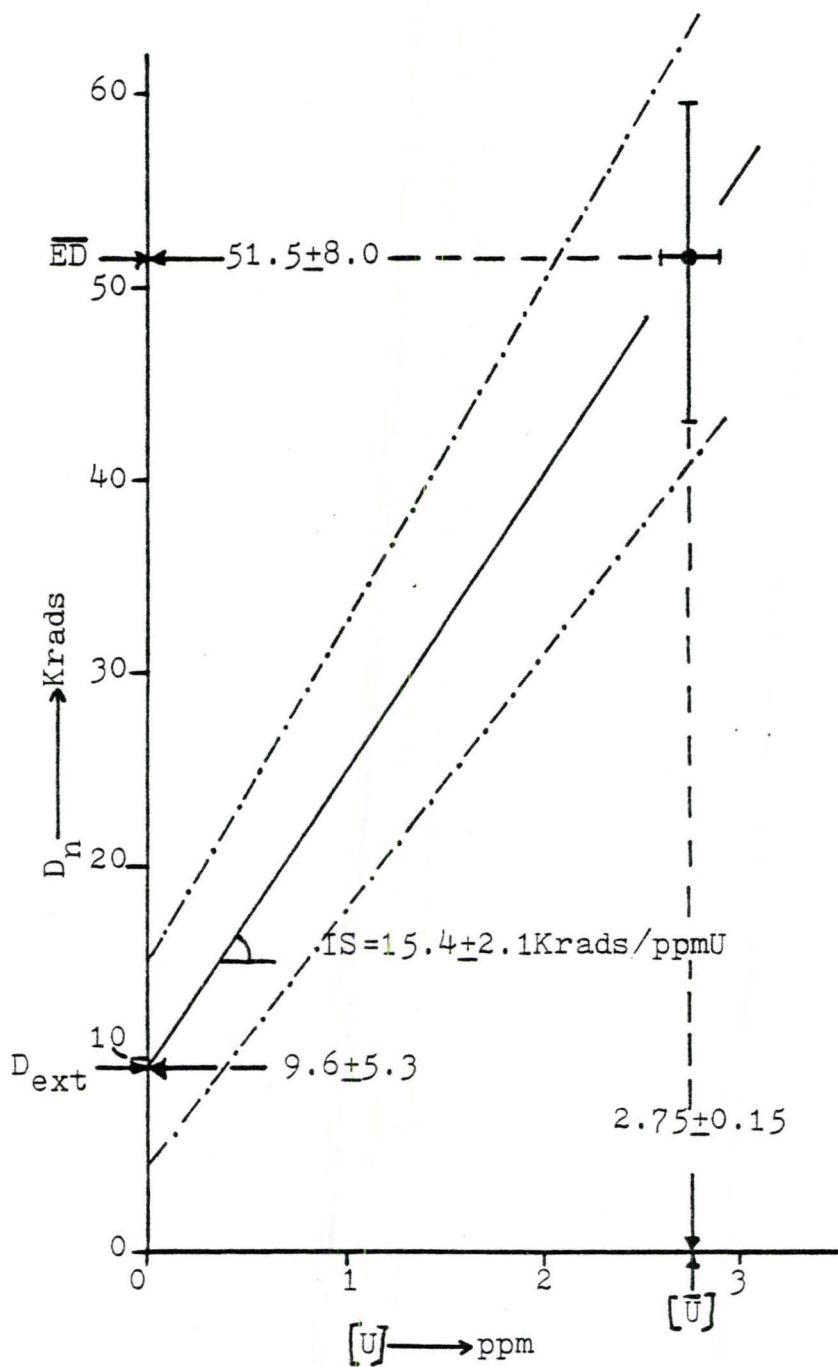


Figure 6.5.3 F/st 77200. 'Real' isochron line and data point for the E layer ( $\overline{ED}$ ,  $[U]$ ).

Thus, the average age of the EF-0 layers, about the average age of the speleothem 77200, seems to be  $t \cong 320 \pm 50$ , and  $\overline{R}_{\text{ext}} = D_{\text{ext}}/t = 30.0 \pm 9.1$  mrad/yr, which is a reasonable value, compared with values from other caves (Figure 4.6.1).

To determine the "average" a-factor ( $\bar{a}$ ) of the EF-0 layers, the equilibrium model is considered ( $t > 200\text{Ka}$ ), as it is interpreted by Bell and Wintle (see section 3.3.2).

(i) Equation (3.5.4) is re-written as:

$\bar{a} = (IS/t - R_{\beta}' - R_{\gamma}')/R_{\alpha}'$ , where IS and  $t$  are as given above,  $R_{\beta}' + R_{\gamma}' = 26.1$  mrad/yr ppmU, and  $R_{\alpha}' = 278.3$  mrad/yr ppmU (no radon loss), the last two as given by Bell (1979). Thus:

$$\bar{a} (\text{Bell}) = 0.08 \pm 0.02$$

(ii) Equation (3.5.3) is re-written as:

$\Delta_1 = IS/ct^*$  where IS and  $t$  are as given above and  $c = 3.7965 \cdot 10^{11} \text{ Ma}^{-1} \text{ ppmU}^{-1}$ . Thus

$\Delta_1 = 12.7 \pm 1.7 \cdot 10^{-11}$  Krads. Figure (6.6.1) shows the linear relation between a-factor and  $\Delta_1$ , according to values given by Wintle (1978). For

$\Delta_1$  as found above, Figure (6.6.1) yields

$$\bar{a} (\text{Wintle}) = 0.11 \pm 0.03.$$

The a-values found above overlap at  $1\sigma$  level. The two values correspond to differing interpretations of effective

\* To illustrate how the approximation  $f(a, p, q, t) \cong \Delta_1 t$  (see section 3.3.2) works we substitute in  $f(a, p, q, t)$  the p, q, t values of the Top 2 cm as found by U/Th dating. We get:

$$f(a, p, q, t) = \Delta_1 t + \Delta_2 \cdot 0.1315 - \Delta_3 \cdot 0.1400 = \Delta_1 t + \Delta_3 \left( \frac{\Delta_2 \cdot 0.1315}{\Delta_3} - 0.1400 \right) \cong \Delta_1 t, \text{ because } \Delta_2 / \Delta_3 = 1.08 \pm 0.03$$

for any a-value.

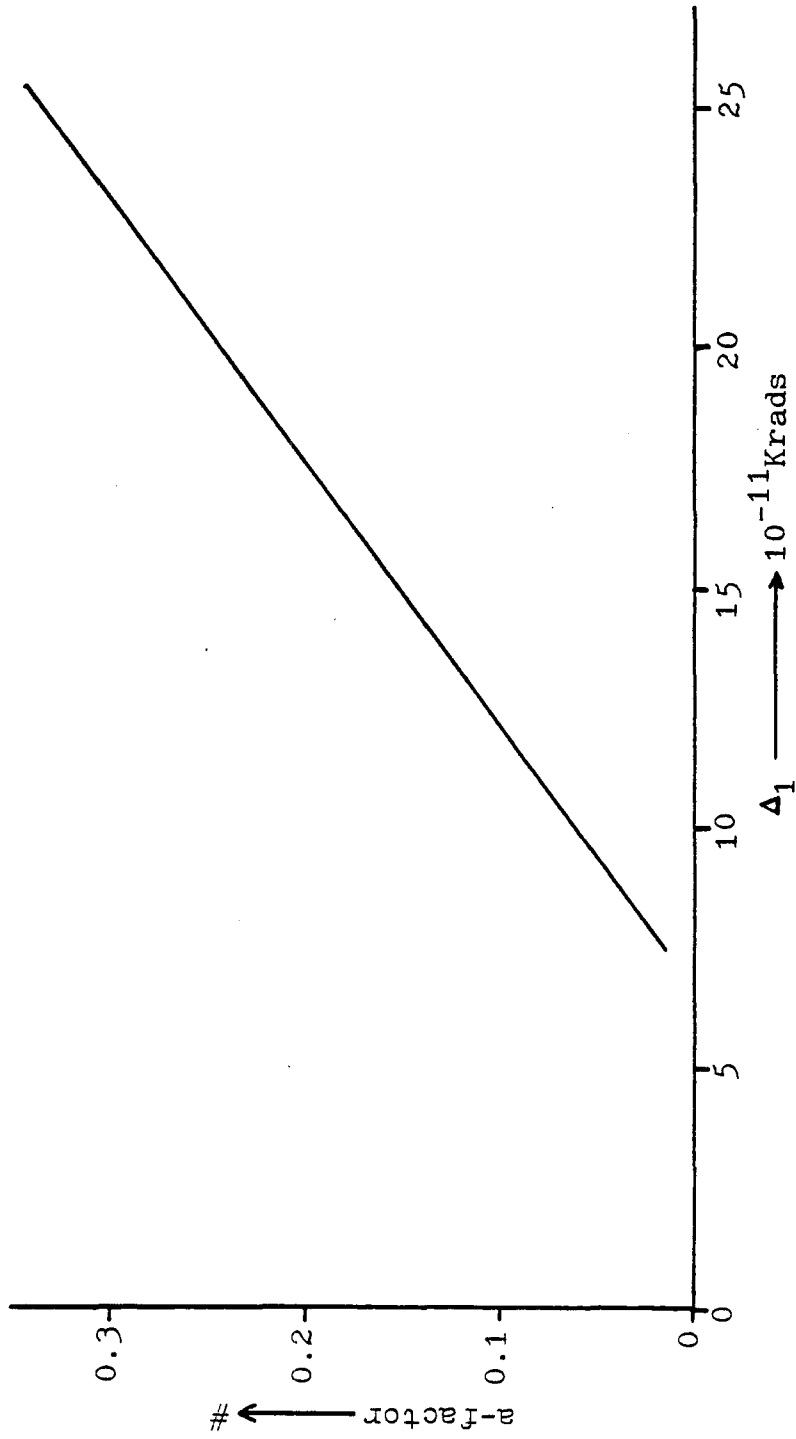


Figure 6.6.1 a-factor as a function of  $\Delta_1$  (Wintle, 1978).

$\alpha$ -doses used by Bell and Wintle respectively. The experimental determinations of  $\alpha$ -value for  $E_3$  gave approximately  $0.12 \pm 0.02$  (ESR, see section 6.4.2) and approximately  $0.140 \pm 0.014$  (TL, see section 6.8.2). These values are closer to 0.11 than to 0.08, a fact which may support Wintle's consideration, although all four values are very similar and three of them (0.11, 0.12, 0.14) overlap within the precision of the analysis.

### 6.7 Determination of the age $t$

Having determined both IS and  $\alpha$ -factor, what is left for  $t$  determination is to decide if a disequilibrium or an equilibrium approach should be considered. The preliminary test (see section 3.6.1) is shown in Figure (6.7.1) and indicates an age greater than 200 Ka. Thus the equilibrium model is appropriate and equations (3.5.4) and (3.5.3) can be used. The available data is:  $IS = 15.4 \pm 2.1$  Krads/ppmU  
 $\alpha = 0.13 \pm 0.02$ ,  $c = 3.7965 \cdot 10^{11} \text{ Ma}^{-1}/\text{ppmU}$ ,  $R'_\alpha = 278.3$  mrads/yr ppmU and  $R'_\beta + R'_\gamma = 26.1$  mrads/yr ppmU (no radon loss),

$\Delta_1 = 13.8 \pm 1.0 \cdot 10^{-11}$  Krads (as inferred from Figure (6.6.1) for  $\alpha = 0.13 \pm 0.02$ ). So: equation (3.5.4)  $\rightarrow t = 247 \pm 34$  Ka (Bell) and equation (3.5.3)  $\rightarrow t = 294 \pm 40$  Ka (Wintle). Though these dates overlap at  $1\sigma$  level, the second one fits better with the U/Th dates of this speleothem. This may support Wintle's consideration on the effective alpha doses, as in

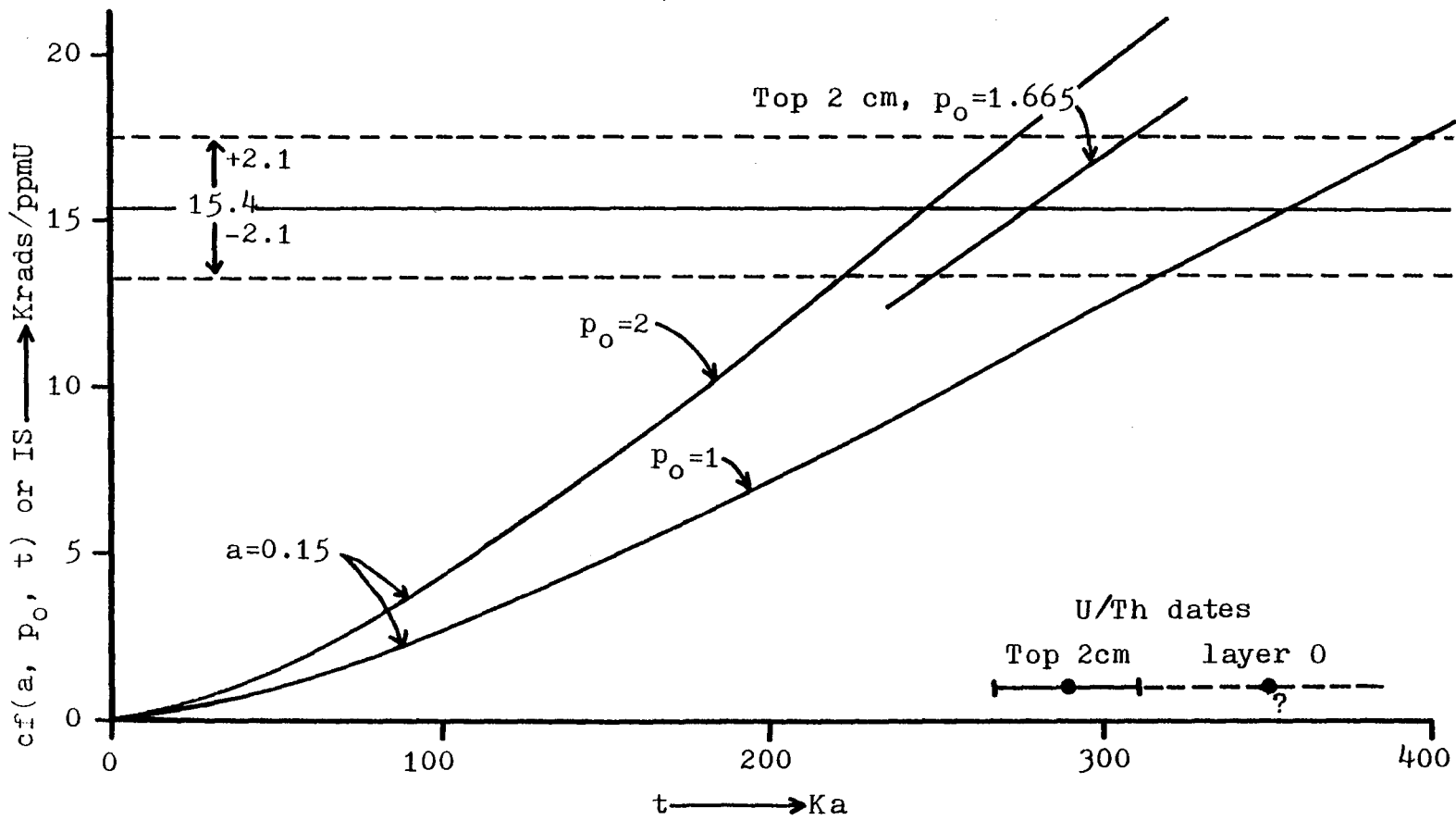


Figure 6.7.1 F/st 77200. Preliminary test to estimate a gross  $t$ .

the case of the  $\bar{a}$  factor (see section 6.6).

The "isochron" date of  $294 \pm 40$  Ka and the assumed average U/Th date of the EF-0 layers of  $320 \pm 50$  Ka agree well at  $1\sigma$  level. The difference of their absolute values ( $294 < 320$ ) may be due to:

- a high  $a$ -value (0.13) and/or an old age (350 Ka) assumed for the 0 layer
- a low IS, because of differences in the 'true' age of EF and 0 layers, which were assumed here to be 'coeval'.

On the other hand, if the 0 layer is ignored, there are two options:

- (i)  $D_{\text{ext}} > 0$ . The best fit line through the  $E_i, F_i$  points (isochron plot) yields  $IS = 15.6 \pm 5.9$  Krads/ppmU and  $D_{\text{ext}} = 9.0 \pm 16.5$  Krads. Equation (3.5.3) gives a date of  $t = 298 \pm 84$  Ka. The  $\pm 28\%$  standard error is too high and the  $D_{\text{ext}}$ -value is actually useless.
- (ii)  $D_{\text{ext}} \cong 0$ . Though there is no evidence other than the  $O_i$  points' location on the isochron plot that such might be the case, a zero  $D_{\text{ext}}$  can give an upper limit of the age of layer EF. The  $IS_{\text{max}}$  (see section 6.5) yields:  $t_{\text{max}} = 363 \pm 61$  Ka.

The above discussion shows that the role of  $D_{\text{ext}}$  in the evaluation of  $t$  is not insignificant, and the  $O_i$  points have to be included in the determination of IS. The age assumption about the 0 layer seems to be less conducive to error than

ignorance of  $D_{\text{ext}}$ . The U/Th and ESR isochron dates for the various cases considered above are displayed in Figure (6.7.2).

### 6.8 TL study

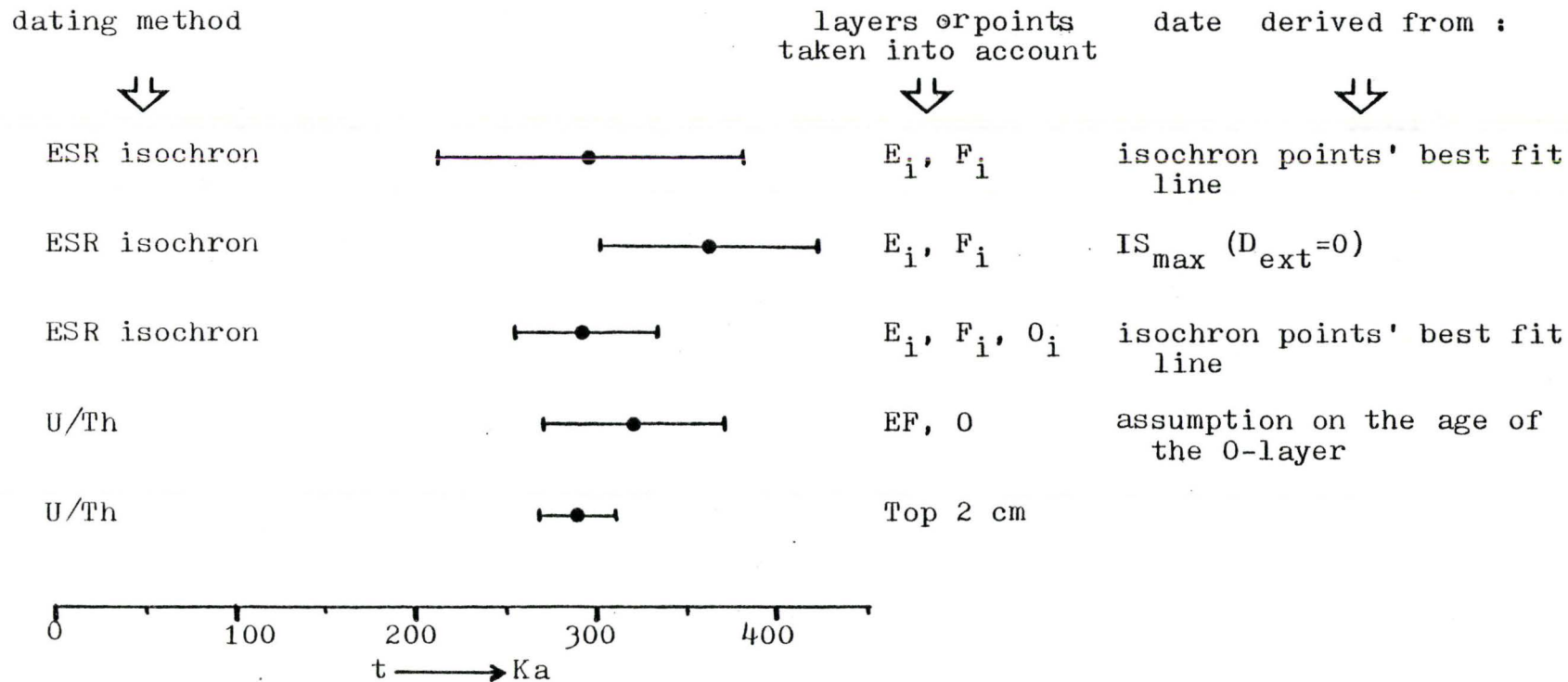
Two samples of the E layer, namely  $E_2$  and  $E_3$ , were studied by TL in order to check the ESR results. Fine powders ( $< 75 \mu\text{m}$ ), not treated with acid, were sent to D.J. Huntley. He separated by settling finer fractions of these powders and did alpha and gamma irradiations, TL measurements, and ED and a-factor evaluations. As a matter of fact, each one of the  $E_3$  aliquots which were given alpha doses were divided in two portions, one of them used for TL and the other sent for ESR (see section 6.4.2). To improve the TL signal to thermal radiation ratio a Corning 5-58 filter was used. To check if this filter transmitted the light emitted by the dating TL peak, the samples which first measured with the 5-58 filter were radiated again and remeasured, this time with a Corning 4-70 filter. The dating TL peak was about 25 times larger with the 4-70 than the 5-58 filter, but so were the other peaks. The TL constant annealing rate was  $\beta = 3^\circ\text{C}/\text{sec}$ .

#### 6.8.1 TL experimental results

The first glow curves of the natural and gamma



Figure 6.7.2 F/st 77200. ESR isochron and U/Th dates for various cases discussed in section(6.7)

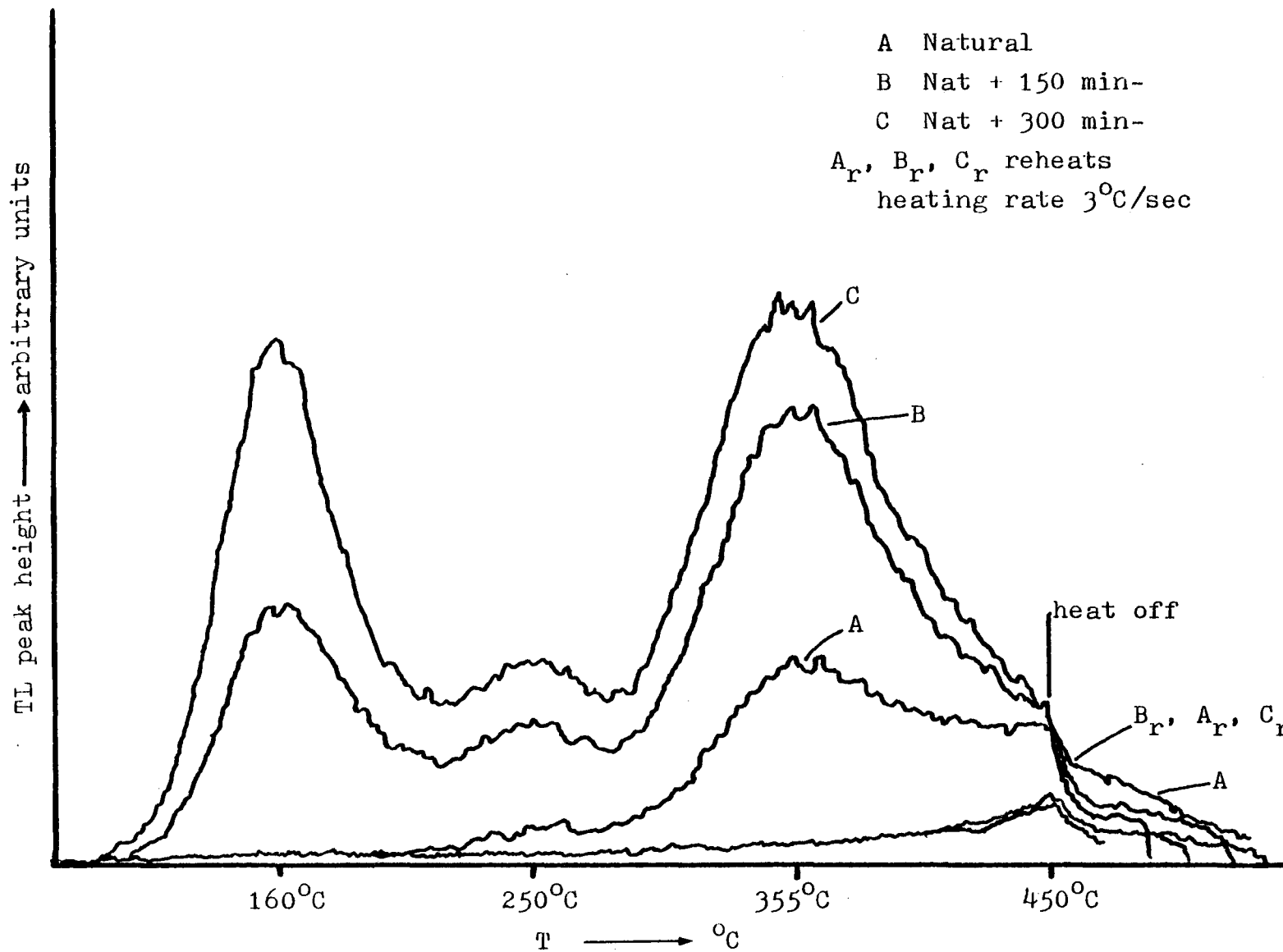


irradiated  $E_3$  are shown in Figure (6.8.1.1). The natural sample displays two peaks of fading temperatures:  $250^\circ\text{C}$  and  $355^\circ\text{C}$  respectively. The TL peak of  $T^*=250^\circ\text{C}$  is correlated to the ESR signal of  $T^*=230^\circ\text{C}$  (Figure 6.4.2), the  $20^\circ\text{C}$  difference being due to the distinct annealing ways. The TL peak of  $355^\circ\text{C}$  has a prominent height but it is more likely due to spurious effects (D.J. Huntley, pers. comm.). The ESR signal of  $T^*\cong 390^\circ\text{C}$  (Figure 6.4.2) cannot be correlated with that peak. It may be correlated with a very weak TL peak of  $T^*\cong 420^\circ\text{C}$  which presumably has been covered by the very strong spurious peak. Irradiated samples display an additional peak of  $T^*=160^\circ\text{C}$  which may be correlated with the ESR signal of  $T^*\cong 110^\circ\text{C}$  ( $g\cong 2.012$ ), found in ESR spectra of other speleothems (Chapter 7). The dating TL peak of  $T^*=250^\circ\text{C}$  ( $3^\circ\text{C}/\text{sec}$ ) indicates a trap, the electrons of which have lifetime  $\tau_0 \geq 6 \text{ Ma}$  (Appendix II) for cave temperature  $T_0 \cong 10^\circ\text{C}$  (see section 5.1). Thus,  $\tau_0$  is at least 20 times greater than the sample's age (see section 2.5) and guarantees thermally stable electrons.

To determine EDs, two out of three aliquots of each sample were given 150 min and 300 min of  $\gamma$ -doses ( $0.231 \text{ Krads}/\text{min}$ ) respectively. First glow growths of  $E_2$  and  $E_3$  are shown in Figures (6.8.1.2) and (6.8.1.3) respectively. The results are as follows:

- (i) sample  $E_2$ : grain sizes  $< 75 \mu\text{m}$  or an average of  $35 \pm 5 \mu\text{m}$ . If we consider linear growth, Figure

Figure 6.8.1.1 F/st 77200-E<sub>3</sub>. TL first glow curves of natural and gamma irradiated material.



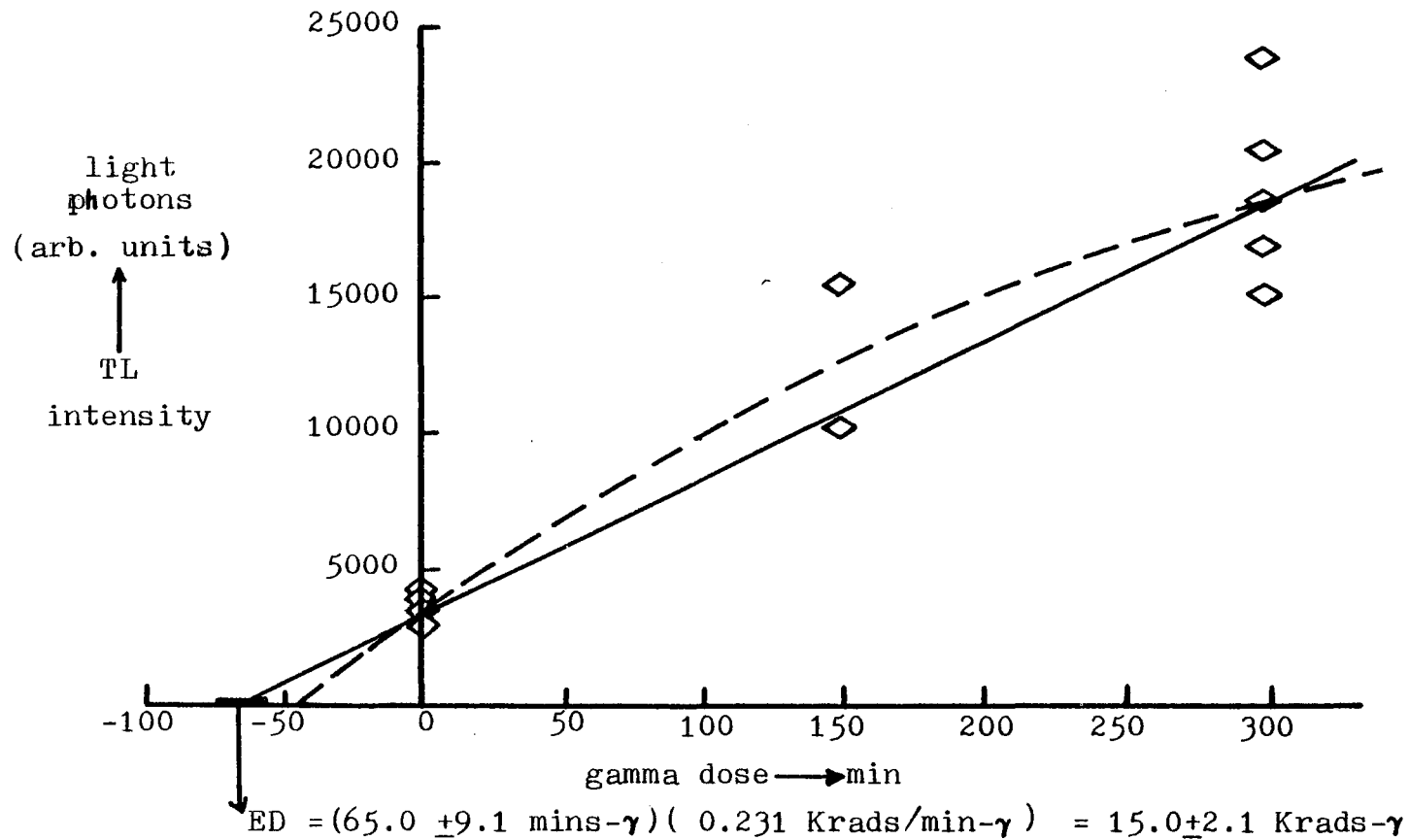


Figure 6.8.1.2 F/st 77200-E<sub>2</sub>. TL intensity response to additive  $\gamma$ -doses for the dating TL peak.

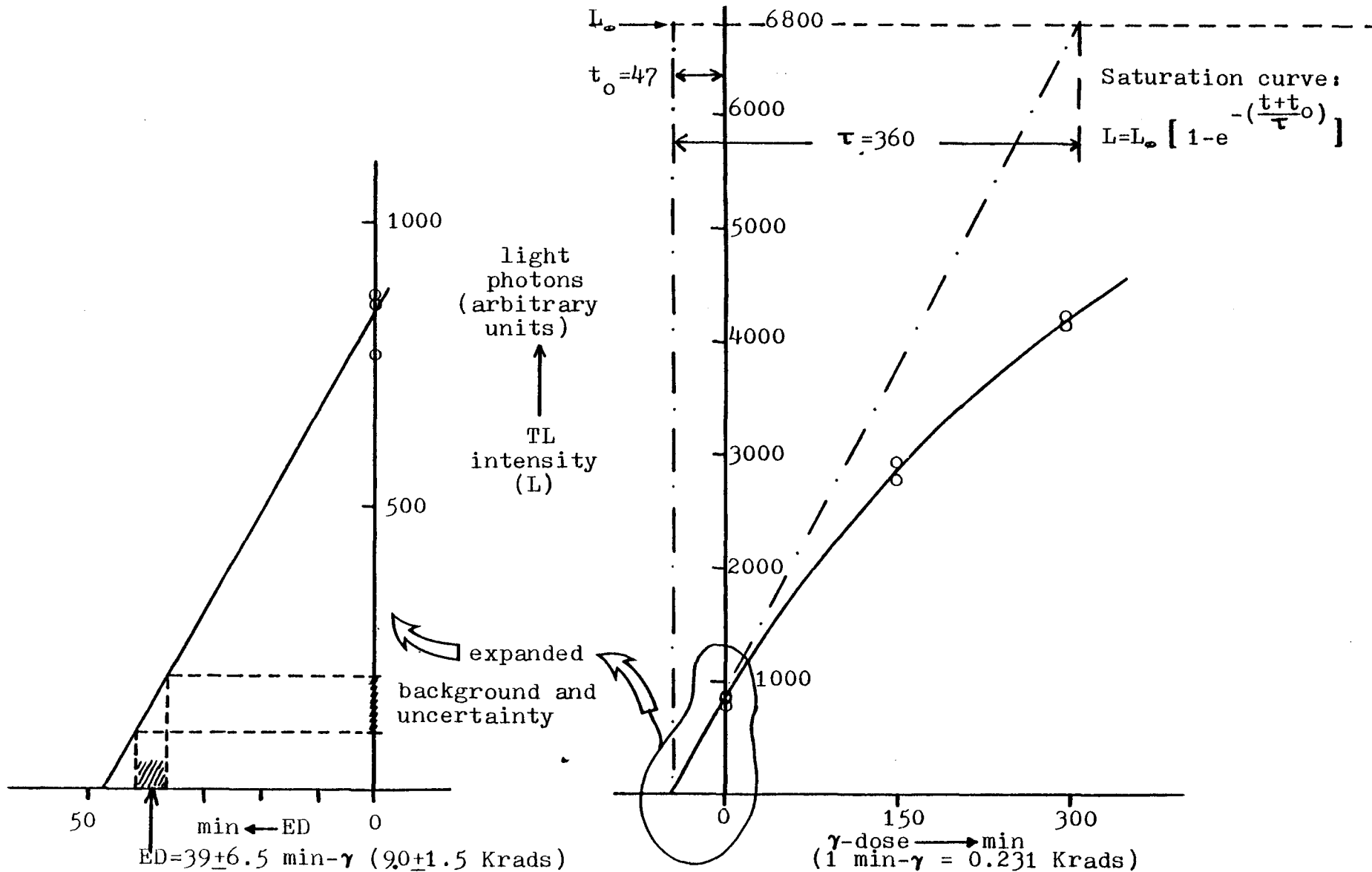


Figure 6.8.1.3 F/st 77200-E<sub>3</sub>. First glow growth with gammas of the dating TL peak.

(6.8.1.2) yields an ED of  $15.0 \pm 2.1$  Krads, while a saturation effect (see below) reduces this value to  $ED_2 \cong 12$  Krads.

- (ii) sample E<sub>3</sub>: grain sizes range: 2-10  $\mu\text{m}$  or an average of  $\sim 6\mu\text{m}$ . Figure (6.8.1.3) shows a clear saturation curvature and yields an  $ED_3 = 9.0 \pm 1.5$  Krads<sup>⊗</sup>

Two more aliquots of E<sub>3</sub> were given 3h and 6h of  $\alpha$ -doses respectively; their first glow curves are shown in Figure (6.8.1.4). The relation of these glow peaks (Figure 6.8.1.5) is obviously linear, yielding an ED due to alphas of  $2.5 \pm 0.2\text{h}$ <sup>⊗</sup>. To evaluate a-factor, the formula (1.6.2.3) has been used; the parameter  $\underline{x}$  has been calculated from the formula (1.6.2.4) or from the ratio  $\gamma\text{-ED} / \alpha\text{-ED}$ . In fact, the average of these two x-values was used ( $(0.33 + 0.26) / 2$  min- $\gamma$  / min- $\alpha$ ), and the a-value was found to be:  $0.140 \pm 0.014$ .

### 6.8.2 Comparison of TL and ESR results. Interpretation: the "grain size effect"

Comparing the data of TL with that of ESR, it is seen that something is wrong; though the a-values of both TL and ESR agree within the experimental error, the EDs of TL are much lower than those of ESR ( $ED_{\text{TL}} \cong 20\% ED_{\text{ESR}}$ ).

---

<sup>⊗</sup>  $\pm$  error due to instrument's background

Figure 6.8.1.4 F/st 77200-E<sub>3</sub>. TL first glow curves of natural and alpha irradiated material

D Natural  
G Nat. + 3h  
H Nat. + 6h  
D<sub>r</sub>, G<sub>r</sub>, H<sub>r</sub> reheats  
Heating rate 3°C/sec.

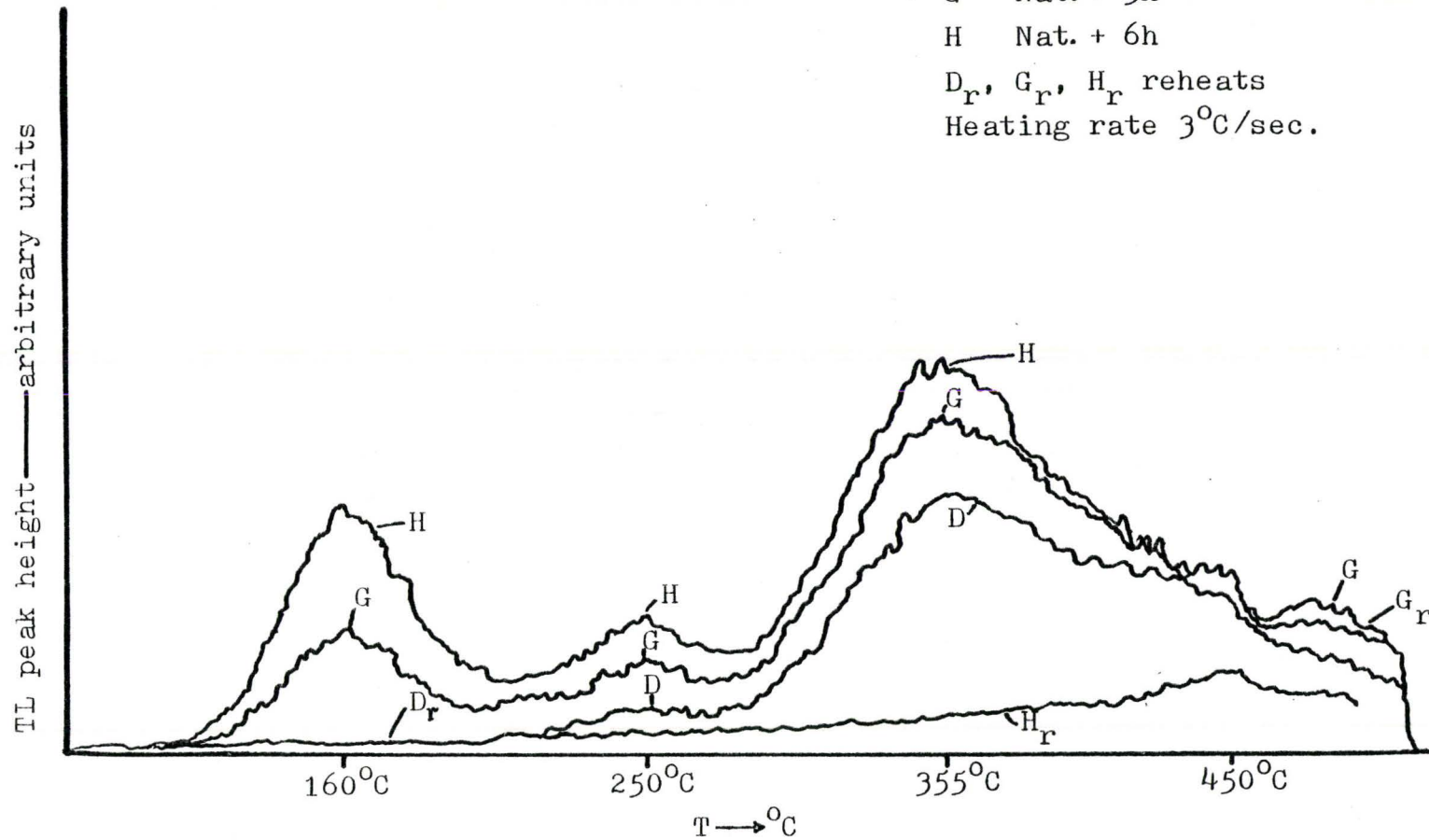
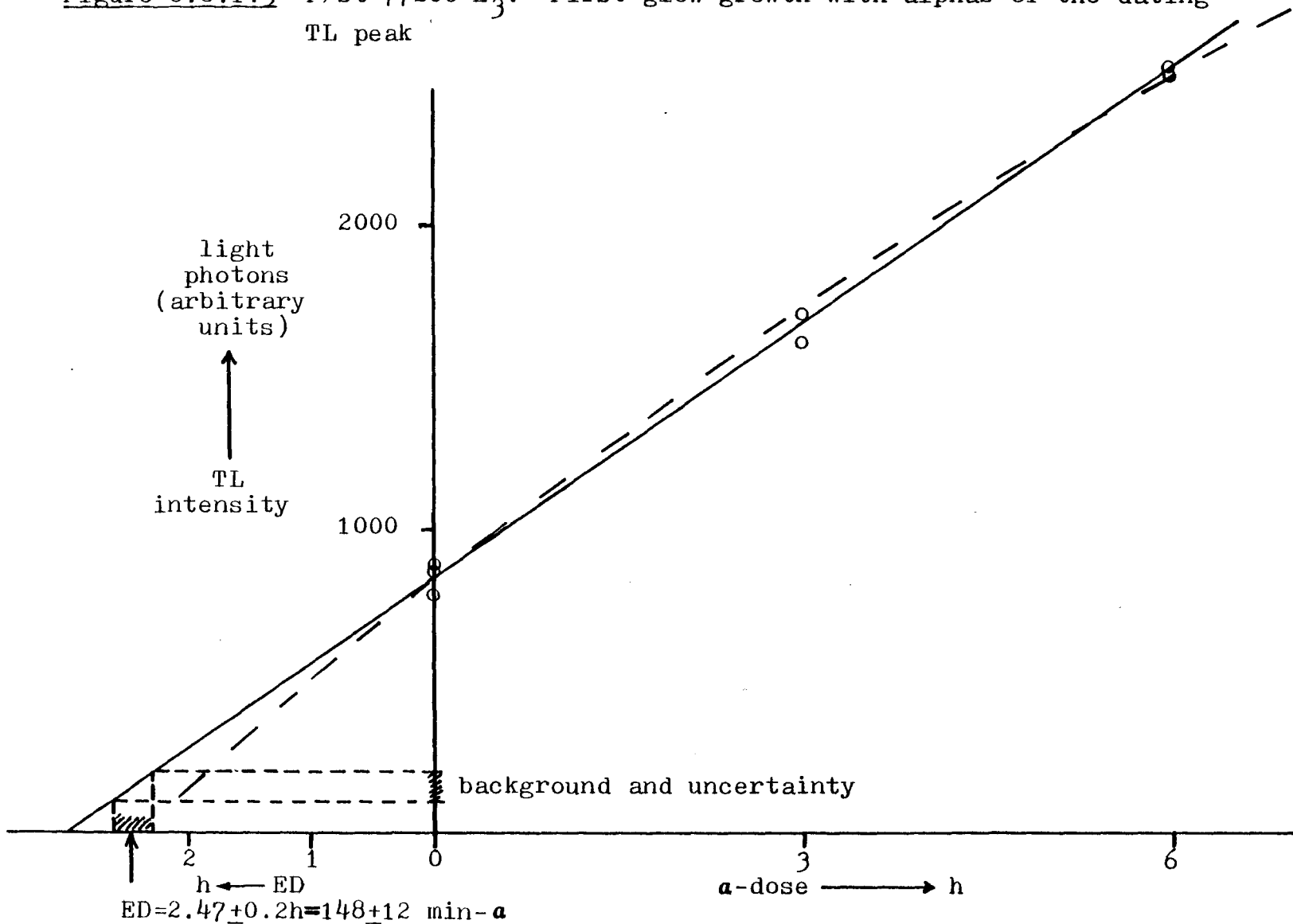


Figure 6.8.1.5 F/st 77200-E<sub>3</sub>. First glow growth with alphas of the dating TL peak





The ED's of TL yield a maximum age for the speleothem<sup>⊗</sup>:

$$t_{\max} \cong 90 \pm 10 \text{ Ka.}$$

Ikeya has estimated ED's of several speleothem samples by means of both TL and ESR methods. He found either very good agreement (Miki and Ikeya, 1978) or a trend of TL-ED's to be a bit higher rather than lower than the ESR ones (Ikeya, 1978a). Ikeya, however, used the same grain sizes in both methods, while we used very fine grains for TL and large grains for ESR. Besides, our fine grains were not treated with acid to eliminate possible surface effects caused during sample preparation, as Wintle (1975) suggests. Such treatment was avoided due to the fear that very fine grains would be readily dissolved and the amount of  $<10 \mu\text{m}$  powder, required for ESR measurements, would become too small. Our study of the grain size effect on natural ESR intensity of samples not treated with acid (Figure 6.8.2.1) indicates that samples of grain size

$\sim 6 \mu\text{m}$  are expected to yield  $I_n$  approximately 40% lower than that of grains of 150-300  $\mu\text{m}$ . Assuming that sensitivity to gammas does not depend on grain size, we would expect the  $\sim 6 \mu\text{m}$  powder of  $E_3$  to have an  $ED_{\text{ESR}} \cong 60\%$ .

$\cdot (51.5 \pm 8 \text{ Krads}) = 31 \pm 5 \text{ Krads}$ , but not as low as  $9 \pm 1.5 \text{ Krads}$ ,

---

<sup>⊗</sup>For  $ED_3 = 9.0 \pm 1.5 \text{ Krads}$  and  $[U] = 275 \pm 0.15 \text{ ppmU}$ , the maximum  $IS = ED/[U]$  becomes  $IS_{\max} = 3.3 \pm 0.5 \text{ Krads/ppmU}$ . For  $a = 0.140 \pm 0.014 \cong 0.15$  and  $p_0 \cong 1.66$ , Figure (6.7.1) gives  $t_{\max} \cong 90 \pm 10 \text{ Ka}$ .

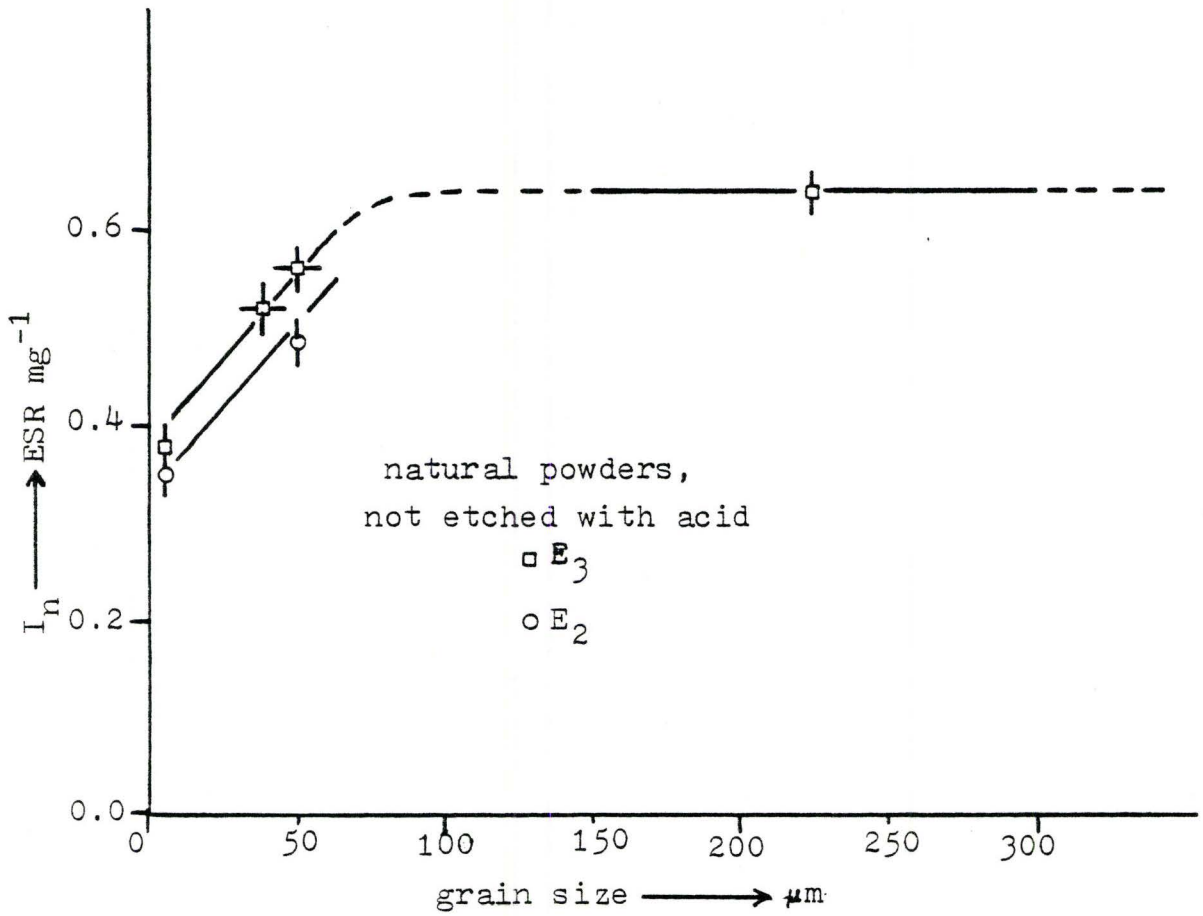


Figure 6.8.2.1 F/st 77200-E. The "grain size effect".

as found by TL.

Lewis (1968) studied the grain size effect of gamma irradiated limestones and dolomites on their TL peak intensities. He found that:

- (i) TL intensity displays a maximum at  $\sim 70-125 \mu\text{m}$  (average grain sizes), and slowly decreases for larger grains.
- (ii) a change from  $\sim 80 \mu\text{m}$  to  $\sim 25 \mu\text{m}$  drops the TL intensity by 30-60% off.

The ranges given in both (i) and (ii) depend on the particular TL peak used for the measurement. The ESR intensities of both  $E_2$  and  $E_3$  calcites seem to reach a maximum when the average grain size is greater than  $80 \mu\text{m}$ . Miki and Ikeya (1978) found good agreement between ESR- and TL-EDs, but they used powders of grain sizes greater than  $180 \mu\text{m}$ . This, and Wintle's (1975, 1978) successful TL studies of speleothems (grain sizes greater than  $75 \mu\text{m}$ ) indicate that TL and ESR may have similar behaviour for sizes greater than  $80 \mu\text{m}$ . Thus, the decrement in TL for large grains found by Lewis in limestones and dolomites ((i) above) does not seem to occur in speleothems, and may be due to the high impurity content of the former materials. On the other hand, the sharp drop of the TL intensity with decreasing grain size ((ii) above) could be common to all carbonates. If this trend becomes more intense for finer grains ( $< 25 \mu\text{m}$ ), a 80% drop of the TL intensity for

~6  $\mu\text{m}$  grains of speleothems would not be surprising.

The previous discussion indicates that a possible difference in the way ESR and TL respond to the grain size effect may exist, TL showing more dependence on grain size. Figure (6.8.2.2) illustrates how we would expect ED to depend on grain size of powder not treated with acid. A model is proposed by Wintle (1975) to explain the low ED's in terms of TL processes. She studied viced and drilled samples of the same grain size (75-250  $\mu\text{m}$ ) and proposed that non-radiative centers are activated on the grain surface during the drilling process. These centers are not refilled with charges during a subsequent irradiation and compete with TL activators, e.g.  $\text{Mn}^{2+}$  etc. (Medlin, 1968b), for the untrapped electrons. This model can explain our TL results with the assumption that prolonged grinding produces very fine grains with activated, non-radiative centers on their surfaces<sup>⊗</sup>, as drilling does on the surfaces of the large grains. Besides, grinding may have partially emptied the traps responsible for the 250°C TL peak, so that the 230°C ESR signal becomes lower for very

---

⊗ There are two reasons that such centers may have had increased density on the surfaces of very fine grains:

- (i) the finer the grains the more the elaboration they undergo during grinding, thus the more centers which may be activated.
- (ii) the finer the grains the higher the ratio: surface area/volume of grains.

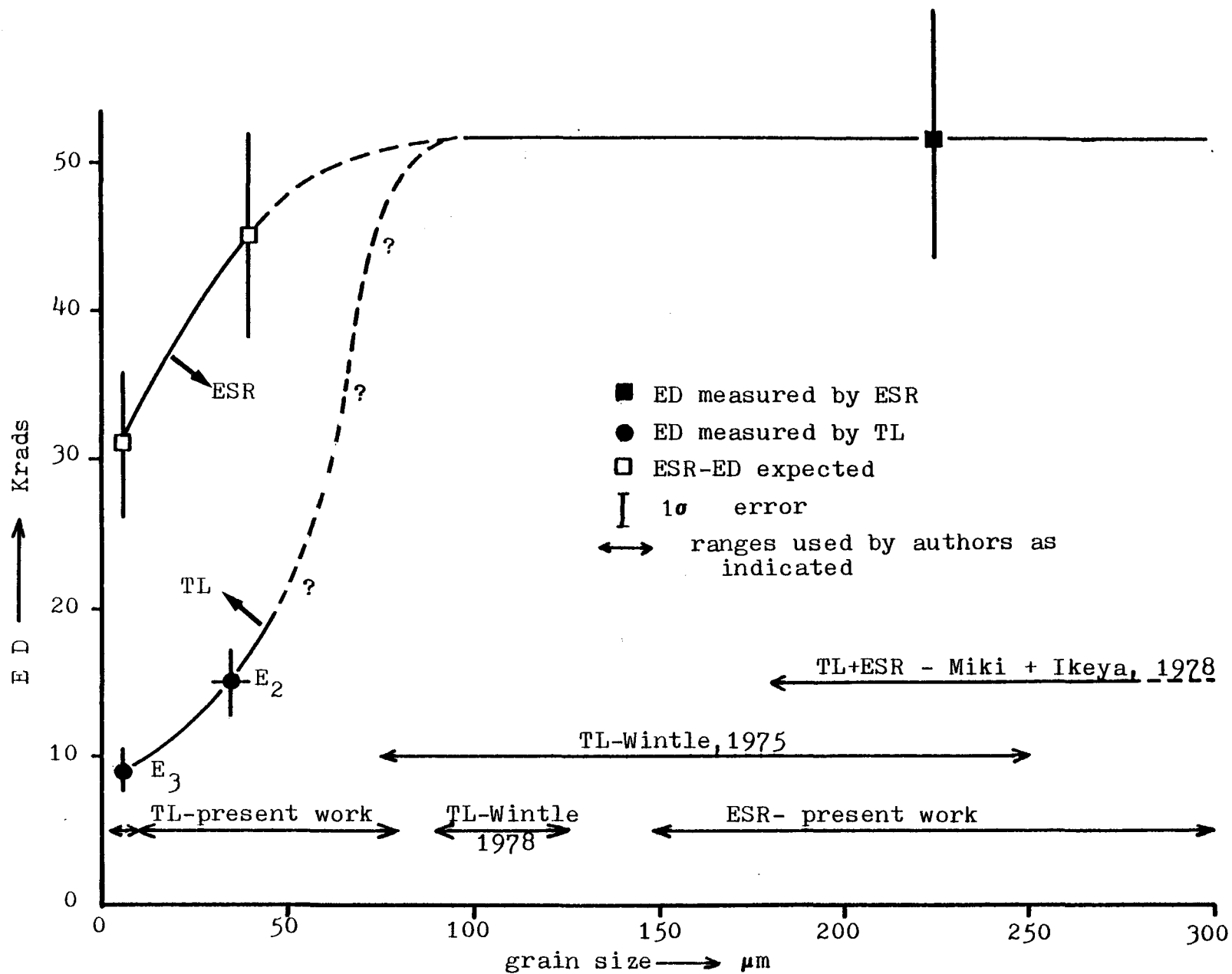


Figure 6.8.2.2 F/st 77200-E. Equivalent dose versus grain size of powders not treated with acid

fine grains. We suggest that these two processes are combined in TL, thus explaining:

- (i) the sharp drop of the natural TL intensity, mentioned previously,
- (ii) the otherwise unexplained divergence of alpha ED's as found by ESR ( $11.4 \pm 0.5h$ ) and TL ( $2.5 \pm 0.2h$ ), though the samples measured had identical range of grain size (2-10  $\mu m$ ).

Wintle's experiments did not indicate any partial evacuation of traps because the grains of the viced sample she used were large enough, i.e. population of activated centers and emptied traps low enough, so that treatment with 0.5 % acetic acid did not alter the TL characteristics. On the other hand, her finding that both drilled and viced samples, despite their differences on ED's and natural TL intensities, displayed the same sensitivity to gammas, supports the assumption we made previously that  $s(\gamma)$  is independent of grain size. Therefore, the agreement in a-values found by ESR and TL is not surprising.

#### 6.9 Supplementary ESR data

In the process of dating speleothem 77200, several assumptions were made due to lack of adequate experimental data. Recent ESR tests on 77200, performed in our laboratory<sup>⊗</sup> after the present work had been integrated (June, 1982),

---

⊗ by Tammy Middleton

supplied new data, which could be considered to support our assumptions and the "isochron" idea in general.

Eight samples have been taken, 4 from each of the EF and K layers of 77200 (indices: a,b,c,d). The analytical procedure was much the same as for the  $E_i$  samples. This time the additive  $\gamma$ -doses were at least up to 40 Krads. Figure (6.9.1) shows the ESR intensity growth with gammas, for some of the samples; this growth is not linear in general. Such a behaviour resembles the TL intensity growth curve of sample  $E_3$  (Figure 6.8.1.3) where linearity is destroyed above  $\sim 120$  min of  $\gamma$ -dose (28 Krads). If the natural dose ( $\sim 47$  min) is added to that, electron trap saturation, as it is ascertained by TL, seems to begin after sample  $E_3$  has absorbed a total dose equivalent to  $\sim 170$  min of  $\gamma$ -dose (40 Krads). The value of  $ED = 51.5 \pm 8.0$  Krads, used to determine the ESR isochron age, stands above that level and may be an overestimation of ED. However, the range of additive  $\gamma$ -doses we used is quite small (0-9.4 Krads), and the assumption about linear growth over a total dose of  $\sim 61$  Krads (51.5 natural +9.4 artificial) may not be conducive to significant error. This is supported by the good agreement of the ESR isochron and U/Th dates.

The determination of EDs from the growth curves of Figure (6.9.1) is problematic for two reasons:

- (i) The exponential growth data requires computer

Samples

- △ K-a
- K-c
- EF-a
- EF-b

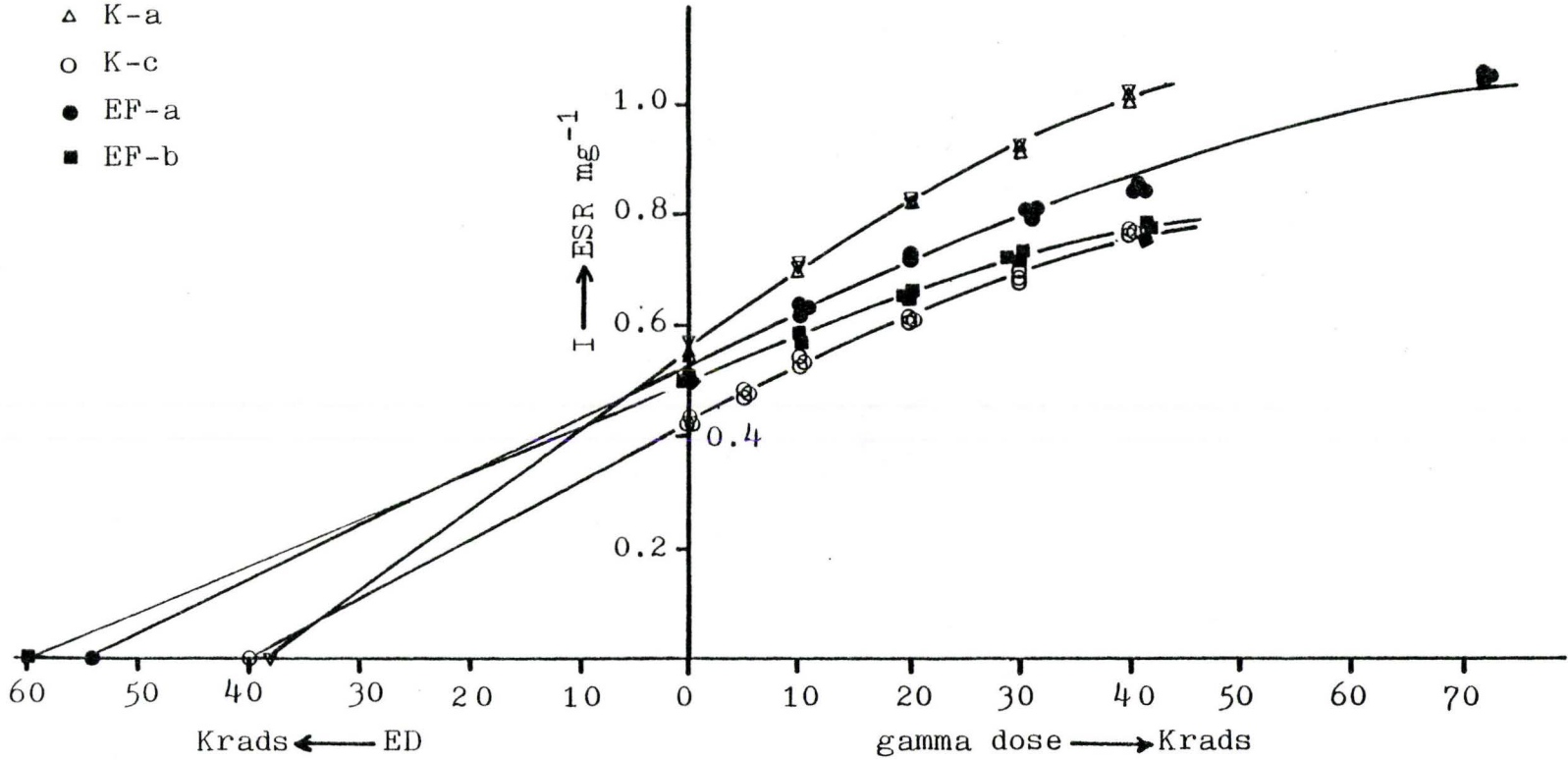


Figure 6.9.1 F/st 77200 - K and EF layers. ESR signal  $S_{1A}$ -growth with additive gamma doses.



processing to give a curve<sup>⊗</sup> fitting the points. It was temporally impossible to do that. The alternative was to draw curves by means of a French Curve.

- (ii) It is not known how far from the beginning of the growth line the linearity is destroyed. Linear growth up to ~60 Krads, however, might be acceptable, as it was noticed previously. The curve tangent at the  $I_n$  point extrapolated back to  $I=0$  gives  $ED < 60$  Krads for almost all the samples.

The ED's determined by the approximate graphic way described above, the maximum ED's derived by fitting all the points to a linear relation and extrapolating back to  $I=0$ , and the U-content of the corresponding samples are displayed in the following table:

Sample	EF-a	EF-b	EF-c	EF-d	K-a	K-b	K-c	K-d
[U] ppm	2.56	2.66	2.71	2.26	2.21	2.24	2.47	2.07
ED Krads	50-60	55-65	50-60	50-60	35-45	--	35-45	35-45
maxED Krads	73.4	72.3 ±1.8	74.1 ±1.8	62.6 ±0.8	62.8	57.5	51.9 ±0.2	52.7 ±0.6

⊗ The curve is expressed by:  $I = I_0 \left[ 1 - \exp\left(-\frac{ED^* + D}{I_0 / s^*}\right) \right]$  where  
 $I$  and  $D$  are the ESR intensity and gamma dose respectively  
 $I_0$  is the ESR intensity saturation level  
 $ED^*$  is the intersection of the curve with the  $\gamma$ -dose axis  
 $s^*$  is the slope of the curve tangent (sensitivity) at the  $ED^*$  point.

These values are plotted in a diagram of ED versus [U] (Figure 6.9.2) where the old data from Figure (6.5.3) is also shown. We note that almost all the new ED-ranges lie in the area determined by the experimental error of the ESR intensity isochron. Furthermore, the new data's tendency to give higher ED for increased [U] is quite clear.

The similar range of linear growth with additive  $\gamma$ -doses that TL and ESR intensities seem to display implies that such a similarity might occur for the growth with alphas. Thus, the assumption made in section(6.4.2) that the ESR intensity of sample E<sub>3</sub> should have linear response to additive  $\alpha$ -doses seems to be reasonable because the TL intensity of the same sample displays such a linearity (Figure 6.8.1.5).

### 6.10 Discussion

Reviewing the above process of dating speleothem 77200, our attention is focussed on the low  $D_n$  at which saturation indications arise. It would be expected for saturation to begin above ED+100 Krads of  $\gamma$ -dose (see section 2.8) but not from as low as 40-60 Krads. The Mn concentration in the EF layer is  $\sim 10$ -20 ppm, that is much lower than the value required to cause saturation (100-1000 ppm) due to Mn-trap interaction (Ikeya, 1981). It is

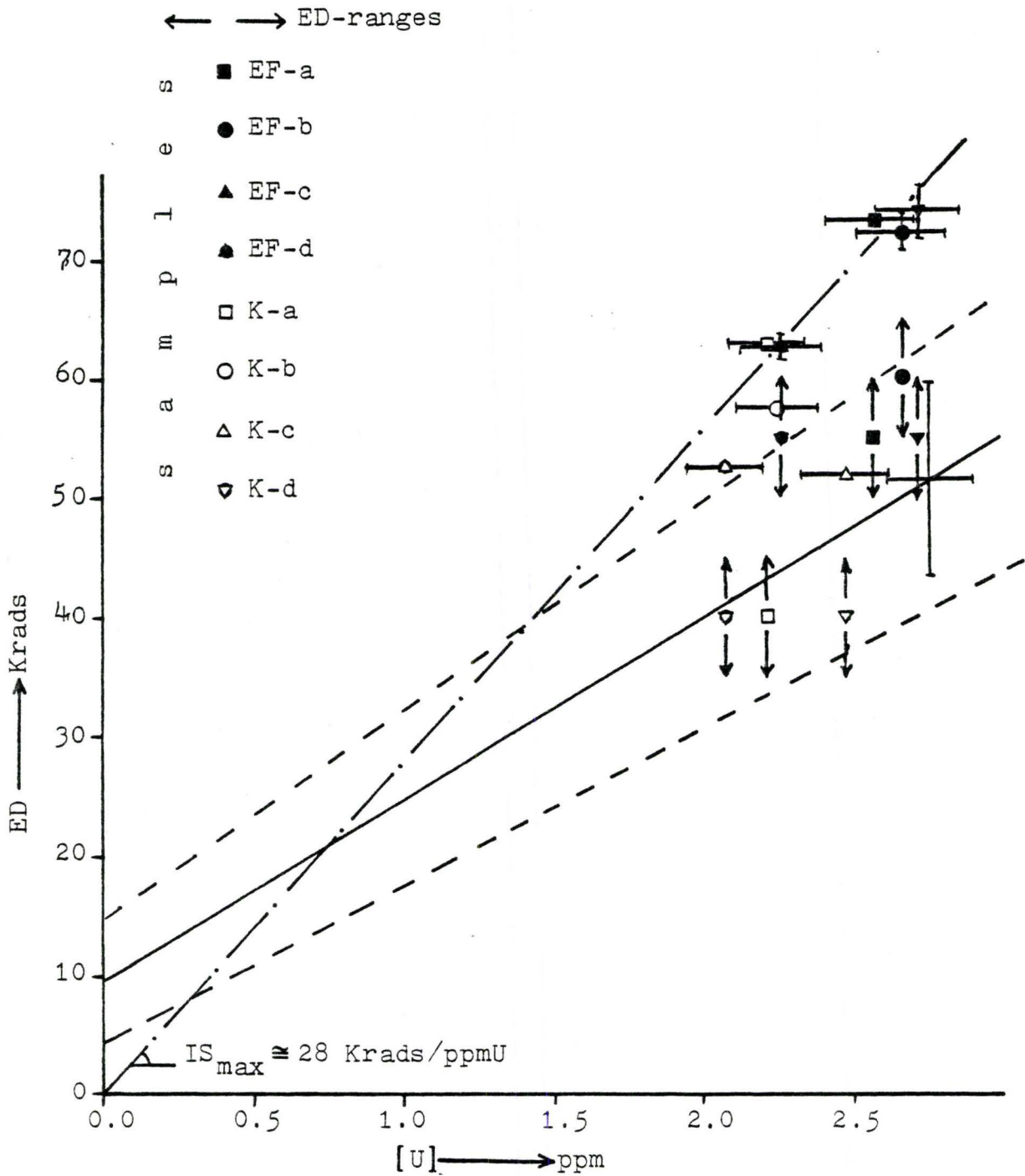


Figure 6.9.2 F/st 77200. Isochron plot including data from Figure (6.5.3) and from the table in section (6.9).

possible that the  $Y^{3+}$  cations, presumably responsible for the dating ESR signal (see section 2.3.1), have quite low concentration. Another possibility is that the ESR signal used for dating ( $S_{1A}$ ) may be the co-effect of two centers, one being present in both natural and irradiated states (stable up to  $T^* \cong 230^\circ\text{C}$ , Figure 6.4.2), and the other produced during irradiation (unstable, interfering signal:  $100^\circ\text{C} < T^* < 230^\circ\text{C}$ ). Both centers may have very similar g-values, thus being indistinguished by our ESR techniques. Such a possibility is indicated from the TL first glow curves of sample  $E_3$  (Figure 6.8.1.1) where a peak at  $T^*=160^\circ\text{C}$  is produced after irradiation. This peak, however, seems to have linear growth with gammas. For the speleothem 77200, thermal study of irradiated samples has not been carried out; such an annealing, therefore, is recommended (see section 3.8 (ii)-a).

As far as the reliability of the conditional isochron dating is concerned, it is hoped that further study, i.e. step annealing and accurate calculation of ED's if saturation persists, will allow a 'real' isochron line or even better two separate lines for the EF and K layers to be defined, thus monitoring the intensity 'isochron' line. To draw an isochron through the maximum ED's of the EF-a, -b, -c, -d points may lead to overestimation of the age of layer EF and underestimation of the external dose. Such an isochron line, however,

could be used to obtain an upper limit for the age. Thus, for  $IS_{\max} \cong 28$  Krads/ppm (Figure 6.9.2) and  $a=0.13$ , equation (3.5.3) yields:  $t_{\max} \cong 530$  Ka. It is not certain whether or not this value might indicate an age for layer EF older than the U/Th date. A young U/Th date could have origin in the presence of a hiatus between any of the Top layers, from A to E (Figure 6.3.1), but such a thing is not manifested by a visual examination (Plate 6.2.1). Otherwise, it is too early for the 'newborn' ESR isochron dating method to judge results of the 'mature' U/Th dating method.

## CHAPTER 7: Annealing and grain size effects of various speleothems

### 7.1 Introduction

This chapter includes some of the results of our preliminary studies, when we were trying to find an appropriate analytical procedure for normal ESR use before the "isochron" tests are performed. Two issues were examined regarding the trapped electron stability.

- (i) thermal behaviour, by applying step annealing (see section 4.4 (ii))
- (ii) response to mechanical treatment (grinding), by studying powders of variable grain size.

The need to do thermal study was realized quite clearly that time, but such a thing did not happen regarding the grain size. It was the TL studies of Lewis (1968) and Wintle (1975) (see section 6.8.2) that motivated us to examine the possibility of a "grain size effect" on the ESR intensity, despite the information found in the literature that such an effect had not been observed to occur in speleothems (section 4.2).

7.2 Speleothem 76165 . Given data and details on analytical procedure.

76165 consists of a number of pieces of flowstone, white non-porous calcites, taken from the Lost John's Cave. The following data are available (Gascoyne, 1979, p.456).

Sample	[U] ppm	p	p <sub>0</sub>	q	<sup>230</sup> Th/ <sup>232</sup> Th	t ka
1 piece	9.35	0.938	0.914	0.649	111	115.5 <sup>+12.3</sup> <sub>-11.0</sub>

The <sup>230</sup>Th/<sup>232</sup>Th indicates a material free of detrital impurities. After extraction of the sample from the flowstone, it was ground and sieved. Two fractions were separated: coarse grains ( > 0.1 mm) were used for irradiations, and both coarse and fine ( < 0.1 mm) fractions were used for thermal studies. Treatment with acid was omitted because this experiment was done during our preliminary investigations. However, this omission is possibly of minor importance, since studies of other speleothems (77200, 77032) have showed that the grain size effect is not significant for grains greater than 0.1 mm. Gamma additive doses given to 5 aliquots were: 2.535, 5.07, 7.605, 10.14 and 12.675 Krads. Sample weights in quartz tubes were 190-230 mg. Only the JEOL-ESR spectrometer was used.

### 7.2.1 Experimental results

Thermal study of natural and irradiated materials (Figure 7.2.1.1) revealed four signals as shown in the following table.

Signal's Symbol	g-factor	T*°C	notes
S <sub>1A</sub>	2.00095(+5)	~210	strong signal, used for dating
S <sub>1B</sub>	2.00590(+5)	~370	signal revealed in thermal study only
S <sub>2B</sub>	2.01180(+10)	~100	signal present in irradiated material only
S <sub>X</sub>	2.00315(+10)	~720	signal not related to irradiation

ESR spectra of the natural material at characteristic temperatures are shown in Figures (7.2.1.2)-A and -B. The signals which are sensitive to  $\gamma$ -rays (S<sub>1A</sub>, S<sub>1B</sub>, S<sub>2B</sub>) have g-values similar to those of speleothems 76121 and 77200. The fading temperatures of the 76165 are a bit lower than those of the flowstone 77200-E<sub>3</sub>, due to the longer annealing time used at each temperature step. The signal S<sub>X</sub> appeared after annealing at T > 250°C, reached a maximum at ~600-650°C and disappeared at T > 800°C; its intensity was the same for both natural and irradiated material. The origin of this signal will be discussed later.

The growth of S<sub>1A</sub> and S<sub>2B</sub> with additive gamma doses is shown in Figure (7.2.1.3). A fading process in S<sub>1A</sub> is



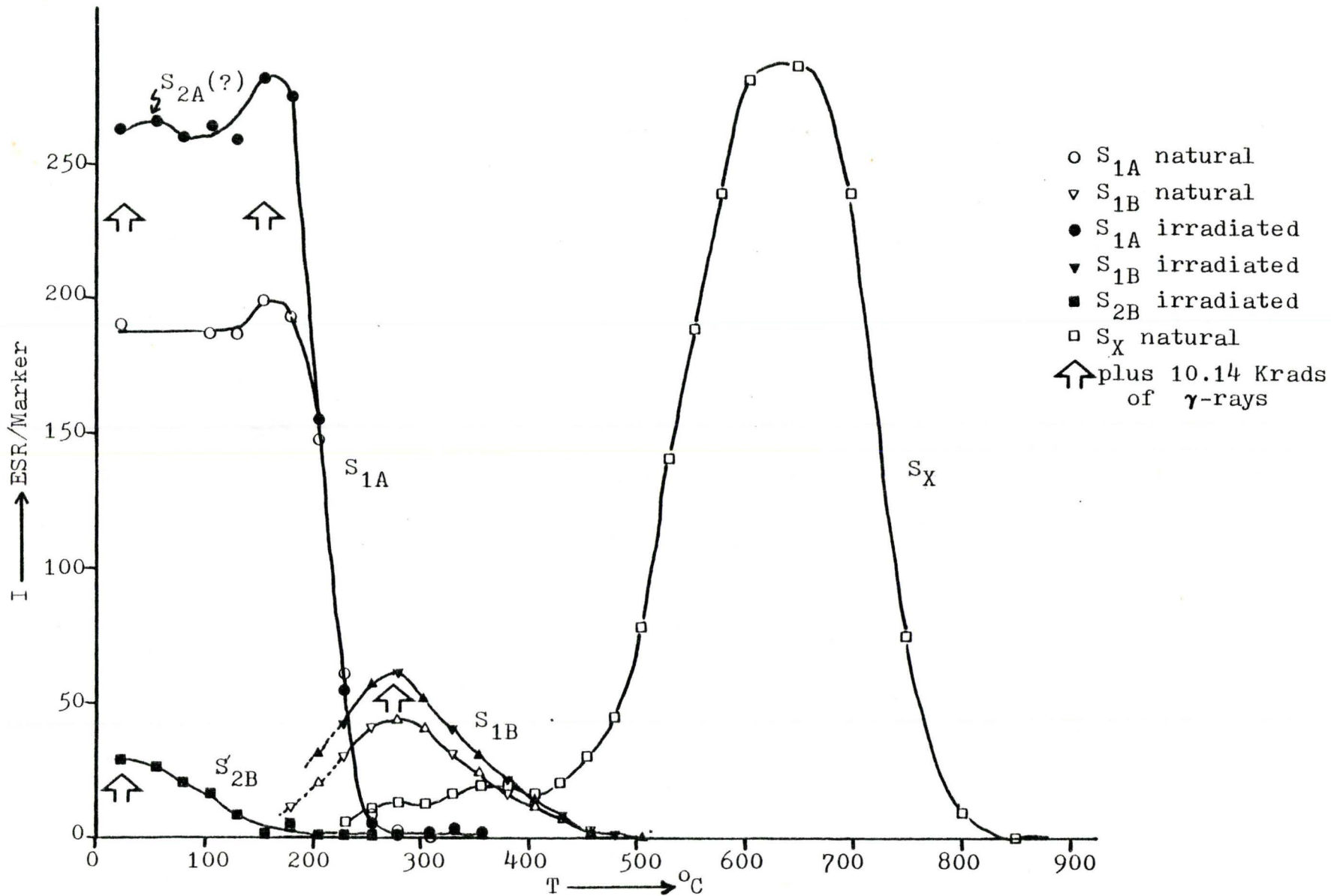


Figure 7.2.1.1 F/st 76165. Step annealing of natural and irradiated powders ( $>100 \mu\text{m}$ ), approximately 6 days after irradiation.

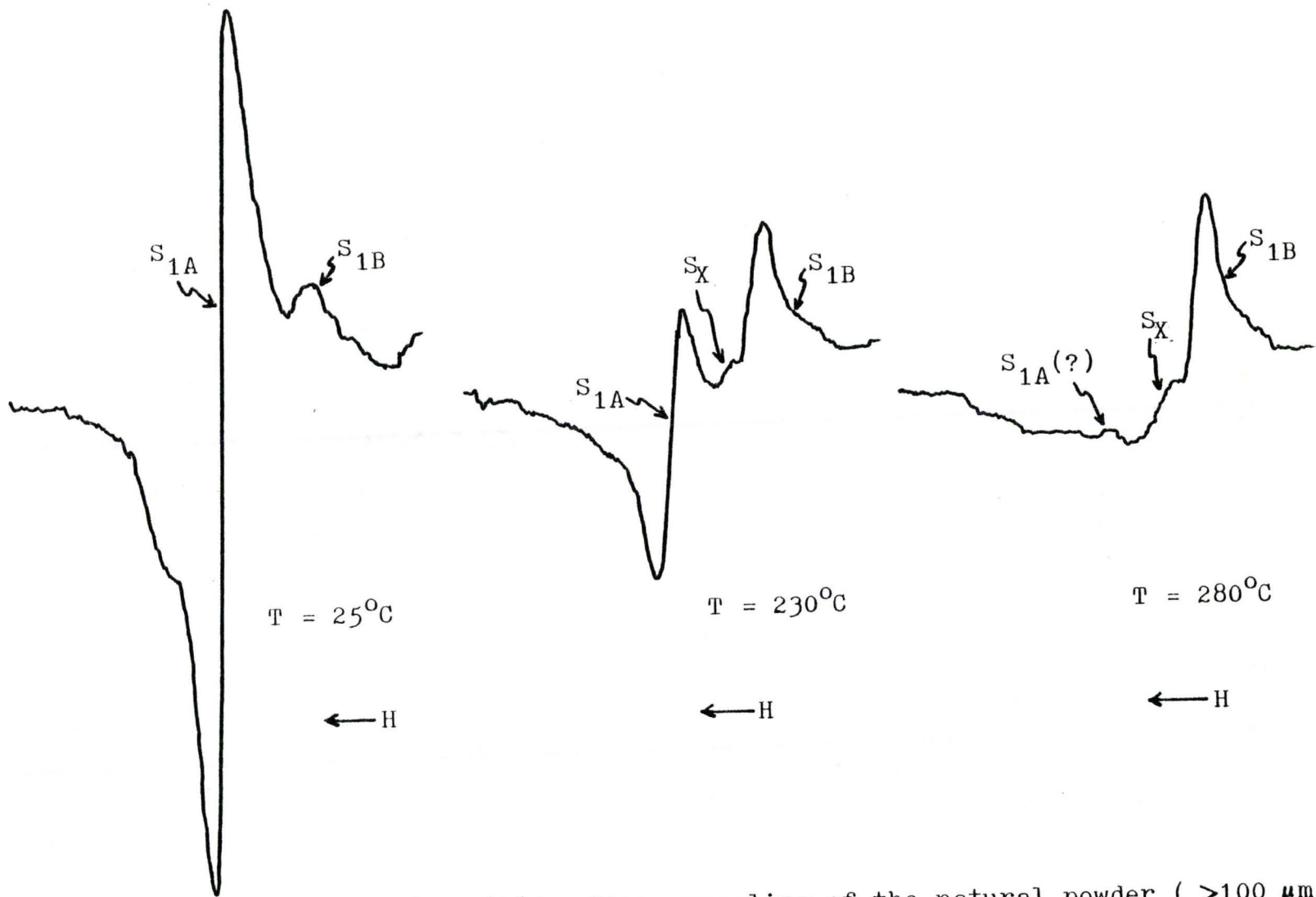


Figure 7.2.1.2.A F/st 76165. Step annealing of the natural powder (>100 μm). ESR spectra at characteristic temperatures. ESR spectrometer: JEOL, Gain = 250.

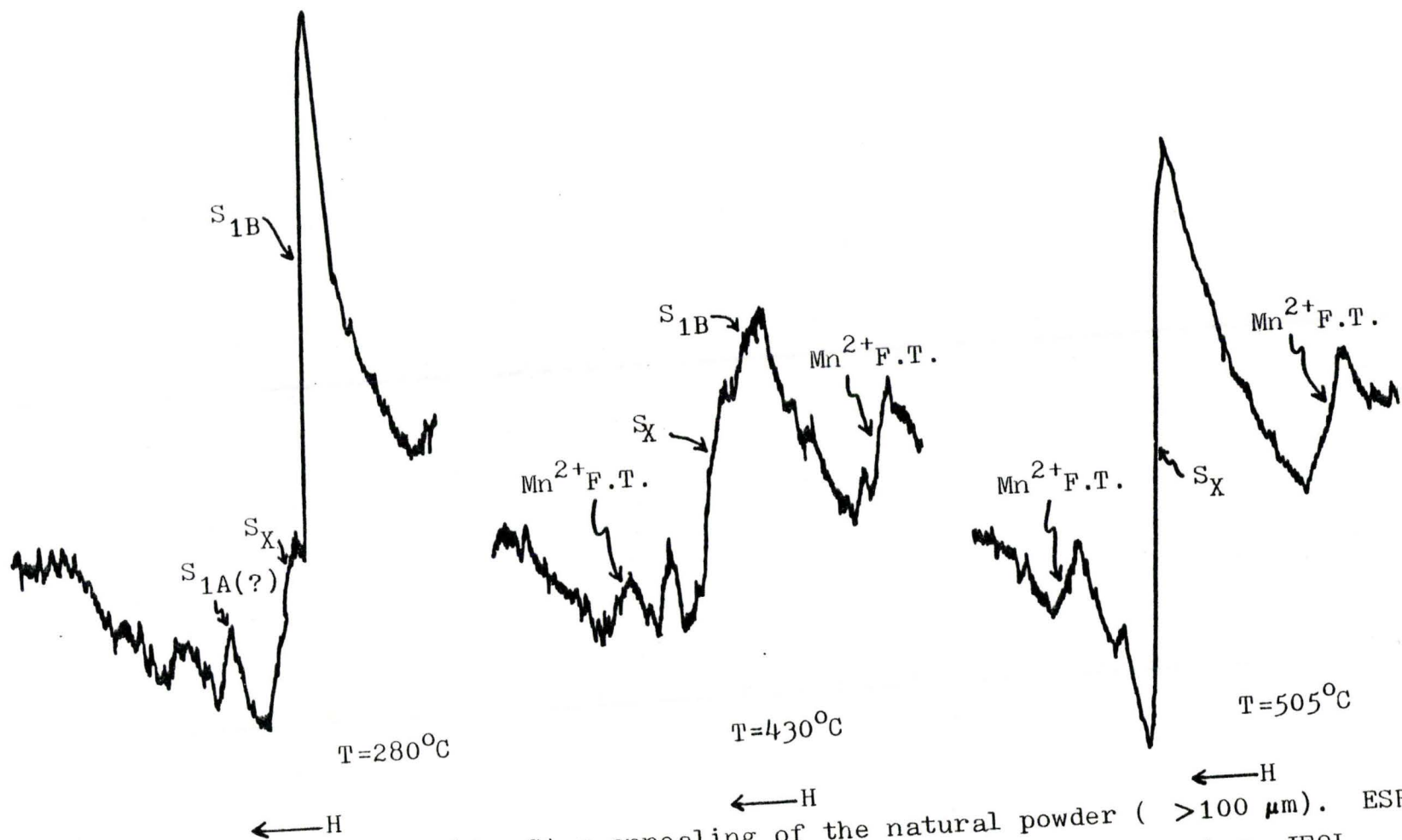


Figure 7.2.1.2.B F/st 76165. Step annealing of the natural powder (>100 μm). ESR spectra at characteristic temperatures. ESR spectrometer: JEOL, Gain = 630.

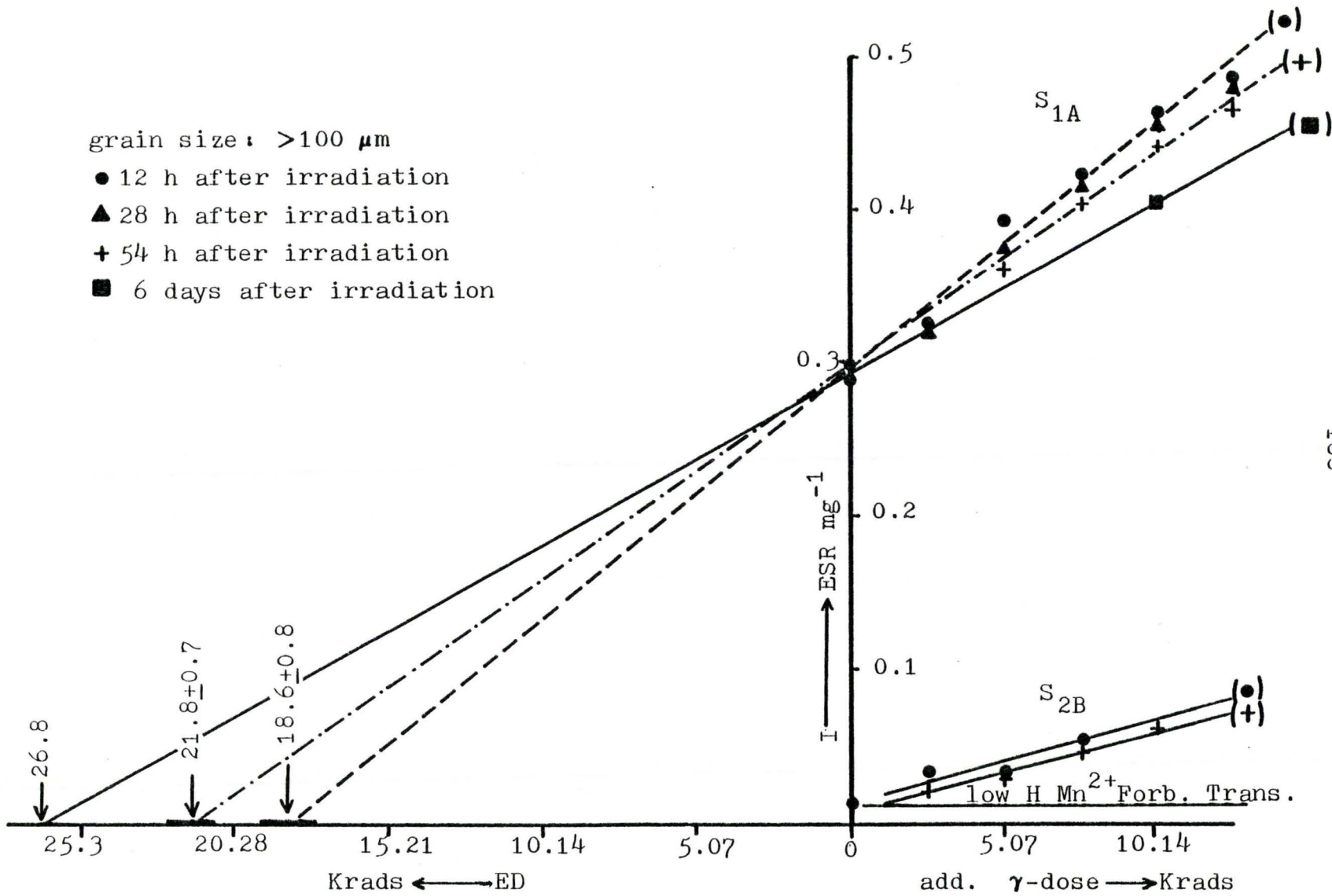


Figure 7.2.1.3 F/st 76165. ESR intensity response to additive  $\gamma$ -doses and fading process.

observed, which is known to become inactive a few days after irradiation (see section 4.4.(i)). This has the effect of causing the EDs obtained to reach presumably a maximum value of  $\sim 27$  Krads about one week after irradiation. The fading of  $S_{1A}$  is assumed to be due to decay of centers of low  $T^*$ , the g-value of which should be very close to 2.001 so that their signal ( $S_{2A}$ ) is completely overlapped by the strong  $S_{1A}$ .

To determine ED, signal  $S_{1B}$  could be used as well. However, the ESR signal of peak  $S_{1A}$  overlaps that of  $S_{1B}$  at  $T < 230^\circ\text{C}$  and retrapping occurs at  $230\text{-}280^\circ\text{C}$ . Thus it is questionable what ESR intensity should be used. If the maximum intensities ( $I_{\text{max}}$ ) of  $S_{1A}$  and  $S_{1B}$  are used, the obtained EDs are  $\sim 24$  Krads and  $\sim 28$  Krads, respectively (Figure 7.2.1.4). The figures of ED based on  $S_{1A}$  show that about the same value is obtained from the room temperature intensity ( $I_{\text{r.t.}}$ ) as from  $I_{\text{max}}$ . That is: if  $I_{\text{r.t.}}$  for  $S_{1B}$  also yields the same ED as does  $I_{\text{max}}$  for this signal, then we should be able to use it to date speleothems older than  $10^6$  years, by which time signal  $S_{1A}$  might have faded partly.

### 7.2.2 Estimation of the a-value

Wintle's model can be used to evaluate  $D_{\text{int}}$  and compare it with the ED found previously. If the data of section(7.2) are applied to equation (3.3.1.1), we get:

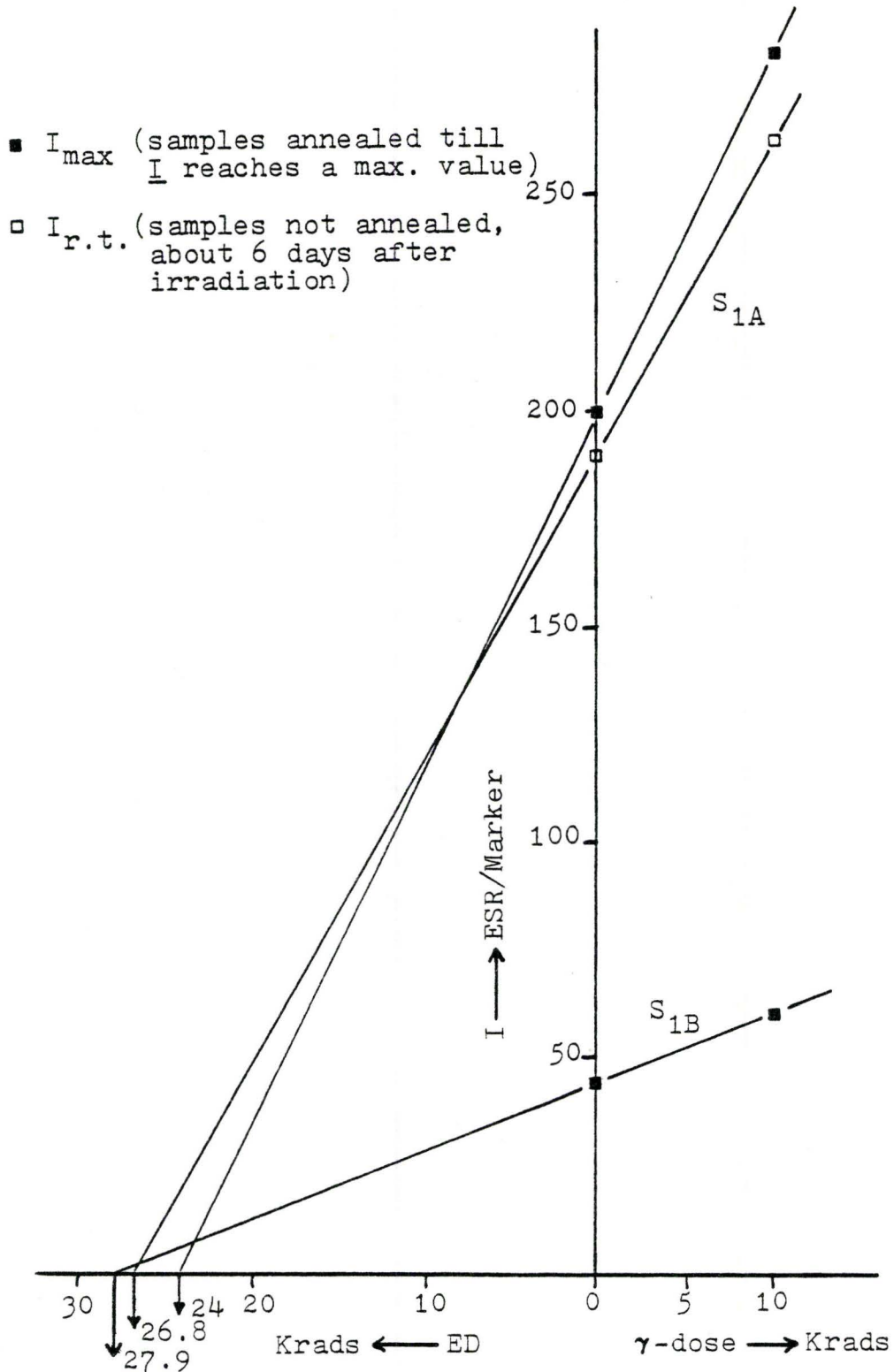


Figure 7.2.1.4 F/st. 76165. ESR signal growth with gammas (data taken from Figure 7.2.1.1).

$D_{\text{int}} = 24.3_{-4.4}^{+4.9}$  Krads for  $a=0.1$  and  $D_{\text{int}} \cong 67$  Krads for  $a=0.5$ .  
 The  $[U]$  value used is that of IDA, and is probably lower than the 'true'  $[U]$  value that would be found by NAA (section 4.6). The  $D_{\text{int}}$  values given above are therefore lower limits of the 'true'  $D_{\text{int}}$ , so that:  $D_{\text{int}} \geq 24.3_{-4.4}^{+4.9}$  Krads for  $a=0.1$  and  $D_{\text{int}} \geq 67$  Krads for  $a=0.5$ . It is obvious that  $ED \cong D_{\text{int}}$  for  $a=0.1$ . A larger  $a$ -value would require  $D_{\text{int}} > ED$  which is impossible since  $ED = D_{\text{ext}} + D_{\text{int}}$  and  $D_{\text{ext}} \geq 0$ . Therefore, it might be expected the  $a$ -factor of 76165 to be  $\leq 0.1$  but not to be significantly greater than 0.1.

### 7.3 Thermal study at 'low' T of 76165 powders of various grain sizes

Several samples of coarse and fine powders were annealed before and just after irradiation, in order to manifest the presence of signal  $S_{2A}$  and study its fading. Figure (7.3.1) shows that significant retrapping occurs, leading to the appearance of two maxima at approximately  $60^{\circ}\text{C}$  and  $160^{\circ}\text{C}$ . Minimum ESR intensities ( $I_{\text{min}}$ ) are obtained at approximately  $110^{\circ}\text{C}$  for both natural and irradiated samples. The decrement ( $I_{\text{r.t.}} - I_{\text{min}}$ ) which the irradiated samples display is probably due to a shallow trap, the electrons of which fade quickly at approximately  $80^{\circ}\text{C}$ , and at a slower but measurable rate at room temperature. This means that instead of waiting one week to allow  $S_{2A}$

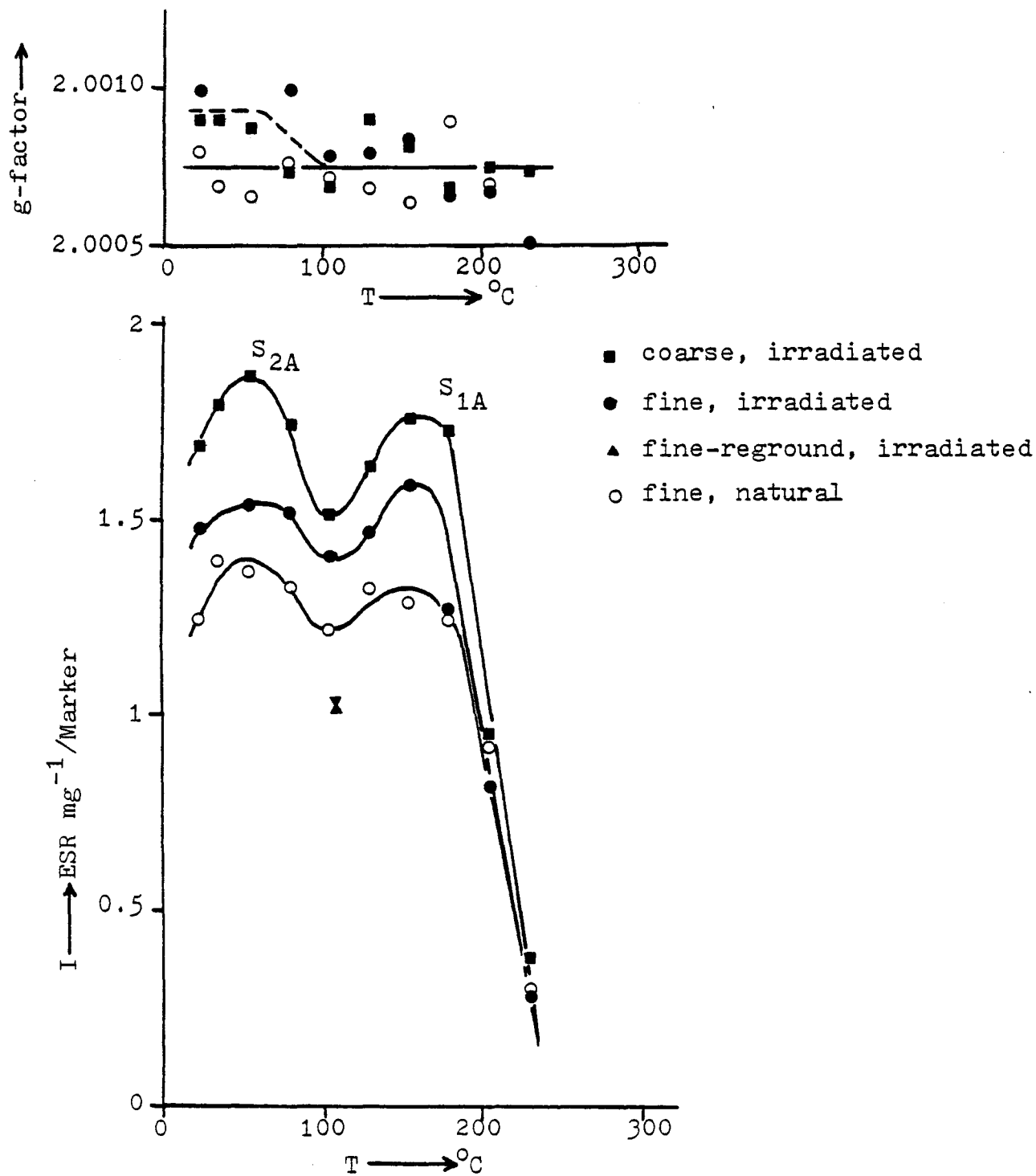


Figure 7.3.1 F/st. 76165. Step annealing ( $\Delta T = 25^\circ\text{C}$ ,  $t^* = 12\text{min.}$ ) at low  $T$  of coarse ( $> 100 \mu\text{m}$ ) or fine ( $< 100 \mu\text{m}$ ) powders, natural or irradiated with 2.46 Krads of gammas. ESR spectra have been taken soon after irradiation.



to fade, one could heat the irradiated samples at about  $110^{\circ}\text{C}$  for about 10 min, thus obtaining the ESR intensity of  $S_{1A}$  without any contribution from  $S_{2A}$ . This procedure has been already followed successfully by several authors (see section 4.4 (i)). The plot of g-factor versus T is also shown in Figure (7.3.1). A trend of the irradiated samples to yield higher g-values for  $T < 100^{\circ}\text{C}$ , though not quite clear, may indicate that the g-value of  $S_{2A}$  is close to 2.001.

The results of this experiment show that ESR intensity decreases with decreasing grain size (Figure 7.3.1). Besides, the difference in ESR intensity between coarse (greater than 0.1 mm) and fine (less than 0.1 mm) grains is significantly less than that between fine and fine-reground grains. Therefore, we may expect further changes in intensity to become negligible for grains greater than 0.1 mm.

#### 7.4 Thermal study at 'high' T

The annealing of 76165 revealed a signal  $S_X$  where ESR intensity does not rise with irradiation. Its occurrence created some problems in the  $S_{1B}$  peak-to-peak height determination, so we decided to study its origin in order to reduce or even better, eliminate its presence, if possible. It is possible that  $S_X$  is due to burned organic impurities,

since heating was done in open air<sup>⊗</sup>. This interpretation was proposed independently by Apers et al. (1981) to explain the occurrence of a signal similar to our  $S_X$  (section 2.4). We repeated step annealing, this time in vacuum of  $\leq 10^{-4}$  atm., but reduction of  $S_X$  was not achieved. It may be that the vacuum was not good enough, since organic impurities in speleothems are present in trace amounts. Artificially precipitated calcite of high purity (ULTREX  $\sim 99.97\%$   $\text{CaCO}_3$ ) should not have contained such organics, but the  $S_X$  was still present in such pure calcite, though displaying smaller intensity than that of 76165. Two more speleothems were tested (807 CW-6, 73107) and these showed large differences in  $S_X$  intensity. The  $E_3$  sample of 77200 did not reveal any  $S_X$ . These results are displayed in Figure (7.4.1).

Signal  $S_X$  does not seem to be related to calcite dissociation ( $\text{CaCO}_3 \xrightarrow{\sim 900^\circ\text{C}} \text{CaO} + \text{CO}_2^\uparrow$ ), since its growth and fading occurs at temperatures well below  $900^\circ\text{C}$ . Another indication which supports this comes from the ESR signals of  $\text{Mn}^{2+}$  impurities inherent into the 76165 samples. Figure (7.4.2) shows that the g-values of some  $\text{Mn}^{2+}$  Forbidden Transitions (those lying between the  $\text{Mn}^{2+}(+\frac{1}{2})$  and  $(-\frac{1}{2})$  peaks) are temperature dependent. At low T ( $24-120^\circ\text{C}$ )

<sup>⊗</sup>for instance:  $\text{M} + \text{RC}_n\text{H}_m \xrightarrow{450-650^\circ\text{C}} \text{M}^+ + \text{RC}_n\text{H}_m^-$  and  $\text{RC}_n\text{H}_m^- + \text{O}_2 \xrightarrow{650-850^\circ\text{C}} \text{CO}_2^\uparrow + \dots$  where M=Trace metal and  $\text{RC}_n\text{H}_m^-$  the organic radical responsible for the signal  $S_X$ .

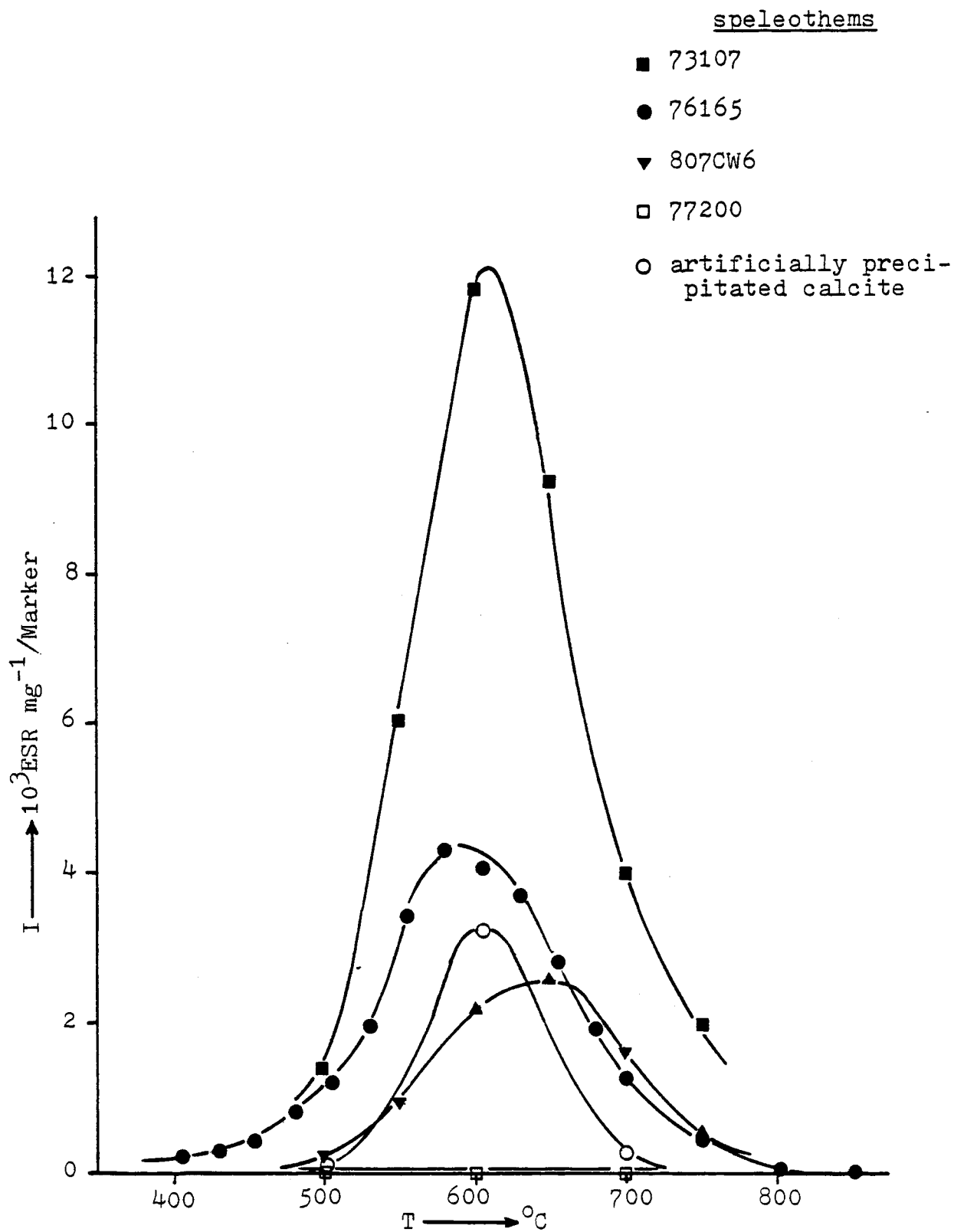


Figure 7.4.1 Step annealing at high  $T$ , for various speleothems.  
 $I \equiv$  ESR intensity of  $S_X$ .

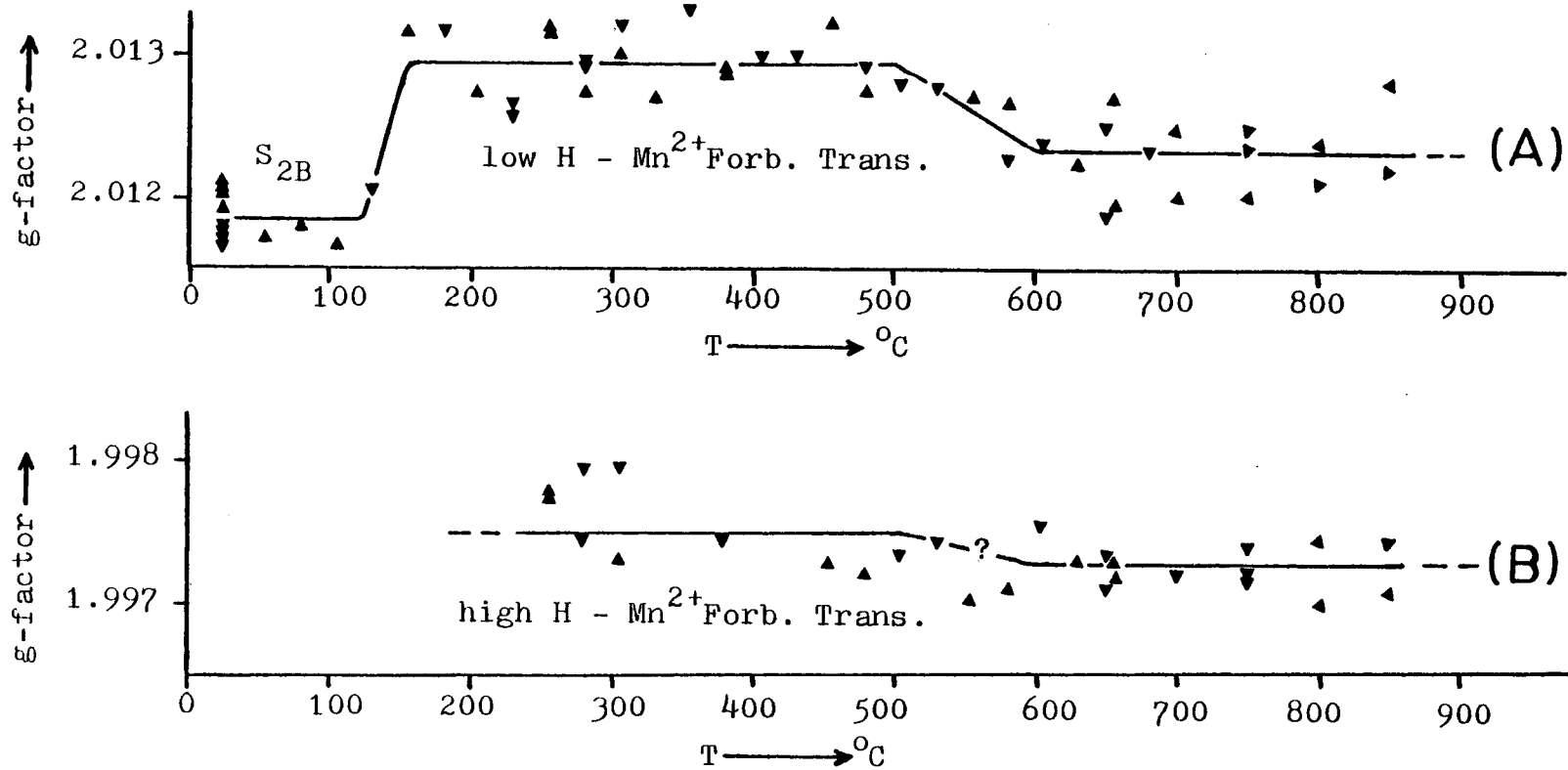


Figure 7.4.2 F/st. 76165. g-value dependence on temperature for low H (A) and high H (B) Mn<sup>2+</sup> Forbidden Transitions.

the low H-Mn<sup>2+</sup> Forb. Trans. (Figure 7.4.2-A) is superimposed by the S<sub>2B</sub> peak, so that the latter predominates. As S<sub>2B</sub> fades, the g-factor reaches its normal value of approximately 2.01295 ( $\pm 15$ ) which remains constant up to about 500°C. From 500 to 600°C, the g-factor decreases and reaches the value of approximately 2.01235( $\pm 15$ ) which remains constant up to 850°C. A similar but less prominent drop of g-values could be considered to occur in the case of the high H-Mn<sup>2+</sup> Forb. Trans. (Figure 7.4.2-B). Kolat and Ozer (1979) have found a change of Mn<sup>2+</sup> g-values to occur during the dissociation of artificially precipitated calcites and speleothems. The dissociation started at 750°C after 15 minutes of heating or at 700°C after 60 minutes heating, and completed after 45-60 minutes or 120-270 minutes respectively. In our case, the temperature at which g-values change is well below 700°C and the heating time (about 10 minutes) much shorter than 60 minutes. Thus, dissociation of calcite is unlikely at least on a large scale.

The above results could be interpreted by considering that S<sub>X</sub> :

- (i) is due to a foreign inorganic substance, incorporated into the calcite lattice during crystallization in various amounts.
- (ii) is related to some structural alteration of calcite at 500-600°C, as is implied from the

drop of  $Mn^{2+}$  Forb. Trans. g-values which suppose to be characteristic of the host crystal structure.

This model, however, could be doubtful for various reasons. What can be said, at the moment, is that  $S_X$  is a free radical induced by heating of natural and artificial calcites, the growth in ESR intensity of which occurs at the same T-range as that at which the drop of the g-value of the low H- $Mn^{2+}$  Forbidden Transition occurs. The nature of the center can only be determined by careful single-crystal studies.

#### 7.5 Speleothems 77032 and 77159 . Given data and details on analytical procedure

77032 is a 15 cm long stalagmite, a dense white-yellow calcite, taken from the Castleguard Cave, Banff National Park Alberta. For the piece we examined (top 2cm) Gascoyne (1979, p.467) gives:  $[U]=2.51$  ppm,  $^{230}Th/^{232}Th=274$ , and  $t=277.8^{+26.1}_{-21.6}$  Ka (U/Th date), that is, both  $[U]$  and  $t$  are relatively high and would be expected to yield a strong ESR signal.

77159 is a piece of flowstone, taken from the Victoria Cave, N.W. England. For the portion we examined (top 1 cm), Gascoyne (1979, p.455) gives:  $[U] = 0.32$  ppm,  $^{230}Th/^{232}Th=9$ , and  $t=92.5^{+9.5}_{-9.0}$  Ka (U/Th date), that is both  $[U]$  and  $t$  are relatively low and should yield a weak

ESR signal.

After extraction of the samples from the speleothems, they were ground and sieved. Several fractions of different range of grain sizes were separated and their natural ESR intensity ( $I_n$ ) was measured on the JEOL spectrometer. Seven fractions of 77032 and three fractions of 77159 were given approximately 2.4 Krads of gammas. Their ESR intensity was measured soon after irradiation and remeasured after heating the samples at approximately 110°C for about 10 minutes. The samples' weights were as follows:

77032 , natural: ~260 mg or ~110 mg, irradiated or heated: approximately 110 mg

77159 , approximately 330 mg for natural, irradiated and heated.

### 7.5.1 Experimental results

Four different radiation sensitive ESR signals were revealed in the examined samples , as shown in the following table.

Speleo- them	g-value	T*°C	present in the natural state	notes	signal's symbol
77032	2.00075 (±5)	>160	YES	strong signal	S <sub>1A</sub> (?)
	2.01190 (±10)	~130	NO		S <sub>2B</sub> '

table continued on next page

Speleo- them	g-value	T*°C	present in the natural state	notes	signal's symbol
77159	2.00380 (±10)	>110	YES	weak signal	S <sub>1A'</sub>
	2.01170 (±5)	<110	NO(?)	see text	S <sub>2B</sub> (?)

Except for the strong signal of 77032 , the rest of the signals displayed peculiarities which distinguish them from the signals of speleothems 76121 , 77200 and 76165 .

- (i) Stal. 77032: the strong signal of  $g=2.00075$  did not fade at  $\sim 160^{\circ}\text{C}$  (12 min.). This signal could be equivalent to the S<sub>1A</sub> of 77200 and 76165 since its g-value is very similar to the g-value of the latter.
- (ii) Stal. 77032: the signal of  $g=2.01190$  fades quickly at approximately  $130^{\circ}\text{C}$  (Figure 7.5.1.1); its decay by time is shown in Figure (7.5.1.2). This signal cannot be equivalent to the S<sub>2B</sub> of 76165 ( $T^* \cong 100^{\circ}\text{C}$ ), despite the fact that both have similar g-values. We call this signal S<sub>2B'</sub> .
- (iii) F/s 77159: the weak signal of  $g=2.00380$  did not fade at approximately  $110^{\circ}\text{C}$  (10 min.). None of the speleothems studied previously showed signals of such a g-value, and no signal was present at  $g \cong 2.001$ , in natural or irradiated material of 77159 . Therefore, the signal



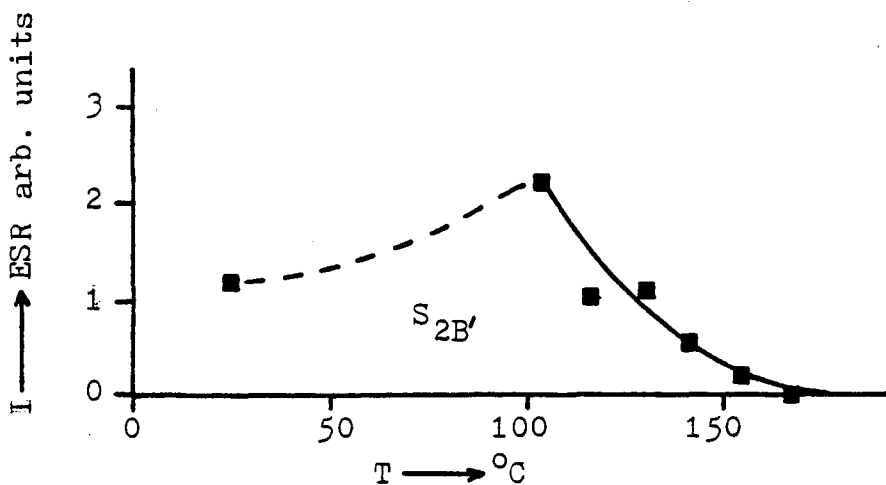


Figure 7.5.1.1 Stal. 77032. Step annealing of powder (300-700  $\mu\text{m}$ ) irradiated with 2.4 Krads gamma and annealed (soon after irradiation).

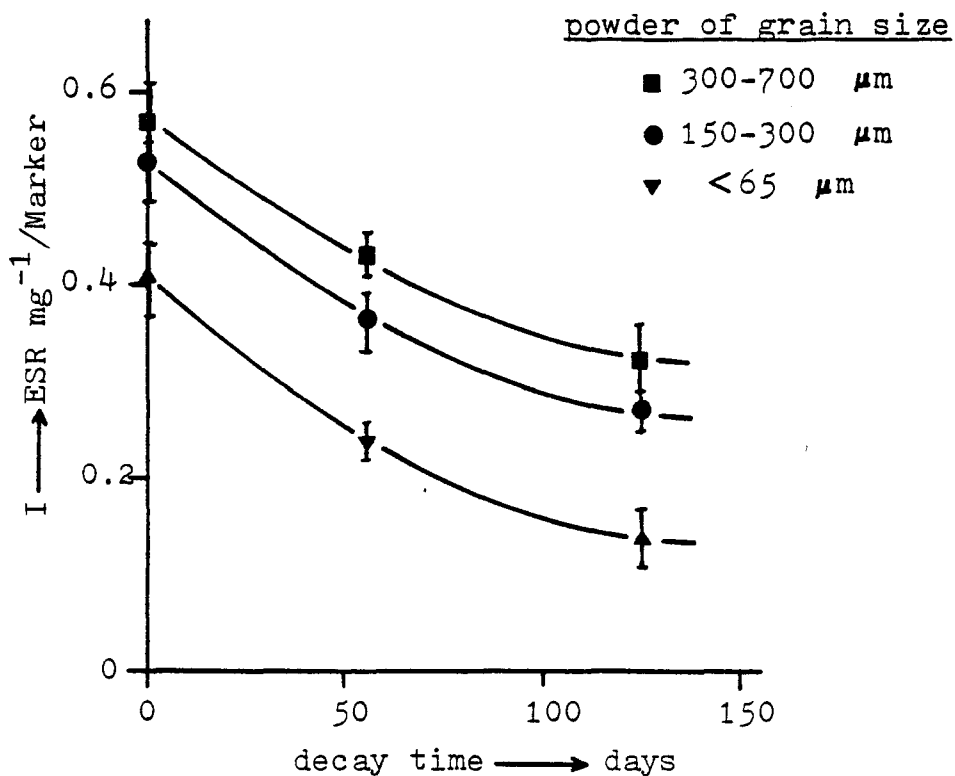


Figure 7.5.1.2 Stal. 77032. ESR signal  $S_{2B'}$ : decay at room temperature.

of  $g \cong 2.004$  was called  $S_{1A}$ .

- (iv) F/s 77159: the signal of  $g=2.01170$  fades quickly at approximately  $110^{\circ}\text{C}$  (10 min.) but only for irradiated material. Besides, this fading does not seem to drop the ESR intensity below the natural level (Figure 7.5.2.2). Such a drop would be expected if the trap responsible for the natural signal has a  $T^* \cong 110^{\circ}\text{C}$ . It seems therefore that the natural ESR intensity represents another signal not sensitive to radiation which has a  $g$ -value very close to 2.0117. The radiation sensitive signal could be identified as  $S_{2B}$ . The 'stable' signal of unknown origin is called  $S_Y$ .

### 7.5.2 The "grain size effect"

The ESR intensity dependence on grain size for various ESR signals of natural and irradiated materials is shown in Figures (7.5.2.1) and (7.5.2.2).

- (i) Stal. 77032,  $S_{1A}$ : it is clear that ESR intensity (I) decreases as grain sizes become  $< 200 \mu\text{m}$ . If  $\Delta I$  represents the intensity increment due to irradiation ( $\Delta I = I_{\text{irradiated}} - I_{\text{natural}}$ ), i.e.  $\Delta I = s(\gamma)D$  where  $D=2.4 \text{ Krads}$ - $\gamma$ , it seems that  $\Delta I$  is not independent of grain size. However, this may be a phenomenological

Figures 7.5.2.1 and 7.5.2.2 Stal. 77032 and F/st 77159. The "grain size effect" for various ESR signals. The powders are natural, irradiated (2.4 Krads of gammas), or irradiated and annealed soon after irradiation at 110°C for about 10 minutes.

Figure 7.5.2.1 Stal. 77032

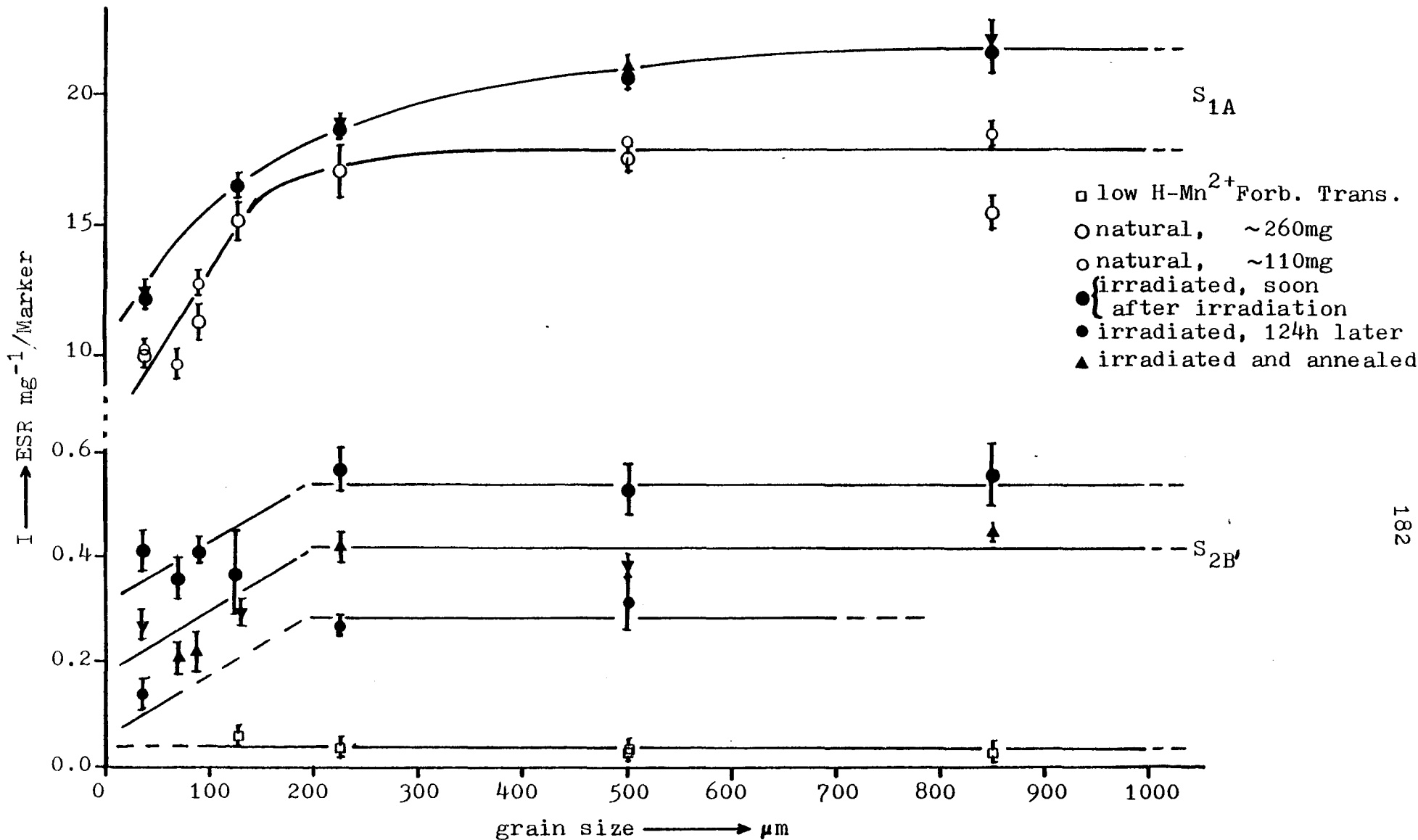
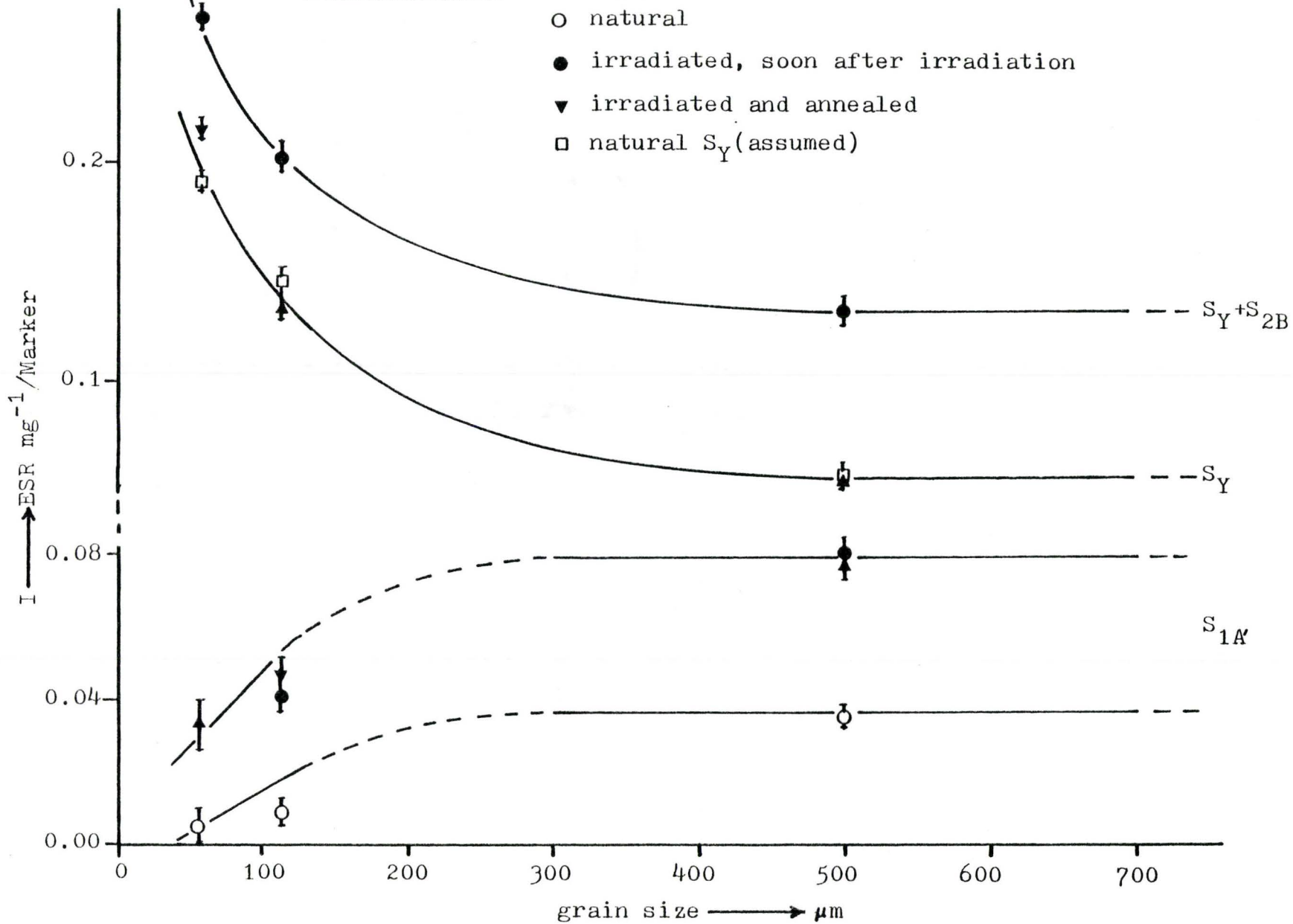


Figure 7.5.2.2 F/st 77159



dependence arising from insufficient resolution of the JEOL spectrometer.

- (ii) Stal. 77032,  $S_{2B}$ : this signal is present only in irradiated materials and overlaps the low H-Mn<sup>2+</sup> Forb. Trans. of  $g=2.01280 (\pm 20)$ , the latter shown only in natural materials. It is obvious that  $\underline{I}$  decreases as grains become less than 200  $\mu\text{m}$ . However, if the  $s(\gamma)$  of this signal was independent of grain size, then the  $\underline{I}$  of irradiated material ought to be the same for any grain size. Besides, the  $\underline{I}$  of fine grains seem to decay faster than that of coarse grains (Figure 7.5.1.2).
- (iii) F/s 77159,  $S_{1A'}$ : this signal displays similar behaviour to that of  $S_{1A}$  (see (i) above).
- (iv) F/s 77159,  $S_{2B}$ : since this signal overlaps the 'stable'  $S_Y$  (see section 7.5.1 (iv)), the 'inverse' relation to grain size is due to the latter. The  $s(\gamma)$  of  $S_{2B}$  seems to be approximately constant for any grain size ( $\Delta I \cong \text{constant}$ ).

The above results show the presence of two kinds of "grain size effect":

- (i) The so called "grain size effect on  $s(\gamma)$ " seems to be related mainly with centers of low  $T^*$  which are not present in natural materials

(signal  $S_{2B}$ ). Its occurrence could be interpreted by considering the  $s(\gamma)$  of these centers to be dependent on grain size.

- (ii) The so called "grain size effect on  $I_n$ " or simply "grain size effect" is related with centers stable at room temperature, the ESR signals of which ( $S_{1A}$ ,  $S_{1A'}$ ) could be used for dating. Its occurrence is probably due to sample preparation (grinding) and the related surface effects (see next section). Such an effect of the grain size on  $I_n$  has been found to occur in other speleothems, too (Figure 6.8.2.1).

It should be pointed out that any  $I_n$  depletion for fine grains is not due to the variable space coarse and fine powders of equal weight occupy into the spectrometer's resonance cavity. On the contrary, this variability should favour fine grains to yield high  $I$ , since the smaller the sample space  $V_s$  the higher the  $I$ , as explained in section(4.5).

### 7.6 Grain size effect and grain 'surface'

The grain size effect has been attributed to surface effects caused during sample preparation (section 6.8.2). To eliminate these effects, other workers commonly treat the grains with 0.5% acetic acid for 1 minute. We tested

that treatment on four fractions of stal. 77032. The results are shown in Figure (7.6.1). It is seen, as expected, that 1 minute acid attack increases the  $\underline{I}$  of fraction 150-300  $\mu\text{m}$  more than that of fraction 300-700  $\mu\text{m}$ . Further acid attack does not change the intensities, suggesting that 1 minute is sufficient for coarse grains to attain maximum  $\underline{I}$ . However, the fine fractions (75-110  $\mu\text{m}$ , less than 65  $\mu\text{m}$ ) have unexpected behaviour: it seems that acid attack does not affect their  $\underline{I}$ . It is not likely that this 'anomalous' finding results from our techniques. On the other hand, very fine grains could have certain peculiarities, not studied so far. If the "grain size effect" is due to production during grinding of a disturbed zone of uniform thickness " $d$ " in which the  $\underline{I}$  is much lower than in undisturbed calcite, then for particles of radius  $r \leq d$ , there will be little effect of acetic acid dissolution, since the whole grain is disturbed. For  $r$  greater than  $d$ , intensity will increase as the disturbed part is stripped off (Figure 7.6.2). We note that the  $\underline{I}$  of the disturbed volume is not zero because  $\underline{I}$  continues to decrease with decreasing  $r$  for  $r$  less than  $d$ , corresponding to separation of grains which have suffered progressively more disturbance per cubic centimeter.



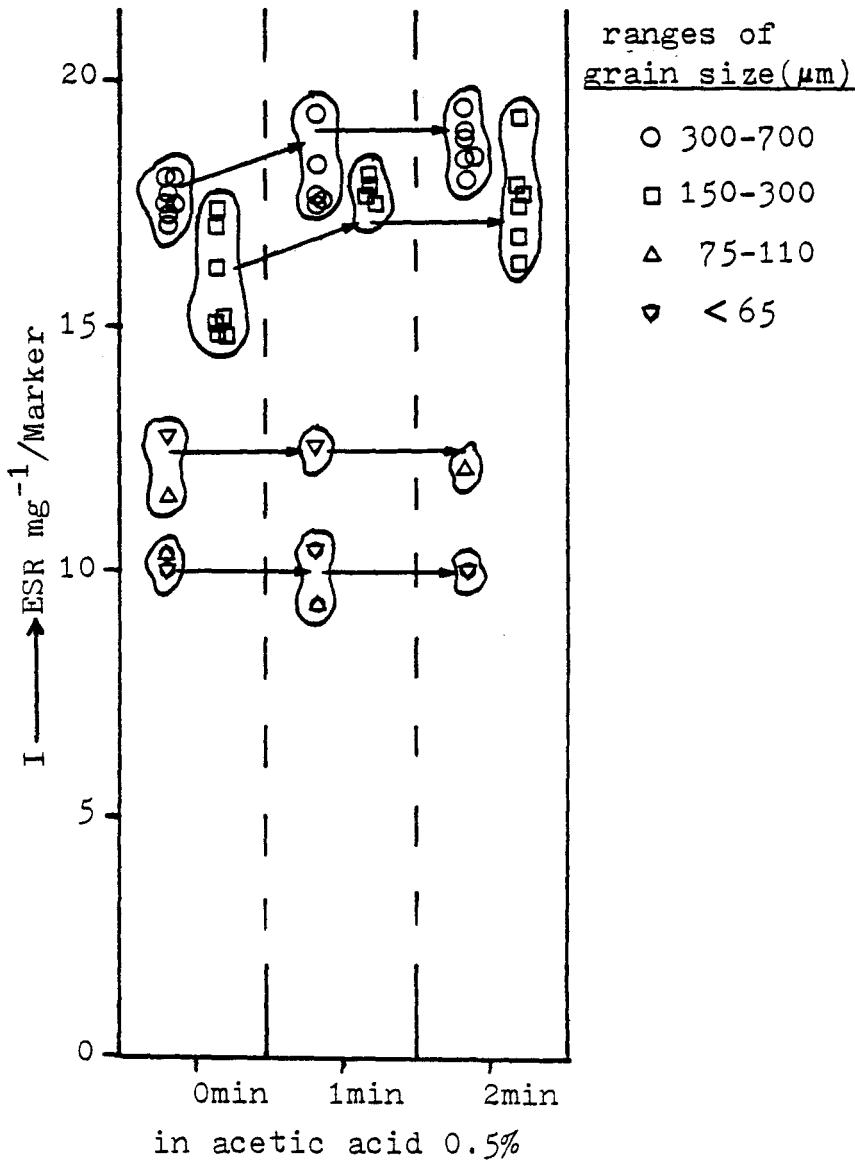


Figure 7.6.1 Stal. 77032. The effect of etching with acetic acid 0.5% on the dating ESR signal ( $S_{1A}$ ) for powders of various ranges of grain size.

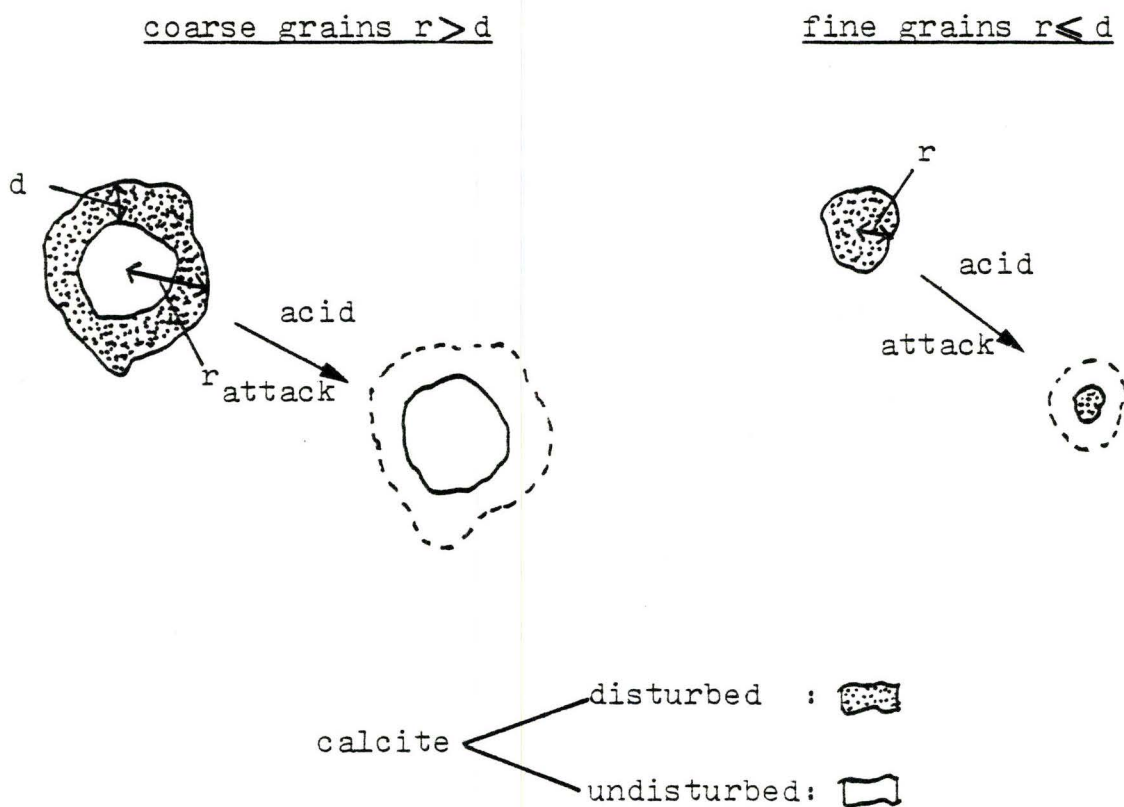


Figure 7.6.2 Acid attack does not affect the ESR intensity of very fine grains ( $< 100 \mu\text{m}$ ).

## 7.7 Discussion

Reviewing the results of this chapter, we note that the so-called "retrapping" of electrons found to occur just before the activation temperature of each trap (section 7.3) has also been observed by other workers (section 2.4, Figure 2.4.1). It is not clear how retrapping can occur, because Levy's model (section 1.4.2) will not allow such electron behaviour. Further, retrapping presumes the presence of a reservoir of non-atomic electrons within the calcite, which need thermal activation before they enter the trap. Such electrons could be found if traps shallower than that responsible for the retrapping are filled at room temperature, some of these being transferred to the deep trap during annealing. However, "retrapping" occurs even in natural materials, where the shallow traps are presumably empty. The lack of a proven model to explain these peculiarities discouraged us from heating irradiated samples (see: section 4.4 - (i)), for determination of ED's.

## CHAPTER 8: Concluding remarks

### 8.1 Introduction

The foregoing chapters have demonstrated the application of ESR isochron dating techniques to speleothems. It was necessary to undertake some preliminary work on the analytical techniques used (chapter 7) because of inadequacies in existing procedures. The purpose of this chapter is to review the results and draw implications from them regarding aspects of dating by ESR isochron methods. Some of these results will also be compared and contrasted with previous ESR work on speleothems.

### 8.2 Distribution of some trace elements in single speleothem layers

The distribution of U and Mn within a single layer of the examined speleothems is not homogeneous. The following table displays [U] and [Mn] ranges for several layers, as well as  $\epsilon$ -values for each TE. The  $\epsilon$ -factor is defined by the equation:

$$\epsilon(\text{TE}) = \frac{[\text{TE}]_{\text{max}} - [\text{TE}]_{\text{min}}}{([\text{TE}]_{\text{max}} + [\text{TE}]_{\text{min}}) / 2} \cdot 100 \% \quad (8.2.1)$$

indicating that the [TE] range is  $\epsilon\%$  of the average of the extreme [TE]-values.

Speleothem	layer	[U] min ppm	[U] max ppm	$\epsilon(U)$ %	[Mn] min ppm	[Mn] max ppm	$\epsilon(Mn)$ %
77200	EF	2.3	3.2	33	5	18	113
	K	2.1	2.5	17	-	-	-
	0	1.6	2.1	27	1	2	67
75037	2	39.3	39.7	1	-	-	-
	4	51.3	58.1	12	-	-	-
	6	40.8	44.6	9	-	-	-

For isochron plots it is necessary to have sufficient [U]-range, i.e. high  $\epsilon(U)$ . In fact, the lower the accuracy in the determination of EDs the higher the  $\epsilon(U)$  that is required. Hence the minimum  $\epsilon(U)$  required for a particular isochron depends on both: a) the dating ESR signal and its peculiarities, and b) the ESR spectrometer resolution, fidelity and possibility of systematic error. In our work, the reproducibility of the ED-values obtained by the JEOL: JES-3BX-X spectrometer was proven inadequate for the demands of  $\epsilon(U) \cong 30\%$ , while the Varian: E104A spectrometer did not show such drawbacks. The 77200 EF and 0 layer  $\epsilon(U)$  results are quite promising for the application of the ESR isochron dating method. In the case where the  $\epsilon(U)$  of a single layer is 'low', multilayer analysis may be the only way to get high  $\epsilon(U)$ , as shown in the following table:

Speleothem	layers	[U] min ppm	[U] max ppm	$\epsilon(U)$ %
77200	EF, K, 0	1.6	3.2	67
75037	1, ..., 6	32.7	58.1	56
76121	Top, Base	1.9	2.6	31

The  $[Mn]$  values within some single layers of the speleothem 77200 range widely ( $\epsilon(Mn)$  up to 113%). Therefore, a high  $\epsilon(Mn)$  combined with the effect of  $[Mn^{2+}]$  on  $I_n$  (see section 6.4.1) may not allow the ESR intensity single layer isochron to be applicable in cases of low  $\epsilon(U)$ .

### 8.3 Detrital uranium and its effect on the isochron slope

The difference between IDA and NAA determinations of  $[U]$  has been attributed to the presence of U in detritus (see section 4.6). The  $\alpha$ -particles of such a detrital U cannot reach calcite itself because of their short range, and calcite true  $D_n(ED)$  should be less than the  $D_n$  expected for total U content. If the dose ED could be attributed to an exclusively 'calcitic' U, the concentration of which can be called "effective  $[U]$ ", then  $[U]_{\text{effective}} < [U]_{\text{total}}$  and therefore IS (based on  $[U]_{\text{total}}$ )  $<$  IS (based on  $[U]_{\text{effective}}$ ). Thus the isochron ages as found by using  $[U]_{\text{total}}$  should be smaller than the 'true' age.

The above model could supply one more explanation for the **low** isochron age of the flowstone 77200 (see section 6.7) and justify the good agreement between ESR isochron and U/Th dates for the stalagmite 76121 (see section 5.7). The 77200 Top 2 cm sample yielded  $[U] = 0.95$  ppm (IDA), a value quite small in contrast with the EF layer, the

[U]-values of which range from 2.3 to 3.2 ppm (NAA). If layers A, B, C, D do not have  $[U] \ll 0.95$  ppm to balance the EF layer high [U], the large difference between IDA and NAA could be interpreted as being due to the detrital U, which should constitute significant portion of the total U of layer EF. On the other hand the 76121 Top 1 cm and Base 2 cm samples yielded IDA [U]-values:  $\sim 2.4$  and  $1.5$  ppm respectively, which are quite close to the NAA [U]-values:  $\sim 2.6$  and  $1.9$  ppm.

#### 8.4 The effect of Mn on the radiation-induced ESR signals

Ikeya's (1975) remark that Mn may suppress  $I_n$  was verified with the study of speleothem 77200 (see section 6.4.1). Results from other speleothems also confirm this "[Mn<sup>2+</sup>]-effect". A piece of the flowstone 76111 yielded: [U] = 0.30 ppm (IDA),  $^{230}\text{Th}/^{232}\text{Th}=15$  and U/Th age, corrected for detrital Th,  $t=26.9_{-3.3}^{+3.4}\text{Ka}$  (Gascoyne, 1979, p.451). Our analysis gave: [U] = 0.3 ppm and [Mn]=94 ppm (NAA). The U content and age of this material, as compared to those of the rest of the speleothem examined, are sufficient for allowing a detectable radiation-induced ESR signal to be seen. No signal other than the very strong Mn<sup>2+</sup> lines was observed in the ESR spectra. The flowstone 77159 S<sub>1A'</sub> natural signal is unusually weak probably because of the high Mn<sup>2+</sup> content, as inferred from the strong Mn<sup>2+</sup> ESR

lines. The U content and age of this material (see section 7.5) do not justify such a low intensity.

### 8.5 Comparison of ESR signals obtained in this work with those in literature

For powdered samples, the parameters: g-factor and  $T^*$  are the only means available in the ESR techniques which can characterize charge traps. Table (8.5.1) displays the g-values and some other characteristic properties of the ESR signals of our speleothems, as well as the symbols adopted for them. The compilation of this table was possible after the observation that many signals were quite common amongst the examined materials. The  $T^*$  and g-values given by other workers (see section 2.4) show only few similarities with those of table (8.5.1). A one-to-one correspondence between g-value and  $T^*$  cannot be established. It seems that the mentioned parameters are not sufficient to identify traps. The g-values of Apers et al. (1981) however match relatively well with our data, as shown in table (8.5.2). There is a tendency for our g-values to be systematically higher than those of Apers et al. This discrepancy could be attributed either to a systematic error of the ESR spectrometer or to the different MW and time constant used in each case. The above discussion shows that interlaboratory determination of  $T^*$  and g-values for identical samples would be very useful.



Table (8.5.1): ESR signal Classification

g-value	Present in Nat. Mat.	Radiation Sensitive	Intensity of Occurrence	T* °C	remarks	symbol adopted
1.981	-	-	-	-	Marker's Mn <sup>2+</sup> (+½): STANDARD	-
1.9975(+3)	-	NO	variable (rather weak)	-	calcite's Mn <sup>2+</sup> (high H Forb. Trans.)	-
2.0001(+2)	NO	NO	very weak	-	arises at $\left\{ \begin{array}{l} T > 200^{\circ}\text{C} \text{ for art. ppt CaCO}_3 \\ T > 650^{\circ}\text{C} \text{ for 76165 speleothem} \end{array} \right.$	-
2.0008(+2)	YES	YES	strong	~220	dating signal, present in most of the speleothem samples	S <sub>1A</sub>
~2.001	NO	YES	very weak	~80	signal parasitic to S <sub>1A</sub>	S <sub>2A</sub>
2.0024(+1)	?	?	very weak	?	present in art. ppt CaCO <sub>3</sub> only	-
2.0032(+2)	NO	NO	variable (rather strong)	-	arises at T > 250°C, fades at ~720°C	S <sub>X</sub>
2.0038(+1)	YES	YES	very weak	>110	present in 77159 spel. only	S <sub>1A'</sub>
2.0059(+1)	YES	YES	weak	~380	-	S <sub>1B</sub>
2.0070(+2)	YES	YES	weak	?	-	S <sub>1B'</sub>
2.0118(+2)	NO NO YES(?)	YES YES NO(?)	weak weak weak	~100 ~130 -	arises in most of the speleothem samples present in 77159 spel. only	S <sub>2B</sub> S <sub>2B'</sub> SY
2.0125(+5)	-	NO	variable (rather weak)	-	calcite Mn <sup>2+</sup> (low H Forb. Trans.)	-
2.033	-	-	-	-	Marker's Mn <sup>2+</sup> (-½)	-

Table (8.5.2): Comparison of ESR data of this work with that of Apers et al., (1981)

		Apers <u>et al.</u> , 1981			Present work			
		g-value	T* or T of occurrence (°C)	symbol , identification	g-value	T* or T of occurrence (°C)	symbol , identification	
radiation induced signals		2.0057	~330	I	2.0059(+1)	~ 380	S <sub>1B</sub>	
		2.0035	~200	II	2.0038(+1)	> 110	S <sub>1A'</sub>	
		2.0002	~220	III	2.0008(+2)	~ 220	S <sub>1A</sub>	
		2.0002	<100	parasitic	~2.001	~ 80	S <sub>2A</sub>	
signals induced by annealing		2.0029	>350	IV	2.0032(+2)	> 250	S <sub>X</sub>	
signals due to impurities		2.0102	-	Mn <sup>2+</sup> lines	2.0125(+5)	-	low H Mn <sup>2+</sup> Forb.Trans.	
experimental conditions	MW (gauss)	0.5			3-4			
	time const. (sec.)	0.5			0.03-0.1			
	step annealing	ΔT (°C)	50			25		
		t* (min)	60			6-12		
		t <sub>o</sub> (min)	30			5-15		

The puzzling results of Yokoyama et al. (1981 b) (see section 2.4) invite some scepticism. They studied samples from "stalagmitic floors" (flowstones) of the cave, "Caune de l'Arago" at Tautavel . Though Apers et al. (1981) have examined samples from the same flowstones, their results are quite different regarding ESR signal  $T^*$  and  $g$ -values. Yokoyama's samples, however, contain appreciable quantities of sediment, presumably limestone particles incorporated into the flowstone during the calcite deposition. Several "stalagmitic calcites" of the said cave have been studied by image intensifier TL (Walton and Dubenham, 1981), who showed that particles of geologically old local limestone are probably present in the matrix of the stalagmite. Such a consideration might explain the discrepancy of  $T^*$  and  $g$ -values between speleothems - pure calcites (materials of the present work) and those contaminated with limestone detritus (Yokoyama's materials). Furthermore, Yokoyama's finding that grain sizes less than  $8 \mu\text{m}$  and greater than  $500 \mu\text{m}$  showed the same  $I_n$ , in contrast to our "grain size effect", might have some relation with the detrital limestone. This thought arises from Lewis' (1968) TL study, where it is shown that limestone natural TL intensity decreases as grain sizes become either less than  $70 \mu\text{m}$  or greater than  $125 \mu\text{m}$ .

### 8.6 Suggestions for further research

The results obtained in this study are sufficiently encouraging that the efforts to improve and expand the isochron dating method should be continued. Several improvements are suggested:

- (i) The ESR signals of both natural and irradiated materials have to be studied thermally, in order to assure high accuracy for EDs.
- (ii) The use of distant samples taken from a well defined broad flowstone growth layer is proposed, in order to obtain high  $\epsilon(U)$ -values.
- (iii) Though a-value approximately equal to 0.1 seems to be common for many pure calcites, such as those examined in this study, an improvement of the isochron plot to account for possible a-value variability could be proven useful. For equilibrium cases (section 3.6.2), instead of plotting ED versus  $[U]$ , the plot of ED versus  $c \Delta_1 [U]$  eliminates any a-value differences and its slope gives directly the isochron age. Such a plot, however, requires determination of the a-factor for each one of the samples individually, which is quite time consuming.

The isochron dating method can be served by ESR as well as by TL since both can determine EDs. Not only that, but

materials other than speleothems might be proven appropriate for isochron dating. Any materials that satisfy several basic criteria required for the conventional ESR or TL dating methods (see for instance: Ikeya, 1978a and Wintle, 1980) can potentially be used.

References

- AITKEN, M.J., 1974: Physics and Archaeology. Clarendon Press, Oxford.
- AITKEN, M.J., 1981: Thermoluminescence dating: introductory review, in R<sub>1</sub>, p. 379-390
- AITKEN, M.J., and S.G.E., BOWMAN, 1975: Thermoluminescent dating: assessment of alpha particle contribution. Archaeometry, 17, 132-138
- AITKEN, M.J., and A.G., WINTLE, 1977: Thermoluminescence dating of calcite and burnt flint: the age relation for slices. Archaeometry, 19(1), 100-105
- APERS, D.J., et al., 1980: A propos d'un essai de datation par RPE de concrétions calcaires originaires de grottes Belges. Radiochem. Radioanal. Letters, 45(6), 427-440
- APERS, D.J., et al., 1981: A criticism of the dating by Electronic paramagnetic resonance (ESR) of the stalagmite floors of the Caune de l'Arago at Tautavel, in R<sub>1</sub>, p.533-550
- ARENA, V., 1971: Ionizing Radiation and Life. The C.V. Mosby Co., Saint Louis
- BELL, W.T., 1976: The assessment of the radiation dose-rate for Thermoluminescence dating. Archaeometry, 18(1), 107-111
- BELL, W.T., 1977: Thermoluminescence dating: revised dose-rate data. Archaeometry, 19(1), 99-100
- BELL, W.T., 1979: Thermoluminescence dating: radiation dose-rate data. Archaeometry, 21(2), 243-245
- BONFIGLIOLI, G., 1968: Thermoluminescence: what it can and cannot show, in R<sub>2</sub>, p. 15-24
- COOPE, G.R., 1975: Climatic fluctuations in northwest Europe since the last interglacial, indicated by fossil assemblages of Coleoptera, in Ice Ages: Ancient and Modern. A. E. Wright and F. Moseley eds., Liverpool. p. 153-168
- DE CANNIERE, P., et al., 1982: ESR study of radiation effects in <sup>210</sup>Po doped calcium carbonate: contribution to the estimation of the paleodose in a stalagmitic floor. Radiochem. Radioanal. Letters, 50(6), 345-353

- ENGE, H., 1970: Introduction to Nuclear Physics. Addison-Wesley Publ. Co., Inc., London
- GASCOYNE, M., 1977: Trace elements in calcite - the only cause of speleothem color? Proceedings of the 1977 NSS Annual Convention, p.39-42.
- GASCOYNE, M., 1979: Pleistocene climates determined from stable isotope and geochronologic studies of speleothem. Ph.D. Thesis, McMaster University, Hamilton.
- GASCOYNE, M., et al., 1978: Uranium series dating and stable isotope studies of speleothems: part I - theory and techniques. Brit. Cave. Res. Assoc., 5(2), 91-111
- HARWELL AERE-R 10044: Report on the Second Uranium-Series Intercomparison Project Workshop, Harwell 23 to 24 June 1980. U.K. Atomic Energy Authority.
- HENNIG, G.J., et al., 1980: Uranium series dating and Thermoluminescence ages of speleothem from Petralona cave, Chalkidiki, Greece. Anthropos (Athens, GR), 7, 174-214.
- HENNIG, G.J., et al., 1981a: ESR-dating of the fossil hominid cranium from Petralona Cave, Greece. Nature, 292, 533-536
- HENNIG, G.J., et al., 1981b: Electron Spin Resonance (ESR) dating of speleothem of the Caune de l'Arago at Tautavel. Notes on problems and progress, in R<sub>1</sub>, p.551-555
- IKEYA, M., 1975: Dating a stalactite by electron paramagnetic resonance. Nature, 255, 48-50
- IKEYA, M., 1976: Natural Radiation Dose in Akiyoshi Cavern and on Karst Plateau. Health Physics, 31, 76-78
- IKEYA, M., 1977: Electron spin resonance dating and fission track detection of Petralona stalagmite. Anthropos (Athens, GR), 4, 152-168
- IKEYA, M., 1978a: Electron spin resonance as a method of dating. Archaeometry, 20(2), 147-158.
- IKEYA, M., 1978b: Spin-Resonance Ages of Brown Rings in Cave Deposits. Naturwissenschaften, 65, 489.

- IKEYA, M., 1980: ESR Dating of Carbonate at Petralona Cave. *Anthropos* (Athens, GR), 7, 143-151
- IKEYA, M., 1981: Dating Methods and limitation by Electron Spin Resonance (ESR), in *R<sub>1</sub>*, p. 437-455
- IKEYA, M., and T., MIKI, 1980a: A New Dating Method with a Digital ESR. *Naturwissenschaften*, 67, 191-192
- IKEYA, M. and T., MIKI, 1980b: Electron Spin Resonance Dating of Animal and Human Bones. *Science*, 207, 977-979
- JEOL: JES-3BS-X ESR Instrument Instruction Manual
- KOLAT, A., and A.M., OZER, 1979: The investigation of chemical decomposition process of stalactites by electron spin resonance (ESR) technique. *Ch. Phys. Let.*, 67 (1), 154-156
- LEVY, P.W., 1968: A Brief Survey of Radiation Effects Applicable to Geology Problems, in *R<sub>2</sub>*, p.25-38
- LEWIS, D.R., 1968: Effect of Grinding on Thermoluminescence of Dolomite, Calcite and Halite, in *R<sub>2</sub>*, p.125-132
- LIRITZIS, Y., 1980:  $^{230}\text{Th}/^{234}\text{U}$  dating of spelaeothems in Petralona. *Anthropos* (Athens, GR), 7, 215-241
- LIRITZIS, Y., and A.N., POULIANOS, 1980: A radiation survey of Petralona cave (Comparison with Majorcan caves). *Anthropos* (Athens, GR), 7, 252-259
- MEDLIN, W.L., 1968a: Thermoluminescence Growth Curves in Calcite, in *R<sub>2</sub>*, p.91-110
- MEDLIN, W.L., 1968b: The Nature of Traps and Emission Centers in Thermoluminescent Rock Materials, in *R<sub>2</sub>*, p.193-223
- MARFUNIN, A.S., 1979: Spectroscopy, Luminescence and Radiation Centers in Minerals. Springer-Verlag, Berlin.
- MARSHALL, S.A., et al., 1964: Electron spin resonance absorption spectrum of  $\text{CO}_2^-$  molecule-ions in single crystal calcite. *Mol. Phys.*, 8, 225-231
- MARSHALL, S.A., et al., 1968: Electron Spin Resonance Absorption Spectrum of  $\text{Y}^{3+}$ -Stabilized  $\text{CO}_3^-$  Molecule-Ion in Single-Crystal Calcite. *J. Chem. Phys.*, 48, 5131-5135



- MIKI, T., and M.,IKEYA, 1978: Thermoluminescence and ESR Dating of Akiyoshi Stalactite. Japan. J. Appl. Phys., 17(9), 1703-1704
- MOORE, G.W., and G.N.,SULLIVAN, 1978: Speleology - The Study of Caves. Zephyrus Press, Inc., Teaneck.
- MULLER, G., 1967: Methods in Sedimentary Petrology. Hafner Publ. Co., N.Y.
- NAMBI, K.S.V., 1979: On ESR Dating of Minerals. Japan. J. Appl. Phys., 18(12), 2319-2320
- POOLE, C.P., 1967: Electron Spin Resonance. Intersc. Publ., N.Y.
- POOLE, C.P., 1972: Electron Spin Resonance, in "Guide to Modern Methods of Instrumental Analysis" ed. by T.H. Gow. Wiley-Interscience, N.Y.
- WALTON, A.J. and N.C.,DEBENHAM, 1981: Image intensifier thermoluminescence studies of stalagmitic calcite, in R<sub>1</sub>, p.403-408
- WINTLE, A.G., 1973: Anomalous Fading of Thermoluminescence in Mineral Samples. Nature, 245, 143-144.
- WINTLE, A.G., 1975: Effects of sample preparation on the Thermoluminescence characteristics of calcite. Modern Geology, 5, 165-167
- WINTLE, A.G., 1977: Thermoluminescence dating of minerals - traps for the unwary. J. of Electrostatics, 3, 281-288
- WINTLE, A.G., 1978: A thermoluminescence dating study of some Qua ternary calcite: potential and problems. Can. J. Earth Sci., 15, 1977-1986
- WINTLE, A.G., 1980: Thermoluminescence dating: a review of recent applications to non-pottery materials. Archaeometry, 22(2), 113-122
- WINTLE, A.G. and M.J.,AITKEN, 1977: Thermoluminescence dating of burnt flint: application to a lower Palaeolithic site, Terra Amata. Archaeometry, 19(2), 111-130
- WERTZ, J.E., and J.R.,BOLTON, 1972: Electron Spin Resonance: Elementary Theory and Practical Applications. McGraw-Hill Inc., N.Y.

- YOKOYAMA, Y., et al., 1980: Some problems encountered in the estimation of annual dose-rate in the ESR dating of fossil bones. Proceedings, Specialist Seminar on TL dating, Sept. 1980, Oxford, PACT Journal
- YOKOYAMA, Y., et al., 1981a: Electron Spin Resonance (ESR) dating of bones of the Caune de l'Arago at Tautavel, in R<sub>1</sub>, p.457-492.
- YOKOYAMA, Y., et al., 1981b: Electron Spin Resonance (ESR) dating of stalagmites of the Caune de l'Arago at Tautavel, in R<sub>1</sub>, p.507-532
- YAVORSKY, B., and A., DETLAF, 1975: Handbook of Physics. Mir. Publ., Moscow.
- ZELLER, E.J., 1968: Use of Electron Spin Resonance for Measurement of Natural Radiation Damage, in R<sub>2</sub>, p.271-279
- ZIMMERMAN, D.W., 1972: Relative Thermoluminescence effects of alpha- and beta-radiation. Radiation Effects, 14, 81-92

- 
- R<sub>1</sub>: Datations Absolues et Analyses Isotopiques en Prehistoire- Methods et Limites. Datation du remplissage de la Caune de l'Arago a Tautavel. Colloque International du CNRS, Tautavel, 22-28 Juin 1981.
- R<sub>2</sub>: Thermoluminescence of Geological Materials, ed. by D.J. McDougall, 1968, Academic Press, London.

APPENDIX IFricke-Calcite conversion factor calculation

The dose D (rad) absorbed by a material which is exposed to radiation of dose R (roentgen) is given by the formula (Arena, 1971, p.218).

$$D = 0.869 \frac{\mu_m \text{ of material}}{\mu_m \text{ of air}} R \quad (I_1)$$

where  $\mu_m$  is the mass absorption coefficient

In Fricke's dosimetry the absorbing medium is almost H<sub>2</sub>O while speleothems are mainly CaCO<sub>3</sub>. If both H<sub>2</sub>O and CaCO<sub>3</sub> are exposed to the same R, the ratio of their D's, as given by eq.(I<sub>1</sub>), gets the form:

$$\frac{D(\text{CaCO}_3)}{D(\text{H}_2\text{O})} = \frac{\mu_m(\text{CaCO}_3)}{\mu_m(\text{H}_2\text{O})} \quad (I_2)$$

(i) Calculation of  $\mu_m$  (CaCO<sub>3</sub>)

Enge (1970, Figure 7-8) gives values of  $\mu_m$  (cm<sup>2</sup>/g) for various elements and  $\gamma$ -energies. For <sup>137</sup>Cs  $\gamma$ -rays:  $\mu_m(\text{O})=0.079$ ,  $\mu_m(\text{C})=0.077$ ,  $\mu_m(\text{Ca})=0.076$ ; the total  $\mu_m$  of a compound is given by the equation (Enge, 1970; p.191).

$$\mu_m \text{ (total)} = \sum_i a_i \mu_{mi} \quad (I_3)$$

where  $a_i$  is the abundance of the "i" element in the compound. Thus, for  $\text{CaCO}_3$  we get:

$$\mu_m(\text{CaCO}_3) = 1/5 \mu_m(\text{Ca}) + 1/5 \mu_m(\text{C}) + 3/5 \mu_m(\text{O}) = 0.078 \text{ cm}^2/\text{g}$$

(ii) Calculation of  $\mu_m(\text{H}_2\text{O})$

Yavorsky and Detlaf (1975, p.867-table ) give values of the attenuation coefficient  $\mu(\text{cm}^{-1})$  of  $\gamma$ -rays in various media for several gamma energies  $E(\text{MeV})$ . The plot of these values for water ( $\mu$  versus  $E$ ) is shown in Figure (I<sub>1</sub>).  $^{137}\text{Cs}$   $\gamma$ -rays have  $E=0.662$  MeV and correspond to a  $\mu = 0.083 \text{ cm}^{-1}$ . Since  $\mu_m = \mu/d$  ( $d$ =density), we get:

$$\mu_m(\text{H}_2\text{O}) = \frac{0.083 \text{ cm}^{-1}}{1 \text{ g/cm}^3} = 0.083 \text{ cm}^2/\text{g}$$

Now, equation (I<sub>2</sub>) gives:

$$\frac{D(\text{CaCO}_3)}{D(\text{H}_2\text{O})} = \frac{0.078 \text{ cm}^2/\text{g}}{0.083 \text{ cm}^2/\text{g}} = 0.9398$$

or  $D(\text{speleothem}) \cong 0.94 D(\text{Fricke})$

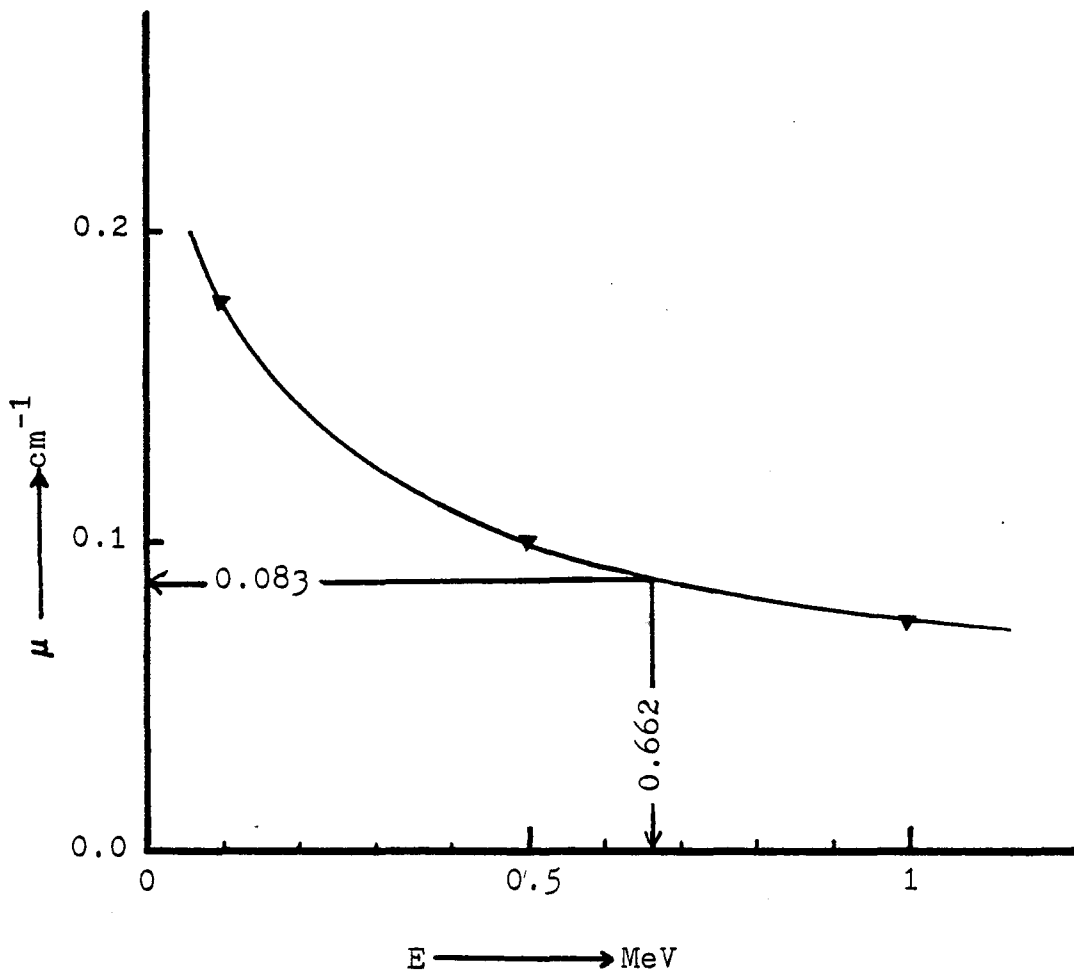


Figure I<sub>1</sub> Attenuation coefficient of  $\gamma$ -rays in water versus gamma energies.

## APPENDIX II

Sample: 77200 E<sub>3</sub>. Calculation of  $\tau_0$  of the TL active defects chosen for dating

The lifetime  $\tau_0$  of trapped charges (see section 1.4.1) can be estimated by means of the equation (1.4.1.3). The obtained value is reliable only if the ratio  $\beta/T^{*2}$  remains relatively constant. The following table displays data from several TL studies on natural calcites.

$\beta$ °C/sec	$T^*$ °K	$T^{*2} 10^4 \text{°K}^2$	Reference
0.5	500	25.00	Medlin, 1968a,b
3	525	27.56	present work
5	550	30.25	Wintle, 1977

The plot of  $\beta$  versus  $T^{*2}$  (Figure II<sub>1</sub>) indicates a fair linear relationship between these parameters. The slope:

$\beta/T^{*2} = 0.1 \pm 0.05 \cdot 10^{-4} \text{°K}^{-1} \text{sec}^{-1}$  can be combined with any  $T^*$  in the range 500-550°K for substitution in equation (1.4.1.3). Here, the average  $T^* = 525^\circ\text{K}$  is used. Wintle gives an  $E = 1.74 \pm 0.02$  eV, while Hennig gives:  $E = 1.65 \pm 0.1$  eV (see section 2.5). If the less favouring  $E = 1.65$  eV is used, the lifetime for  $T_0 = 10^\circ\text{C} = 283^\circ\text{K}$  (see section 5.1) gets a minimum  $\tau_0 \approx 6$  Ma, while for  $E = 1.74$  eV it becomes:  $\tau_0 \approx 30$  Ma.

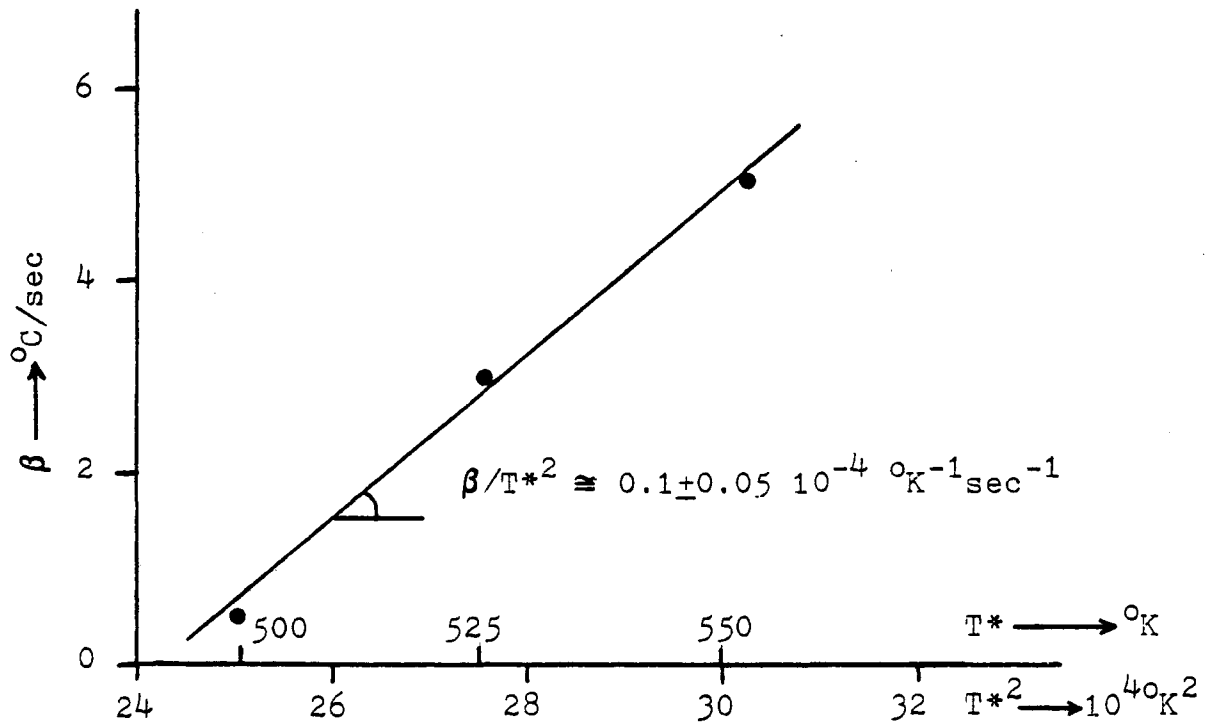


Figure II<sub>1</sub> Annealing rate ( $\beta$ ) dependence on activation temperature ( $T^*$ ).